TECHNICAL REPORT SL-79-8

EARTHQUAKE ANALYSIS OF THE GRAVITY DAM MONOLITHS OF THE RICHARD B. RUSSELL DAM

by

C. Dean Norman, Harry E. Stone

Structures Laboratory
U. S. Army Engineer Waterways Experiment Station
P. O. Box 631, Vicksburg, Miss. 39180

September 1979
Final Report

Prepared for U. S. Army Engineer District, Savannah
Savannah, Ga. 31402

Unclassified

SECURITY CLASSIFICATION OF THIS PAGE *(When Data Entered)*

REPORT DOCUMENTATION PAGE

READ INSTRUCTIONS BEFORE COMPLETING FORM

1. REPORT NUMBER: Technical Report SL-79-8

2. GOVT ACCESSION NO.:

3. RECIPIENT'S CATALOG NUMBER:

4. TITLE *(and Subtitle)*: EARTHQUAKE ANALYSIS OF THE GRAVITY DAM MONOLITHS OF THE RICHARD B. RUSSELL DAM

5. TYPE OF REPORT & PERIOD COVERED: Final report

6. PERFORMING ORG. REPORT NUMBER:

7. AUTHOR(s): C. Dean Norman, Harry E. Stone

8. CONTRACT OR GRANT NUMBER(s):

9. PERFORMING ORGANIZATION NAME AND ADDRESS: U. S. Army Engineer Waterways Experiment Station, Structures Laboratory, P. O. Box 631, Vicksburg, Miss. 39180

10. PROGRAM ELEMENT, PROJECT, TASK AREA & WORK UNIT NUMBERS:

11. CONTROLLING OFFICE NAME AND ADDRESS: U. S. Army Engineer District, Savannah, P. O. Box 889, Savannah, Ga. 31402

12. REPORT DATE: September 1979

13. NUMBER OF PAGES: 136

14. MONITORING AGENCY NAME & ADDRESS *(if different from Controlling Office)*:

15. SECURITY CLASS. *(of this report)*: Unclassified

15a. DECLASSIFICATION/DOWNGRADING SCHEDULE:

16. DISTRIBUTION STATEMENT *(of this Report)*

Approved for public release; distribution unlimited.

17. DISTRIBUTION STATEMENT *(of the abstract entered in Block 20, if different from Report)*

18. SUPPLEMENTARY NOTES

19. KEY WORDS *(Continue on reverse side if necessary and identify by block number)*

Earthquake engineering
Gravity dams
Monoliths
Richard B. Russell Dam

20. ABSTRACT *(Continue on reverse side if necessary and identify by block number)*

Finite element computer analyses were performed for critical concrete sections of the Richard B. Russell Dam using as input several acceleration-time histories recommended by a panel of geologists and seismologists. Response spectra analyses were also performed using the Nuclear Regulatory Commission (NRC) Guide 1.60 design response spectra for a 0.25-g ground acceleration. Both complete time history response calculations and

(Continued)

DD FORM 1 JAN 73 1473 EDITION OF 1 NOV 65 IS OBSOLETE

Unclassified

SECURITY CLASSIFICATION OF THIS PAGE *(When Data Entered)*

20. ABSTRACT (Continued).

simplified approximate analyses are performed and their results compared. The effects of dynamic response parameters such as foundation flexibility and level of structural damping are studied. Conservative aspects of the different analysis procedures are pointed out, and their effects on structural stresses were qualitatively evaluated. A comparison of the results of these types of analyses is made with observations from the earthquake experience of the Koyna Dam during the Indian earthquake of 1967.

Appendix A presents acceleration-, velocity-, and displacement-time histories and response spectra at 5 and 10 percent damping for eight earthquakes. Appendix B presents the results of an earthquake structural analysis of the Koyna Dam of India.

PREFACE

This study was conducted during the period January 1977-April 1979 by personnel of the U. S. Army Engineer Waterways Experiment Station (WES) under the sponsorship of the U. S. Army Engineer District, Savannah.

This work was conducted under the supervision of Messrs. Bryant Mather, Acting Chief, Structures Laboratory (SL), W. J. Flathau, Assistant Chief, SL, and J. T. Ballard, Chief, Structural Mechanics Division (SMD), SL. Various phases of the analyses were performed by Messrs. H. Wayne Jones, Automatic Data Processing Center, and Harry E. Stone and C. Dean Norman, SMD. This report was prepared by Mr. Norman and Mr. Stone.

The Commanders and Directors of WES during the conduct of this study and the preparation of this report were COL J. L. Cannon, CE, and COL Nelson P. Conover, CE. Technical Director was Mr. F. R. Brown.

CONTENTS

CONVERSION FACTORS, U. S. CUSTOMARY TO METRIC (SI)
UNITS OF MEASUREMENT

U. S. customary units of measurement used in this report can be converted to metric (SI) units as follows:

Multiply	By	To Obtain
feet	0.3048	metres
inches	2.54	centimetres
inches per second	2.54	centimetres per second
miles	1.609344	kilometres
pounds (force) per square inch	6.894757	kilopascals

EARTHQUAKE ANALYSIS OF THE GRAVITY DAM MONOLITHS OF THE RICHARD B. RUSSELL DAM

PART 1: INTRODUCTION

1. This report is concerned primarily with the earthquake structural analysis of the concrete nonoverflow section of the Richard B. Russell Dam. Also considered herein are the earthquake analyses of the intake sections and the overflow sections. The analysis of each section will be presented and discussed separately. The tallest nonoverflow monolith was considered the most susceptible to earthquake damage and therefore was analyzed in more detail than the other sections. Consequently, the approach taken in this study was to determine the nonoverflow section's capability to adequately withstand the effects of the maximum design earthquake. Once this capability was established and the conservatism in various aspects of the analysis identified, similar analysis procedures could be used with confidence for the intake and overflow sections. In the final designs for all sections, concrete strengths will be selected that will safely withstand the acting seismic stresses as determined in this study.

2. It should be pointed out here that in general, the analysis procedure used for the Richard B. Russell project yields conservative results. Specific conservative assumptions such as rigid fixed foundation and low levels of damping will be discussed in detail later in this report. These assumptions are conservative in that they force the dam to safely withstand the energy produced by the earthquake forces without allowing for any energy dissipation associated with the flexibility of the foundation, nonlinear response of the dam, or any other energy dissipating effects.

3. To familiarize the reader with what could be interpreted as overall conservatism in the analysis procedure used in this report, a particular earthquake experience can be cited. Koyna Dam, located in India, experienced a magnitude 6.5 earthquake with epicenter near the reservoir on December 11, 1967. The dam had been instrumented earlier

in 1963, and this active instrumentation recorded the acceleration records shown in Figure B.1. Maximum principal stresses were computed by finite element analysis to be near 900-psi* tension on the downstream face near elevation 2060 (Figure B.2) with stresses on the upstream face as high as 600-psi tension. With stresses in this range over a significant area of the cross section, one would expect considerable cracking to occur in the dam. Koyna Dam did experience significant cracking on the upstream and downstream faces near elevation 2060. However, the dam withstood the earthquake without any sudden release of water and the damages incurred were later repaired. The Koyna example demonstrates that assumptions such as rigid foundation, low damping levels, and linear response yield results that are generally conservative. It is also important to note that the computed maximum stresses occurred in the regions where cracking was observed. The overflow monoliths of Koyna Dam were analyzed with a similar finite element procedure, the results of which indicated there would be no cracking. These results were also consistent with the actual earthquake experience since no cracks were observed on the overflow monoliths.

Background

4. The Richard B. Russell Dam is to be constructed on the Savannah River approximately 170 miles upstream from Savannah, Georgia (Figure 1). As can be seen in Figure 2, the damsite falls in a seismic zone 2 which implies design accelerations in the range of 0.05 g. Although these values of design accelerations are used in simplified earthquake analyses for many structures, the U. S. Army Corps of Engineers elected to establish a Design Earthquake Panel (DEP) for the Richard B. Russell Project along with a Design Review Panel (DRP). The DEP was directed to characterize the damsite from a seismic standpoint and recommend general motion-time histories which might be used for engineering analysis and design purposes. It was understood that these time

---

* A table of factors for converting U. S. customary units of measurement to metric (SI) units is found on page 3.

histories would apply to bedrock motions at the site. The DRP was directed to review these free-field time histories and recommend individual records or appropriately equivalent ground motion to be used in the structural analysis of the dam. Furthermore, the DRP would review the engineering application of the ground motion and approve the structural analysis procedures used. The actual earthquake structural analysis would be performed by staff members of the Structures Laboratory of the U. S. Army Engineer Waterways Experiment Station (WES). Members of the above-mentioned panels and analysis staff are listed below.

Design Earthquake Panel	Design Review Panel
Dr. C. Allin Cornell	Dr. Nathan M. Newmark
Dr. David T. Snow	Dr. H. Bolton Seed
Dr. Otto W. Nuttli	Mr. Charles Content
Dr. David B. Slemmons	Mr. Wendell S. Johnson
Dr. Leland Timothy Long	Mr. F. B. Slichter
Dr. Pradeep Talwani	
Fr. Louis Eisele, S. J.	

WES Structural Analysis Staff

Mr. C. Dean Norman
Mr. Harry E. Stone
Mr. H. Wayne Jones

Design Earthquake

5. The maximum design earthquake is defined as the severest earthquake that is believed to be possible at the project site on the basis of geological and seismological evidence. For the maximum design earthquake loading, inelastic structural behavior with associated cracking of the concrete of a gravity dam is permissible as long as the cracking is not severe enough to cause a significant failure of the dam, resulting in release of the reservoir. (Reference ER 1110-2-1806, Earthquake Design and Analysis for Corps of Engineers Dams, pages 3 and 7).

6. The DEP concluded (Reference 1) that there was no evidence of an active fault existing in the general area of the Richard B. Russell Dam site. Furthermore, severe earthquakes have been restricted to the vicinity of Charleston, South Carolina, which is approximately 170 miles from the damsite. Due to the distance, motions attenuated from the

Charleston site would be low. However, an exceptionally conservative approach could be taken where a near-field event is assumed at the damsite. Based on this assumption, the peak motions for bedrock were determined by the panel to be in the range of 0.4 to 0.5 g with velocities from 30 to 45 cm/sec and displacements up to 20 cm with a 5-sec duration. The DEP then selected a group of earthquake time histories with these general characteristics which could be used to form the basis for a dynamic response analysis.

7. After consideration of the site conditions and the characteristics of the structure to be designed, the DRP concluded that a conservative design could be based on a design response spectrum with a ground acceleration of 0.25 g. The recommended response spectrum is described in the NRC Regulation Guide 1.60 as the Safe Shutdown Earthquake. It can be shown that this response spectrum, in general, bounds the effects of earthquake time histories as defined by the DEP (Figure A.25). Details of the rationale used by the DRP in developing the design earthquake are described in "Design Earthquake for Richard B. Russell Dam" dated 1 April 1977.

Summary of the Analyses Performed

8. For the nonoverflow section of the dam, two methods of analysis were used. The first method used is a one-dimensional simplified method of analysis which assumes cantilever beam action only and uses a response spectrum to define the earthquake ground motion. The NRC Regulatory Guide 1.60 response spectrum for 5 percent damping and 0.25-g ground acceleration (Figures 3 and A.25) was used for this analysis. The second method used is a two-dimensional finite element time history method of analysis. For this analysis several of the earthquake time histories listed in the DEP report were used in a special finite element computer program for the earthquake analysis of concrete gravity dams. These time histories are listed in Table 1 and are shown in Appendix A. Five and ten percent damping were used in separate analyses.

9. For the intake and overflow sections of the dam, a

three-dimensional finite element response spectrum method of analysis was used. The NRC Regulatory Guide 1.60 response spectrum for 5 percent damping and 0.25-g ground acceleration was used in a general-purpose finite element computer program for these analyses. The DRP also suggested that uplift pressures on the nonoverflow section be incorporated into the seismic analysis. This analysis was performed by personnel of the U. S. Army Engineer District, Savannah, using McDonnell Douglas's version of STRUDL with the same finite element grid as used in the seismic analysis. Three load cases were considered: (a) full gravity only, (b) uplift only, and (c) combination full gravity and uplift. Comparison of the stresses of load case 1 and load case 2 indicates a maximum net change of 25-psi tension at the heel of the nonoverflow section. Since preliminary studies indicate that the dynamic analysis is conservative, the stresses due to uplift may safely be neglected.

PART II: EARTHQUAKE ANALYSIS, NONOVERFLOW SECTION

Methods of Analysis

Simplified procedure

10. As mentioned previously, the first method of analysis used for the nonoverflow section of the concrete dam was based on the response spectrum method. Details of this analysis procedure are presented in Reference 2. In general, the analysis is based on the assumption that the earthquake response of the dam is adequately described with a single-degree-of-freedom (SDOF) model. The effects of the hydrodynamic interaction are incorporated in the analysis using the theory presented in Reference 3. Essentially the interaction problem is solved using a substructure method in which the dam is one substructure and the reservoir the other. The problem is then solved in the frequency domain. In this analysis procedure, the dam is assumed fixed at the base and only horizontal earthquake components are considered. The geometry and material properties for the dam along with the design response spectra used in this analysis are shown in Figure 3.

11. After the lateral earthquake forces are determined, they are applied to the dam and combined with the loads associated with gravity and hydrostatic water pressure to determine the states of stress at critical locations in the dam. For the purpose of determining stresses, the dam is assumed to respond as a cantilever beam.

Finite element method with hydrodynamic interaction

12. In this method of analysis, the dam is modeled with finite elements and the reservoir is solved as a continuum boundary value problem with compressibility of the water included. The solution is based on the substructure concept and is carried out in the frequency domain. Horizontal and vertical ground motions are input in the form of acceleration-time histories with the final solution obtained by mode superposition. The base of the dam is assumed to be ideally fixed, implying a rigid foundation. Details of this analysis procedure are

presented in Reference 4. The same geometry and material properties as used in the simplified method are used here.

Presentation of Results

Simplified procedure

13. Results of the simplified analysis are presented in Table 2 in the form of maximum stresses at the heel, toe, upstream face at the water level, and downstream face at the water level. One set of stresses is obtained with the earthquake forces acting in the downstream direction while the other set is obtained when the earthquake forces act in the upstream direction. Five percent damping was used in constructing the response spectrum used in this analysis. Tension stresses are considered positive.

Finite element method with hydrodynamic interaction

14. A list of the earthquake time histories used in the finite element analysis is presented in Table 1. Horizontal and vertical components of the scaled earthquake records are presented in Table 1. These records were selected from the list of recommended time histories presented in Reference 1 and generally bracket the type of motion discussed by the DEP and that motion associated with the design response spectrum presented in the NRC 1.60 Guide. Sixteen computer runs were conducted using eight time histories recommended by the DEP, each with two percentages of critical damping. These time histories together with their associated response spectra are shown in Appendix A. For each computer run, four critical areas of the dam were studied: heel, toe, upstream face near the water level, and downstream face near the water level. For each of these critical areas, the principal stress was evaluated at each time step throughout the complete time history. At the time when the stress in a particular critical area reached a maximum, the stresses in all other parts of the dam were evaluated and a stress contour plot was made. These stress contour plots are presented in Figures 4 through 19. For a particular plot, the critical area

considered is indicated in the upper right-hand portion of the plot. A summary of the results of these computer runs is presented in Table 3.

Discussion of Results

General

15. Results from the earthquake structural analyses presented herein should be carefully interpreted in light of the performance criteria specified for the design earthquake. As stated earlier, inelastic structural behavior with associated cracking of the concrete is permissible for the maximum design earthquake response as long as the cracking is not severe enough to cause a failure of the dam resulting in release of the reservoir. Also, the primary intent of this study was to provide a conservative yet rational approach to the dynamic structural analysis of the Richard B. Russell Dam. With these general ideas in mind, a discussion of the results of the simplified and finite element analyses is presented.

Simplified procedure

16. Maximum stresses determined using this procedure are shown in Table 2 for earthquake forces acting in the downstream and upstream directions. Maximum tensile stresses occur on the upstream face when the earthquake forces act downstream and on the downstream face when these forces act upstream. The maximum tensile stresses at 5 percent damping range up to 257 psi on the upstream face to 405 psi on the downstream face. There are several reasons for believing that a properly designed concrete gravity dam can withstand dynamic tensile stresses of this magnitude. First, the high stresses are restricted primarily to four regions of the dam cross section and do not exist over a major portion of the dam. Experiences such as the earthquake performance of Koyna Dam in India (Reference 5) have indicated that concrete dams can continue to maintain their impounded water even after significant cracking in localized areas has occurred. Furthermore, concrete strength in tension and compression is dependent on rate of loading with significant increases

observed in some test programs at loading rates consistent with those occurring in earthquake response (Reference 6). However, additional research is needed to verify the observed strength increases. It should also be mentioned that a fixed base is assumed in the analysis, which would imply rigid foundation rock. Since this is not actually the case with practical foundation materials, one can expect the stresses in the dam in general and near the base particularly to be somewhat less than those indicated by the analyses due to the flexibility of the foundation. Finally, it is reasonable to assume a higher level of damping for a structure stressed at levels considered here (Reference 7). This would imply use of a response spectrum which would yield lower earthquake forces.

Finite element method
with hydrodynamic interaction

17. The maximum tensile stress considering all 16 finite element analyses was 471 psi at the heel due to the N90E and vertical components of the San Fernando earthquake at 5 percent damping and 355 psi at the heel for 10 percent damping. These stresses and other maximum values can be compared using Table 3. The high stresses shown in Table 3 are of less concern when increased concrete strength with strain rate is considered as mentioned earlier. Specifically, for the first earthquake listed in Table 3, an inspection of the stress-time output indicated that the maximum stress changed from 471-psi tension at 3.4 sec to 91-psi compression at 3.5 sec. Therefore, the duration of high tensile stresses is very short. Also, these stresses are localized and do not act over a large portion of the dam. The uncracked area remaining should be sufficient to carry the shear and moment required for stability. The significant reduction in stresses due to higher damping values is evident based on the results of these analyses. When interpreting results from the finite element solution, one should recognize that this procedure will generally yield higher stresses than the simplified procedure at critical areas such as the heel. This is due to the discontinuity at the dam and rigid foundation interface. The finite element analysis recognizes this as a stress concentration at the heel where, in reality,

the flexibility of the foundation would tend to decrease this stress. Stress concentrations such as this can be seen in Figure 4d.

18. In order to obtain a more quantitative understanding of the general effects of dam-foundation interaction, the theory of an earthquake response spectrum analysis can be studied. As mentioned, the analyses previously discussed assume the base of the dam to be rigidly fixed to the foundation. This implies that there will be no displacements or rotations at the foundation level. Model and prototype vibration tests on concrete dams have indicated that this is not strictly correct since the foundation does deform and generally causes the natural periods of the dam-foundation system to lengthen. The effects of including a foundation in a finite element calculation of natural frequencies is illustrated in Figure 20. The effects of foundation interaction on mode shapes is not so great and is demonstrated for the first mode in Figure 21.

19. If the equations of motion for a concrete dam are formulated in terms of base acceleration and the first mode of vibration is considered, the distribution of lateral earthquake forces over the height of the dam is given by (Reference 2)

$$f_1(y) = \alpha_1 \frac{S_a(\tilde{T})}{g} \left[W_s(y)\phi(y) + P(y) \right] \qquad (1)$$

in which

α_1 = 4, equivalent to a mode participation factor

$S_a(\tilde{T})$ = spectral acceleration obtained from the design response spectrum. $\tilde{T}$ is the fundamental period including reservoir effects

g = acceleration of gravity

$W_s(y)$ = weight per unit height of dam

$\phi(y)$ = fundamental mode shape of dam

$P(y)$ = hydrodynamic pressure

20. The quantities α_1, g, $W_s(y)$, and $\phi(y)$ are essentially

the same for a fixed base dam and one in which the foundation is included (e.g., $\phi(y)$ was shown to be insensitive to foundation effects). Therefore, two parameters in Equation 1 are dependent on the foundation effects: $S_a(\tilde{T})$ and $P(y)$. The variation in $\tilde{T}$ is from 0.188 sec for the fixed base and 0.21 sec for the foundation included. Entering the design response spectrum (Figure 3) at the corresponding frequencies of 4.75 and 5.32 Hz, the change in the spectral acceleration $S_a(\tilde{T})$ is hardly noticeable. Therefore, the dependence of $f_1(y)$ on $S_a(\tilde{T})$ is concluded to be negligible in regard to the foundation interaction effect for this particular dam. The final parameter to investigate is $P(y)$. From Reference 2

$$P(y) = \left(\frac{H}{H_s}\right)^2 \bar{P}(y)$$

where (H/H_s), the ratio of reservoir depth to dam height, is the same for a fixed base and for foundation included. $\bar{P}(y)$ is determined from the set of curves shown in Figure 22 where

$$R_2 = \frac{H}{1180\tilde{T}}$$

Note that R_2 for a fixed base is always greater than R_2 for foundation included (H is a constant for each case). Figure 22 then demonstrates that larger values of R_2 imply larger values of $\bar{P}(y)$ and $f_1(y)$. Therefore, based on this analogy, the effect of the foundation flexibility is concluded to be that of lowering the total lateral earthquake forces exerted on the dam and consequently lowering the resulting stresses in the dam. Also, it can be argued that for a given loading on the dam, the overall stresses in the dam which include a foundation will be less than those for a fixed base. This can be argued since the external work would be the same for each system while the material volume to store strain energy is much greater when the foundation is included and therefore the general stress distribution would be less.

Conclusions

21. The general conclusion drawn from this study is that the non-overflow section of the Richard B. Russell Dam as specified by the geometry in Figure 3a can be designed to safely withstand the maximum design earthquakes without failure of the dam. This conclusion was reached after studying the results of state-of-the-art simplified and detailed earthquake structural analysis procedures and the past earthquake response of the Koyna Dam during the 1967 Indian earthquake. The Koyna Dam was subjected to a recorded ground motion of 0.49 g for the transverse (upstream-downstream) component and 0.34 g for the vertical component without a failure. The analysis procedure presented herein was used in analyzing the Koyna Dam, and the results are consistent with the degree of damage which actually occurred in the dam.

PART III: EARTHQUAKE ANALYSIS, INTAKE SECTION

22. A cross-sectional view of the intake section of the Richard B. Russell Dam is presented in Figure 23. For analysis purposes the intake section is approximately 205 ft high and 71 ft wide. The primary openings in the section include the penstock and the gate and bulkhead slots. Substantial reinforcing steel is provided around these openings in the design section.

Finite Element Method with Response Spectrum

23. A three-dimensional (3-D) finite element analysis was performed on the intake section. The SAP IV finite element computer code with the variable node element as described in Reference 8 was used for the analysis. Oblique views of the finite element grid are presented in Figure 24. The vertical plane of symmetry through the center of the intake section and the edge of the intake monolith establish the lateral boundaries of the finite element grid. The boundary condition imposed on these edges is similar to a condition of plane strain. The restraints on displacements of the nodes at the base of the section prescribe a fixed condition. The grid consists of six vertical layers (Figure 25) with a total of 753 elements resulting in 2551 degrees of freedom. Two loading conditions, penstock empty and full, were considered in the analysis. The effects of the reservoir were modeled using a Westergaard added mass concept. This essentially resulted in adding equivalent water mass to the nodes on the upstream face for the empty penstock case. In the full penstock condition a portion of the water in the penstock was considered to act in the same manner as that in an intake tower; the remainder was treated as a Westergaard mass calculated from a projected vertical area concept. This was done since the equivalent mass must be developed on a surface area oriented normal to the direction of motion of the dam during an earthquake. The mass and weight of the gate and bulkhead were added to appropriate nodes where they were supported.

24. The design response spectrum as specified in the NRC

Regulation Guide 1.60 with 0.25-g ground acceleration and 5 percent damping was used in the analysis of the intake section. Four modes of vibration were used in the dynamic analysis. Elements on the upstream and downstream face and those surrounding the penstock opening were of 2.9×10^6-psi modulus concrete, and the remainder of the elements were of 2.6×10^6-psi modulus concrete. It was concluded by DRP that for the intake and overflow sections this method of analysis would be adequate for design purposes.

Presentation of Results (Intake Section)

25. A complete printout of stresses in all elements of the grid is being furnished to the Savannah District. In this report only stresses in a few critical areas of the section are presented. The coordinate system and identification of grid layering is shown in Figure 25. The element numbering for each layer was the same and is presented in Figure 26. The critical elements were selected near the heel, toe, and the upstream face near the water level. Stresses in elements on the downstream face near the water level were small. The stresses (tension is positive) produced in these elements based on the response spectrum analysis using one mode of vibration are presented in Table 4. In Table 4 the element and layer where the highest stresses were computed are presented along with vertical stresses due to gravity. The σ_z dynamic stresses and σ_z total stresses are also based on one mode of vibration. σ_{max} is determined from a principal stress calculation which considers the gravity stresses and the dynamic stresses. The complete states of stress for different critical elements are presented in Table 5. In Table 5 four modes of vibration are considered and a root sum square of the displacement is used to calculate stresses. σ_z stresses presented in Table 5 can be compared with the one-mode approximation (σ_z total) stresses presented in Table 4 in evaluating the one-mode calculation.

Conclusions

26. The maximum principal stress computed for one mode response in the intake section was 439-psi tension and occurred at the heel. In structures of this type subjected to earthquake loadings, usually 90 to 95 percent of the total response is contained in the fundamental mode; therefore, the above value for maximum principal stress is significant. As observed from Tables 4 and 5, the only tensile stresses of sizable value occurred in the heel element 1. The same logic used previously in interpreting the heel stress for the nonoverflow monolith should be used here. Essentially, that is to say that there is a stress concentration due to the sharp angle between the dam and the foundation and that it was observed that this high stress was localized and would tend to relieve itself as the actual dam structure responded to the earthquake loadings. Generally, it can be concluded that the intake section of the Richard B. Russell Dam as shown in Figure 23 can be designed to safely withstand the maximum design earthquakes without failure.

PART IV: EARTHQUAKE ANALYSIS, OVERFLOW SECTION

27. A cross-sectional view of the overflow section of the Richard B. Russell Dam is shown in Figure 27. Openings for the sluice and gallery were not modeled in this analysis. Piers and the tainter gate were included in the analysis. The overflow section is 60 ft wide and approximately 136 ft high with a pier width of approximately 10 ft. As in the intake section, substantial reinforcing steel is provided around openings in the overflow section and in the piers, which must support loads from the tainter gates.

Finite Element Method with Response Spectrum

28. Essentially the same type finite element analysis was used for the overflow section as was used in the analysis of the intake section. Views of the 3-D finite element grids are shown in Figure 28. Due to the symmetry of the overflow section, a grid 30 ft deep was used in the analysis with the same boundary conditions as used for the intake section.

29. In constructing the finite element grid with 1282 degrees of freedom, 335 elements were used. A Westergaard-type analysis was used to model the reservoir effects. The mass of the tainter gate and the Westergaard mass calculated in the region of the tainter gate were concentrated at the nodes in the region of the trunnion reaction. The weight of the tainter gate was supported proportionately by nodes along the crest of the section and near the trunnion reaction. Elements in contact with the water on the upstream face and downstream face were of 3.3×10^6-psi modulus concrete with the remainder of the elements in the overflow section itself being of 2.7×10^6-psi modulus concrete. For those elements in the pier, except at the level of the trunnion reaction (where 4.3×10^6-psi modulus concrete was used), 3.0×10^6-psi modulus concrete was used.

Presentation of Results (Overflow Section)

30. As is the case for the intake section, a complete printout of

stresses for the overflow section is being furnished to the Savannah District. The stresses in critical areas will be presented herein. Coordinate system and grid layering for the overflow section are presented in Figure 29. Element numbers for the finite element grid are shown in Figure 30. For the overflow section, the critical areas for stress determination were selected near the heel, toe, crest of the section, and at the trunnion reaction. These stresses were determined in the same manner as for the intake section and are presented in Tables 6 and 7.

Conclusions

31. Stresses computed for the overflow section follow the same pattern as those determined for the previous two sections. However, there is one region of significantly high tensile stress near the trunnion reaction. This high stress should present no real problem since there is substantial reinforcing steel provided in this area to resist the loads from the tainter gate. Generally, it can be concluded that the overflow section of the Richard B. Russell Dam as shown in Figure 27 can be designed to safely withstand the maximum design earthquakes without failure.

REFERENCES

1. Geological and Seismological Evaluation of Earthquake Hazards at the Richard B. Russell Project, March 1977.

2. A. K. Chopra, "Earthquake Resistant Design of Concrete Gravity Dams Considering Dynamic Effects of Earthquakes," November 1977.

3. P. Chakrabarti and A. K. Chopra, "Earthquake Response of Gravity Dams Including Reservoir Interaction Effects," Report No. EERC 72-6, December 1972.

4. P. Chakrabarti and A. K. Chopra, "A Computer Program for Earthquake Analysis of Gravity Dams Including Hydrodynamic Interaction," Report No. EERC 73-7, Earthquake Engineering Research Center, University of California, Berkeley, CA, May 1973.

5. P. Chakrabarti and A. K. Chopra, "The Earthquake Experience at Koyna Dam and Stresses in Concrete Gravity Dams," International Journal of Earthquake Engineering and Structural Dynamics, Vol. 1, No. 2, October-December 1972, pp. 151-164.

6. J. M. Raphael, "The Nature of Mass Concrete in Dams," Douglas McHenry Symposium Volume, American Concrete Institute, Detroit, MI, 1977.

7. N. M. Newmark, "Comments on Conservatism in Earthquake Resistant Design," Urbana, IL, September 1974.

8. K. Bathe, E. Wilson, and F. Peterson, "SAP IV, A Structural Analysis Program for Static and Dynamic Response of Linear Systems," Report No. EERC 73-11, June 1973.

9. P. Morrison, et al., "Earthquake Recordings on or Near Dams," USCOLD Committee on Earthquakes, November 1977.

10. A. K. Chopra, "Earthquake Resistant Design of Concrete Gravity Dams Considering Dynamic Effects of Earthquakes," A report to Office, Chief of Engineers and U. S. Army Engineer Waterways Experiment Station, November 1977.

Table 1

Earthquakes Used in Finite Element Analysis

Earthquake	Scaled Peak Ground Motion				
	Horizontal Acceleration cm/sec^2	Acceleration, g		Velocity, cm/sec	
		H*	V*	H*	V*
San Fernando Earthquake Hollywood Storage P.E. Lot CIT D058, N90E	414	0.42	0.18	42.2	10.0
San Fernando Earthquake Griffith Park Obs. CIT 0198, S00W	352.0	0.36	0.24	41.0	14.8
San Fernando Earthquake Pacoima Dam CIT C041, S16E	382.7	0.39	0.24	37.7	19.4
San Fernando Earthquake 445 Figueroa CIT C054, N52W	294.2	0.30	0.11	34.8	21.4
San Fernando Earthquake 1625 Olympic Blvd. CIT 0199, N62W	238.0	0.24	0.15	21.3	10.4
San Fernando Earthquake 3411 Wilshire Blvd. CIT S265	125.0	0.13	0.05	18.2	6.79
Parkfield Earthquake Cholame Shandon Array No. 2 CIT B033, N65E	239.8	0.24	0.10	39.0	7.05
Helena, Montana, Earthquake CIT B025, N90E	427.5	0.44	0.27	39.9	28.5

* H = horizontal, V = vertical.

Table 2

Maximum Stresses Computed from Simplified Analysis Procedure Using NRC 1.60 Guide Response Spectrum with 5 Percent Damping

Direction of Earthquake Forces	Maximum Principal Stresses, psi				Maximum Vertical Stresses, psi			
	Heel	Toe	Upstream Face	Downstream Face	Heel	Toe	Upstream Face	Downstream Face
Upstream	-339	283	-336	405	-339	167	-336	280
Downstream	196	0 (-625)*	257	0 (-451)*	196	-369	257	-312

* ( ) indicates minimum stress or largest compressive stress.

Table 3

Summary of Maximum Stresses from Finite Element Analysis for Two Damping Ratios

Earthquake	Damping %	Maximum Tensile Stress, psi		
		Heel	Upstream	Downstream
San Fernando, N90E	5	471	337	440
San Fernando, N90E	10	355	237	322
San Fernando, S00W	5	348	247	292
San Fernando, S00W	10	258	168	231
San Fernando, S16E	5	242	171	198
San Fernando, S16E	10	195	142	150
San Fernando, N52W	5	254	98	139
San Fernando, N52W	10	209	65	96
San Fernando, N62W	5	204	106	149
San Fernando, N62W	10	170	89	120
San Fernando, Wilshire Blvd.	5	132	62	109
San Fernando, Wilshire Blvd.	10	112	51	82
Parkfield, N65E	5	121	18	66
Parkfield, N65E	10	118	7	51
Helena, N90E	5	339	237	308
Helena, N90E	10	256	188	225

Table 4

Stresses in Critical Areas of Intake Section, Richard B. Russell Dam, Due to Design Response Spectrum at 5 Percent Damping

Element	Layer	σ_z Gravity psi	σ_z Dynamic psi (1 Mode)	σ_z Total psi (1 Mode)	σ_{max} psi (1 Mode)
1	6	-38*	464	426	439
55	5	-72	-133	-205	7.3
23	6	-47	-63	-110	19
80	5	-26	-55	-81	4.4
79	1	-66	163	97	100

* Tension (+).

Table 5

Complete States of Stress, Intake Section, Richard B. Russell Dam,
Design Response Spectrum at 5 Percent Damping

Layer	Element		σ_x	σ_y	σ_z	τ_{xy}	τ_{yz}	τ_{zx}
			Gravity Stresses, psi					
6	1		-6.4	-12.6	-38.1	-0.3	-0.3	-5.8
5	55		-26.7	-29.2	-72.0	11.9	-33.7	43.1
6	23		-8.0	-51.1	-47.3	-17.1	26.5	18.5
5	80		-5.5	-8.9	-26.3	0.4	0.1	6.1
1	79		-19.4	-14.1	-65.8	-0.1	-1.1	1.1
			Gravity ± Dynamic (4 Modes)*, psi					
6	1	(+)	92.3	159.3	431.8	-0.25	0.05	60.2
		(-)	-105.1	-184.5	-508.0	-0.35	-0.65	-71.8
5	55	(+)	16.6	23.8	63.6	37.0	24.3	124.6
		(-)	-70.0	-82.2	-207.6	-13.2	-91.7	-38.4
6	23	(+)	-3.8	16.9	18.4	11.5	64.4	50.0
		(-)	-12.2	-119.1	-113.0	-45.7	-11.4	-13.0
5	80	(+)	38.0	27.2	36.6	9.6	3.5	71.7
		(-)	-49.0	-45.0	-89.2	-8.8	-3.3	-59.5
1	79	(+)	-3.6	9.1	133.2	1.0	1.6	21.8
		(-)	-35.2	-37.3	-264.8	-1.2	-3.8	-19.6

* Column of plus and minus signs in parentheses indicates the addition or subtraction of the dynamic stresses to or from the gravity stresses.

Table 6

Stresses in Critical Areas of Overflow Section, Richard B. Russell Dam, Due to Design Response Spectrum at 5 Percent Damping

Element	Layer	σ_z Gravity psi	σ_z Dynamic psi (1 Mode)	σ_z Total psi (1 Mode)	σ_{max} psi (1 Mode)
1	4	-75	-43	-118	-3.5
2	4	-30	-8	-38	-6.5
51	4	-31	259	228	262
72	4	-10	290	280	297
21	4	-8	290	282	875*

* σ_x gravity = 221 , σ_x dynamic = 647 at element 21.

Table 7

Complete States of Stress, Overflow Section, Richard B. Russell Dam,
Design Response Spectrum at 5 Percent Damping

Layer	Element		σ_x	σ_y	σ_z	τ_{xy}	τ_{xy}	τ_{zx}
			Gravity Stresses, psi					
4	1		-18.0	-18.6	-75.2	0	0	25.5
4	2		-5.6	-7.1	-29.7	0	0	5.5
4	51		-31.7	-12.5	-30.9	0	0	53.8
4	72		-19.3	-21.1	-9.6	4.3	4.0	10.2
4	21		220:6	6.0	-8.1	-0.45	1.8	16.7
			Gravity ± Dynamic (4 Modes)*, psi					
4	1	(+)	-3.0	-6.5	-29.5	0	0	59.3
		(-)	-33.0	-30.7	-120.9	0	0	-8.3
4	2	(+)	3.5	-3.5	-20.4	0	0	16.5
		(-)	-14.7	-10.7	-38.9	0	0	-5.5
4	51	(+)	5.1	47.9	234.2	0	0	83.9
		(-)	-68.5	-72.9	-296.0	0	0	23.7
4	72	(+)	-3.9	8.8	308.6	36.3	48.0	56.9
		(-)	-34.7	-51.0	-327.8	-27.7	-40.0	-36.5
4	21	(+)	903.4	24.6	359.5	6.2	10.1	136.9
		(-)	-462.2	-12.6	-373.7	-7.1	-6.5	-103.6

* Column of plus and minus signs in parentheses indicates the addition or subtraction of the dynamic stresses to or from the gravity stresses.

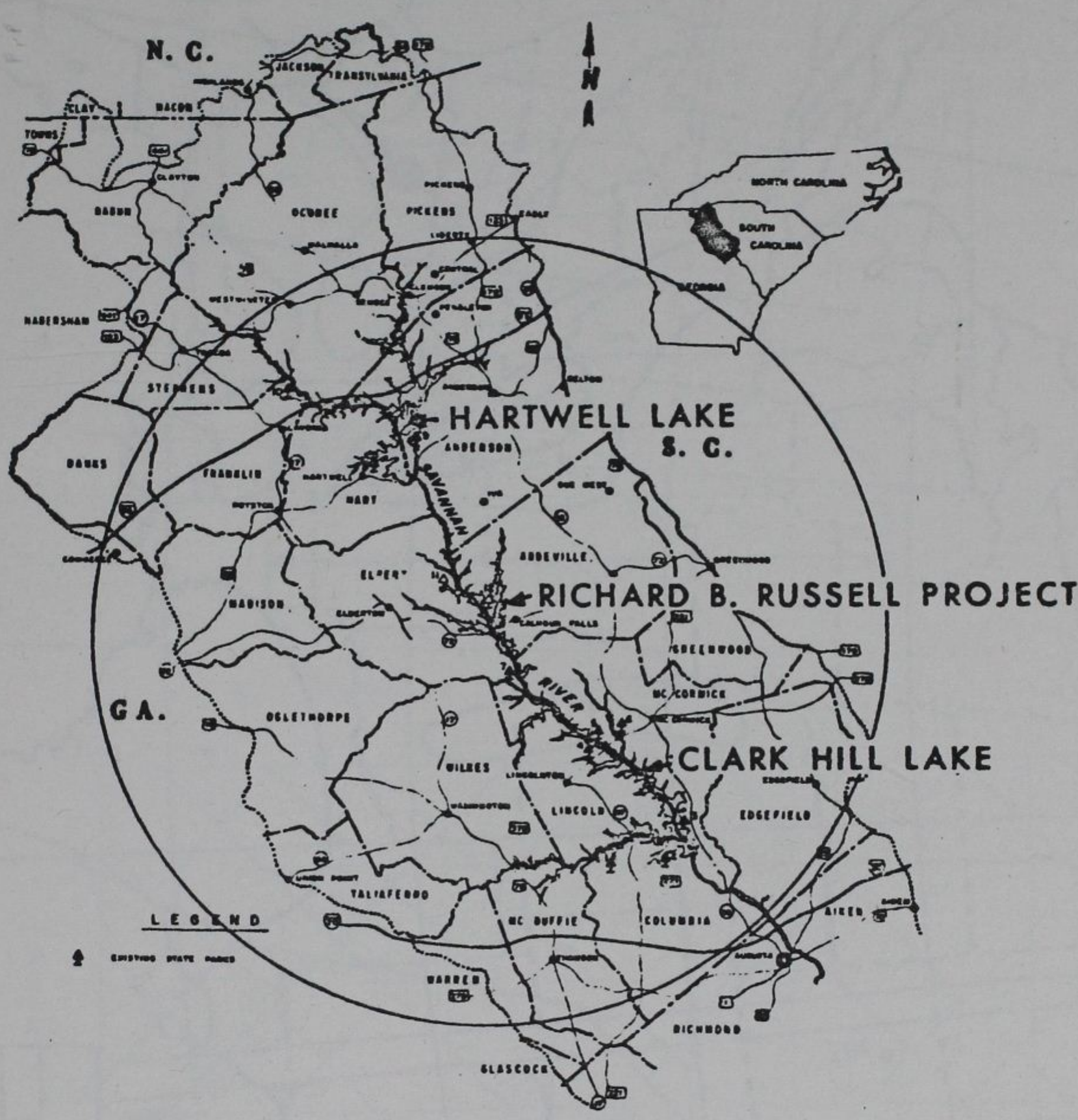

Figure 1 Geographic location of Richard B. Russell Dam site.

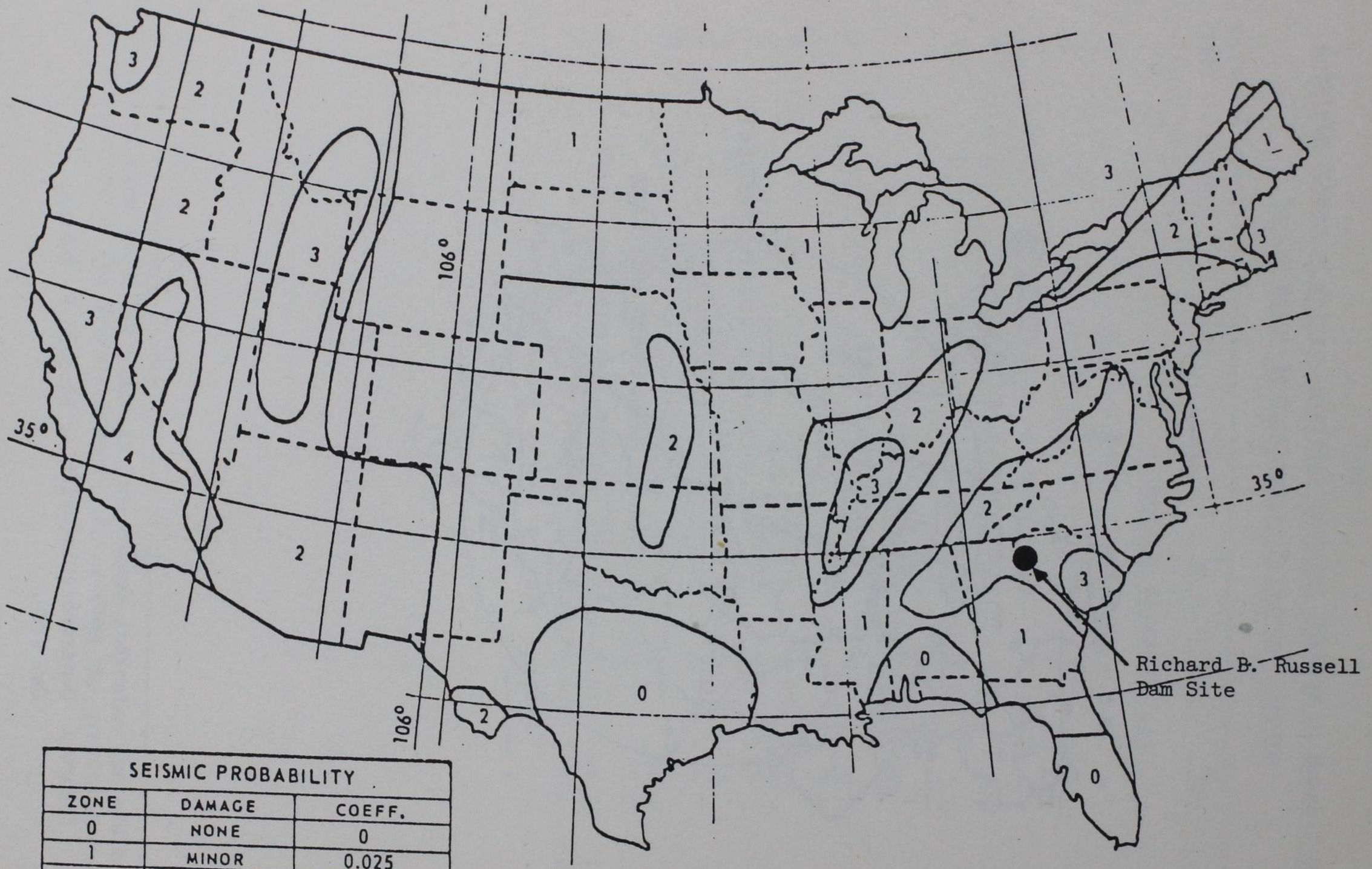

SEISMIC PROBABILITY		
ZONE	DAMAGE	COEFF.
0	NONE	0
1	MINOR	0.025
2	MODERATE	0.05
3	MAJOR	0.10
4	GREAT	0.15

Figure 2 Seismic zone map of contiguous states.

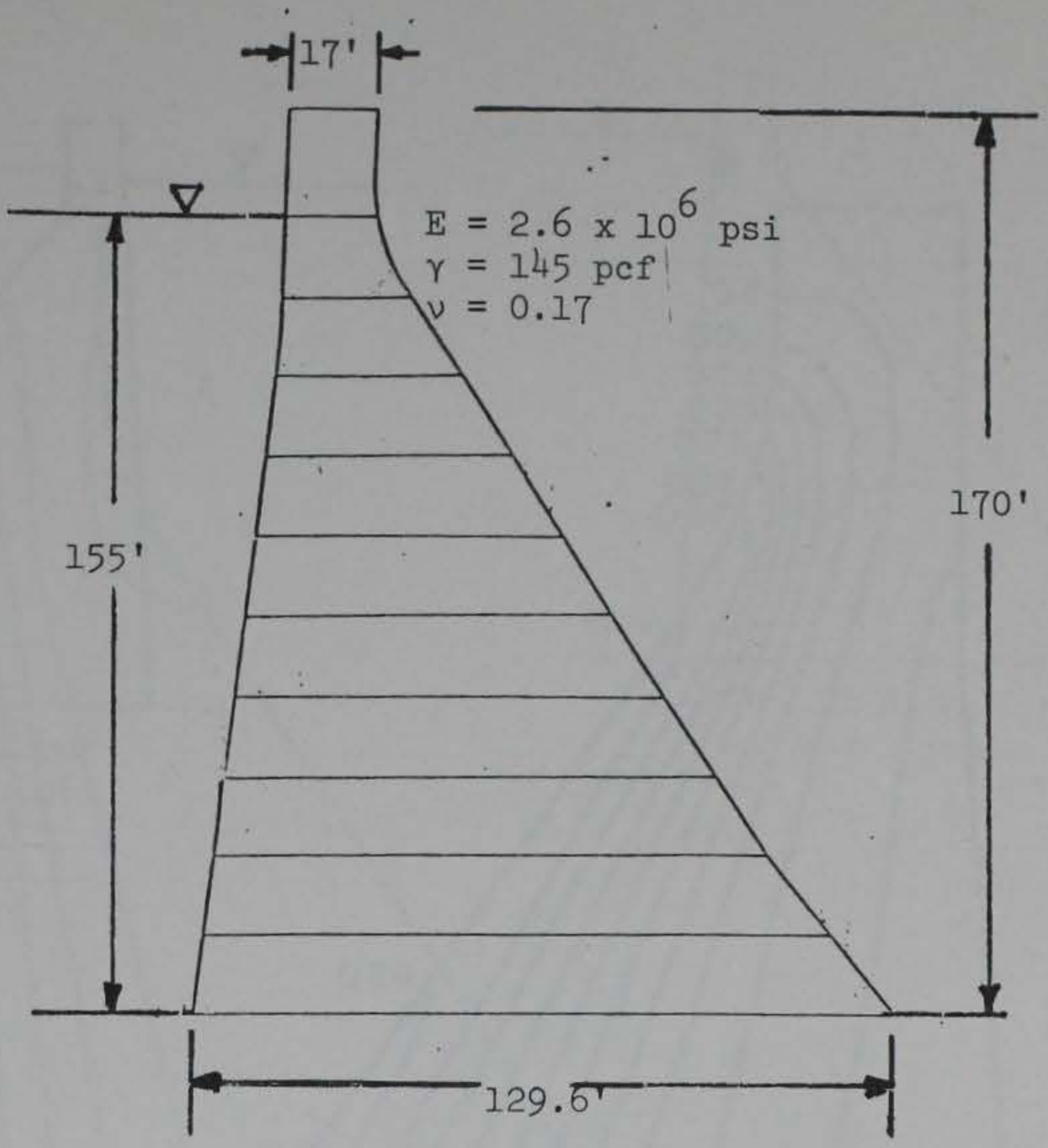

a. Geometry of nonoverflow section.

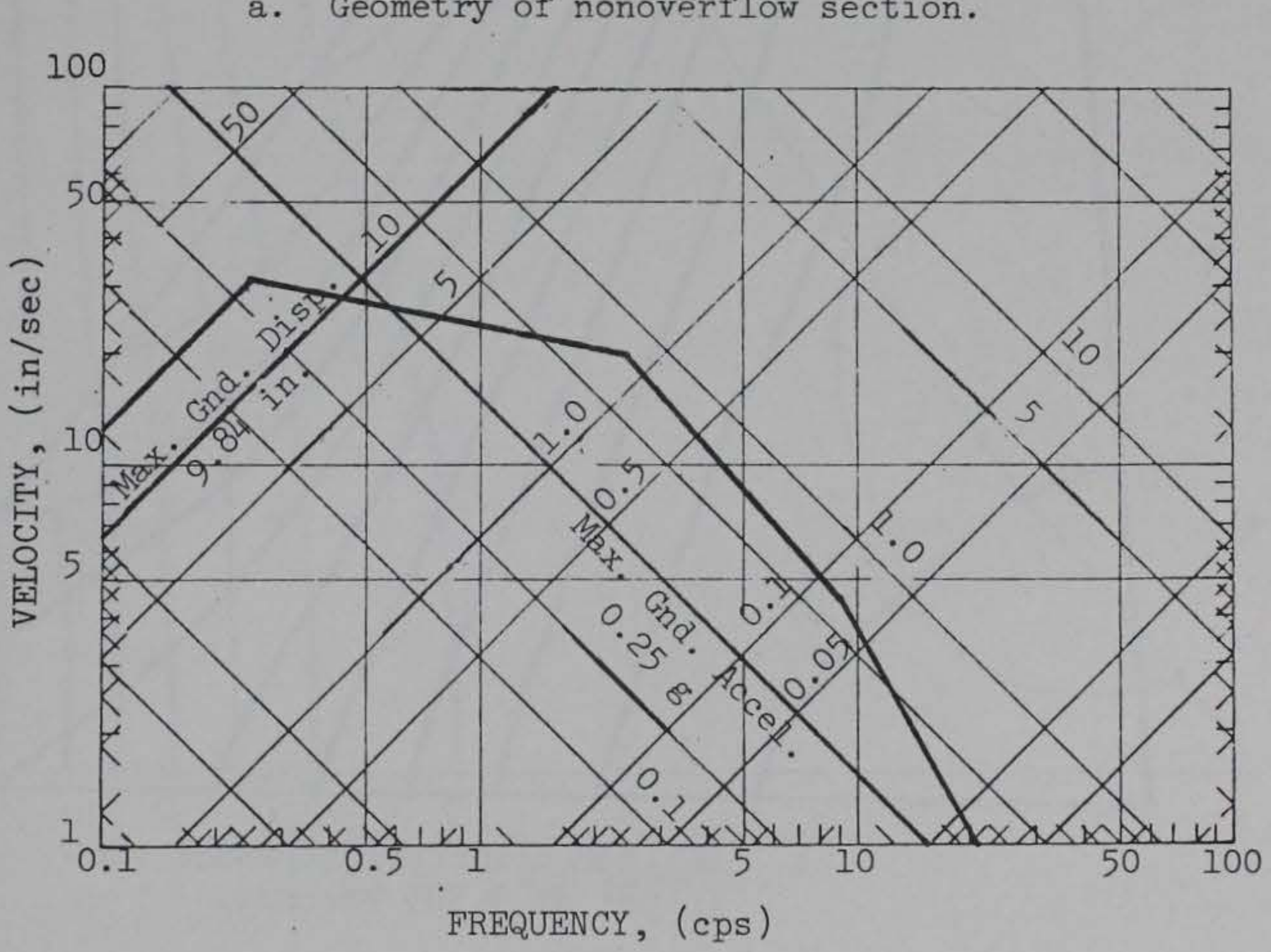

b. Design response spectrum, 5 percent damping.

Figure 3 Geometry and design response spectrum.

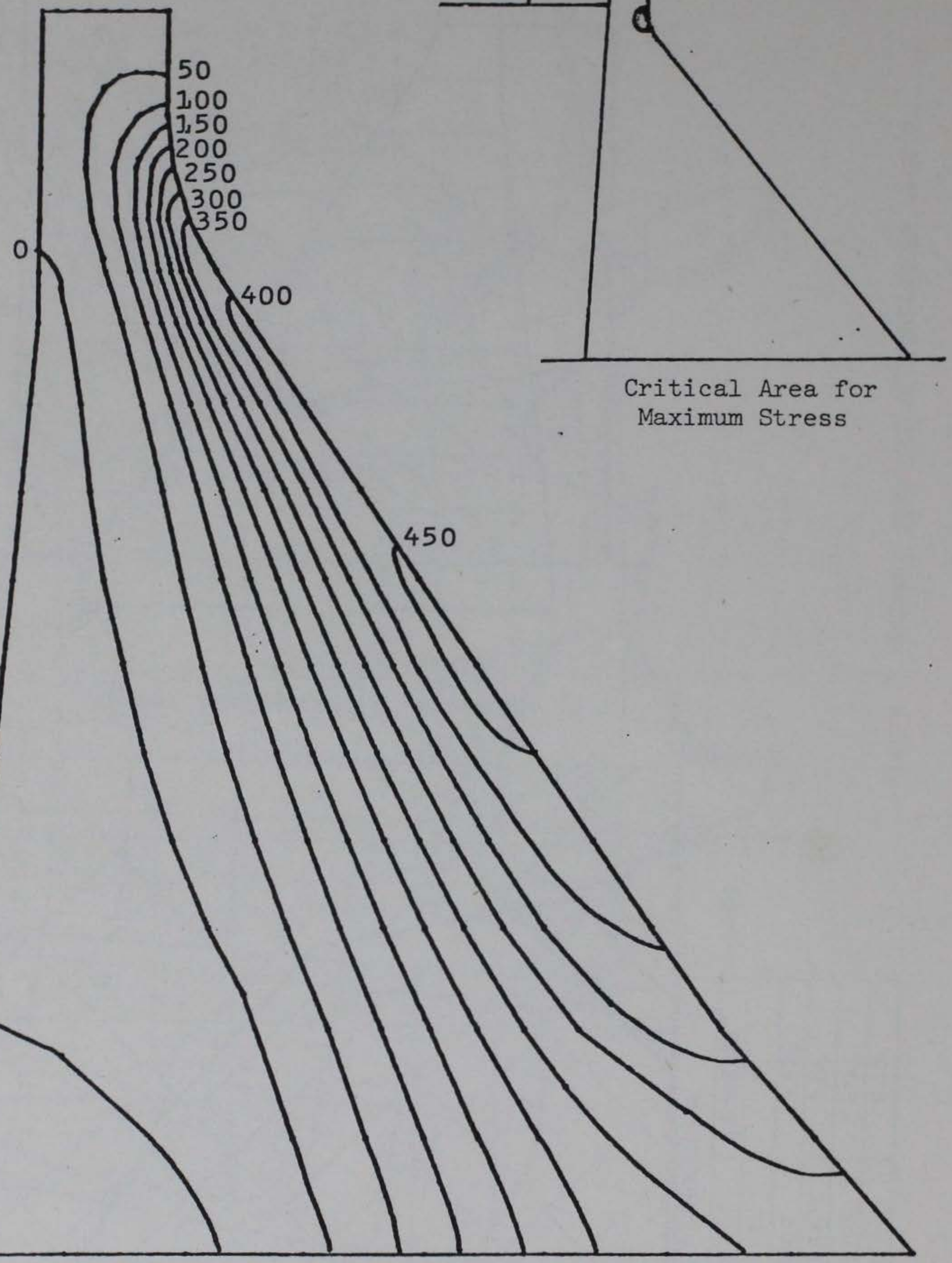

Critical Area for
Maximum Stress

a. Maximum principal stresses
in psi at 3.505 seconds.

Figure 4 Maximum principal stresses in Richard B. Russell Dam due to N90E and vertical components of San Fernando Earthquake, 5 percent damping (sheet 1 of 4).

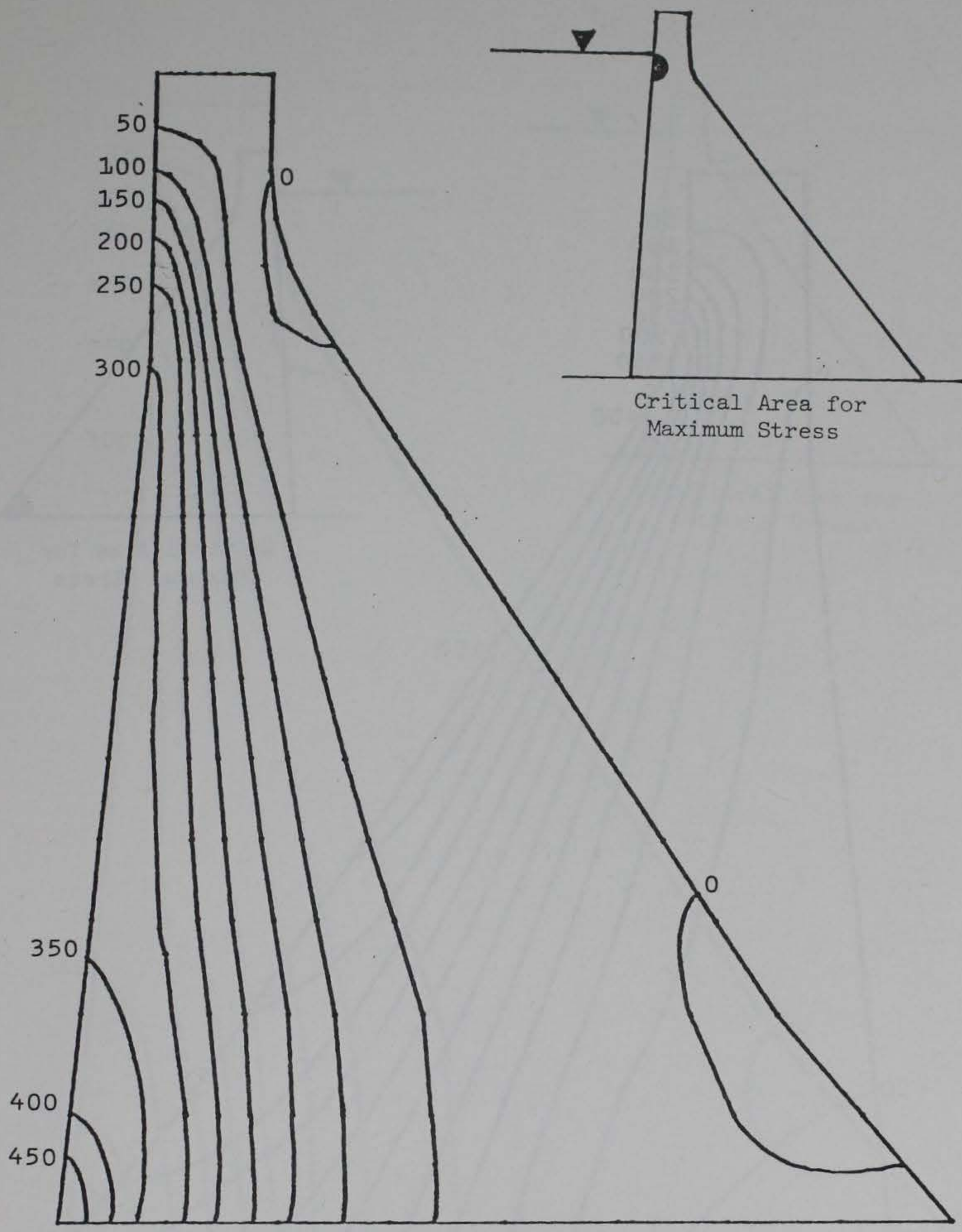

b. Maximum principal stresses
in psi at 3.410 seconds.

Figure 4 (sheet 2 of 4).

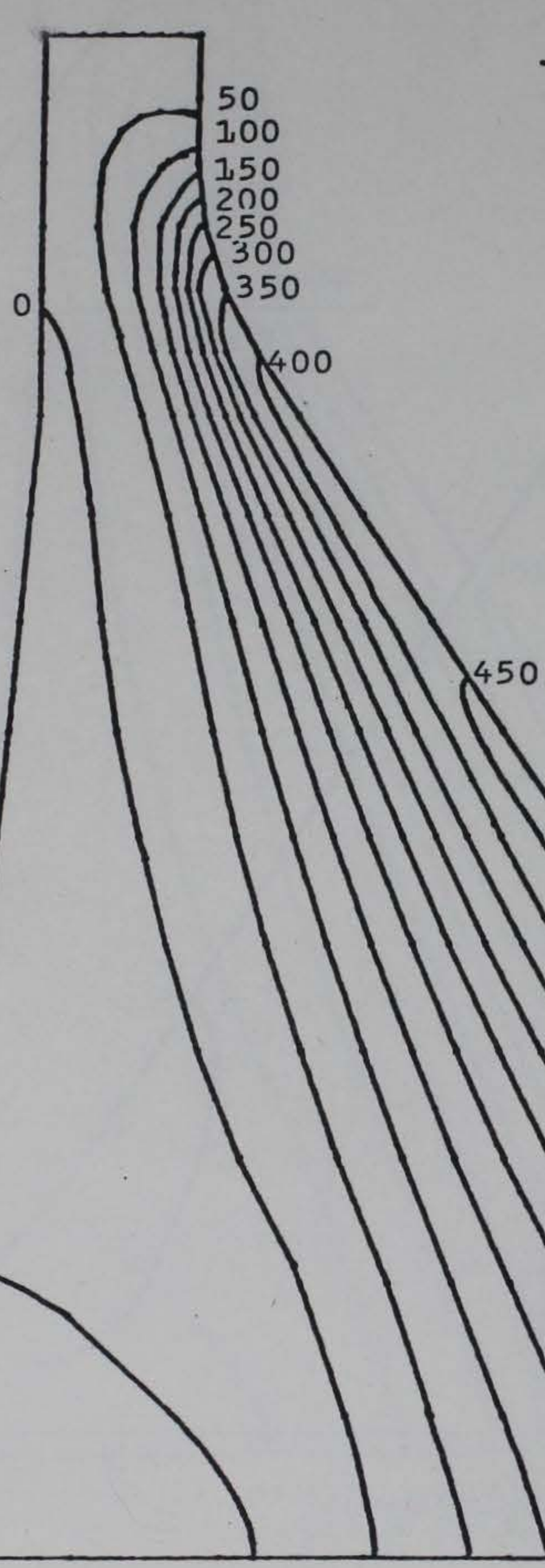

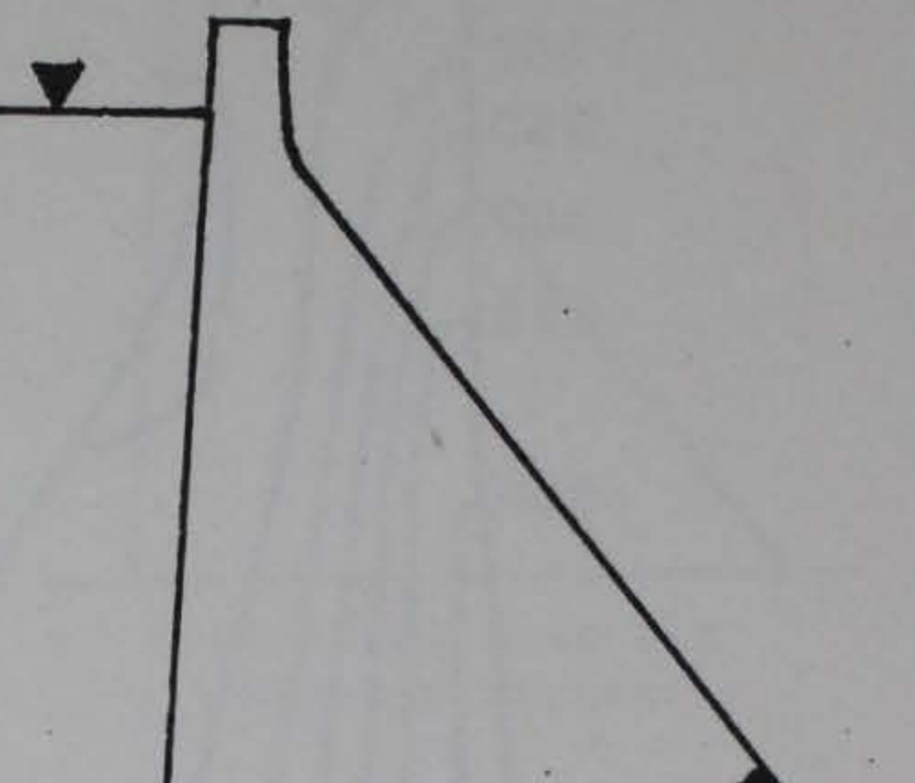

Critical Area for
Maximum Stress

c. Maximum principal stresses
in psi at 3.50 seconds.

Figure 4 (sheet 3 of 4).

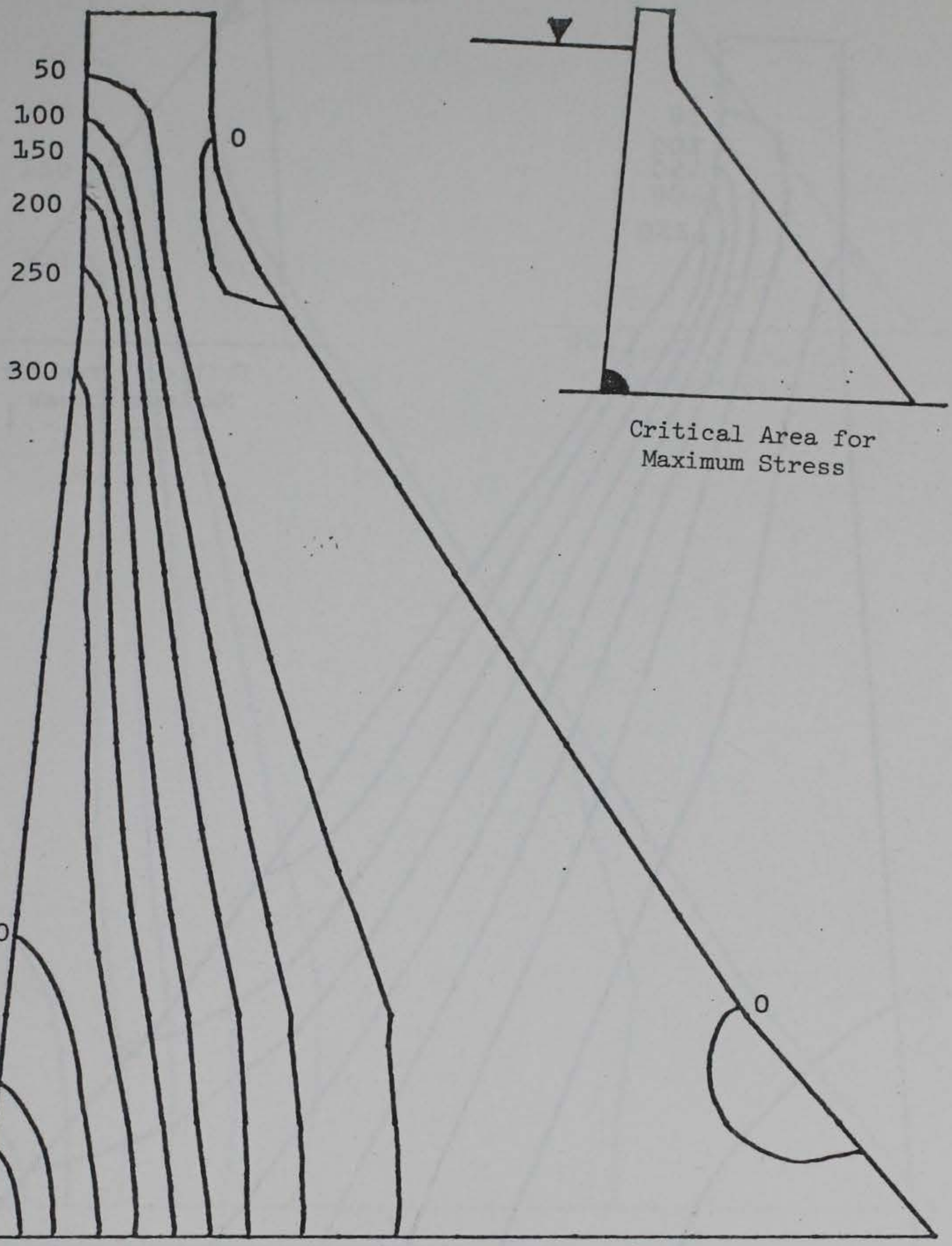

d. Maximum principal stresses in psi at 3.40 seconds.

Figure 4 (sheet 4 of 4).

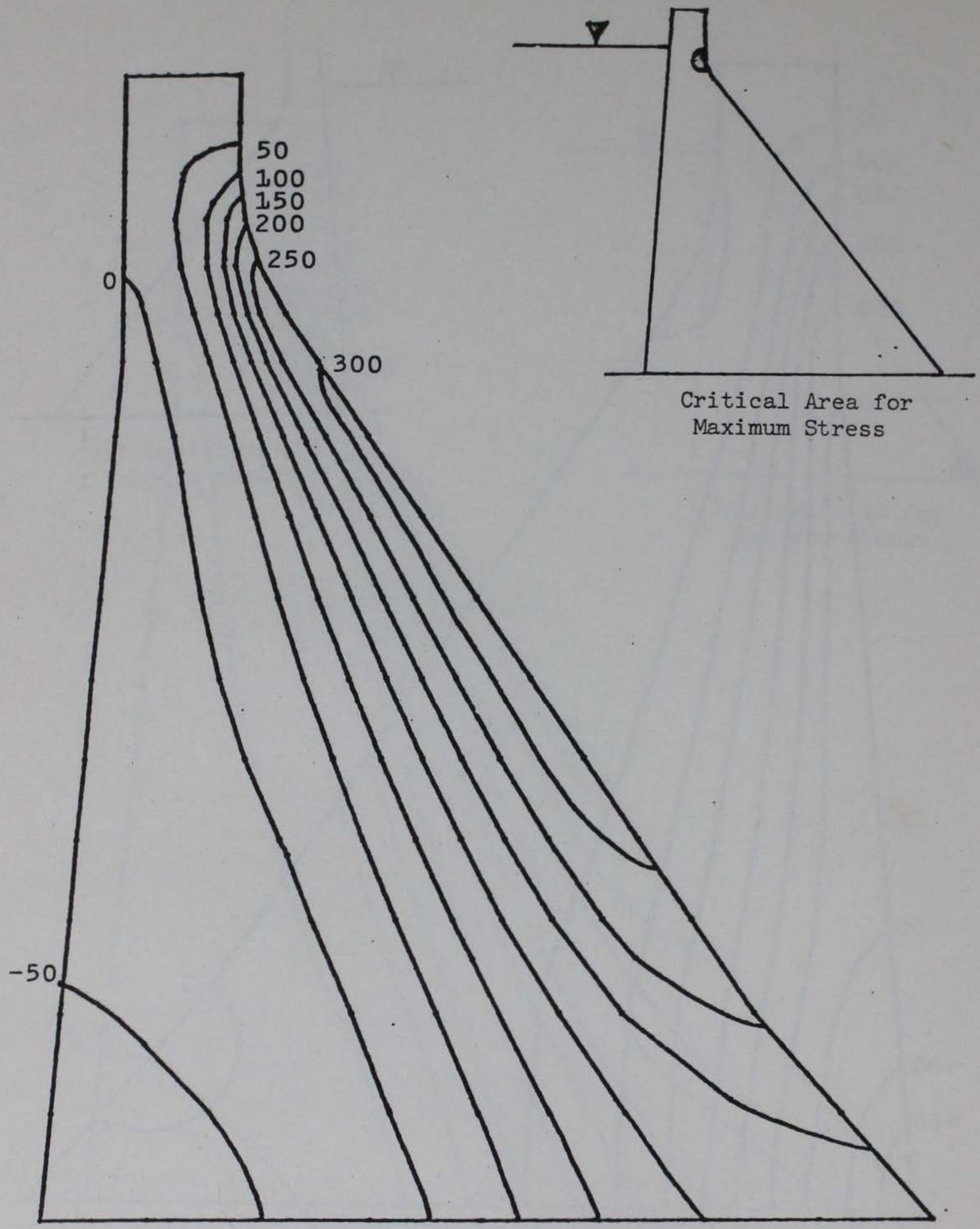

a. Maximum principal stresses in psi at 3.51 seconds.

Figure 5 Maximum principal stresses in Richard B. Russell Dam due to N90E and vertical components of San Fernando Earthquake, 10 percent damping (sheet 1 of 4).

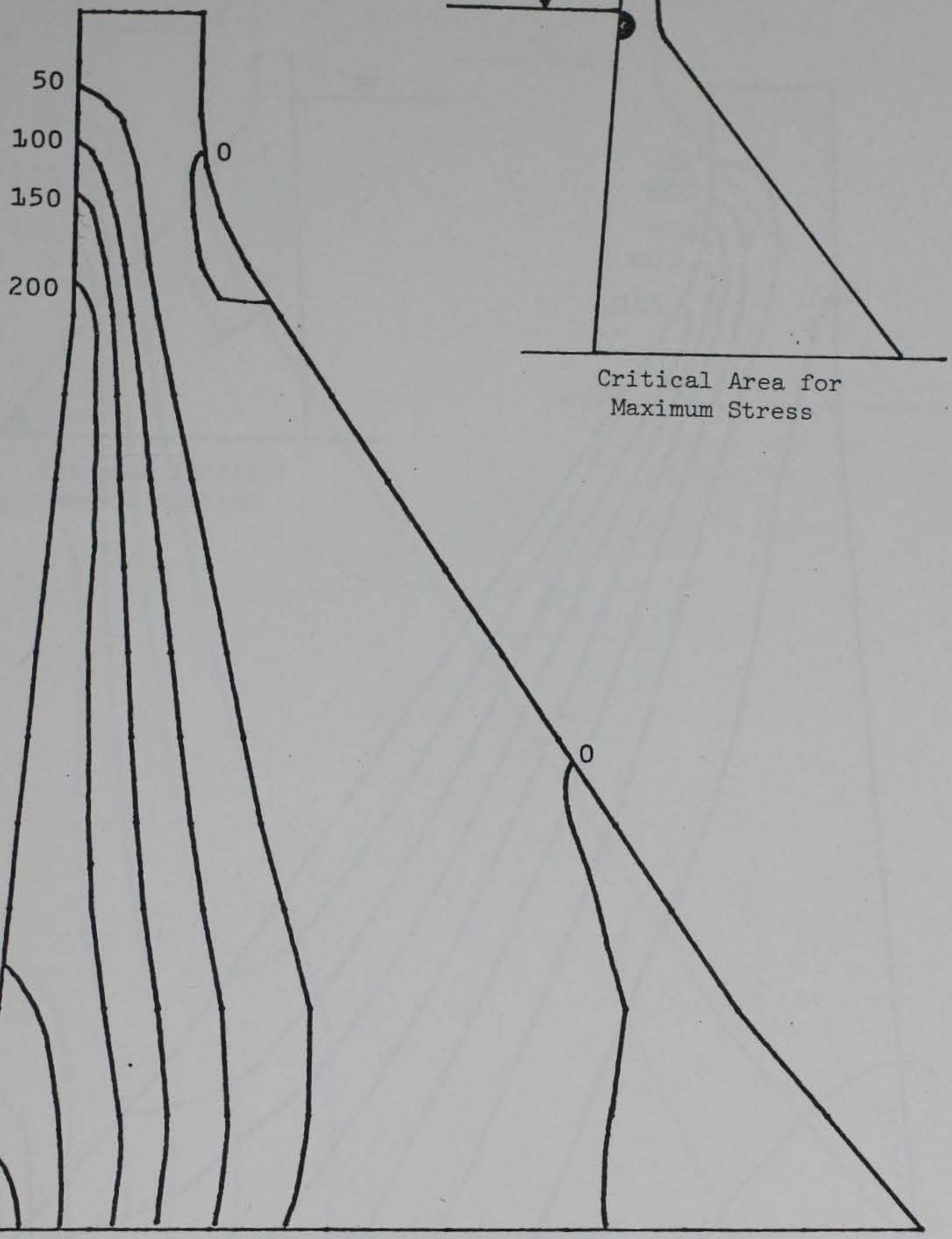

b. Maximum principal stresses
in psi at 3.415 seconds.

Figure 5 (sheet 2 of 4).

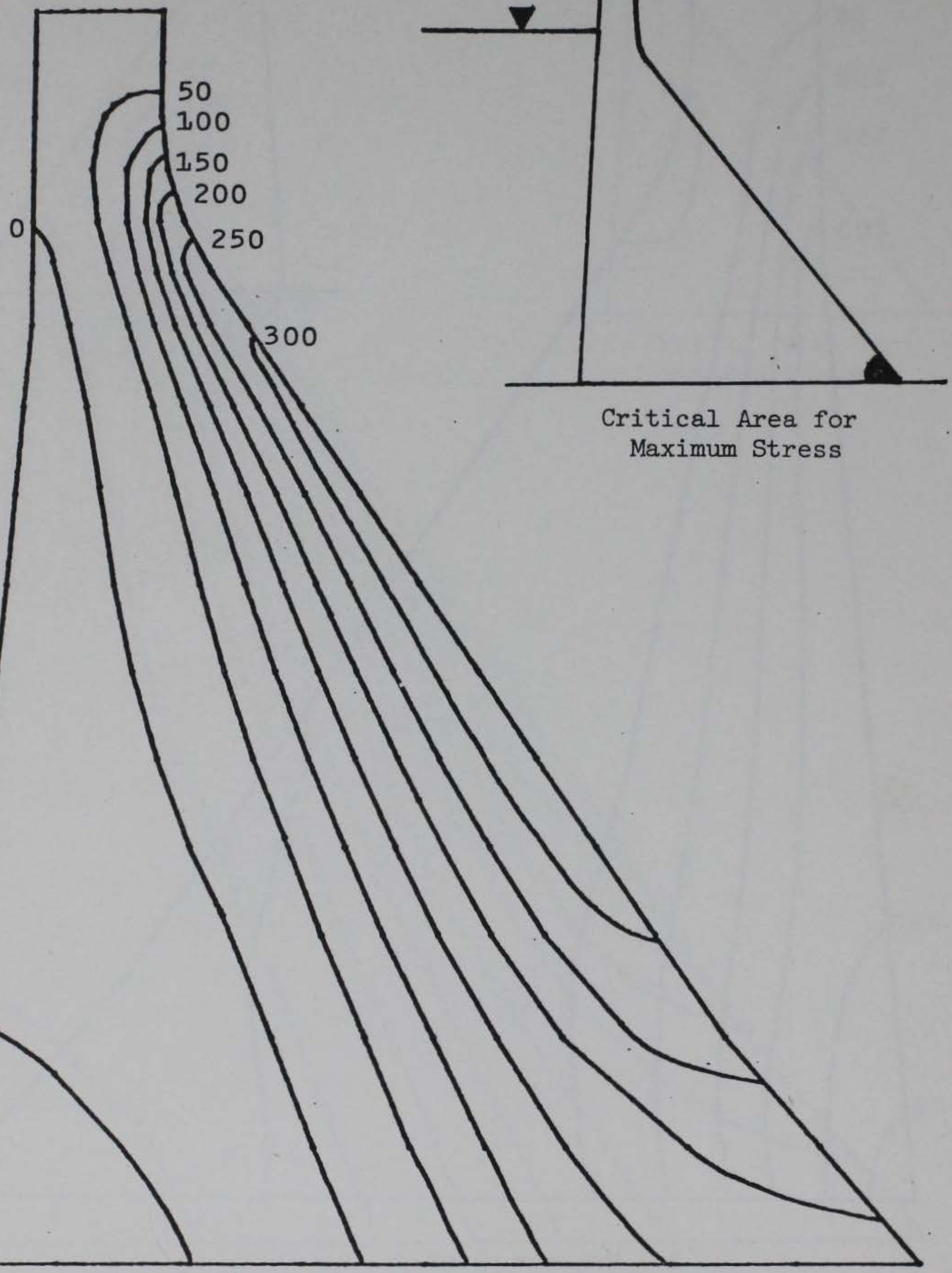

Critical Area for
Maximum Stress

c. Maximum principal stresses
in psi at 3.50 seconds.

Figure 5 (sheet 3 of 4).

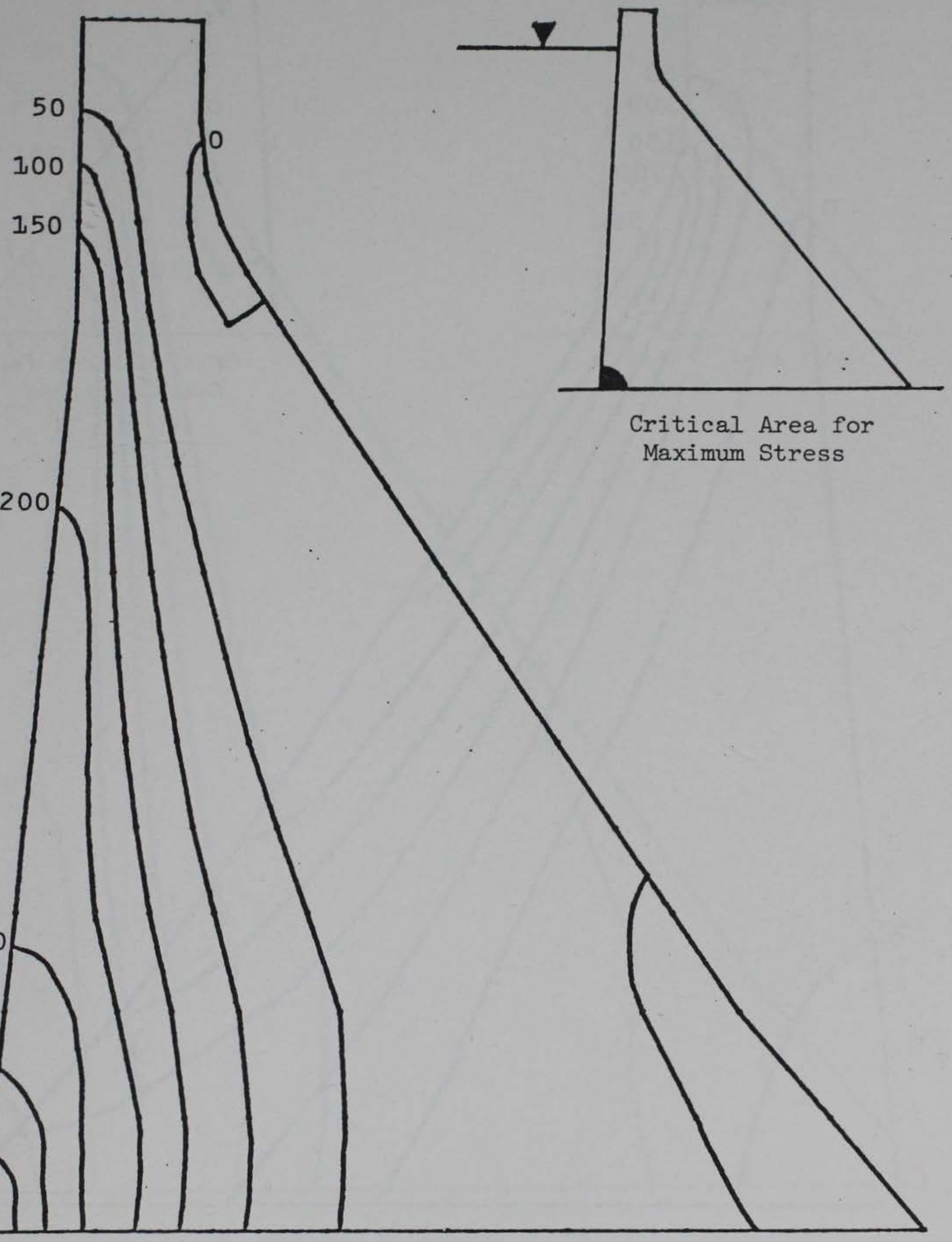

Critical Area for
Maximum Stress

d. Maximum principal stresses
in psi at 3.40 seconds.

Figure 5 (sheet 4 of 4).

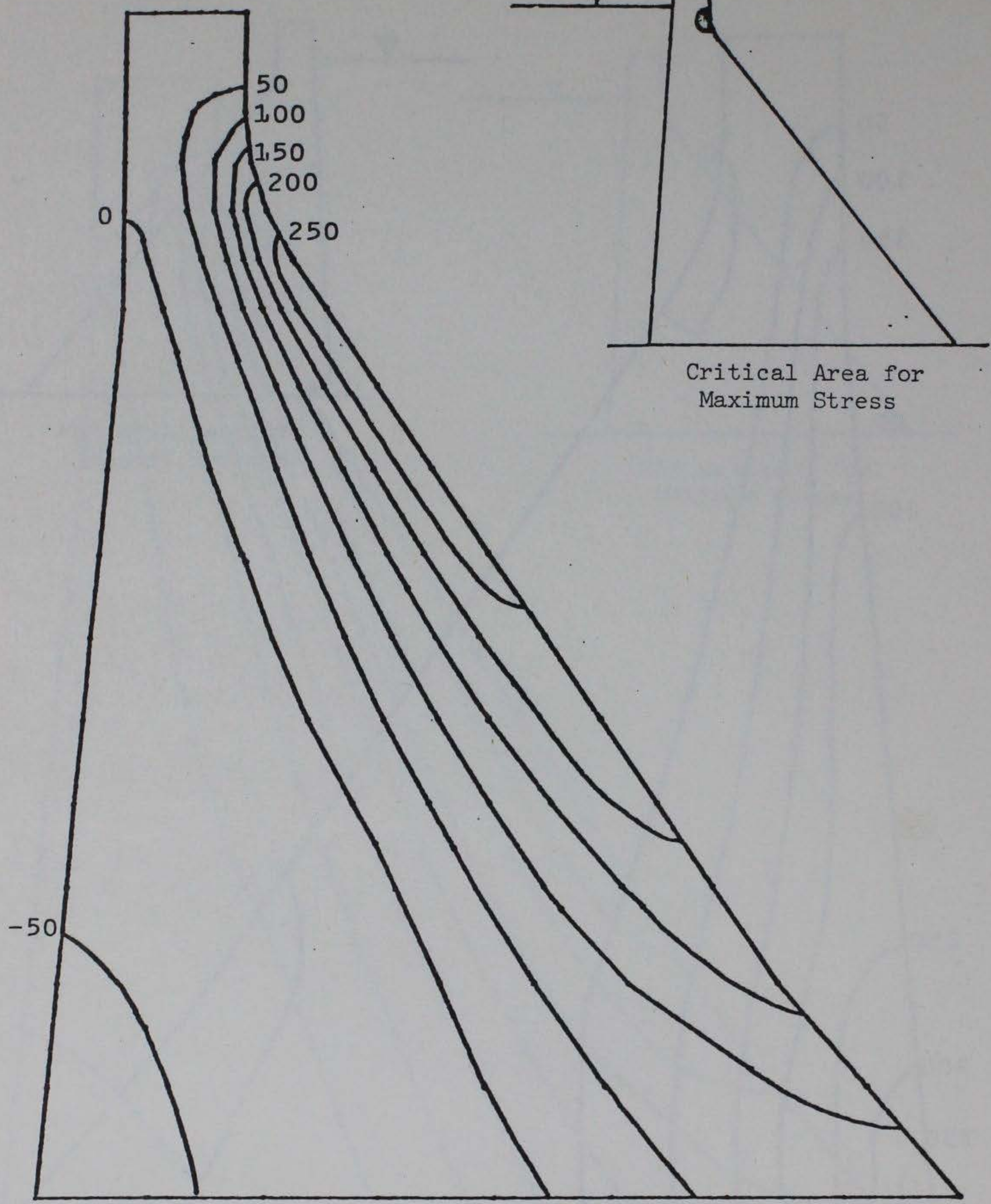

Critical Area for
Maximum Stress

a. Maximum principal stresses
in psi at 4.18 seconds.

Figure 6 Maximum principal stresses in Richard B. Russell Dam due to S00W and vertical components of San Fernando Earthquake, 5 percent damping (sheet 1 of 4).

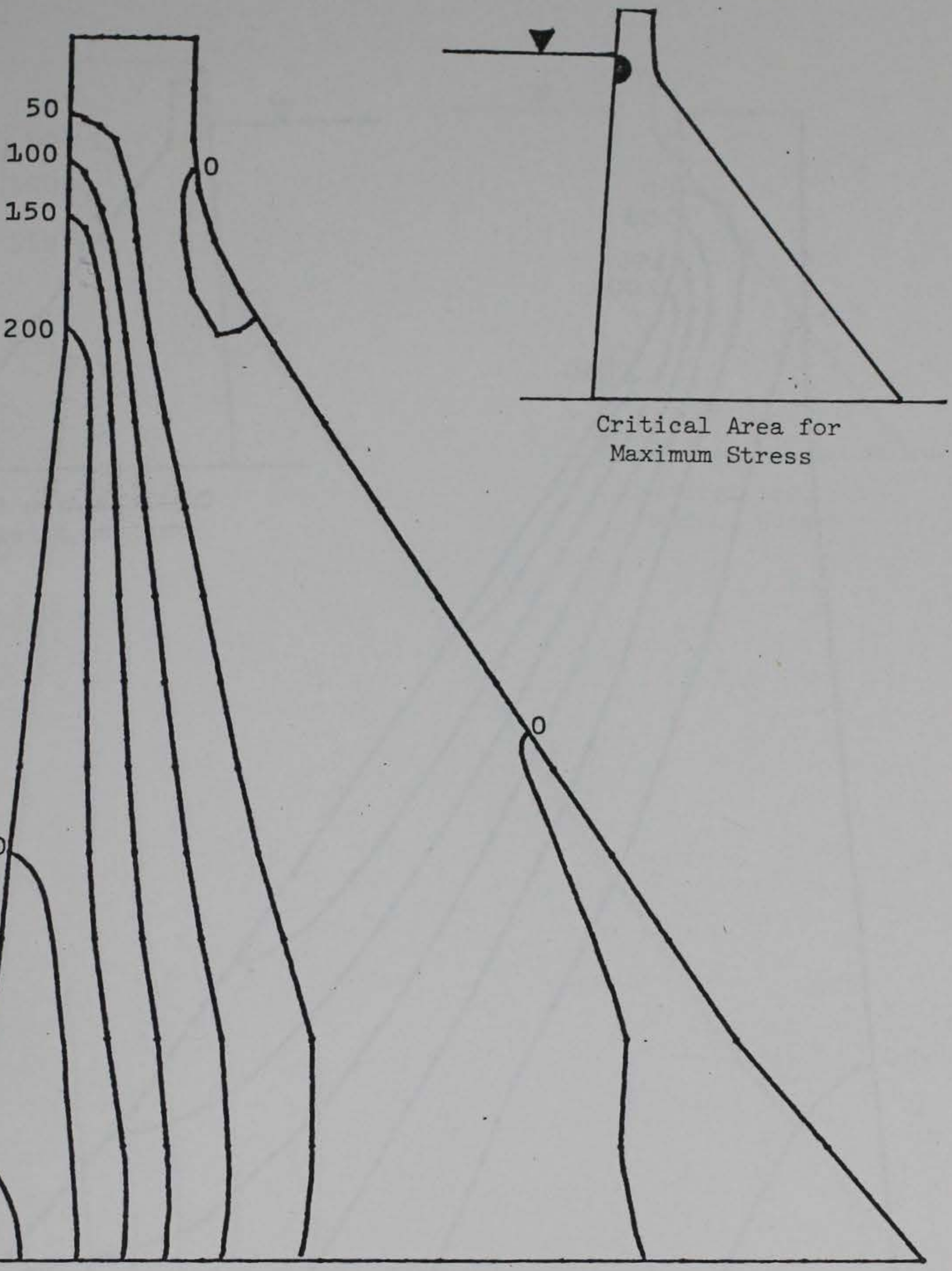

b. Maximum principal stresses
in psi at 4.26 seconds.

Figure 6 (sheet 2 of 4).

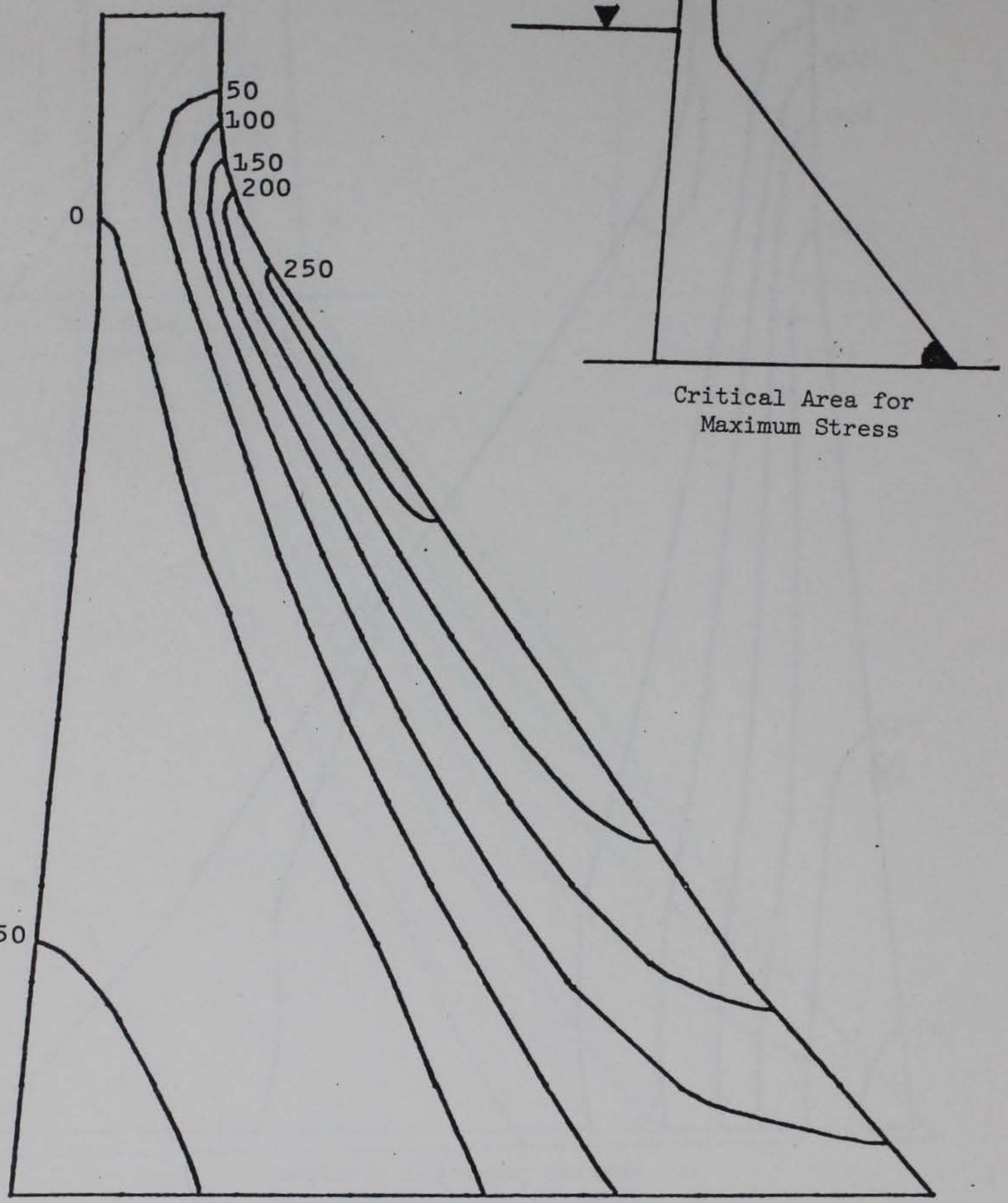

Critical Area for
Maximum Stress

c. Maximum principal stresses
in psi at 4.17 seconds.

Figure 6 (sheet 3 of 4).

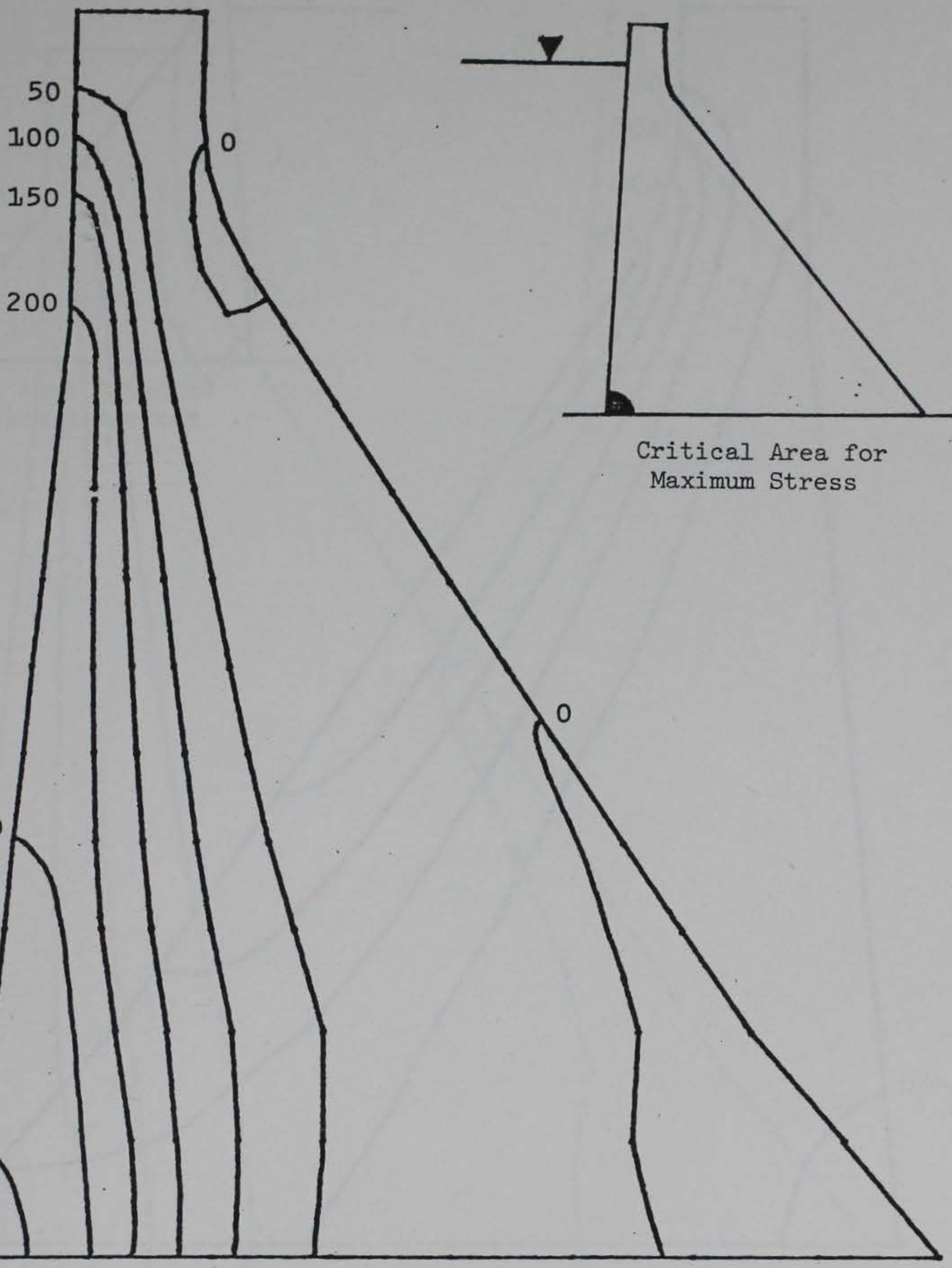

d. Maximum principal stresses
in psi at 4.26 seconds.

Figure 6 (sheet 4 of 4).

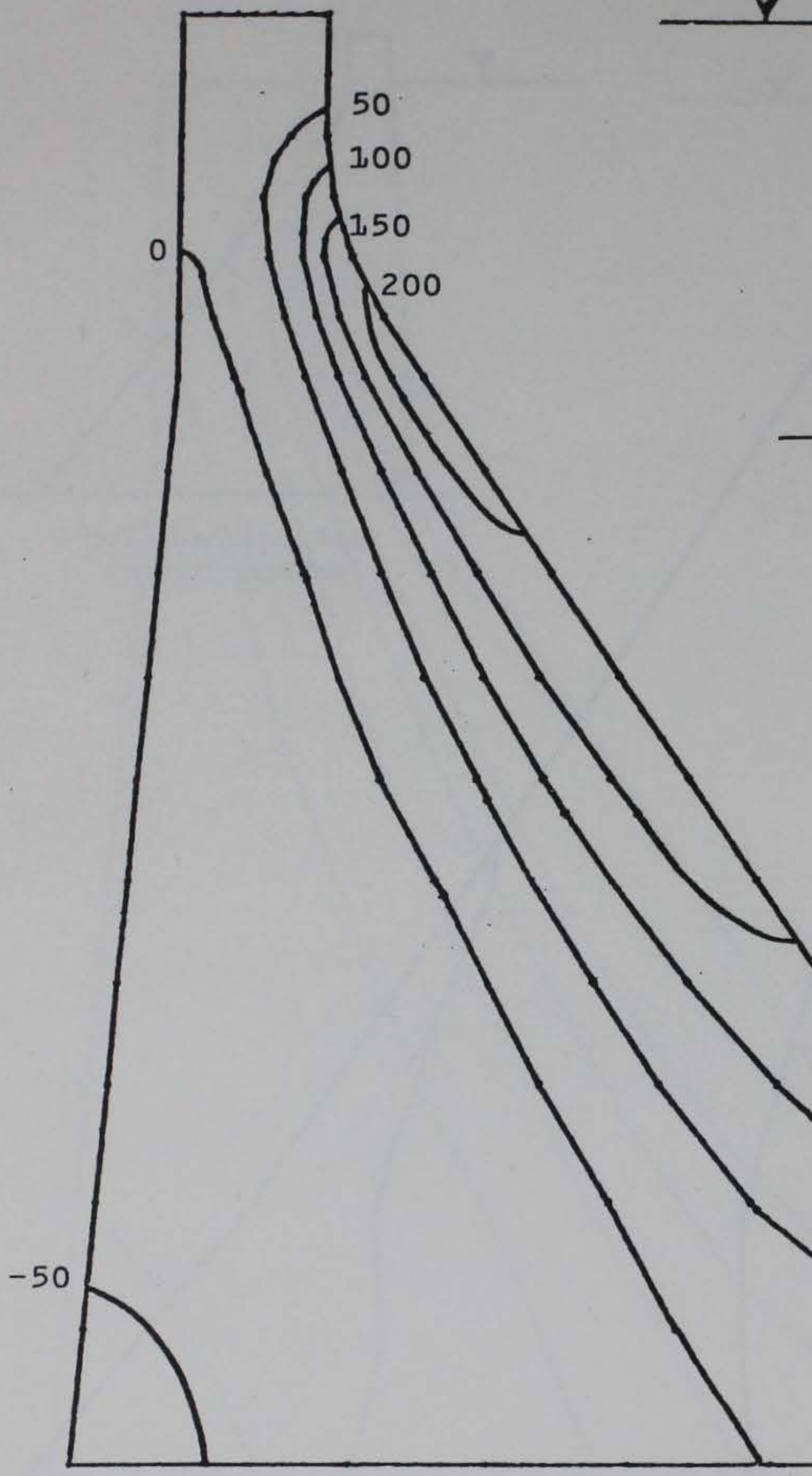

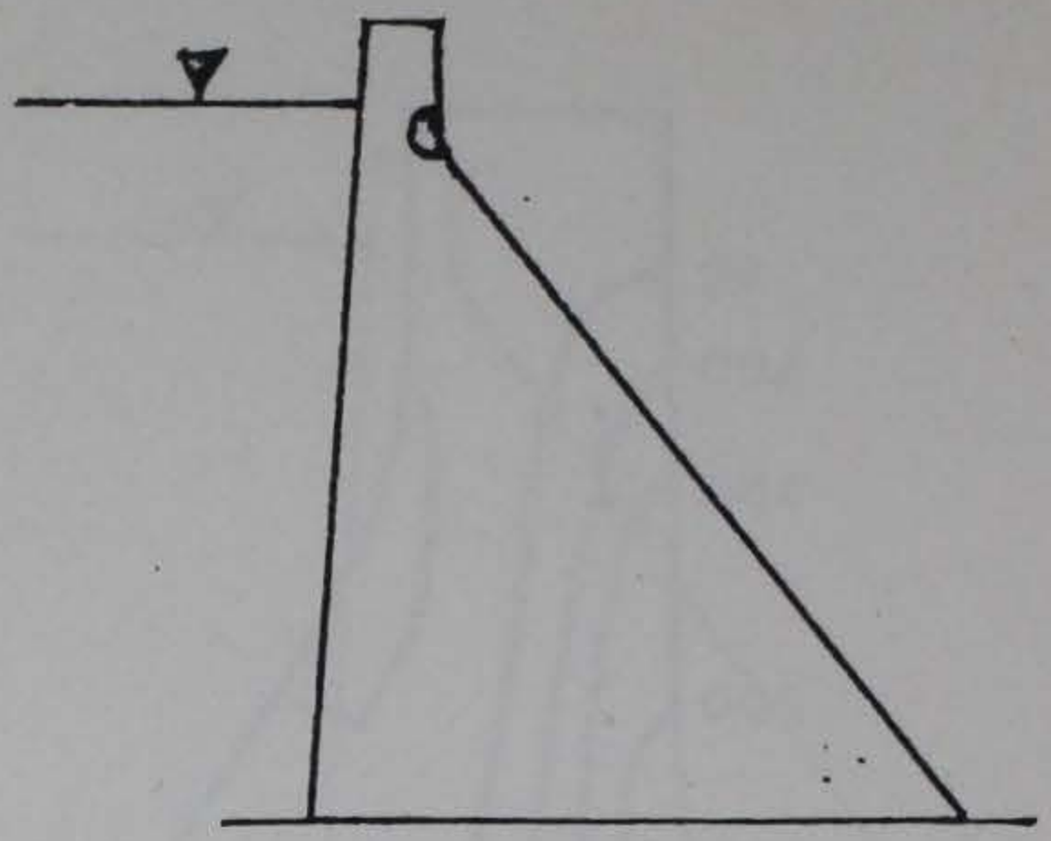

Critical Area for
Maximum Stress

a. Maximum principal stresses
in psi at 4.18 seconds.

Figure 7 Maximum principal stresses in Richard B. Russell Dam due to S00W and vertical components of San Fernando Earthquake, 10 percent damping (sheet 1 of 4).

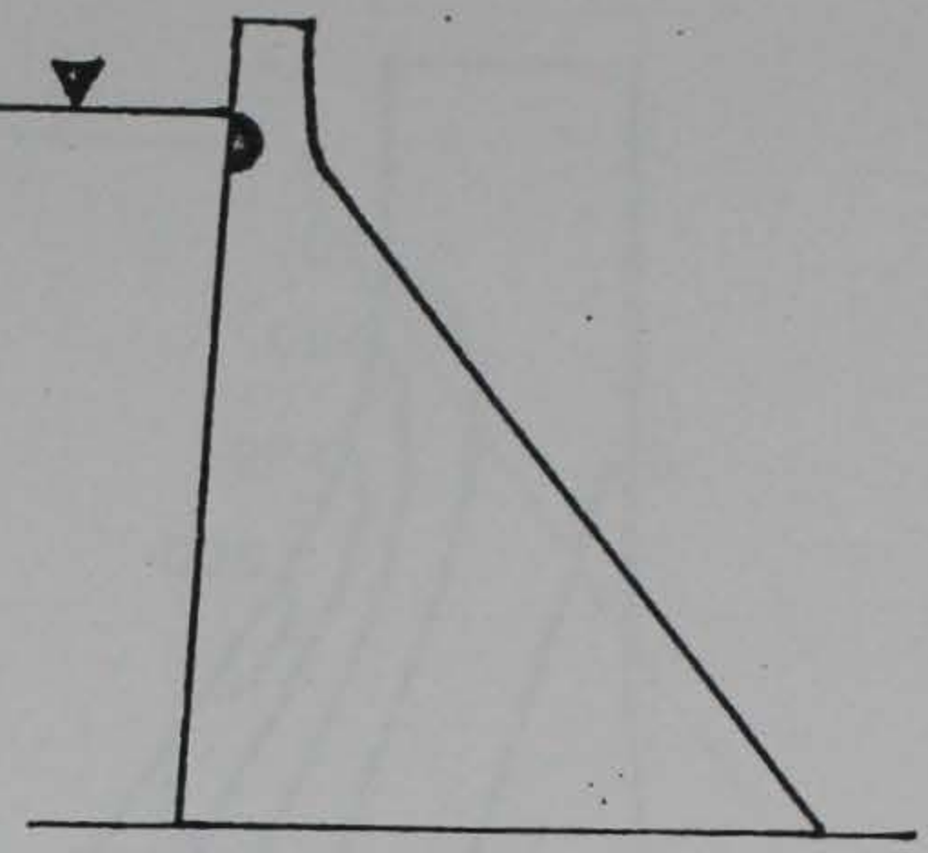

Critical Area for
Maximum Stress

b. Maximum principal stresses
in psi at 4.26 seconds.

Figure 7 (sheet 2 of 4).

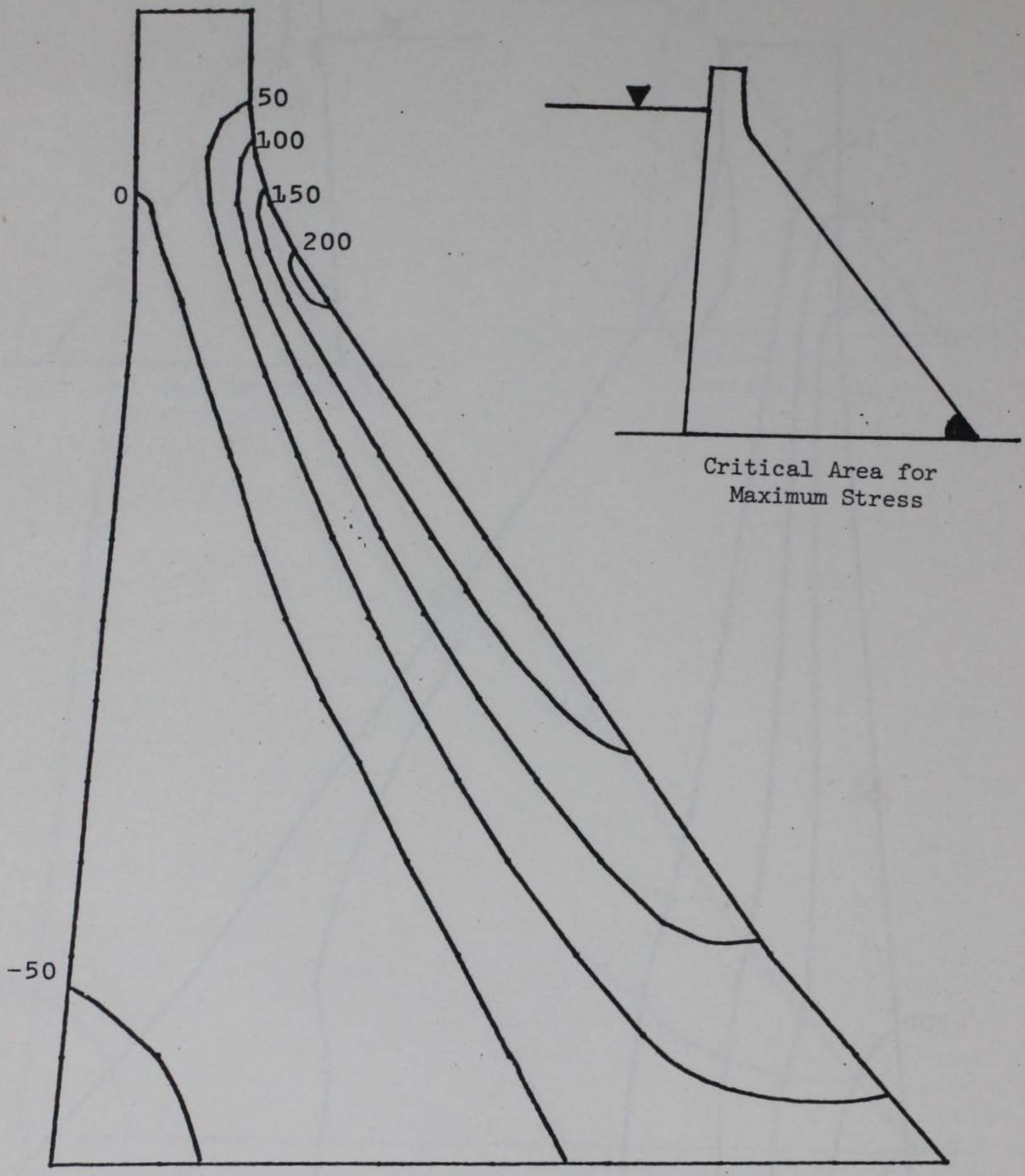

Critical Area for
Maximum Stress

c. Maximum principal stresses
in psi at 4.17 seconds.

Figure 7 (sheet 3 of 4).

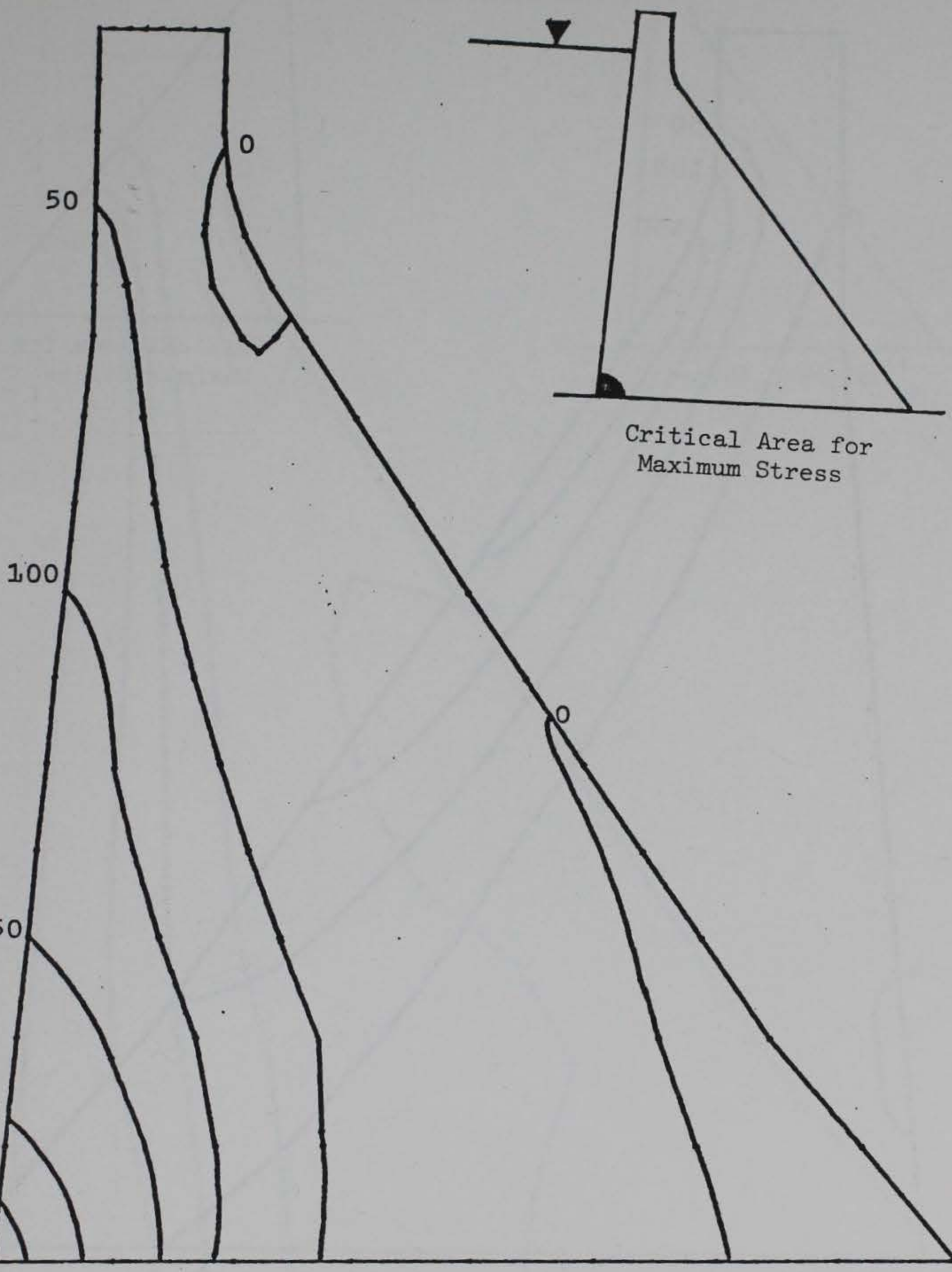

Critical Area for
Maximum Stress

d. Maximum principal stresses
in psi at 4.08 seconds.

Figure 7 (sheet 4 of 4).

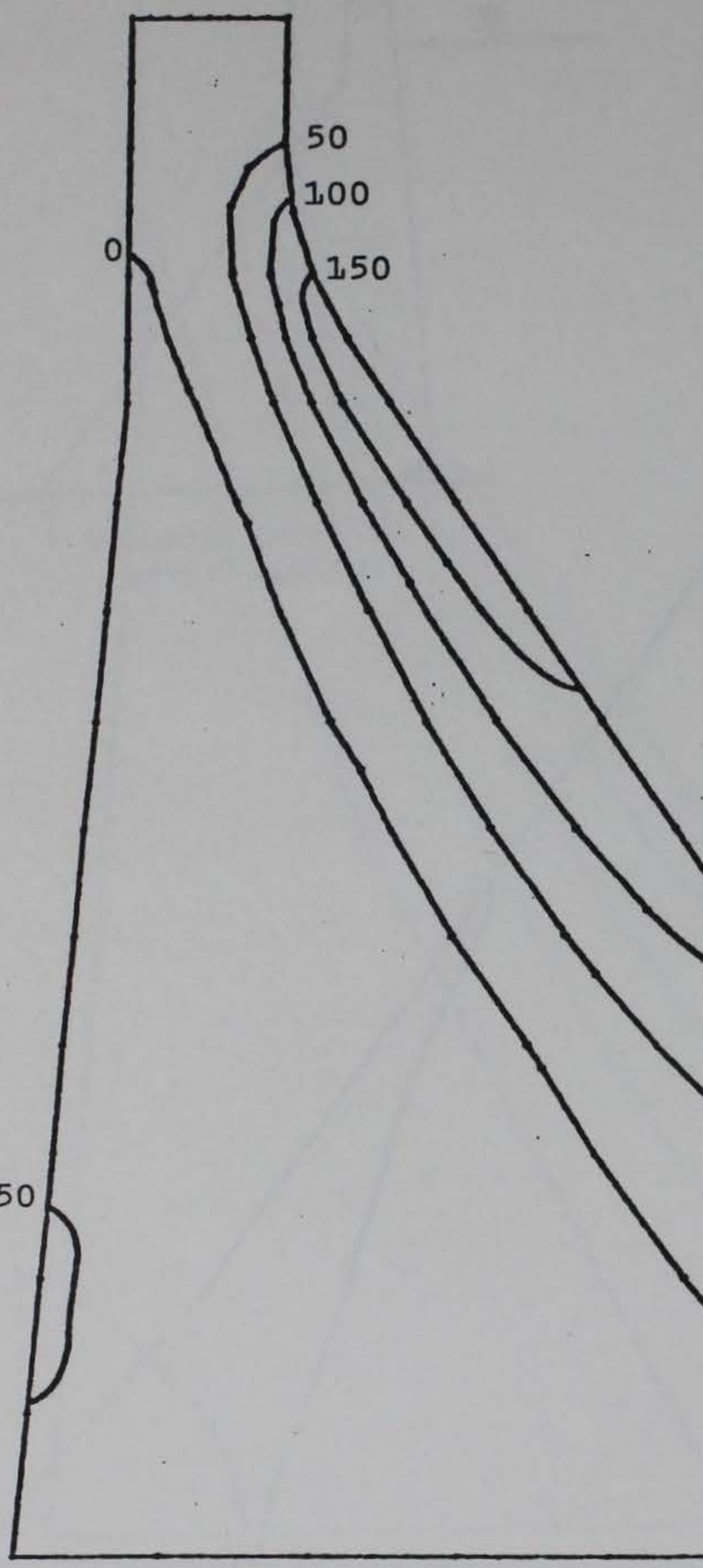

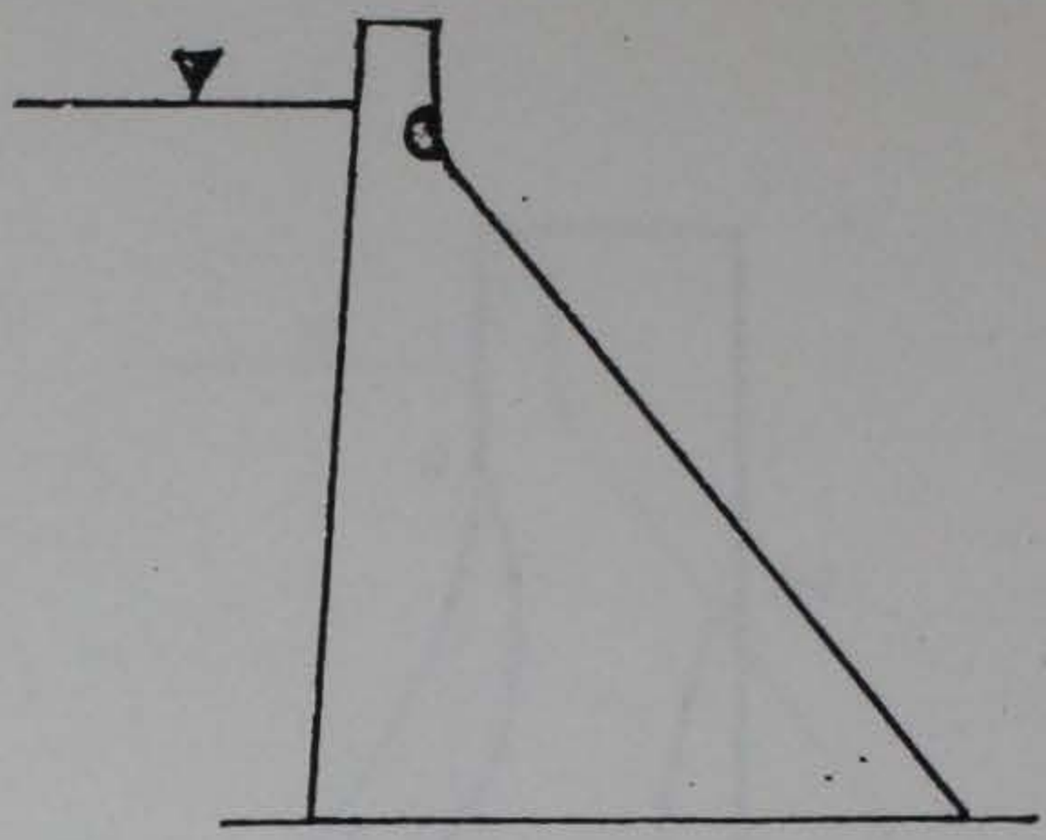

Critical Area for
Maximum Stress

a. Maximum principal stresses
in psi at 8.55 seconds.

Figure 8 Maximum principal stresses in Richard B. Russell Dam due to S16E and vertical components of San Fernando Earthquake, 5 percent damping (sheet 1 of 4).

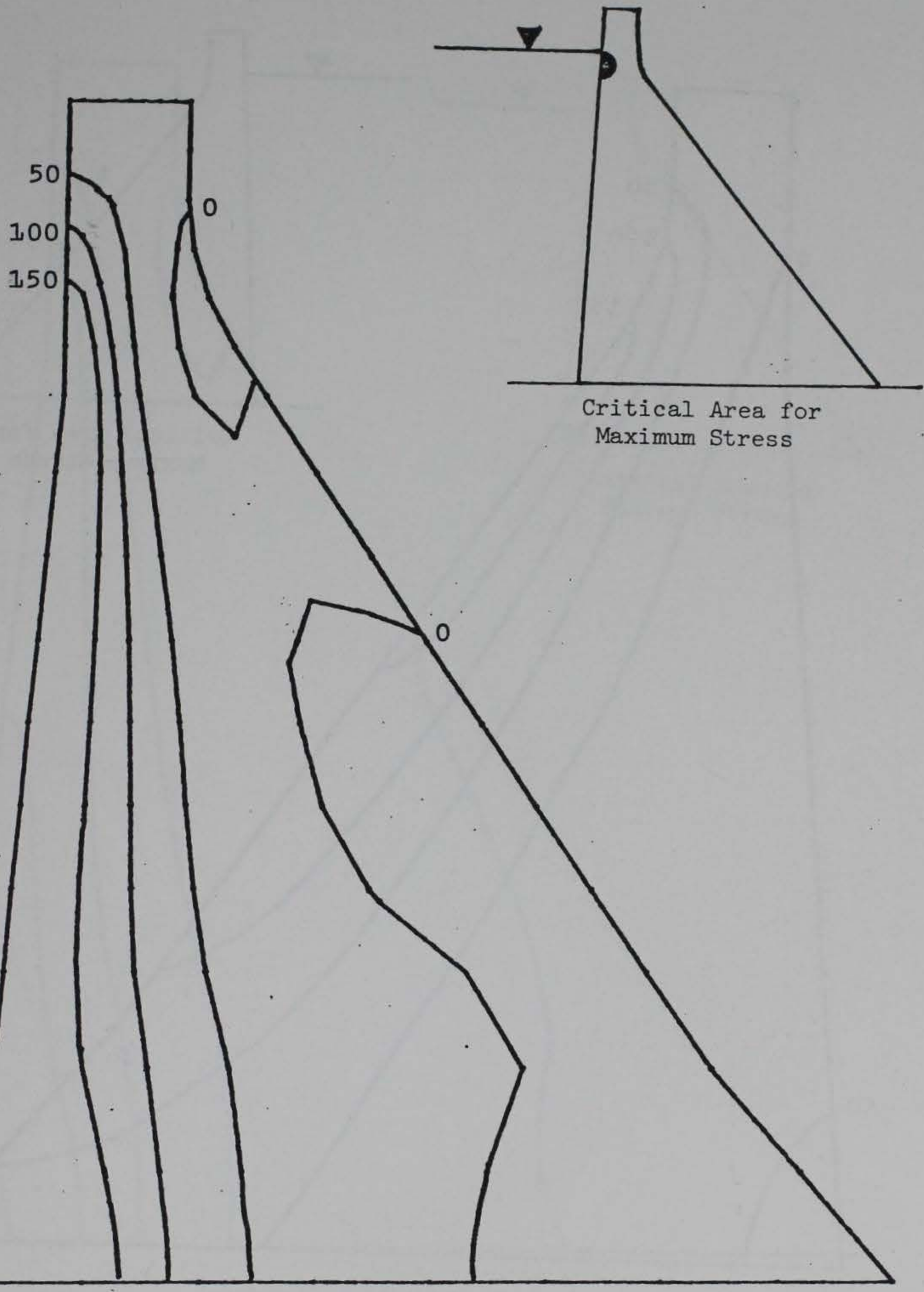

Critical Area for
Maximum Stress

b. Maximum principal stresses
in psi at 8.615 seconds.

Figure 8 (sheet 2 of 4).

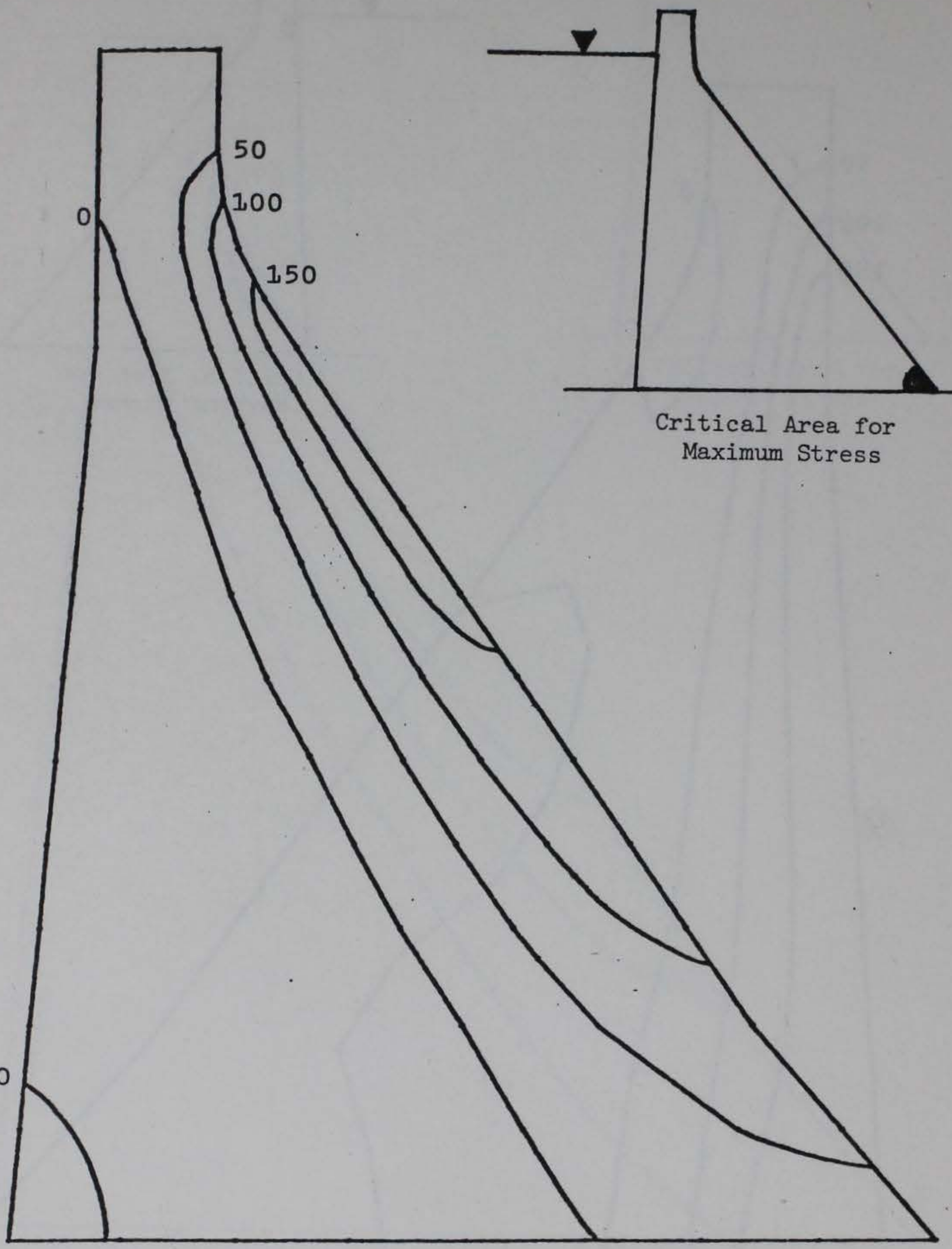

Critical Area for
Maximum Stress

c. Maximum principal stresses
in psi at 8.895 seconds.

Figure 8 (sheet 3 of 4).

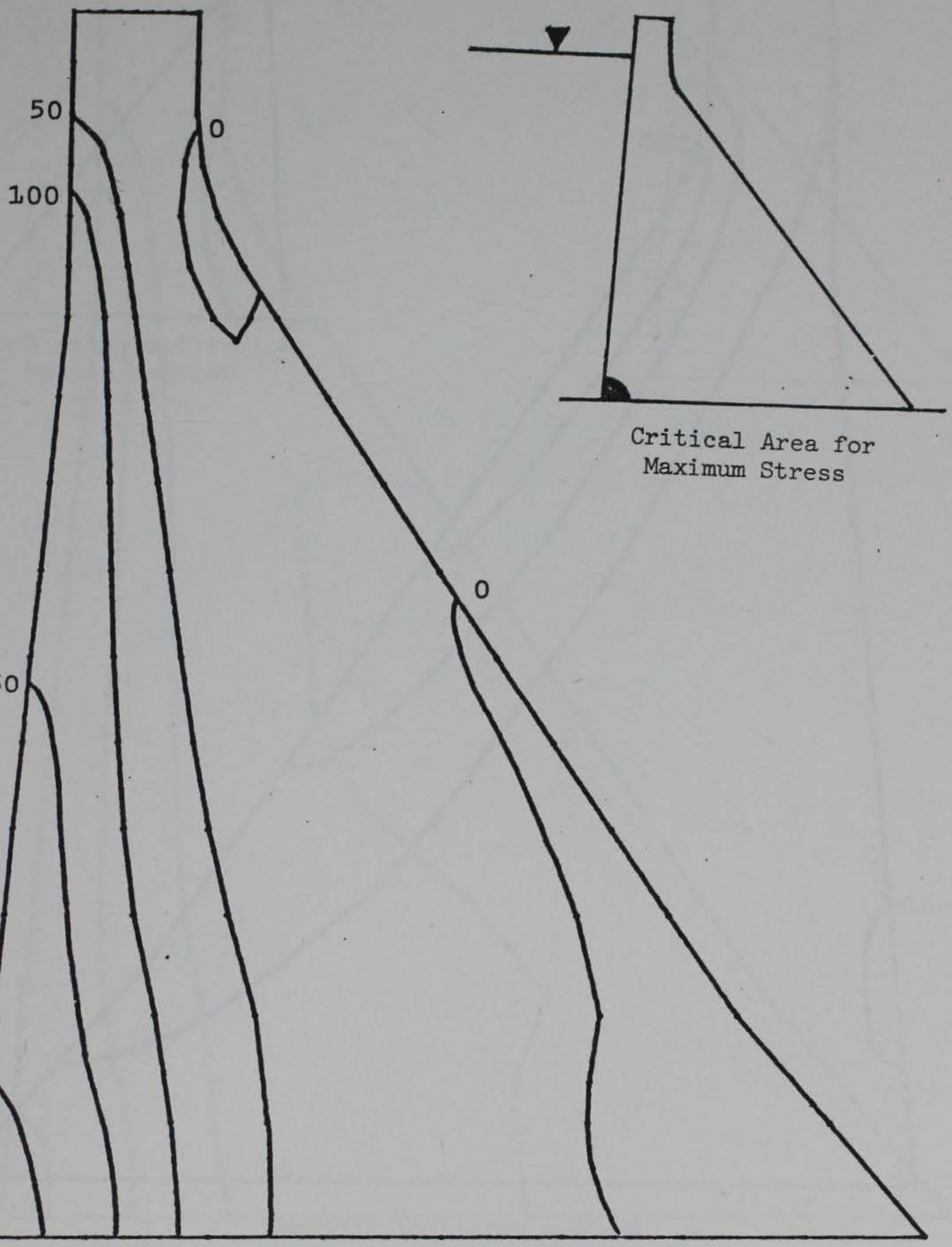

Critical Area for
Maximum Stress

d. Maximum principal stresses
in psi at 8.99 seconds.

Figure 8 (sheet 4 of 4).

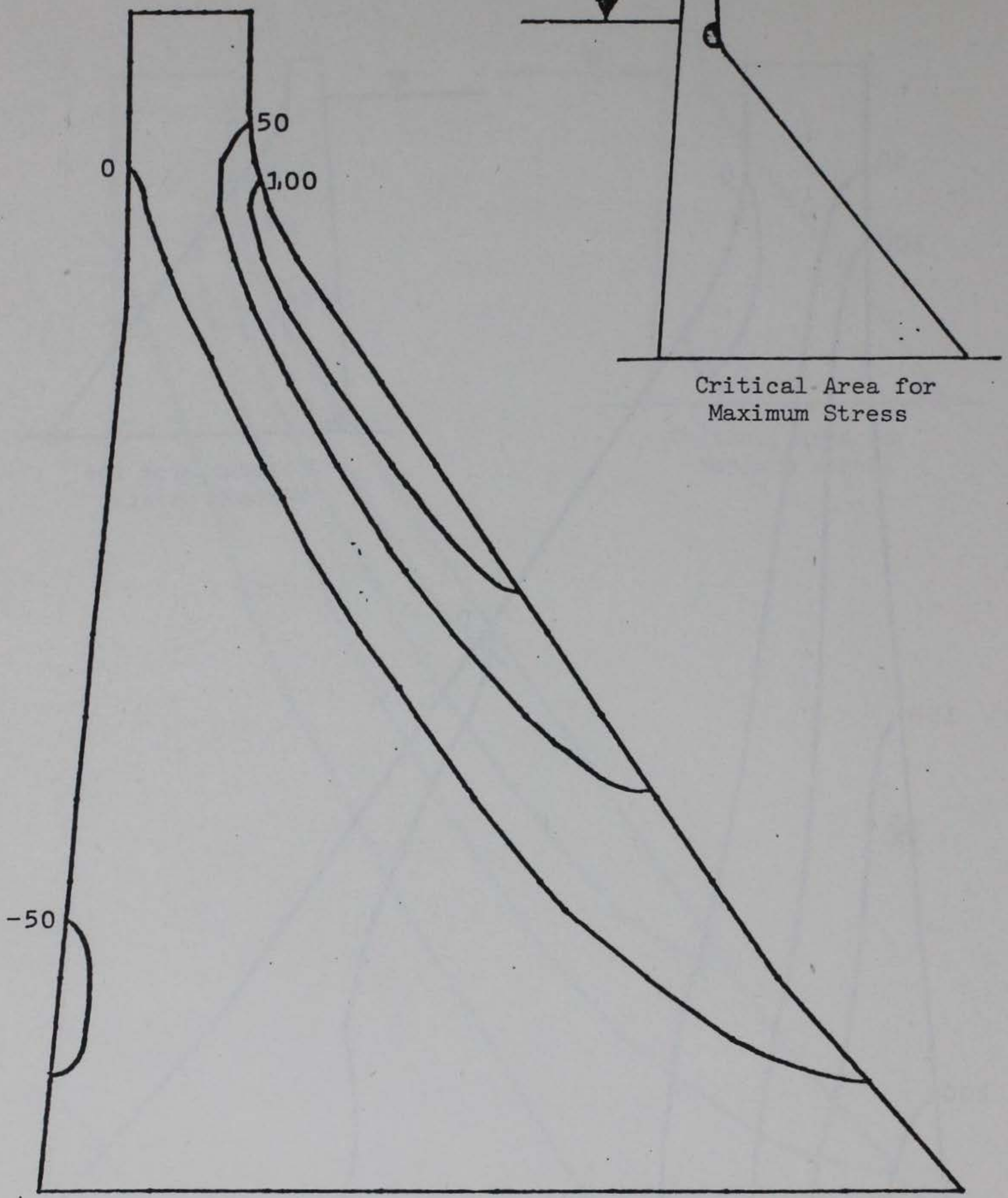

Critical Area for
Maximum Stress

a. Maximum principal stresses
in psi at 6.55 seconds.

Figure 9 Maximum principal stresses in Richard B. Russell Dam due to S16E and vertical components of San Fernando Earthquake, 10 percent damping (sheet 1 of 4).

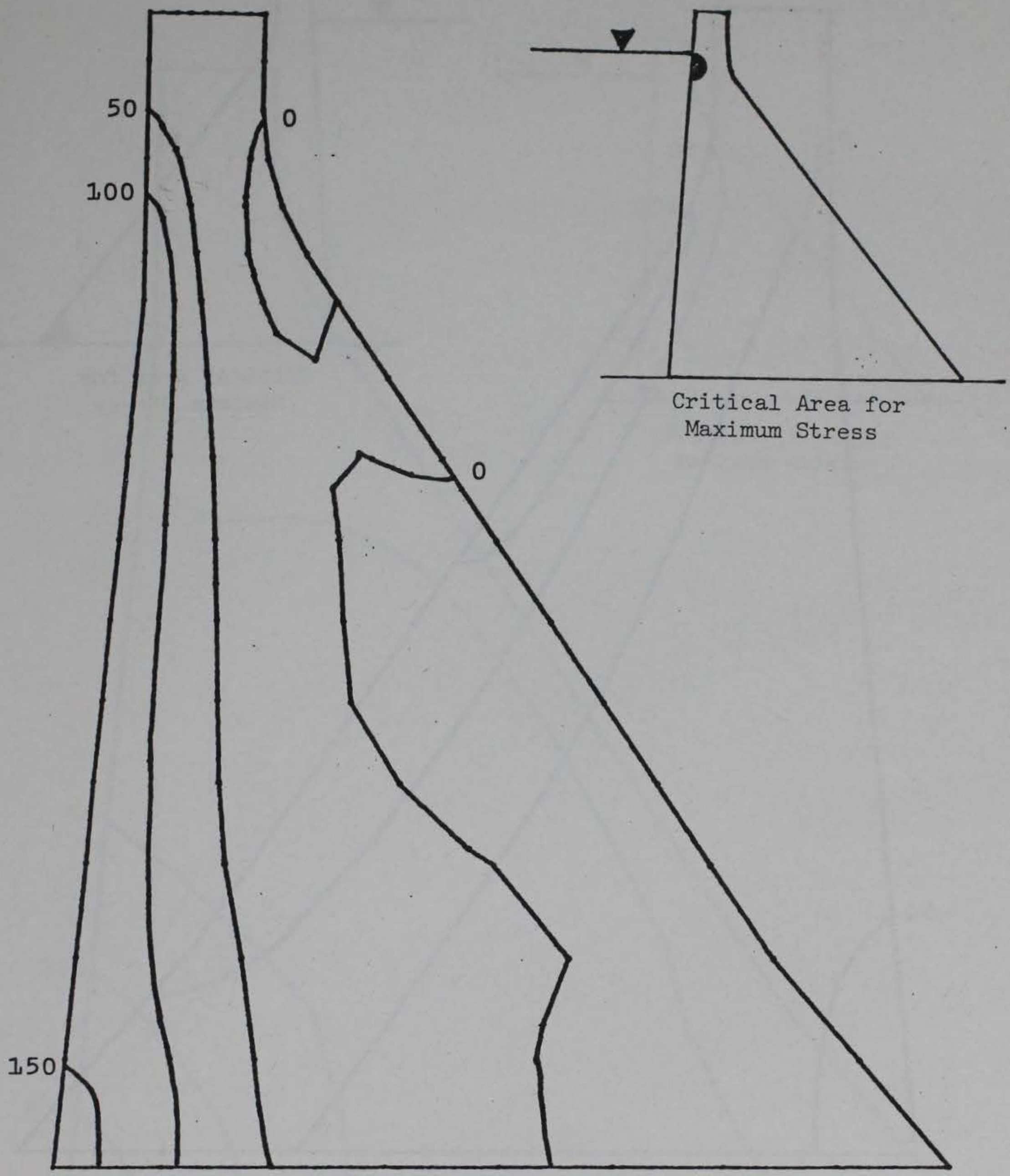

Critical Area for
Maximum Stress

b. Maximum principal stresses
in psi at 8.615 seconds.

Figure 9 (sheet 2 of 4)

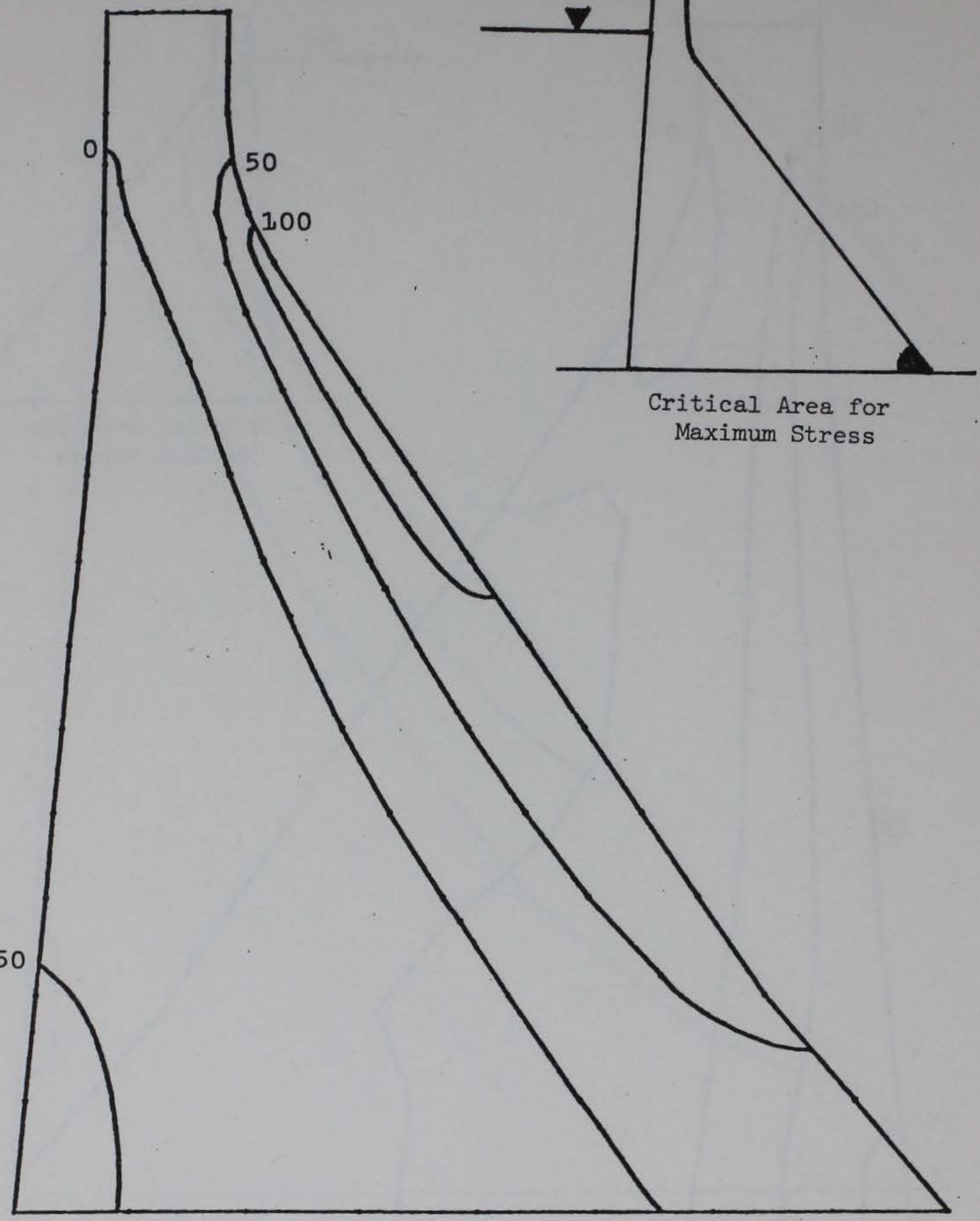

Critical Area for
Maximum Stress

c. Maximum principal stresses in psi at 8.525 seconds.

Figure 9 (sheet 3 of 4)

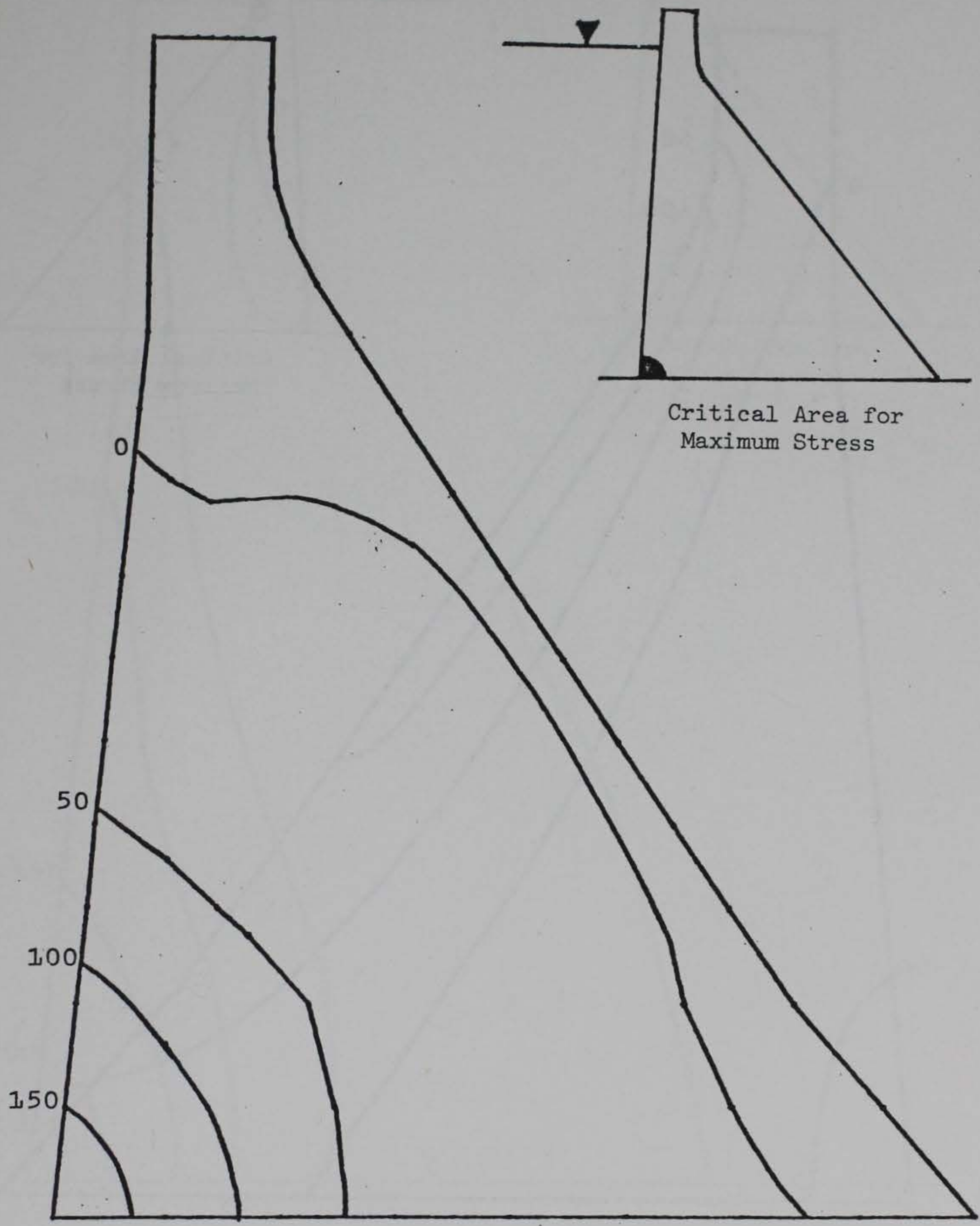

Critical Area for
Maximum Stress

d. Maximum principal stresses
in psi at 7.775 seconds.

Figure 9 (sheet 4 of 4).

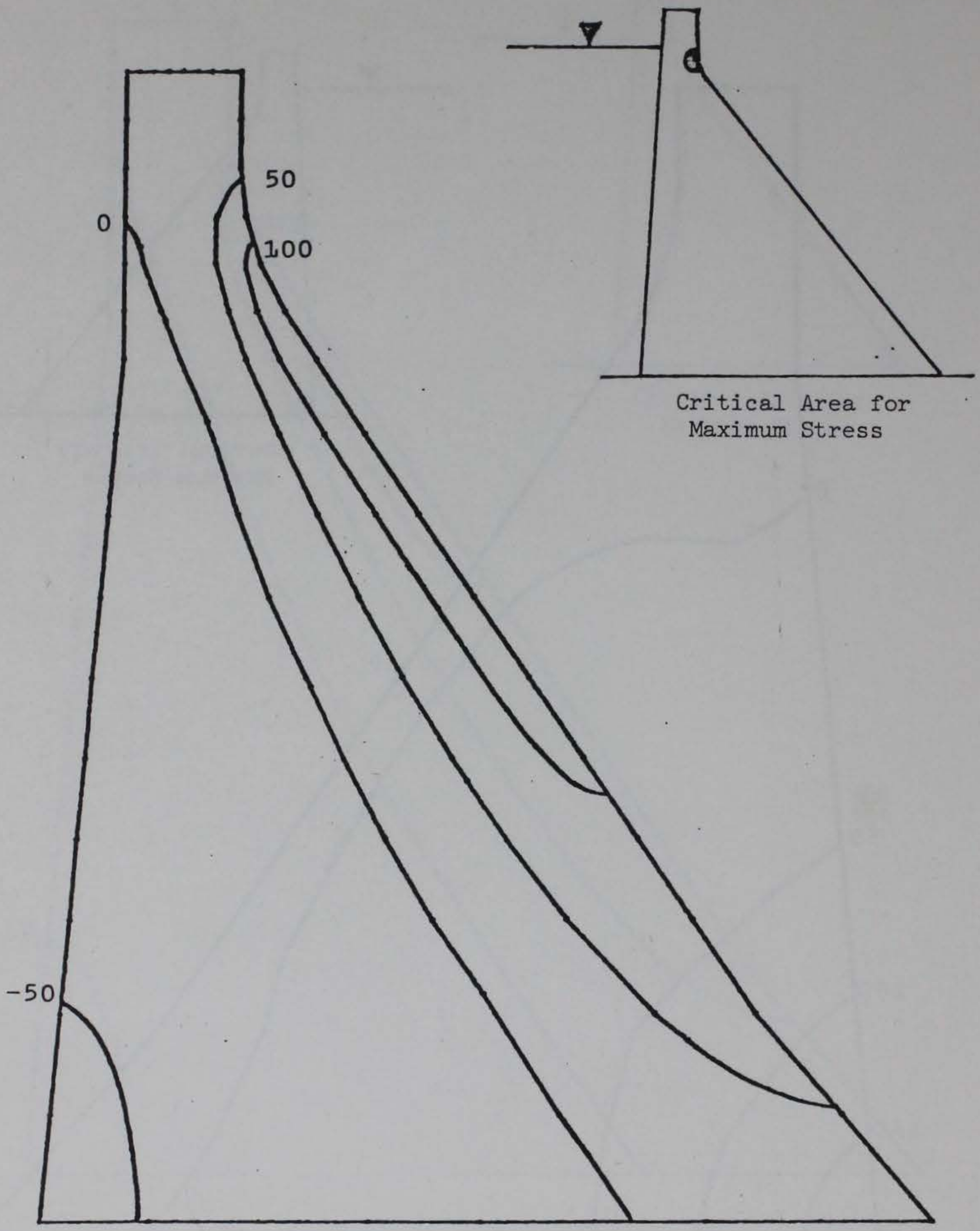

Critical Area for
Maximum Stress

a. Maximum principal stresses
in psi at 7.455 seconds.

Figure 10 Maximum principal stresses in Richard B. Russell Dam due to N52W and vertical components of San Fernando Earthquake, 5 percent damping (sheet 1 of 4).

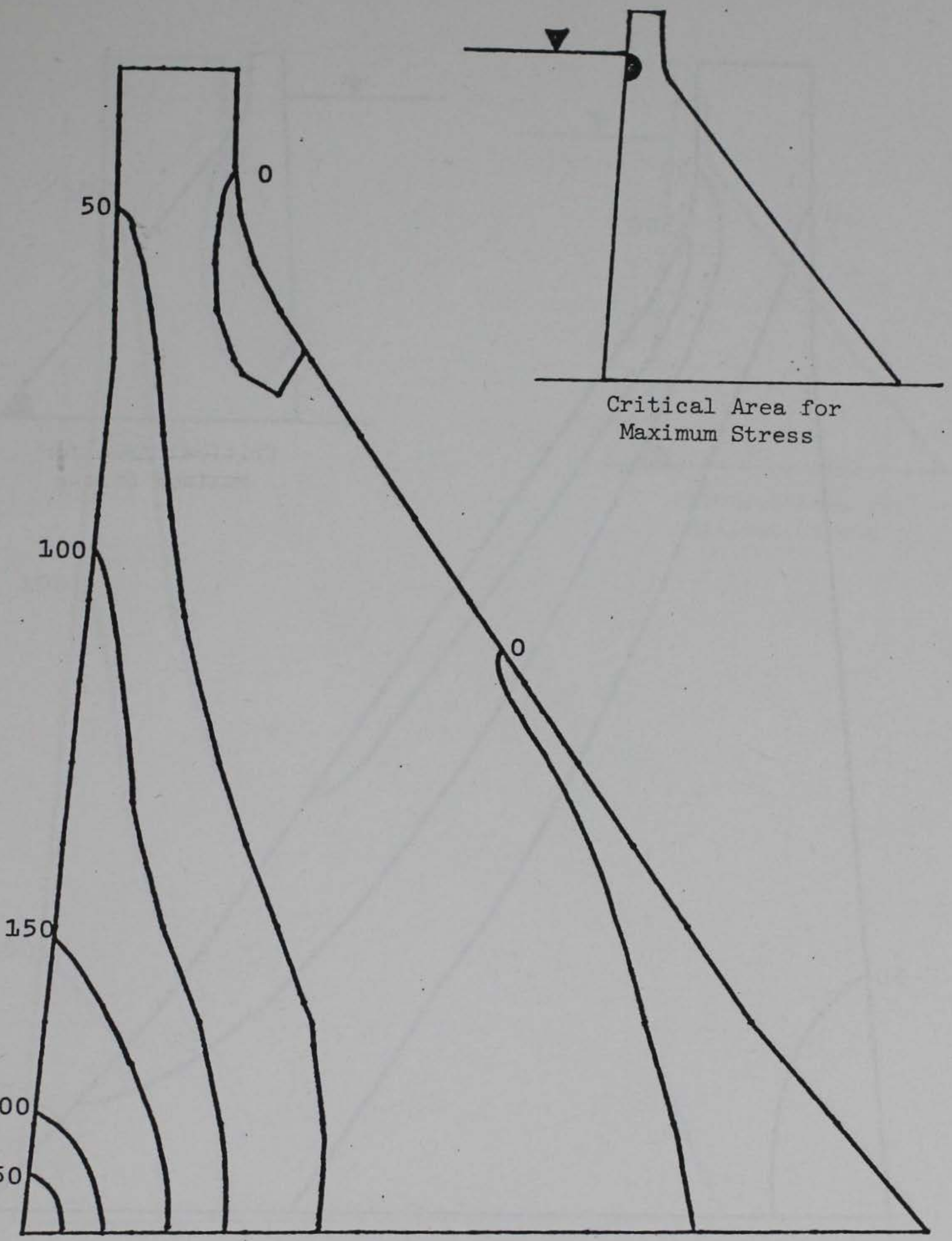

b. Maximum principal stresses
in psi at 7.355 seconds.

Figure 10 (sheet 2 of 4).

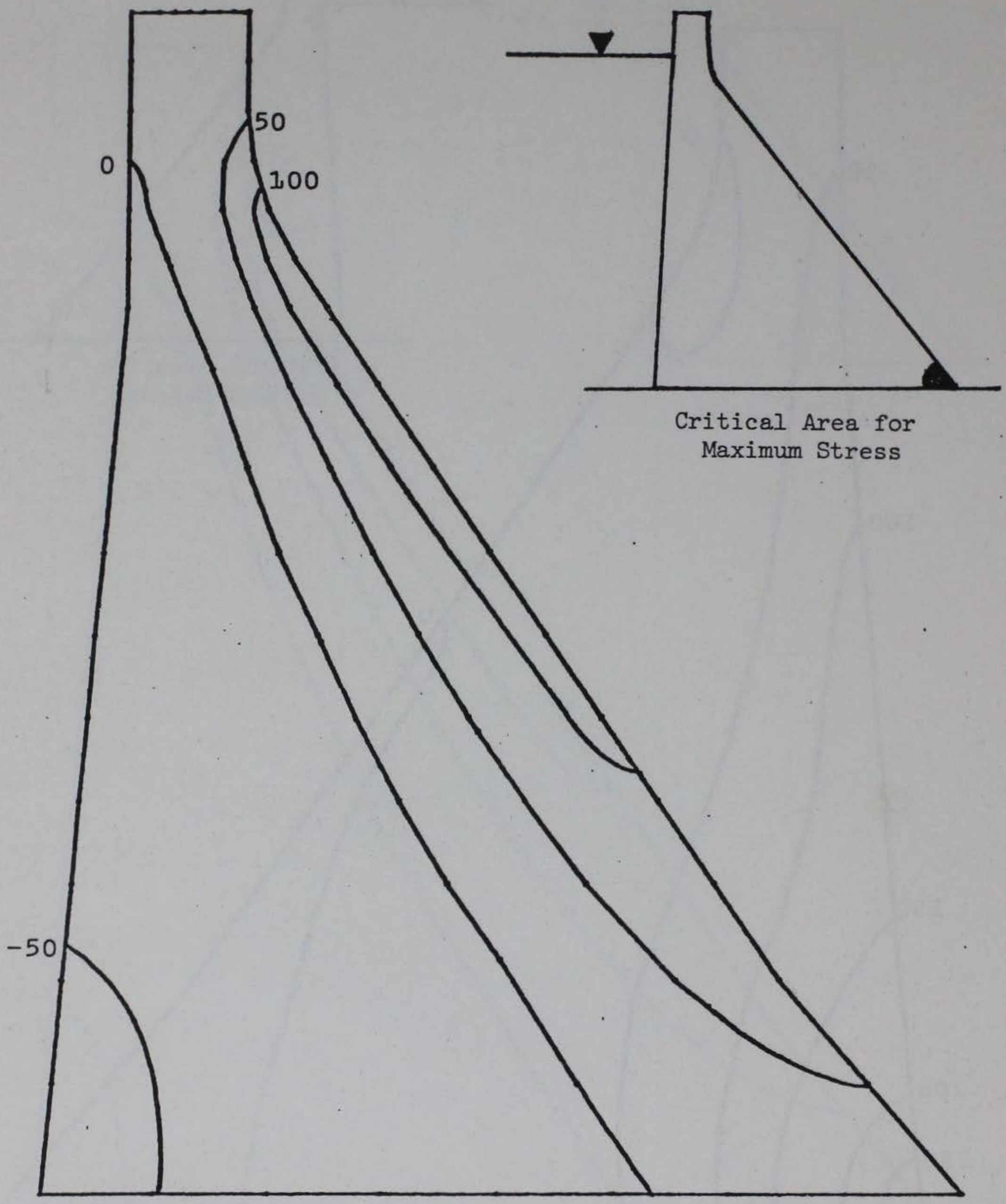

Critical Area for
Maximum Stress

c. Maximum principal stresses
in psi at 7.46 seconds.

Figure 10 (sheet 3 of 4)

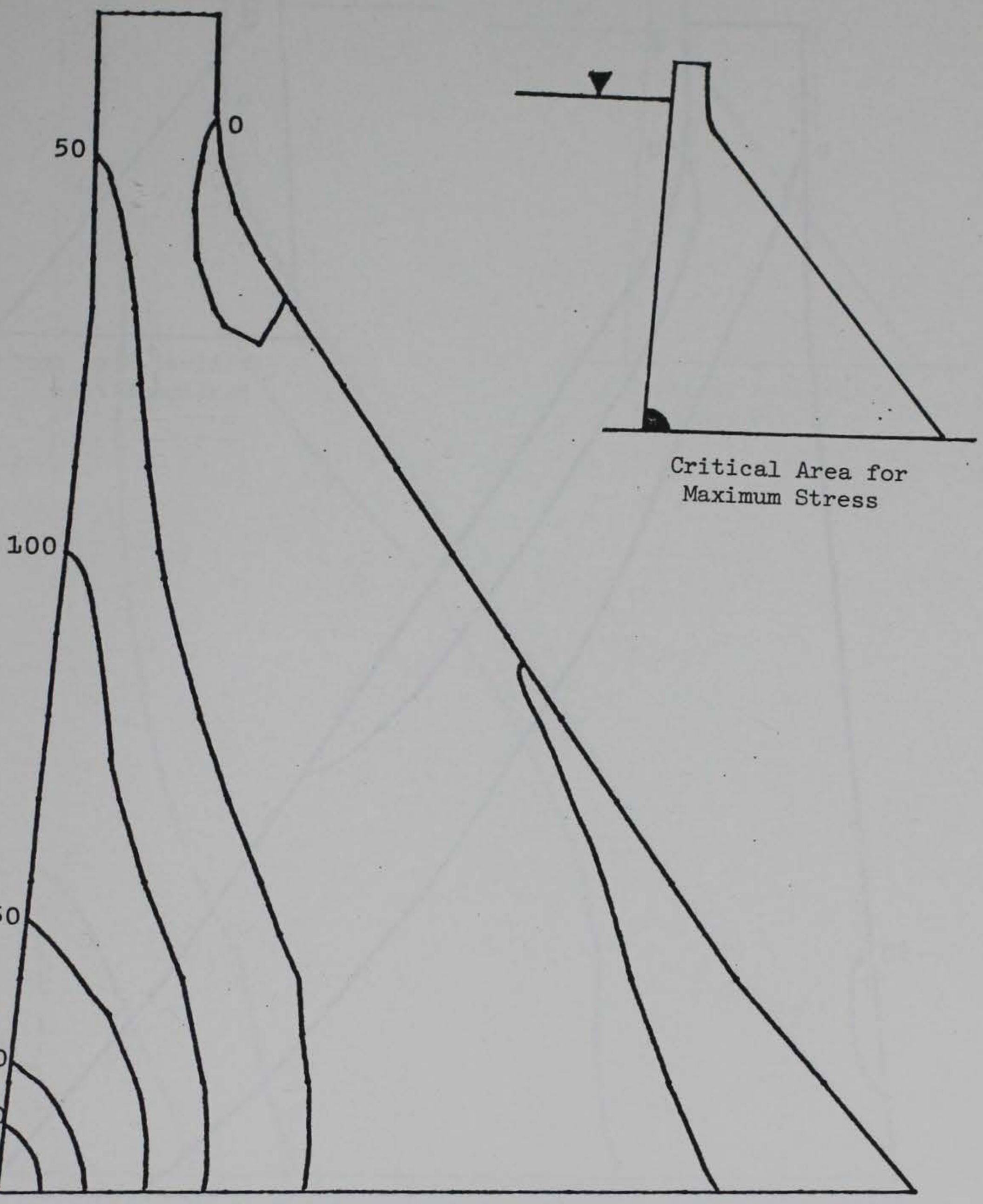

Critical Area for
Maximum Stress

d. Maximum principal stresses
in psi at 7.35 seconds.

Figure 10 (sheet 4 of 4).

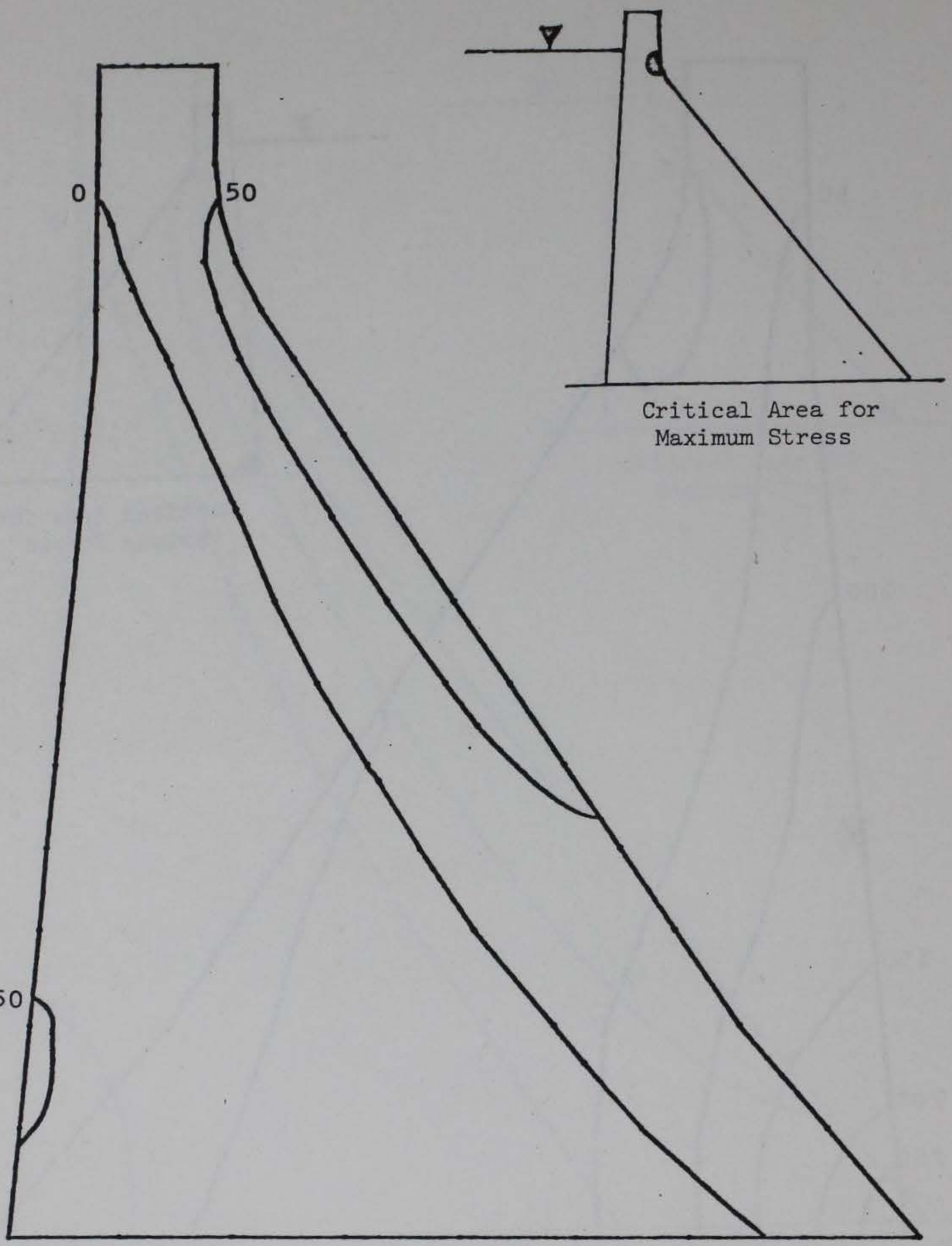

Critical Area for
Maximum Stress

a. Maximum principal stresses
in psi at 7.46 seconds.

Figure 11 Maximum principal stresses in Richard B. Russell Dam due to N52W and vertical components of San Fernando Earthquake, 10 percent damping (sheet 1 of 4).

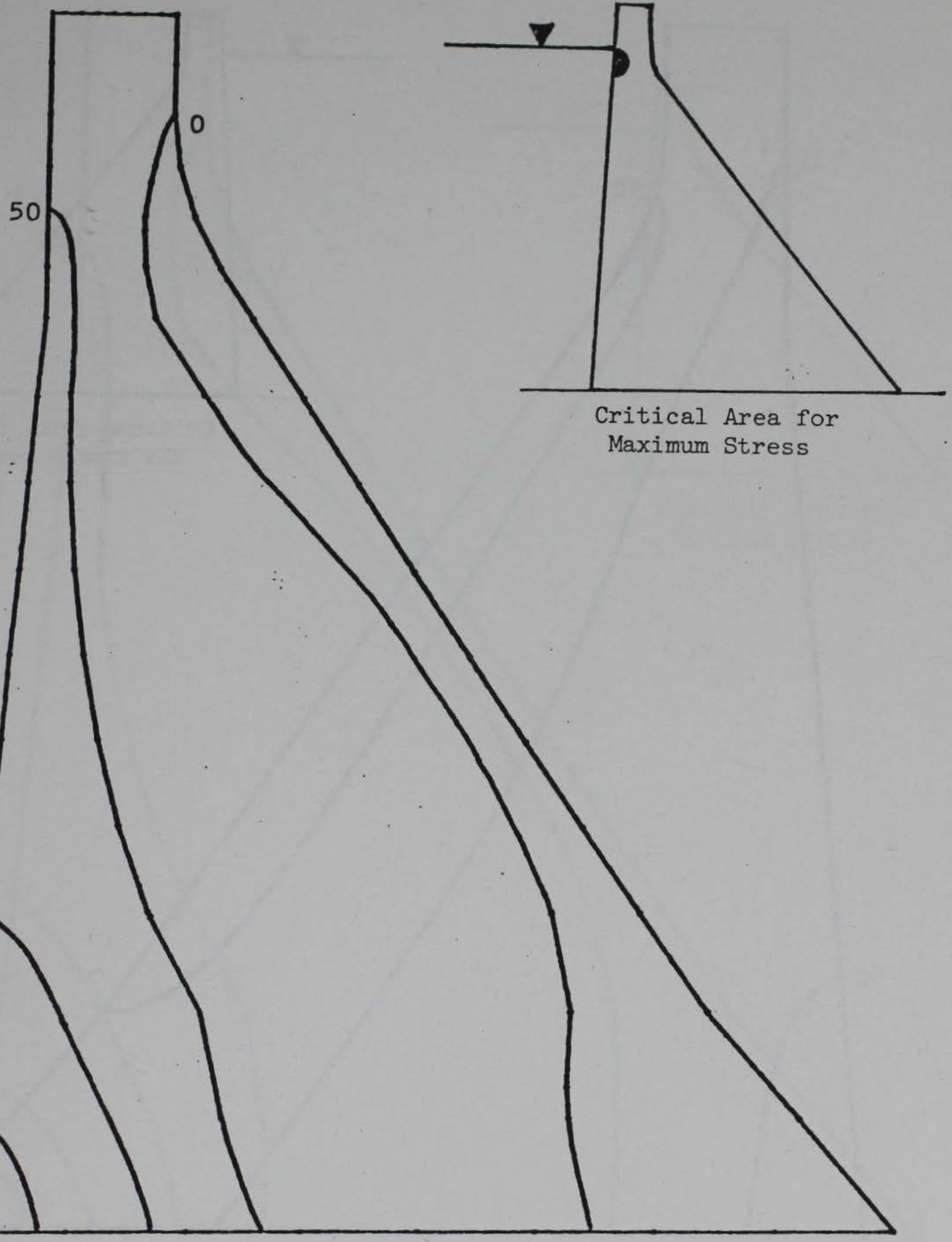

b. Maximum principal stresses
in psi at 7.365 seconds.

Figure 11 (sheet 2 of 4).

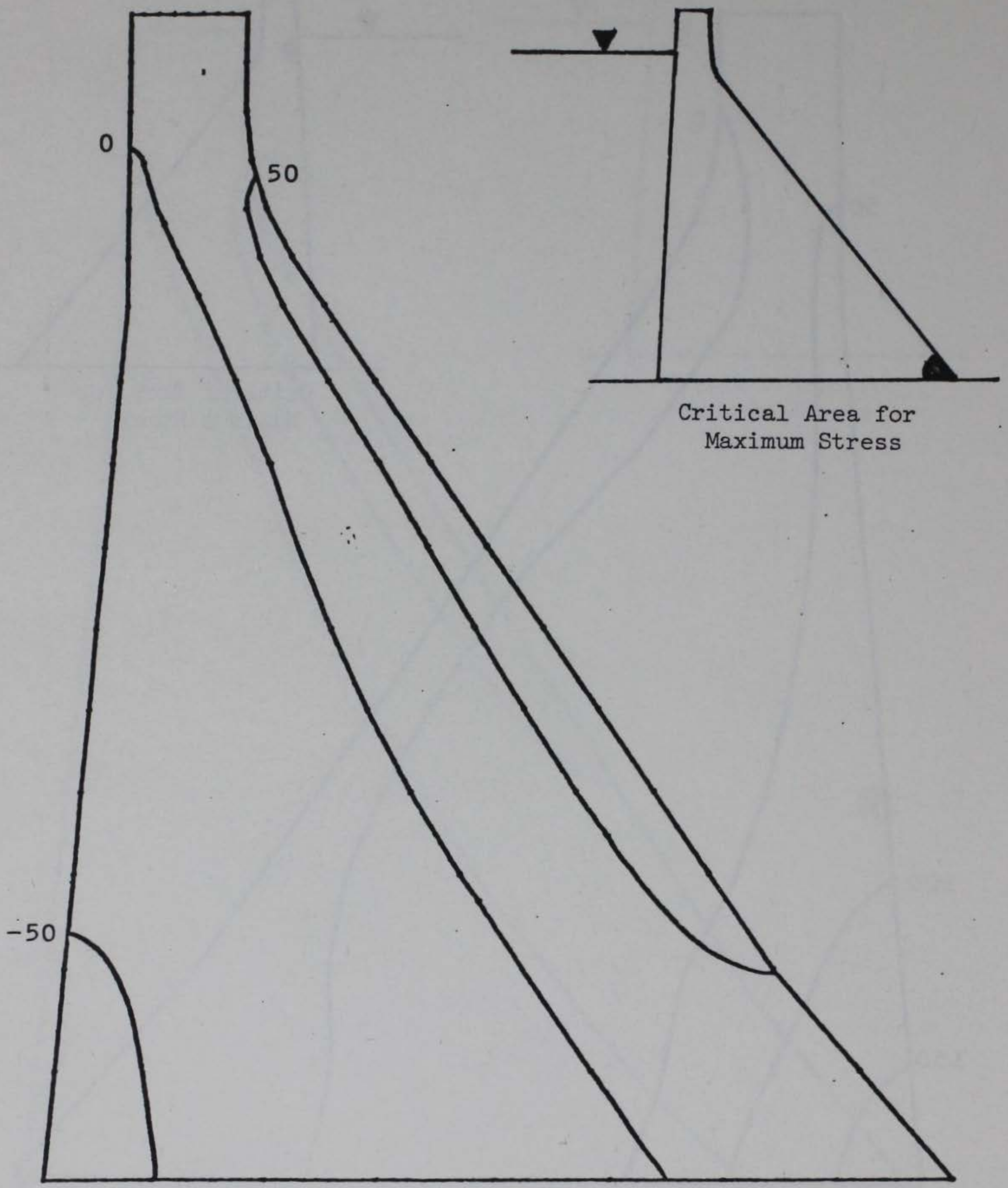

Critical Area for
Maximum Stress

c. Maximum principal stresses
in psi at 4.745 seconds.

Figure 11 (sheet 3 of 4).

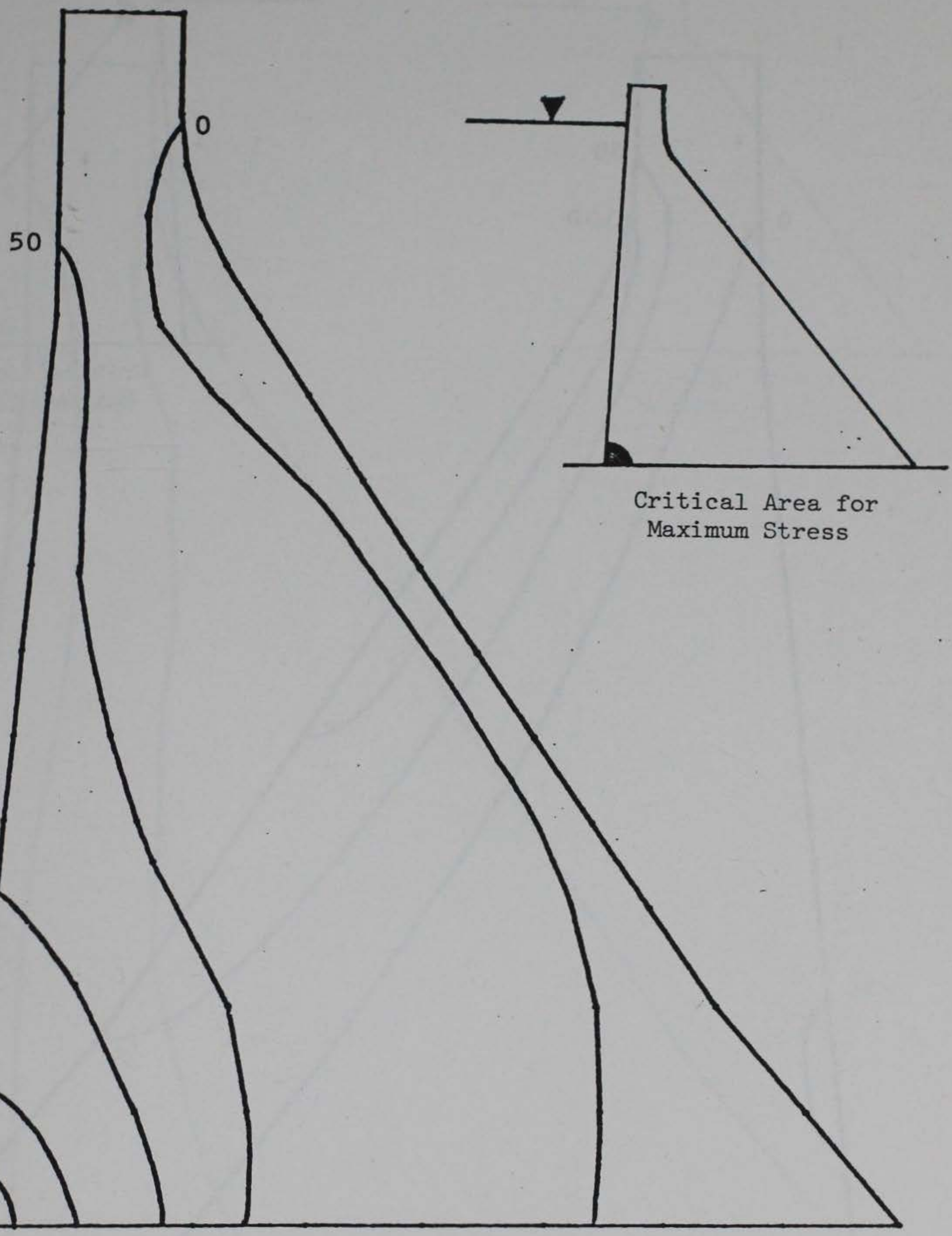

Critical Area for
Maximum Stress

d. Maximum principal stresses
in psi at 7.35 seconds.

Figure 11 (sheet 4 of 4).

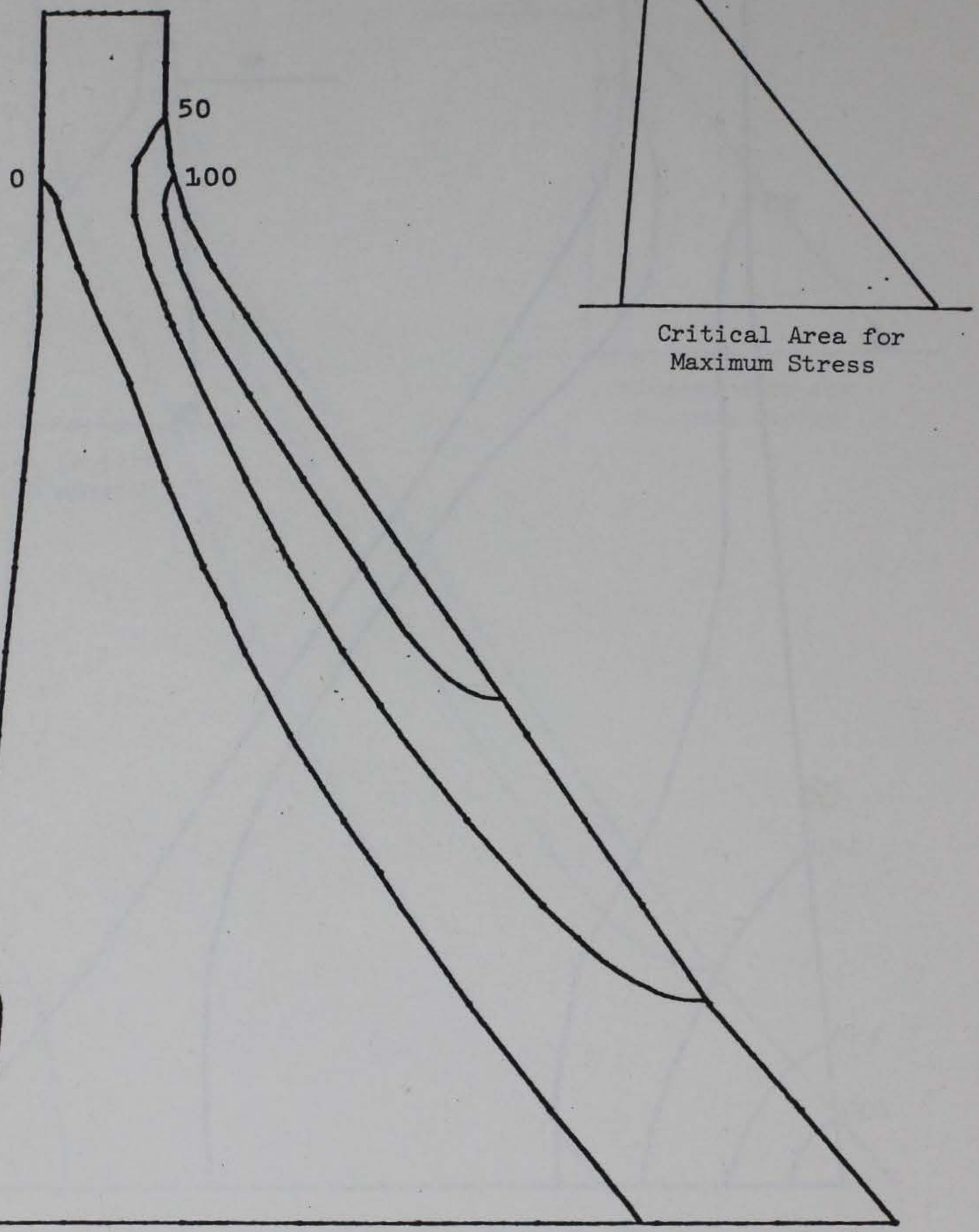

a. Maximum principal stresses in psi at 1.1275 seconds.

Figure 12 Maximum principal stresses in Richard B. Russell Dam due to N62W and vertical components of San Fernando Earthquake, 5 percent damping (sheet 1 of 4).

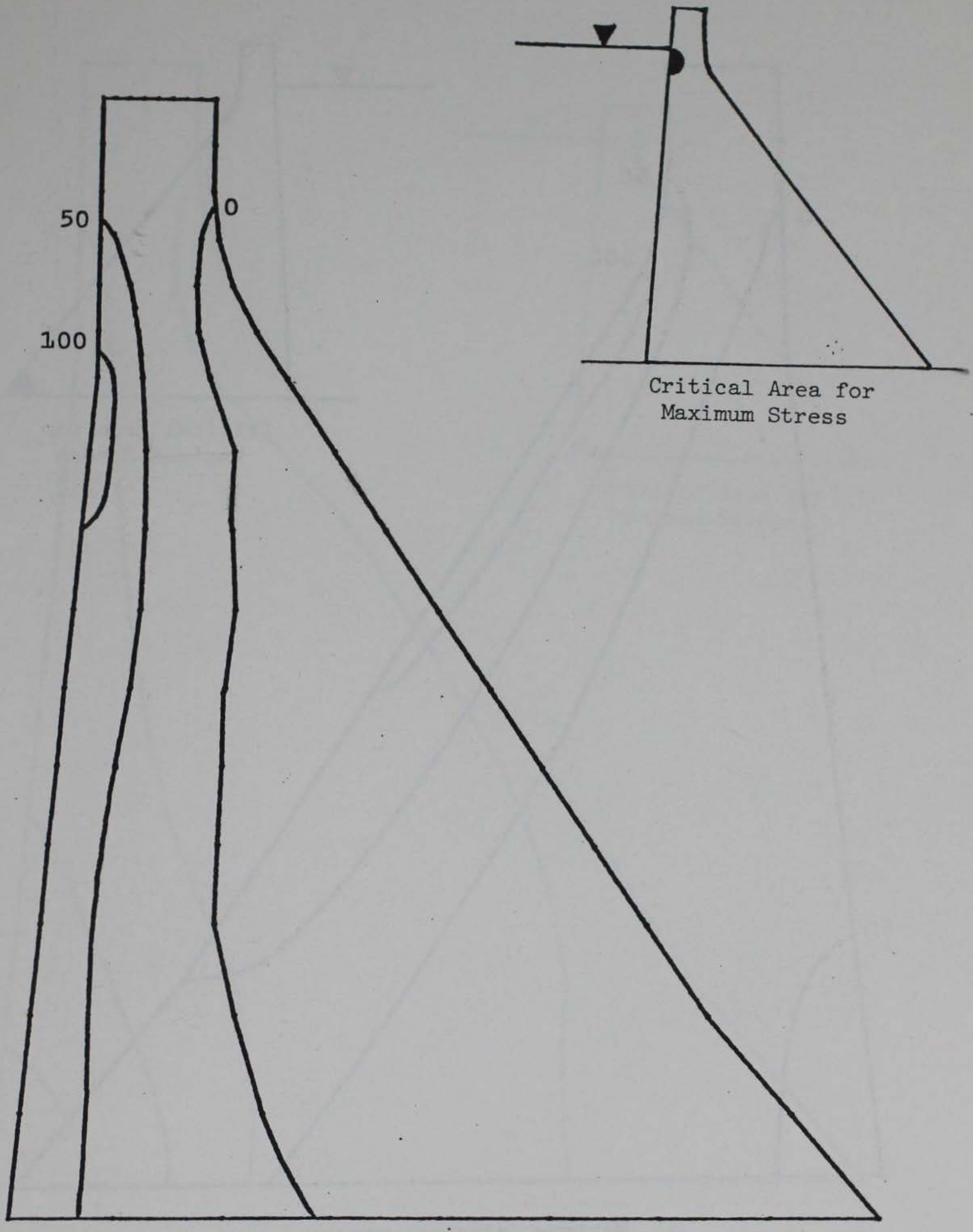

b. Maximum principal stresses
in psi at 1.233 seconds.

Figure 12 (sheet 2 of 4).

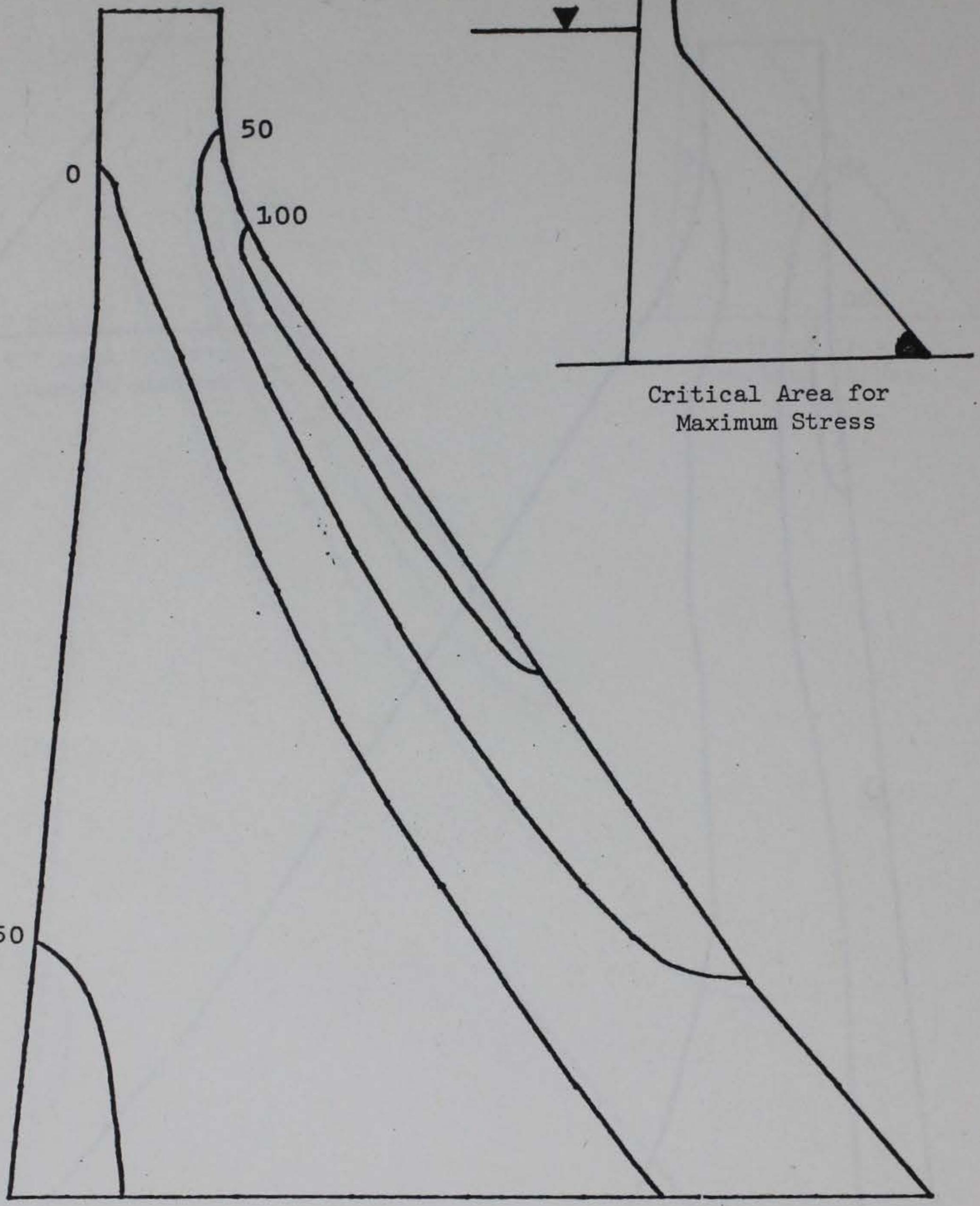

Critical Area for
Maximum Stress

c. Maximum principal stresses
in psi at 1.147 seconds.

Figure 12 (sheet 3 of 4).

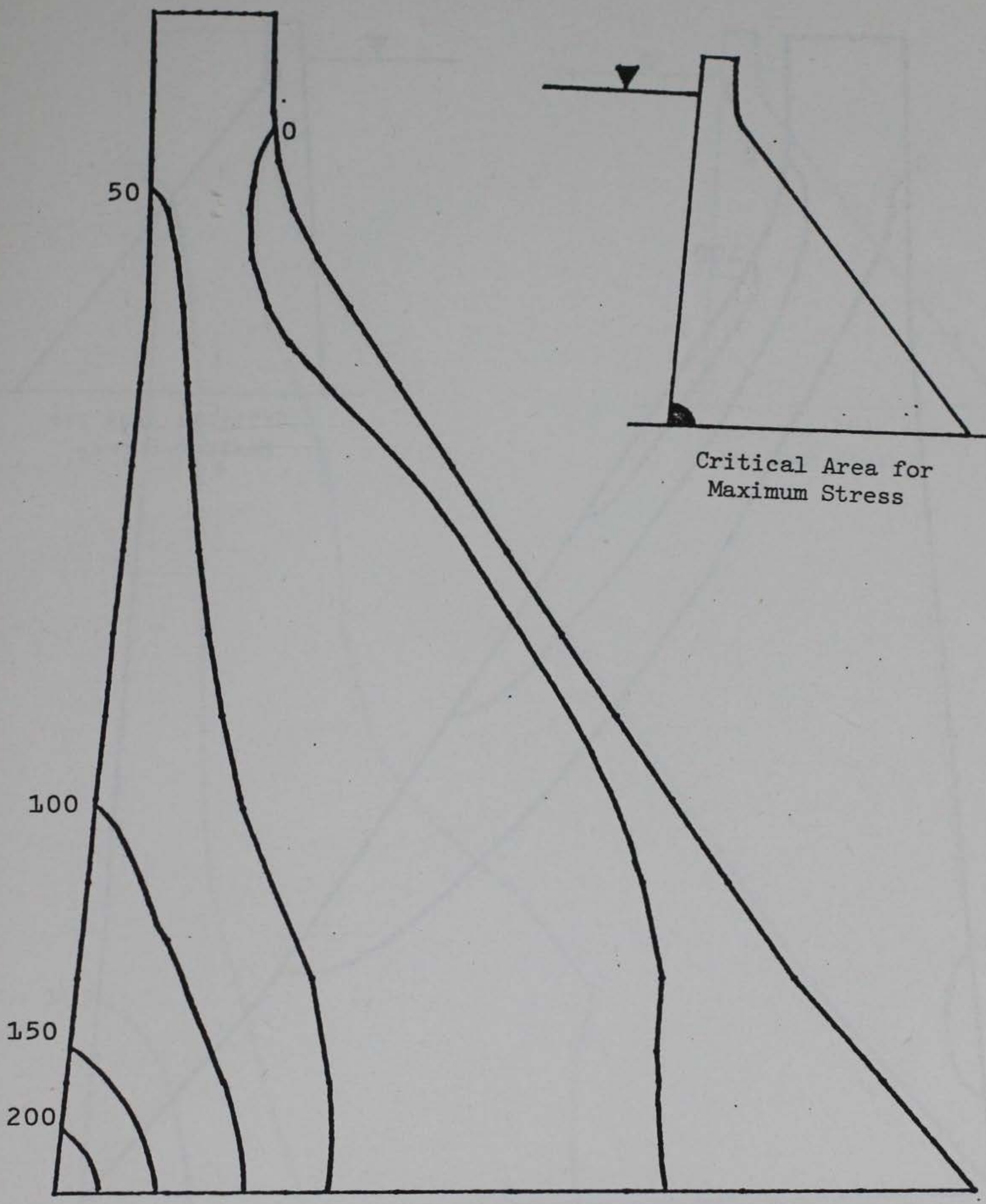

Critical Area for
Maximum Stress

d. Maximum principal stresses
in psi at 9.86 seconds.

Figure 12 (sheet 4 of 4).

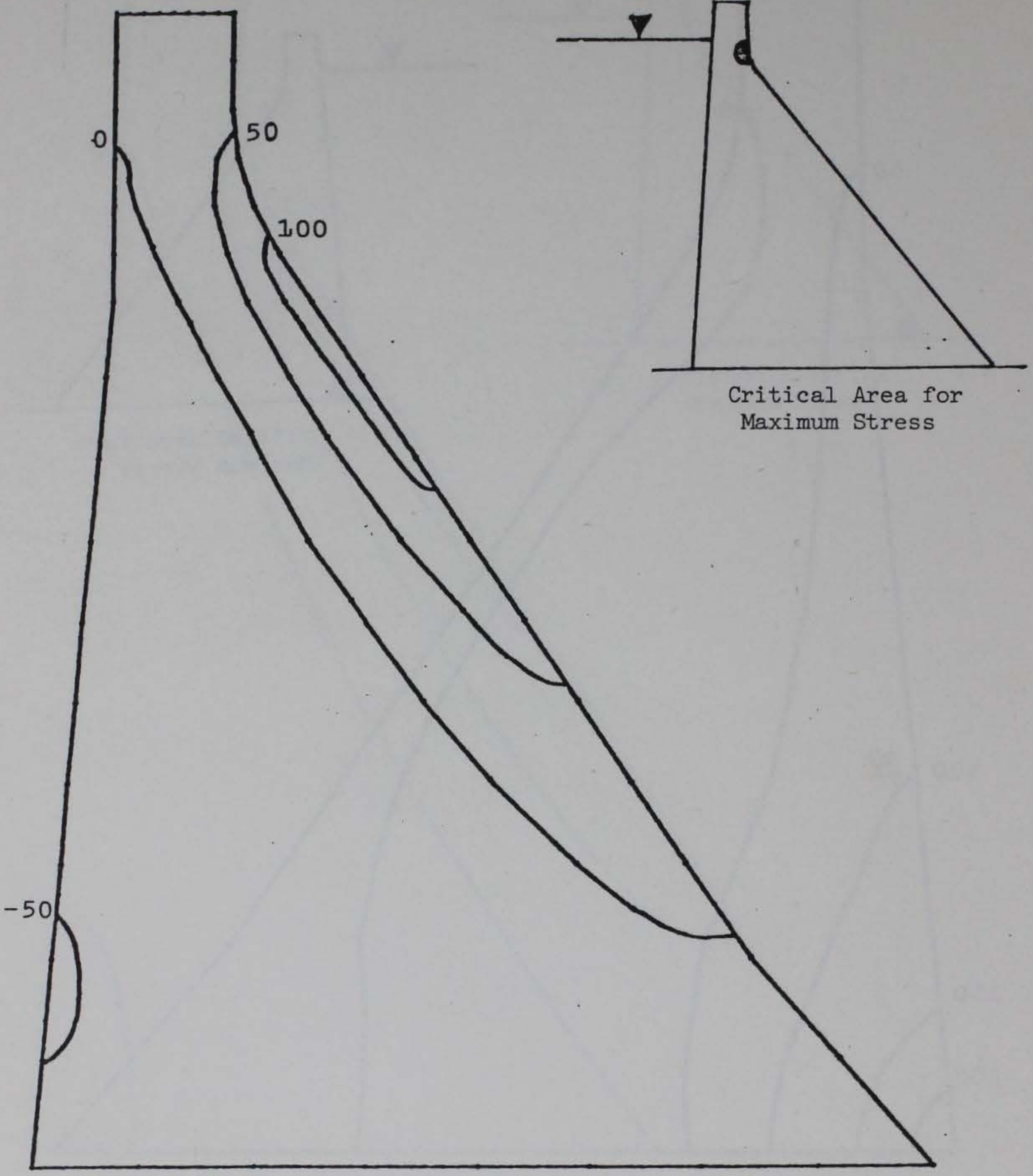

a. Maximum principal stresses
in psi at 1.2535 seconds.

Figure 13 Maximum principal stresses in Richard B. Russell Dam due to N62W and vertical components of San Fernando Earthquake, 10 percent damping (sheet 1 of 4).

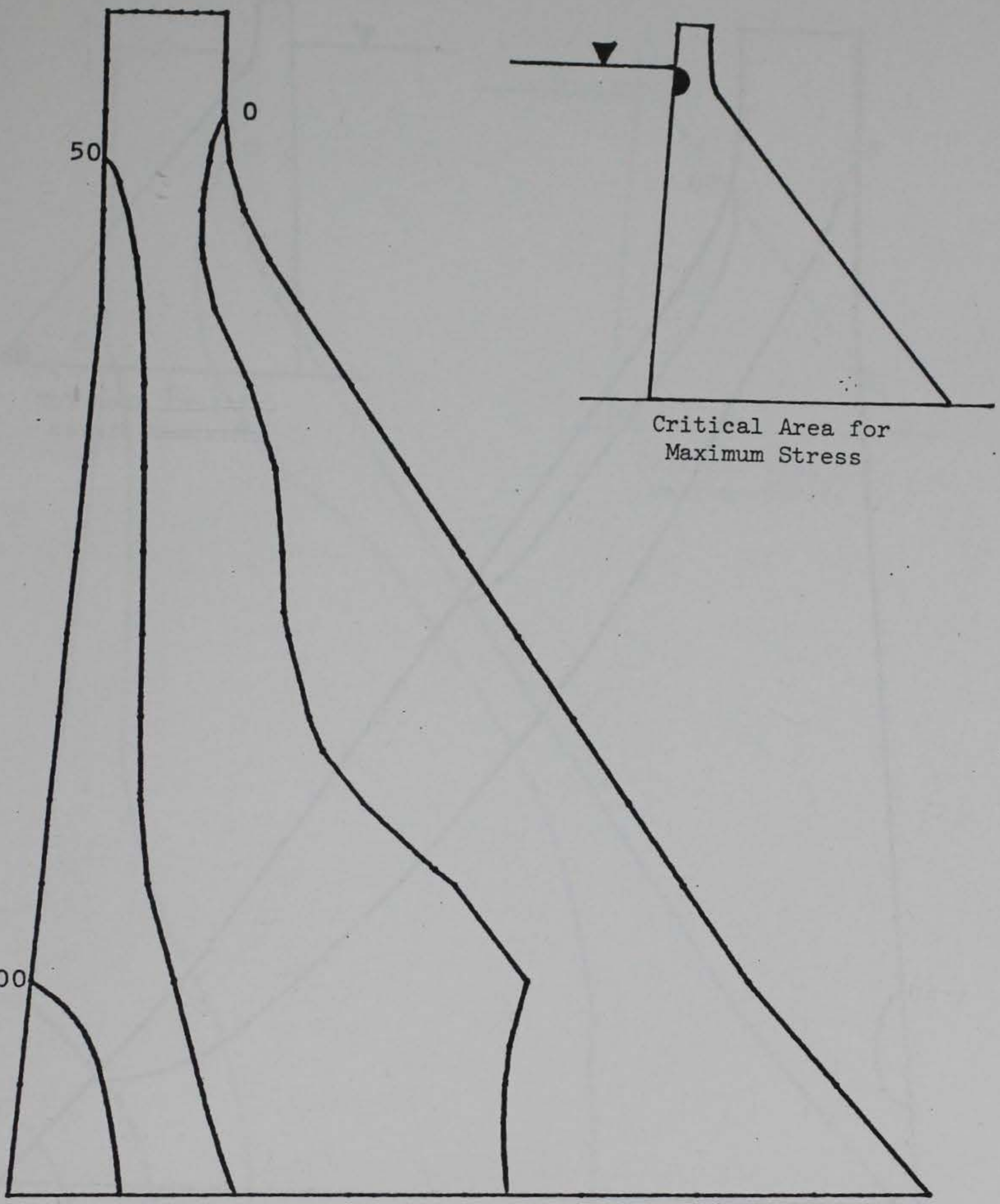

b. Maximum principal stresses
in psi at 1.2615 seconds.

Figure 13 (sheet 2 of 4).

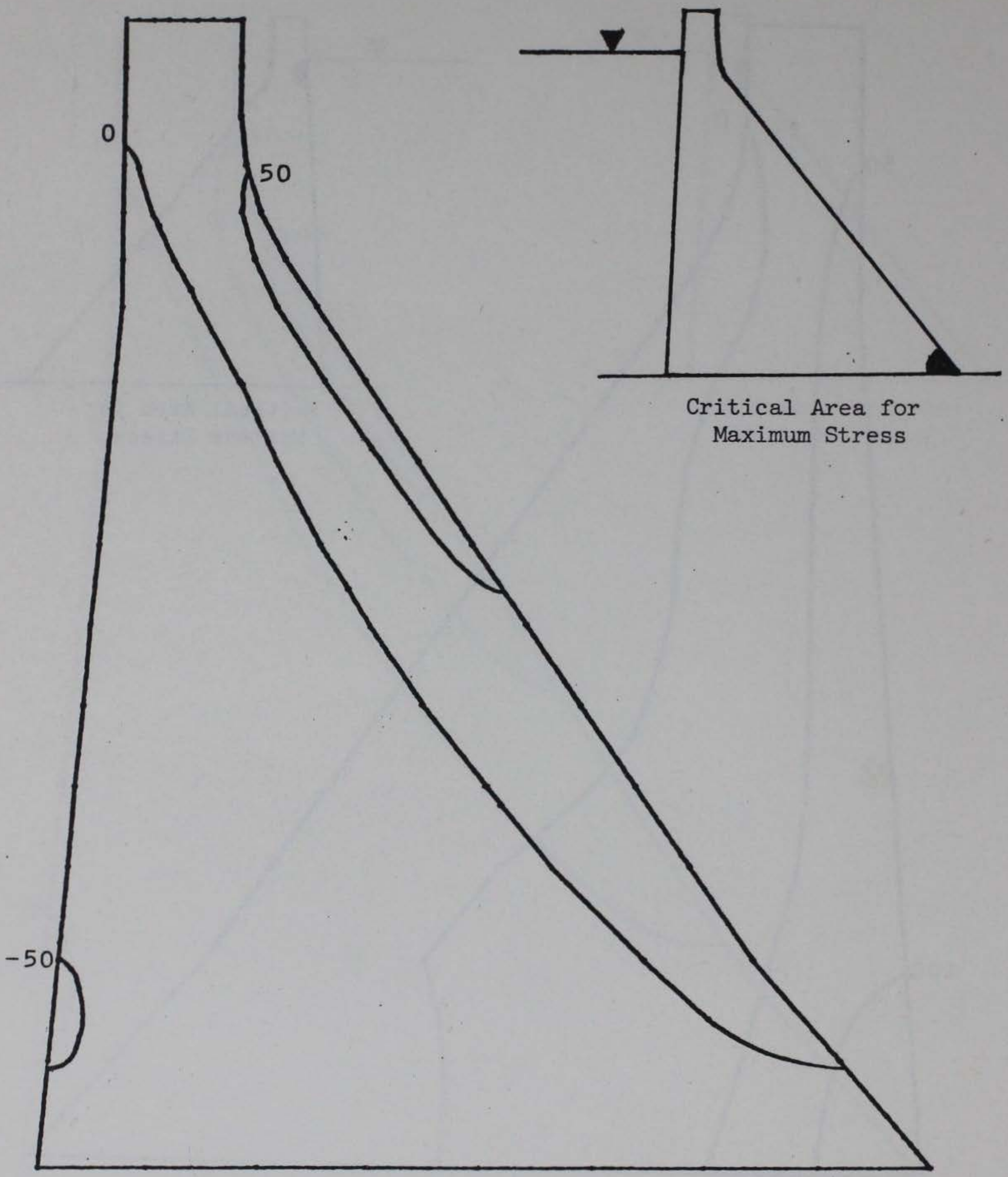

Critical Area for
Maximum Stress

c. Maximum principal stresses
in psi at 1.1475 seconds.

Figure 13 (sheet 3 of 4).

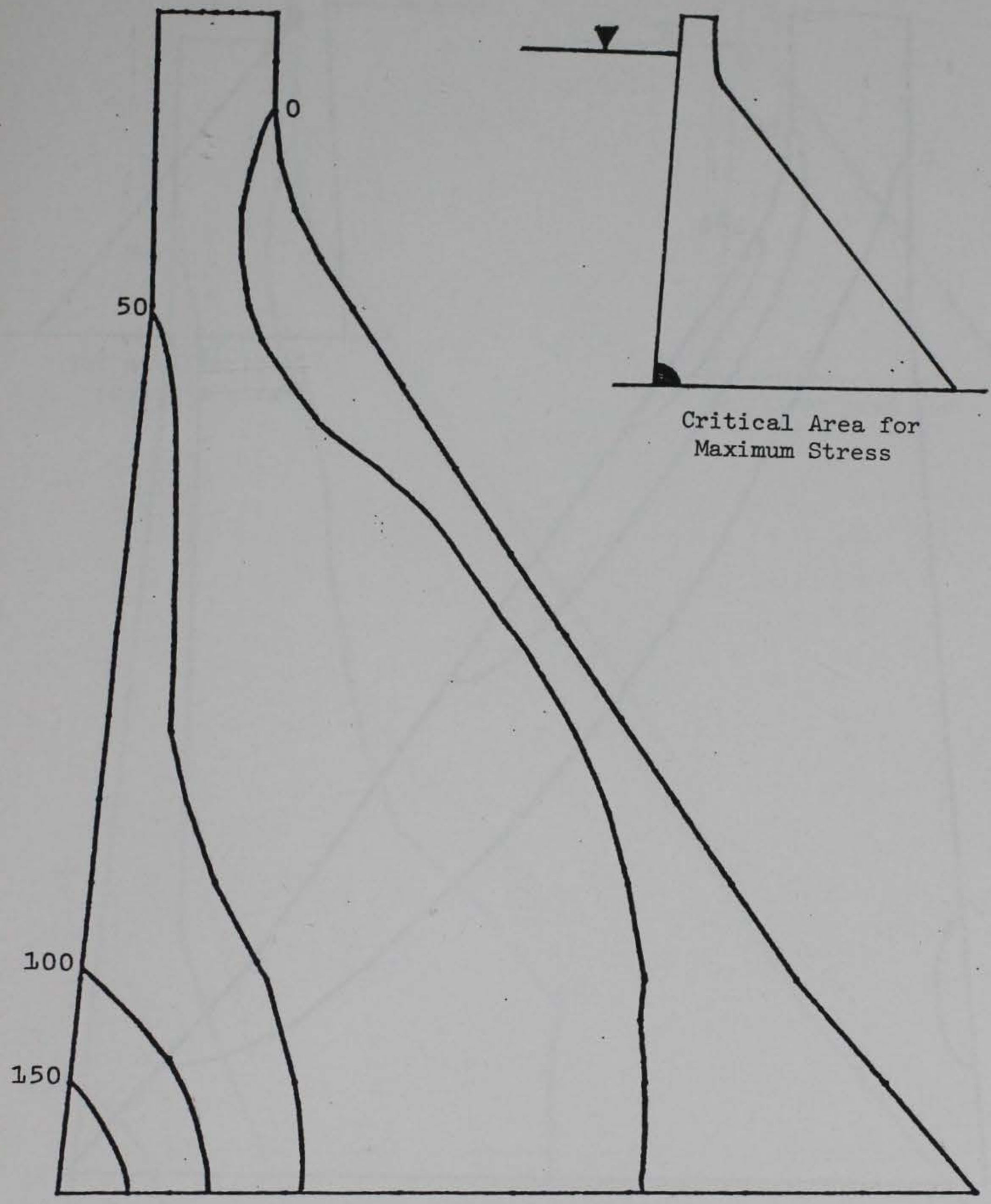

Critical Area for
Maximum Stress

d. Maximum principal stresses
in psi at 9.86 seconds.

Figure 13 (sheet 4 of 4).

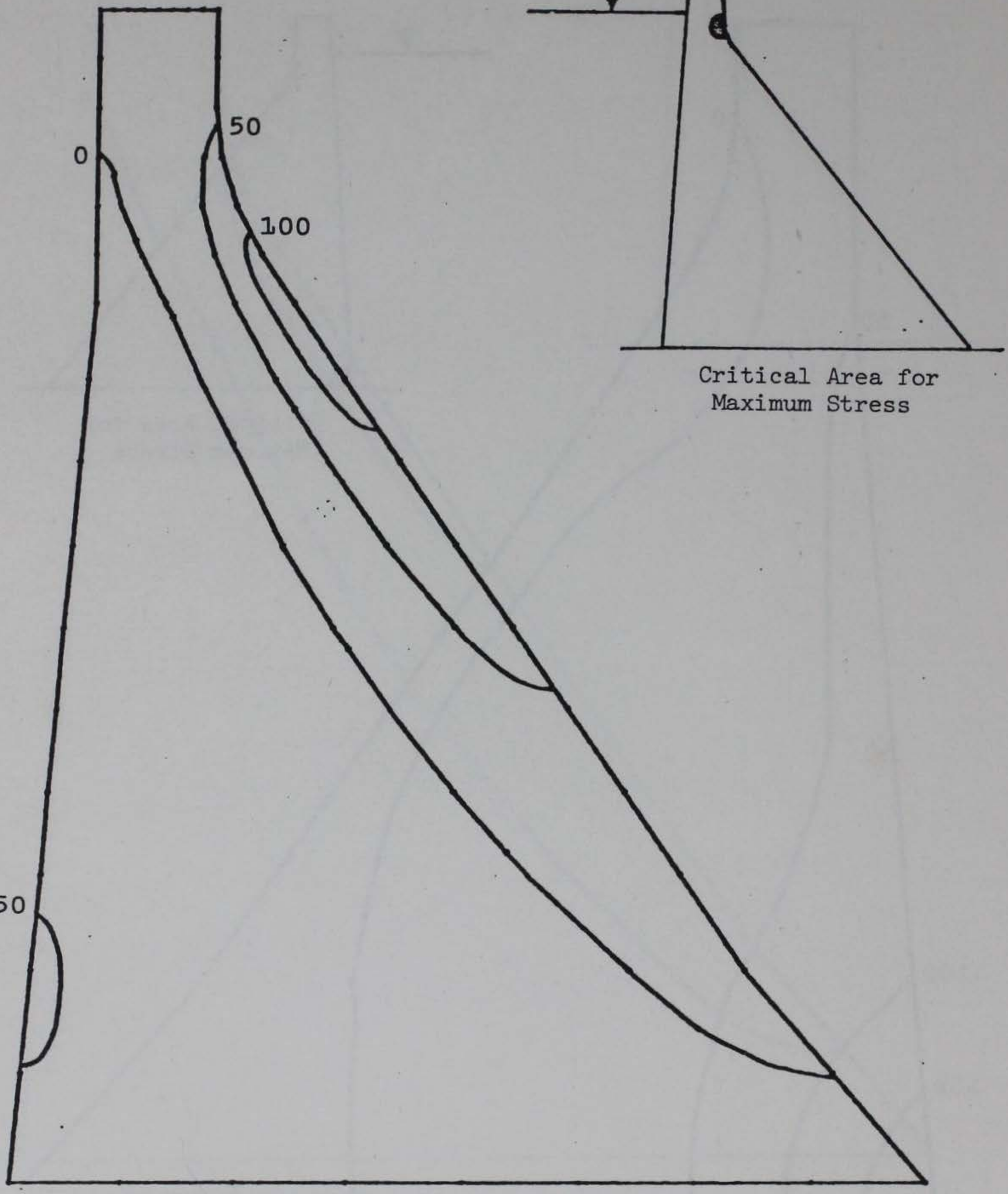

Critical Area for
Maximum Stress

a. Maximum principal stresses
in psi at 6.35 seconds.

Figure 14 Maximum principal stresses in Richard B. Russell Dam due to WILSH and vertical components of San Fernando Earthquake, 5 percent damping (sheet 1 of 4).

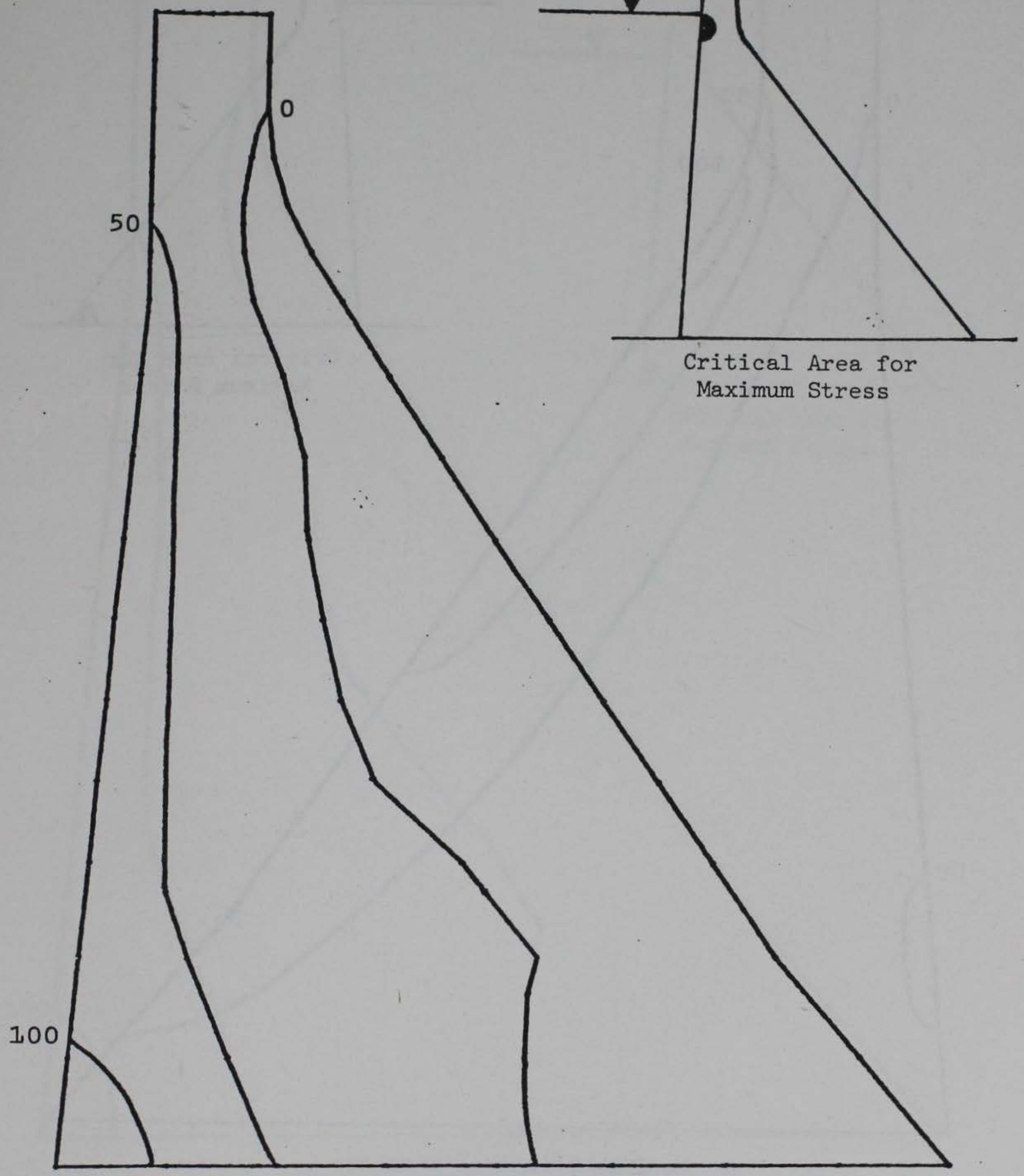

Critical Area for
Maximum Stress

b. Maximum principal stresses
in psi at 6.645 seconds.

Figure 14 (sheet 2 of 4).

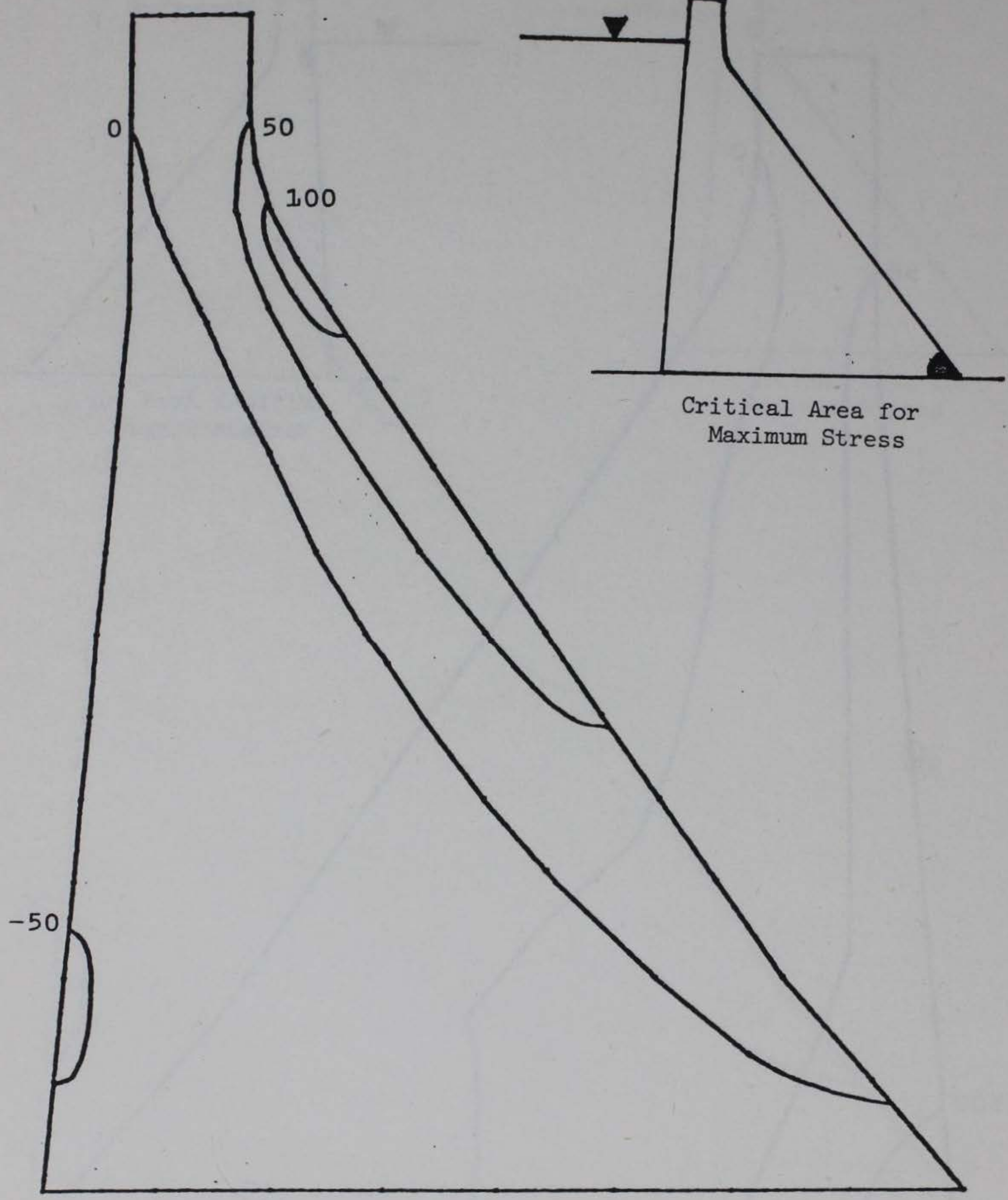

Critical Area for
Maximum Stress

c. Maximum principal stresses
in psi at 6.355 seconds.

Figure 14 (sheet 3 of 4).

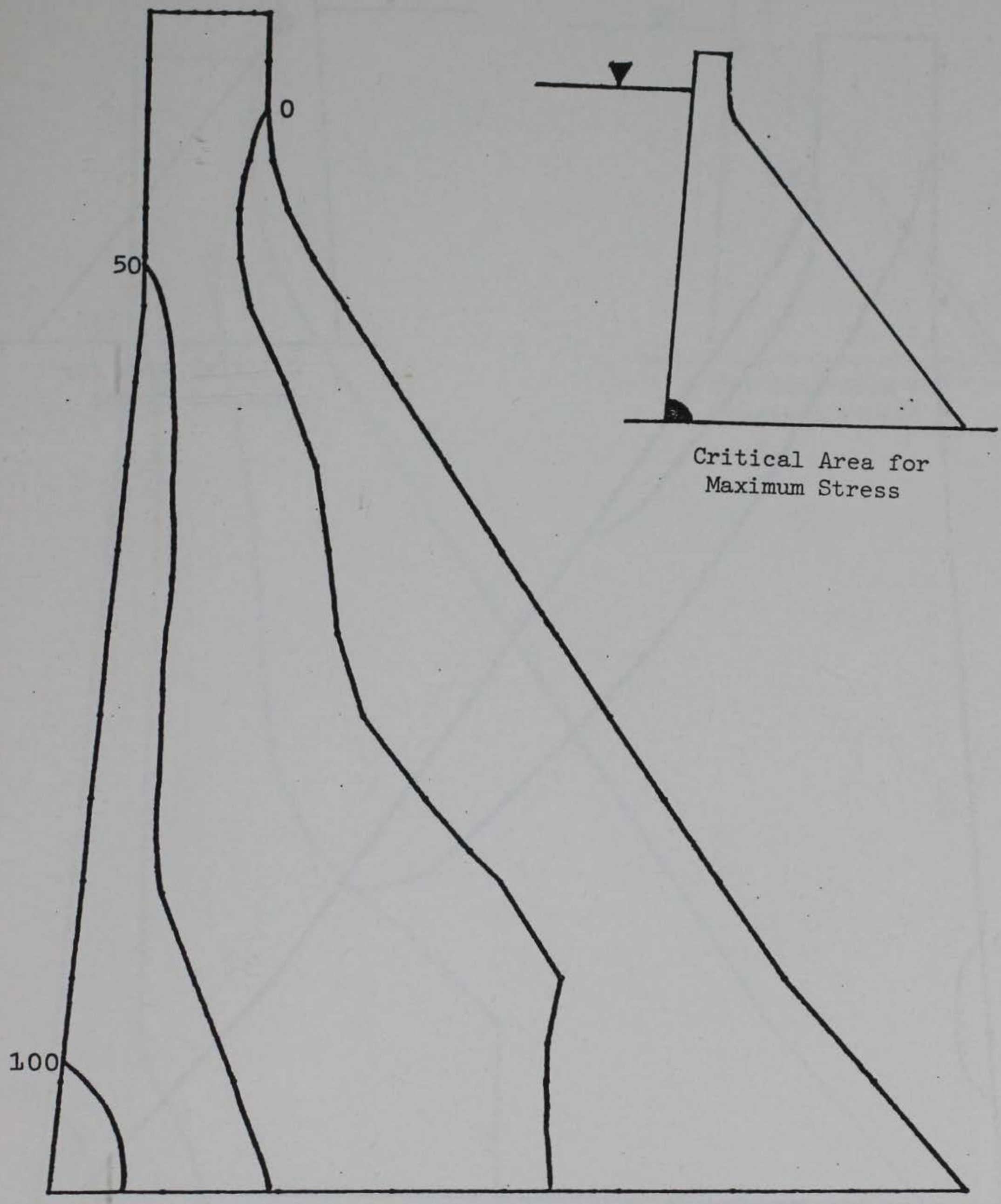

Critical Area for
Maximum Stress

d. Maximum principal stresses
in psi at 6.635 seconds.

Figure 14 (sheet 4 of 4).

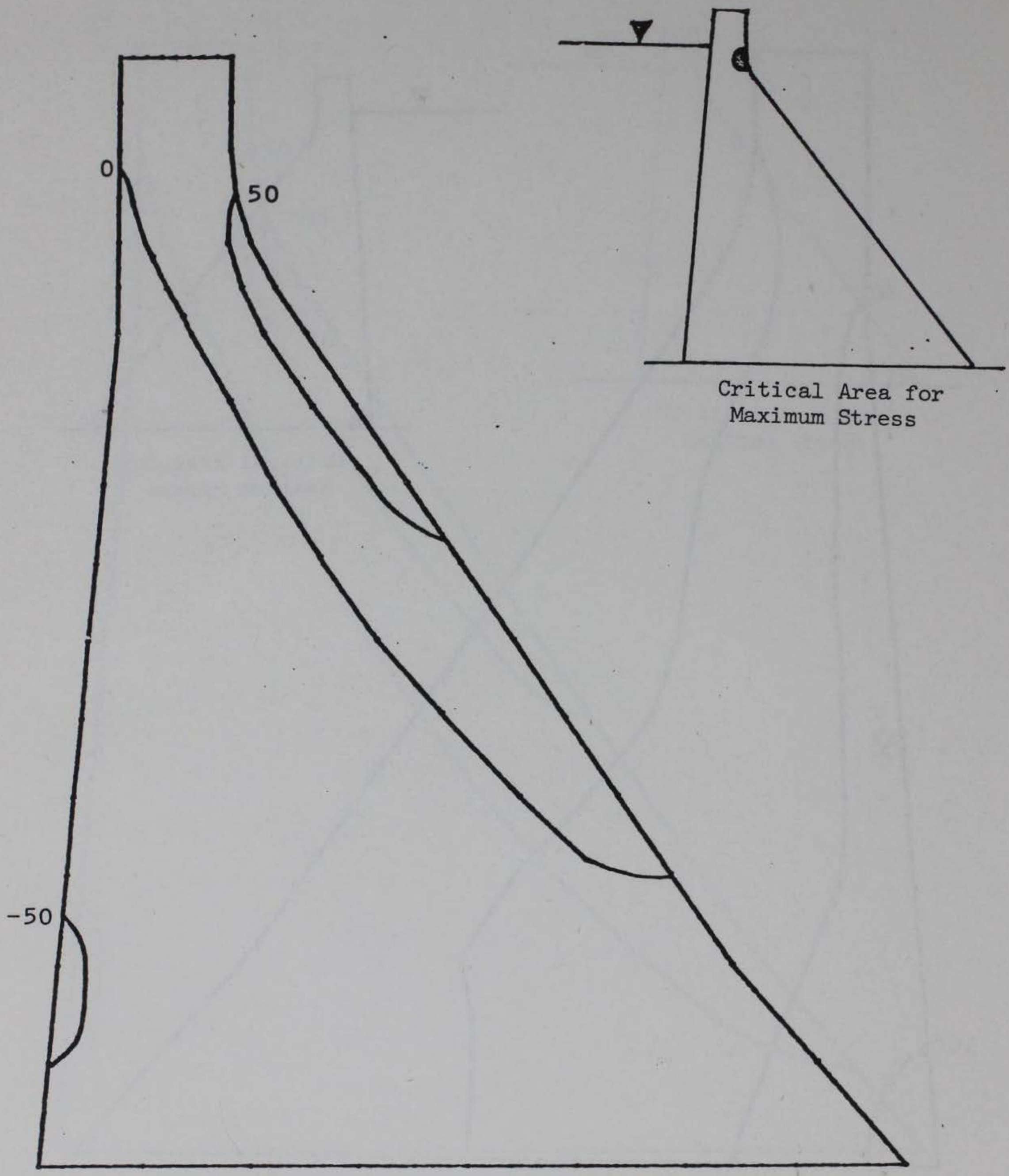

Critical Area for
Maximum Stress

a. Maximum principal stresses
in psi at 6.355 seconds.

Figure 15 Maximum principal stresses in Richard B. Russell Dam due to WILSH and vertical components of San Fernando Earthquake, 10 percent damping (sheet 1 of 4).

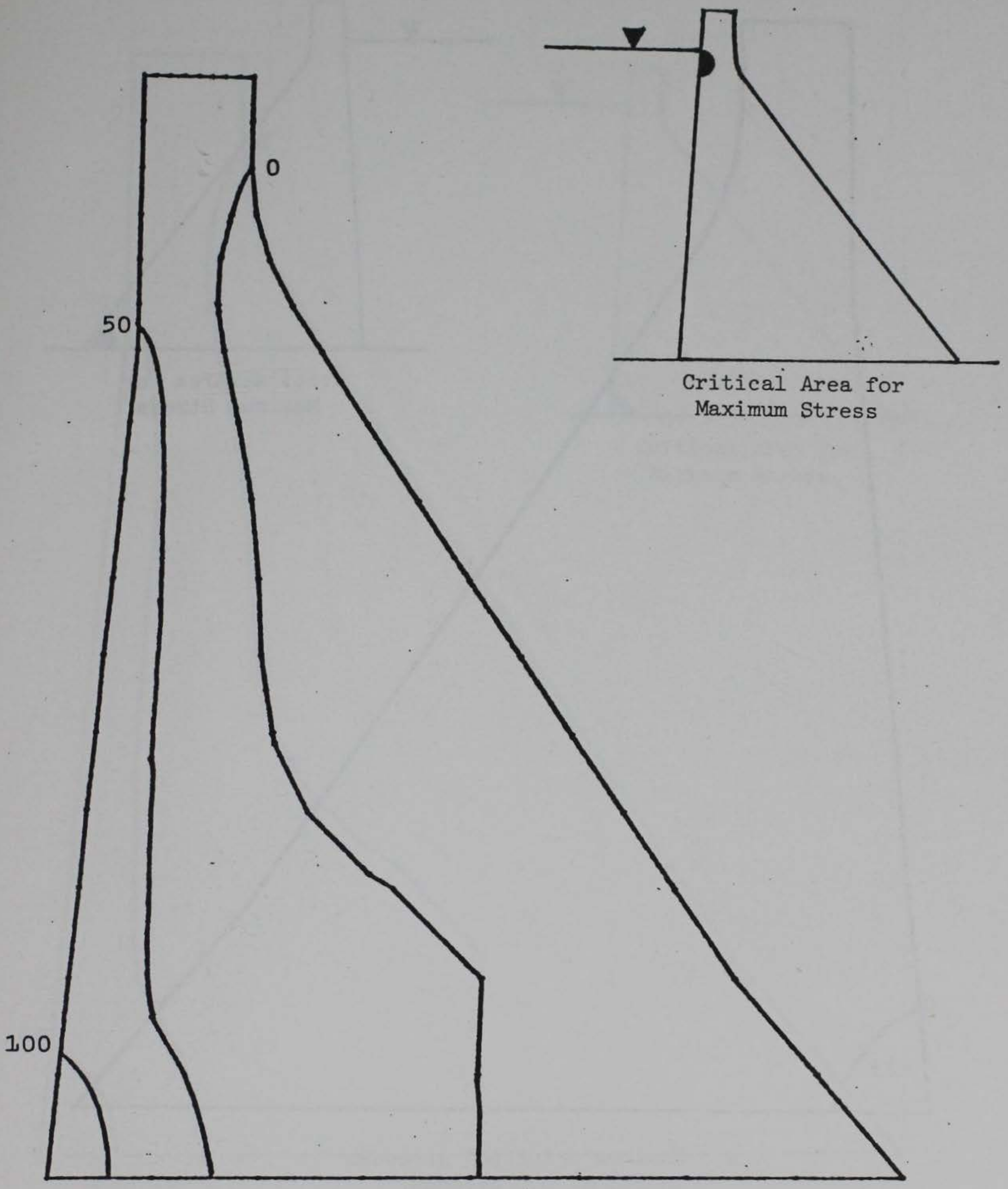

Critical Area for
Maximum Stress

b. Maximum principal stresses
in psi at 7.97 seconds.

Figure 15 (sheet 2 of 4).

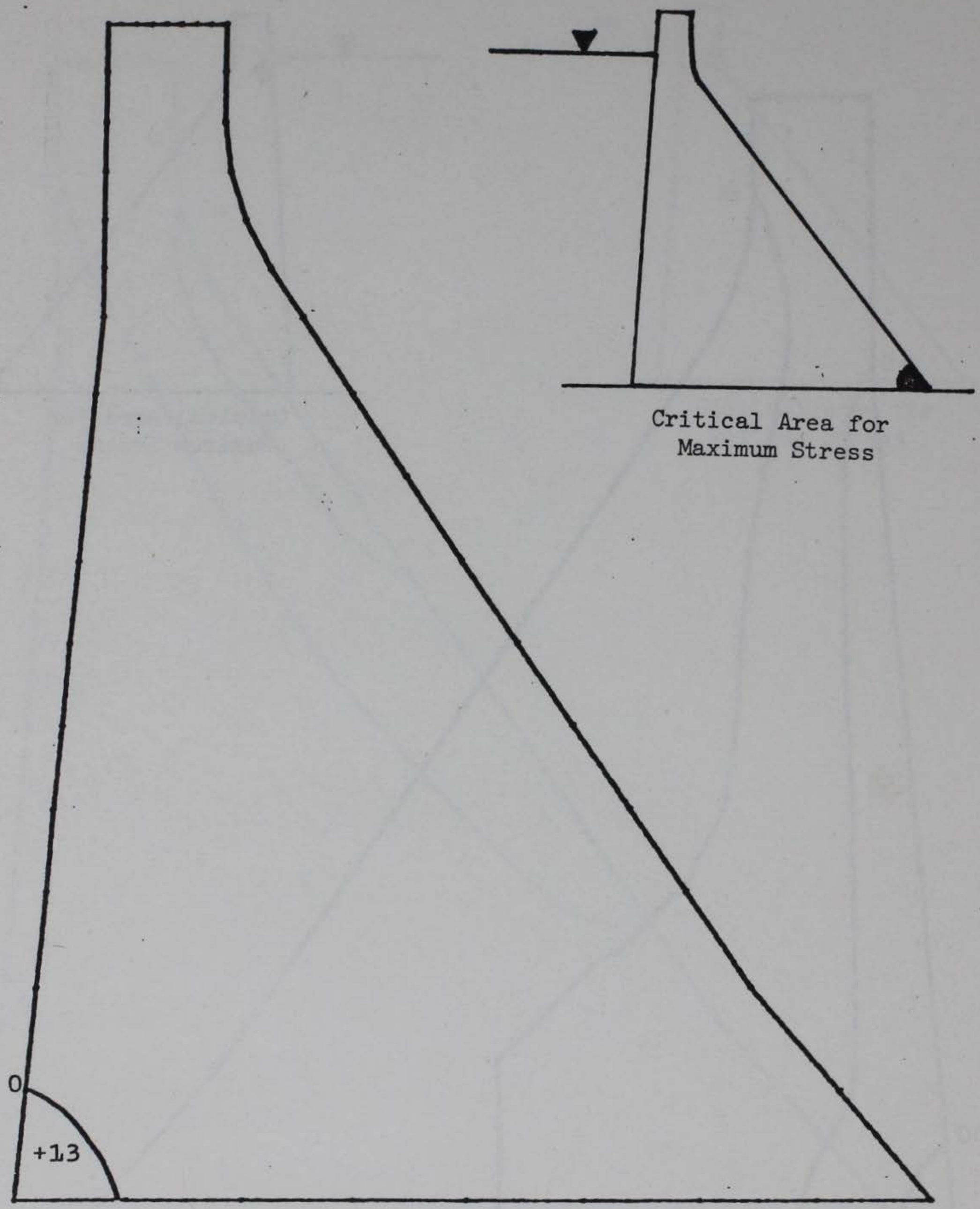

c. Maximum principal stresses in psi at 0.0 seconds.

Figure 15 (sheet 3 of 4).

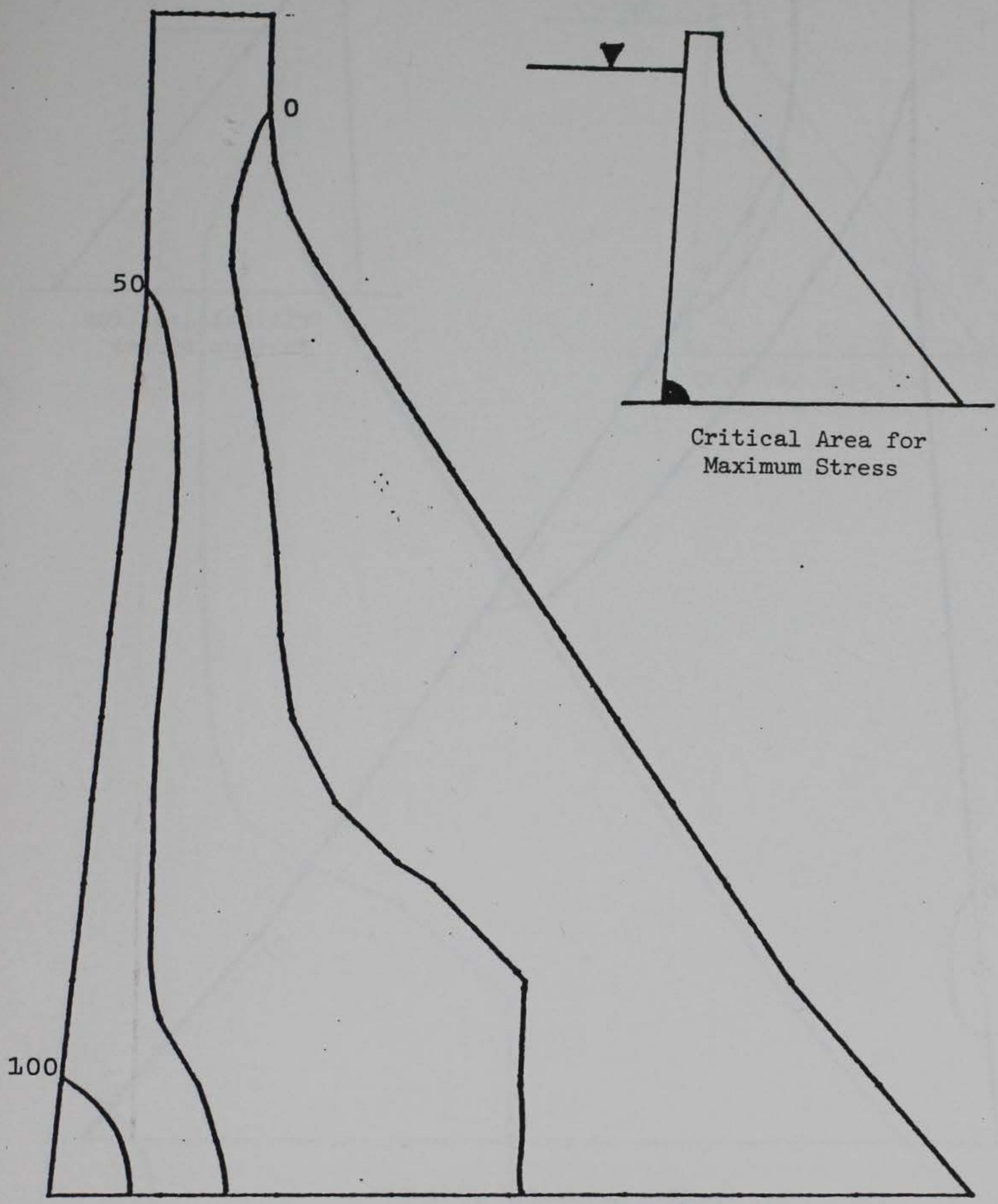

Critical Area for
Maximum Stress

d. Maximum principal stresses
in psi at 7.965 seconds.

Figure 15 (sheet 4 of 4).

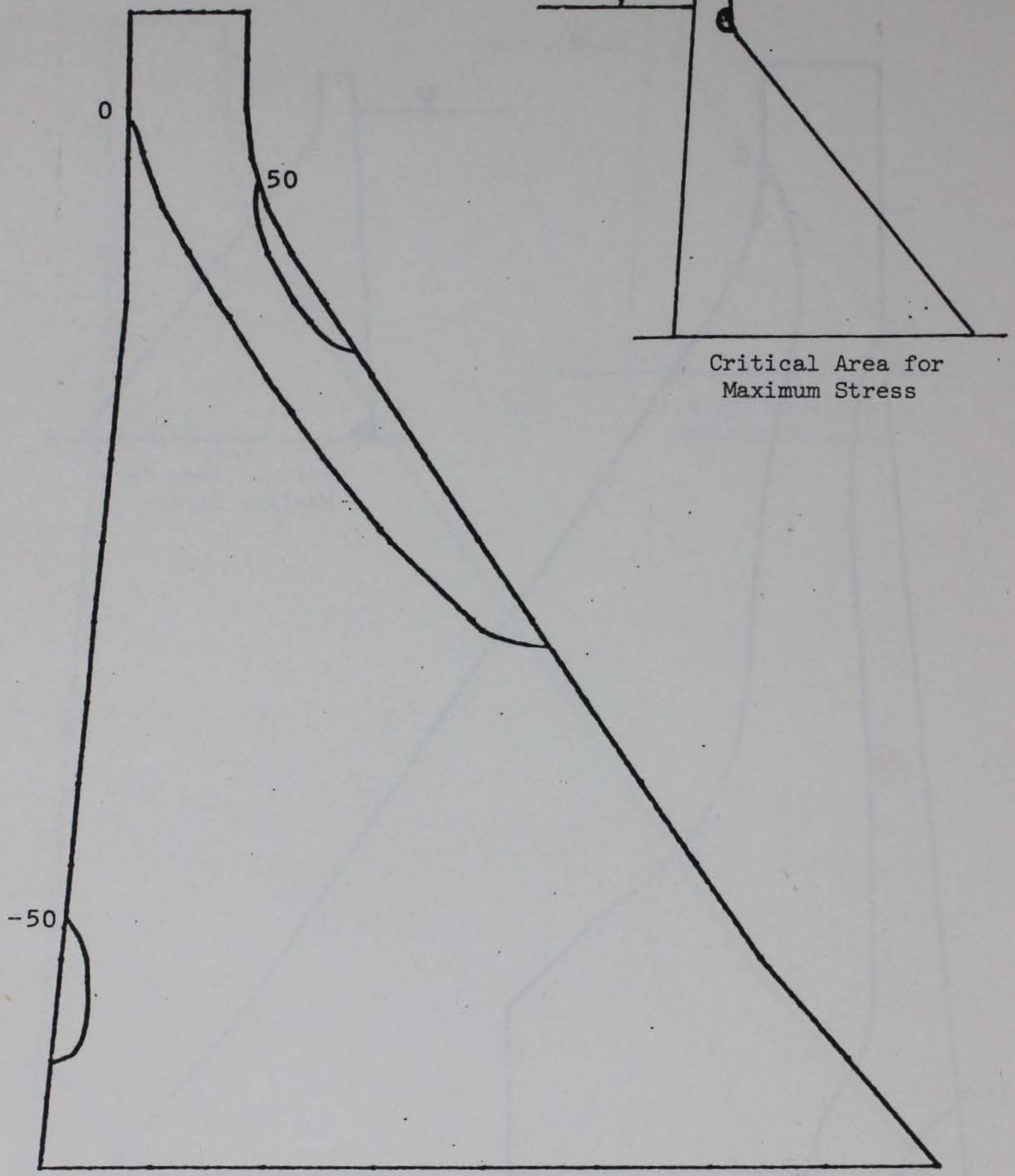

Critical Area for
Maximum Stress

a. Maximum principal stresses
in psi at 1.87 seconds.

Figure 16 Maximum principal stresses in Richard B. Russell Dam due to N65E and vertical components of Parkfield-Cholame Earthquake, 5 percent damping (sheet 1 of 4).

Critical Area for
Maximum Stress

b. Maximum principal stresses
in psi at 4.325 seconds.

Figure 16 (sheet 2 of 4).

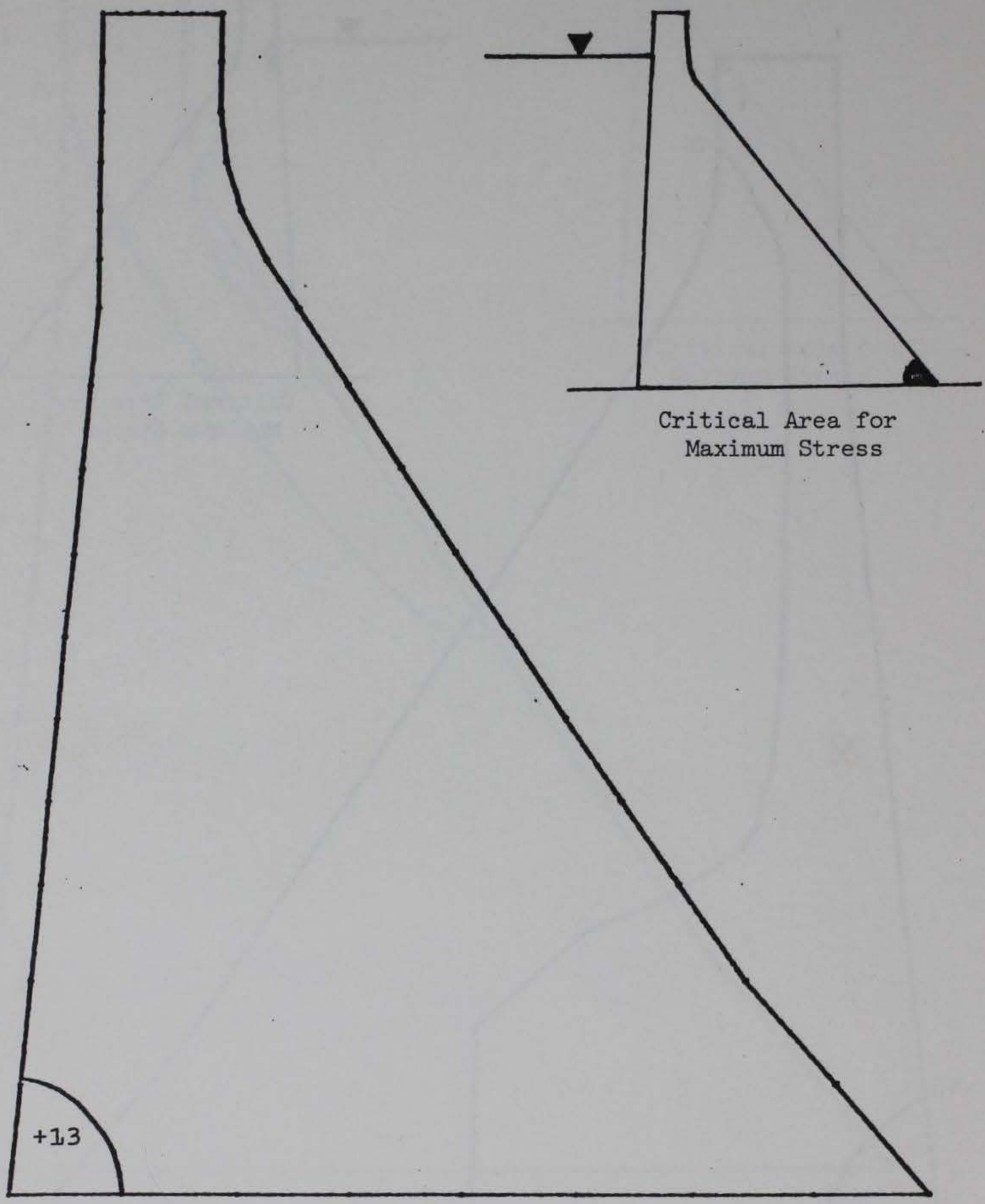

Critical Area for
Maximum Stress

c. Maximum principal stresses
in psi at 0.0 seconds.

Figure 16 (sheet 3 of 4).

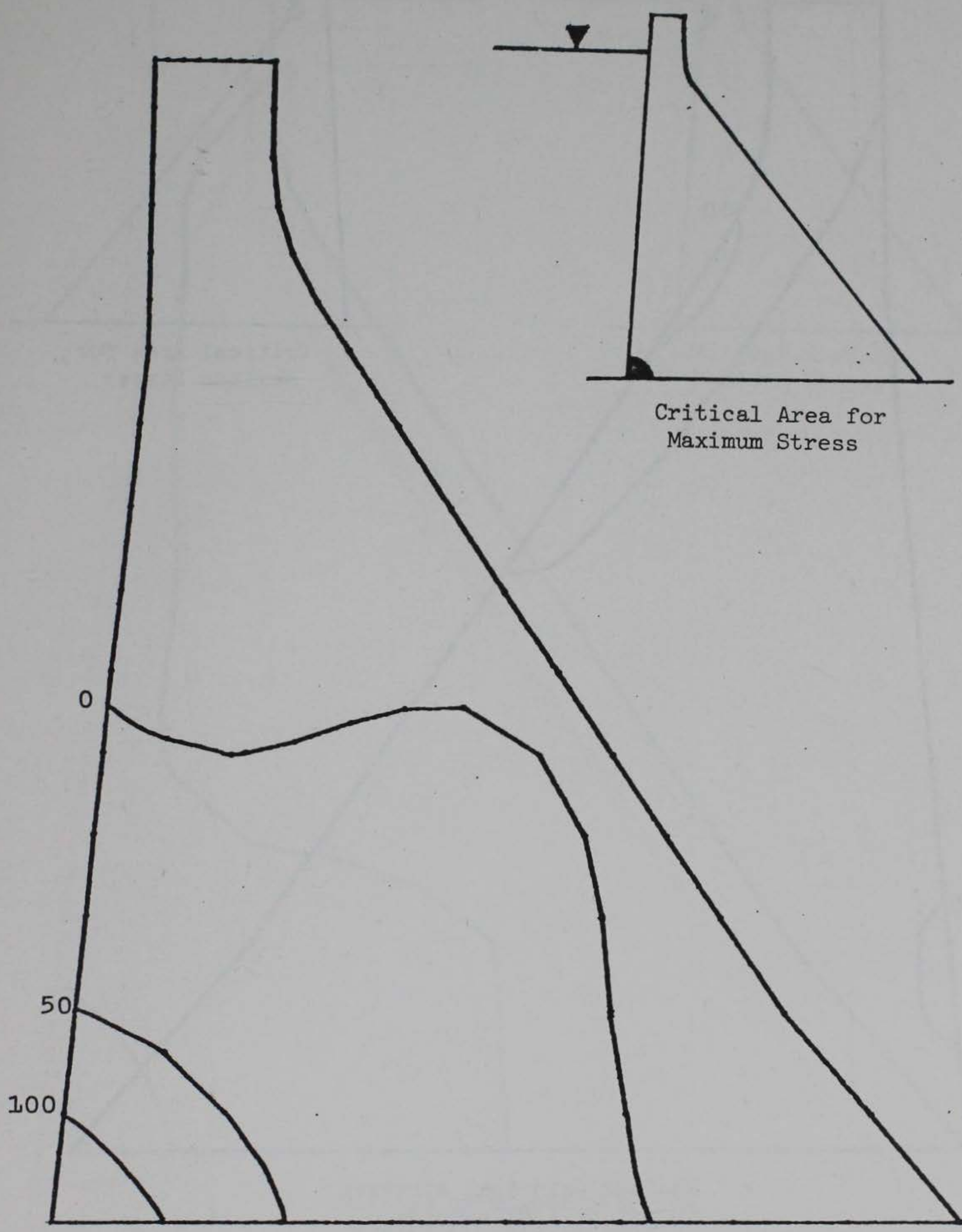

Critical Area for
Maximum Stress

d. Maximum principal stresses
in psi at 3.765 seconds.

Figure 16 (sheet 4 of 4).

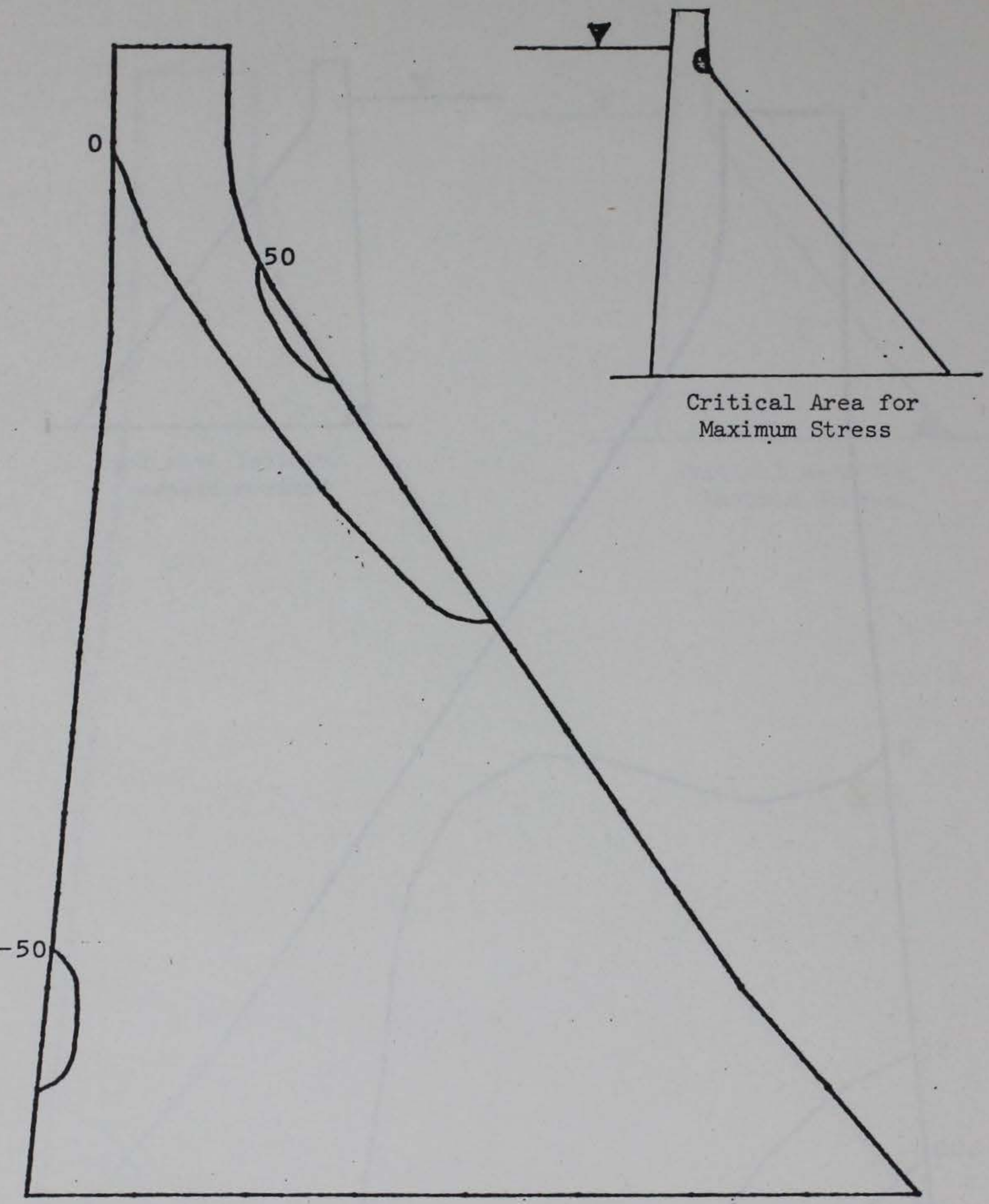

Critical Area for
Maximum Stress

a. Maximum principal stresses
in psi at 1.87 seconds.

Figure 17 Maximum principal stresses in Richard B. Russell Dam due to N65E and vertical components of Parkfield-Cholame Earthquake, 10 percent damping (sheet 1 of 4).

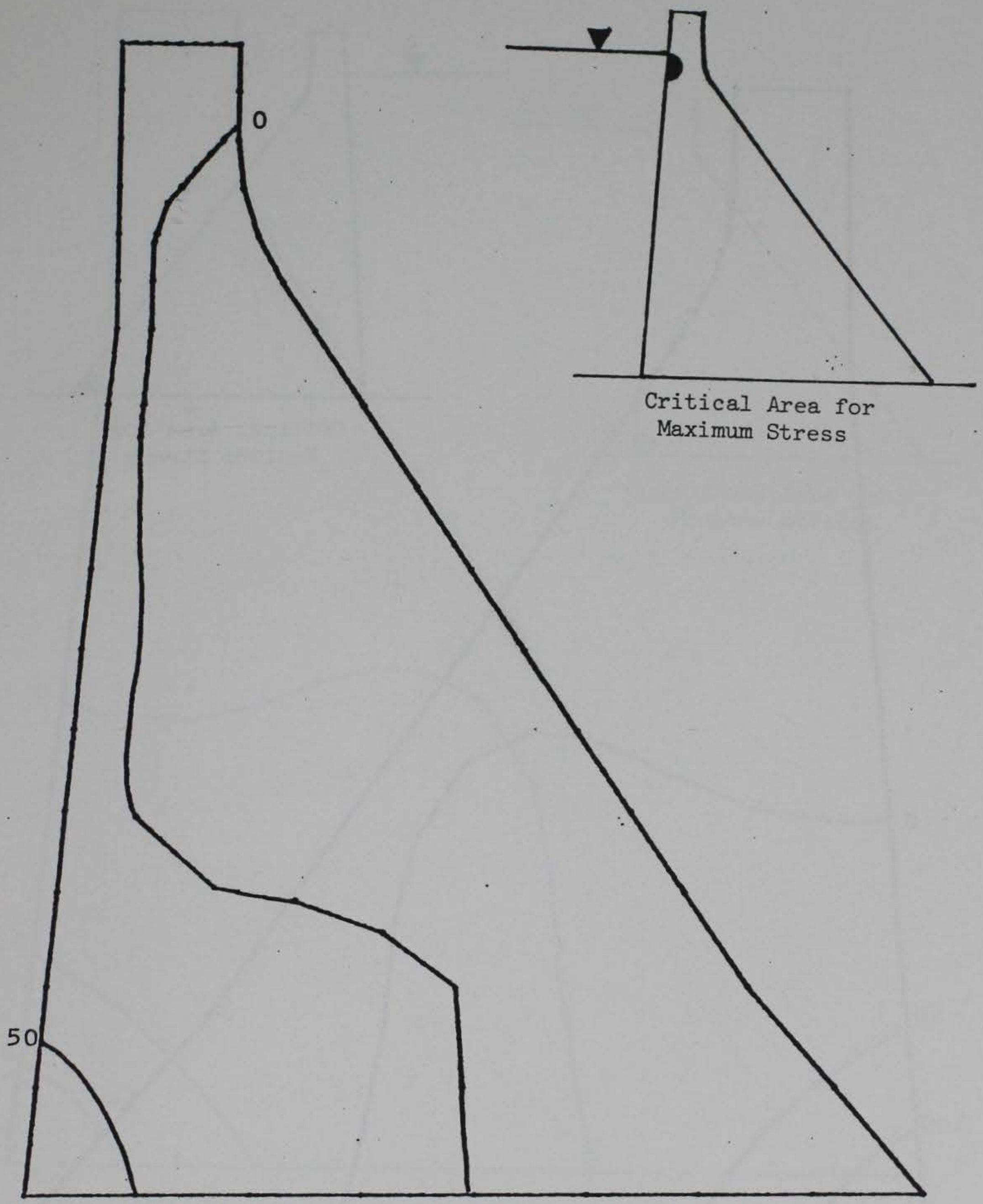

b. Maximum principal stresses
in psi at 4.325 seconds.

Figure 17 (sheet 2 of 4).

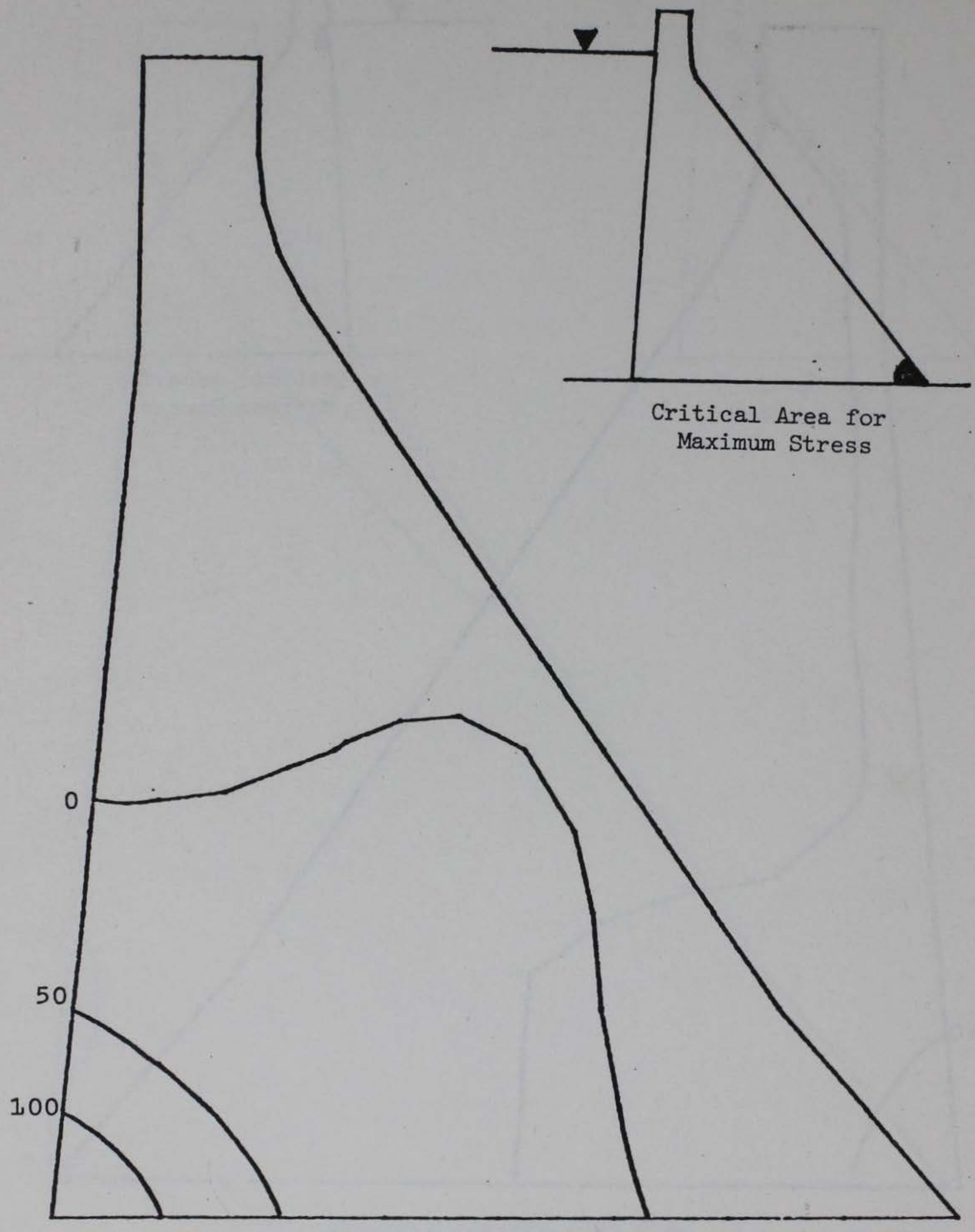

Critical Area for
Maximum Stress

c. Maximum principal stresses
in psi at 3.755 seconds.

Figure 17 (sheet 3 of 4).

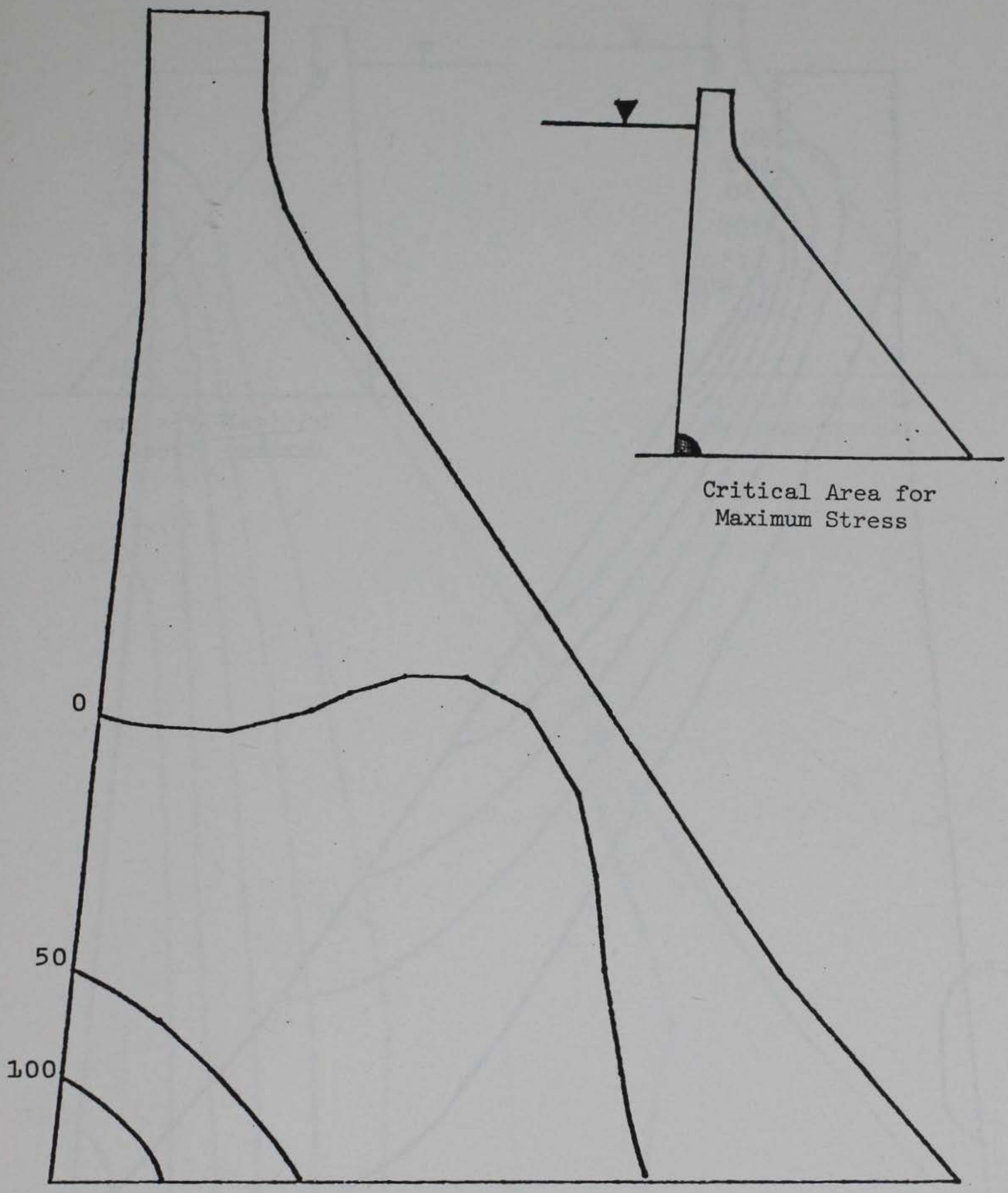

Critical Area for
Maximum Stress

d. Maximum principal stresses
in psi at 3.765 seconds.

Figure 17 (sheet 4 of 4).

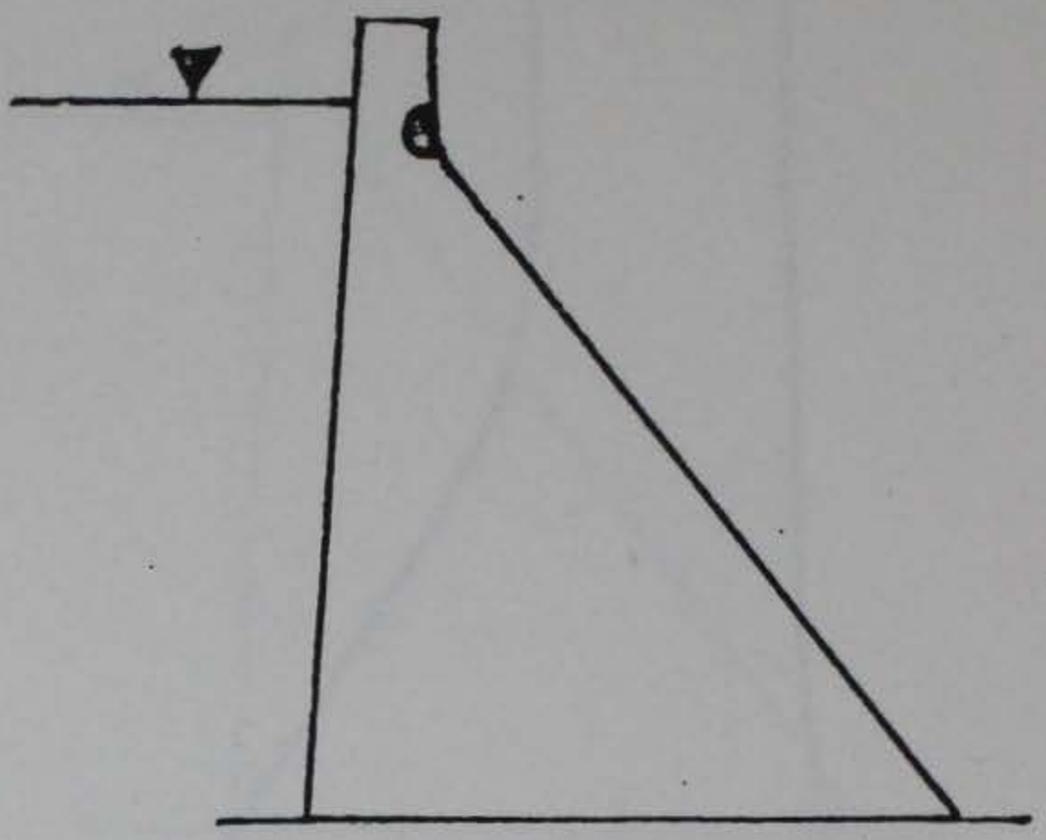

Critical Area for
Maximum Stress

a. Maximum principal stresses
in psi at 2.645 seconds.

Figure 18 Maximum principal stresses in Richard B. Russell Dam due to N90E and vertical components of Helena Earthquake, 5 percent damping (sheet 1 of 4).

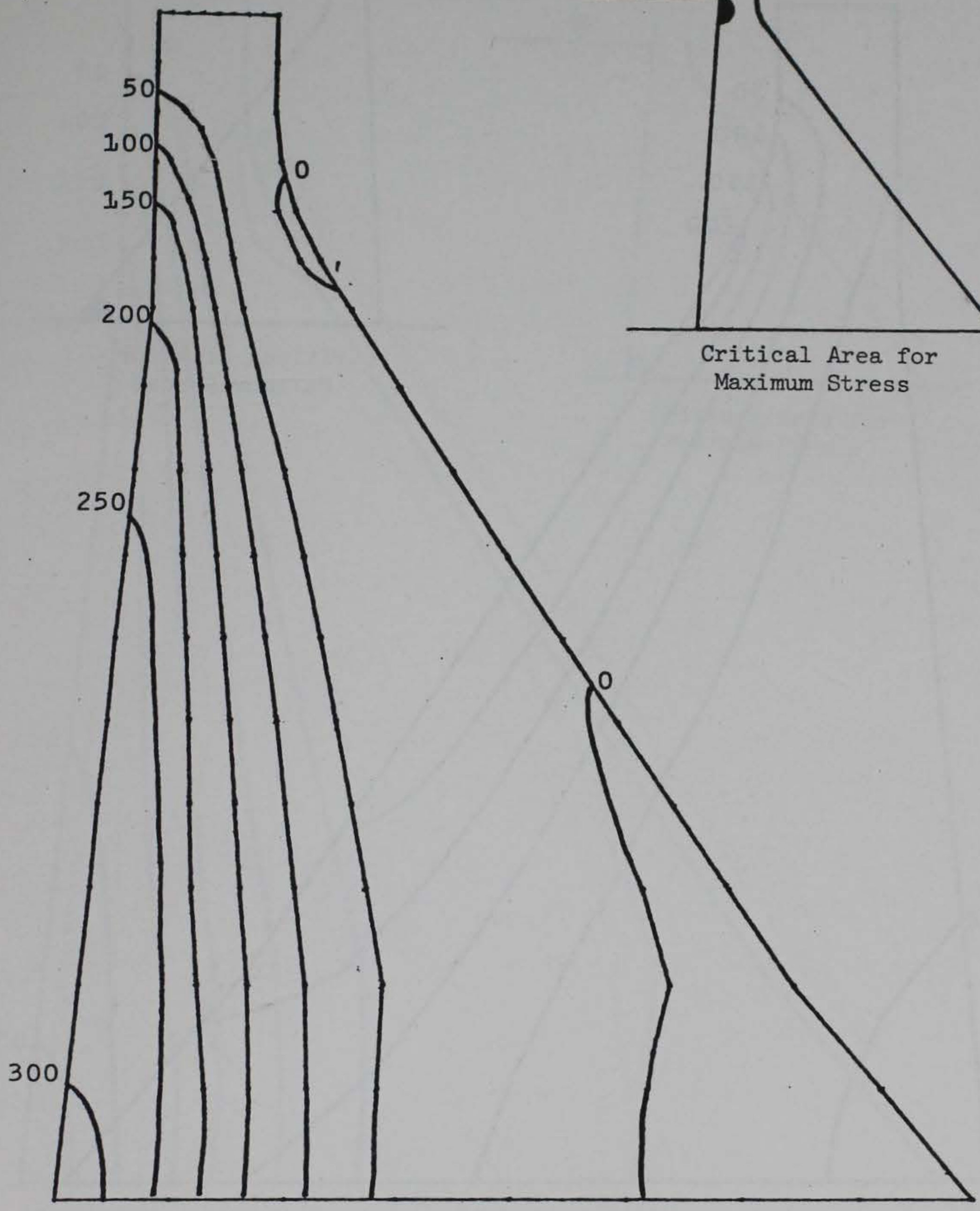

Critical Area for
Maximum Stress

b. Maximum principal stresses
in psi at 2.71 seconds.

Figure 18 (sheet 2 of 4).

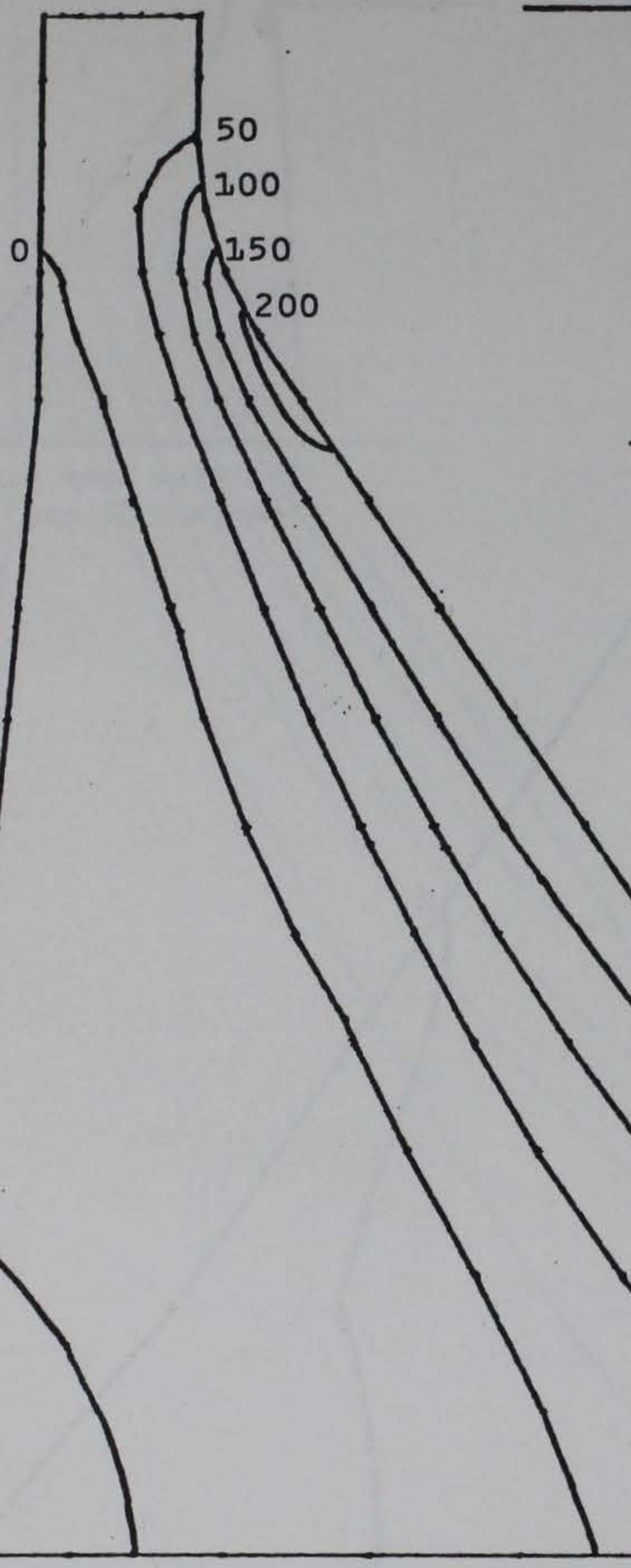

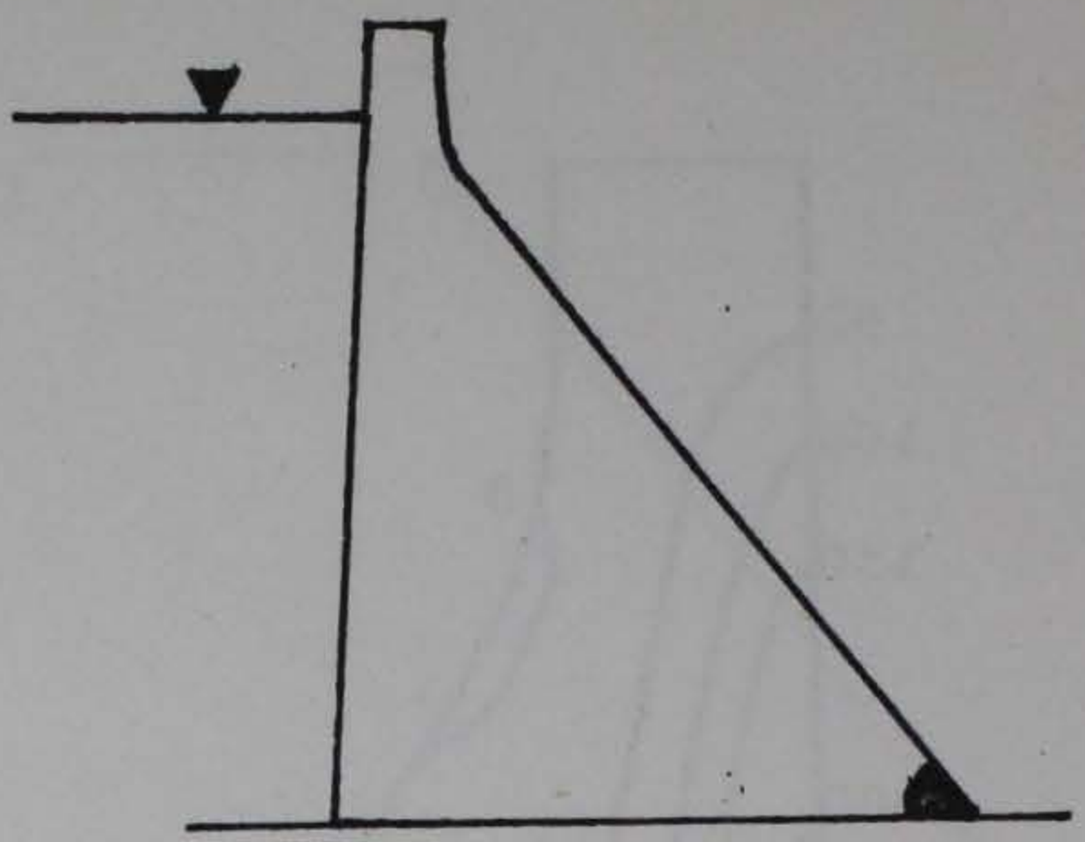

Critical Area for
Maximum Stress

c. Maximum principal stresses
in psi at 2.97 seconds.

Figure 18 (sheet 3 of 4).

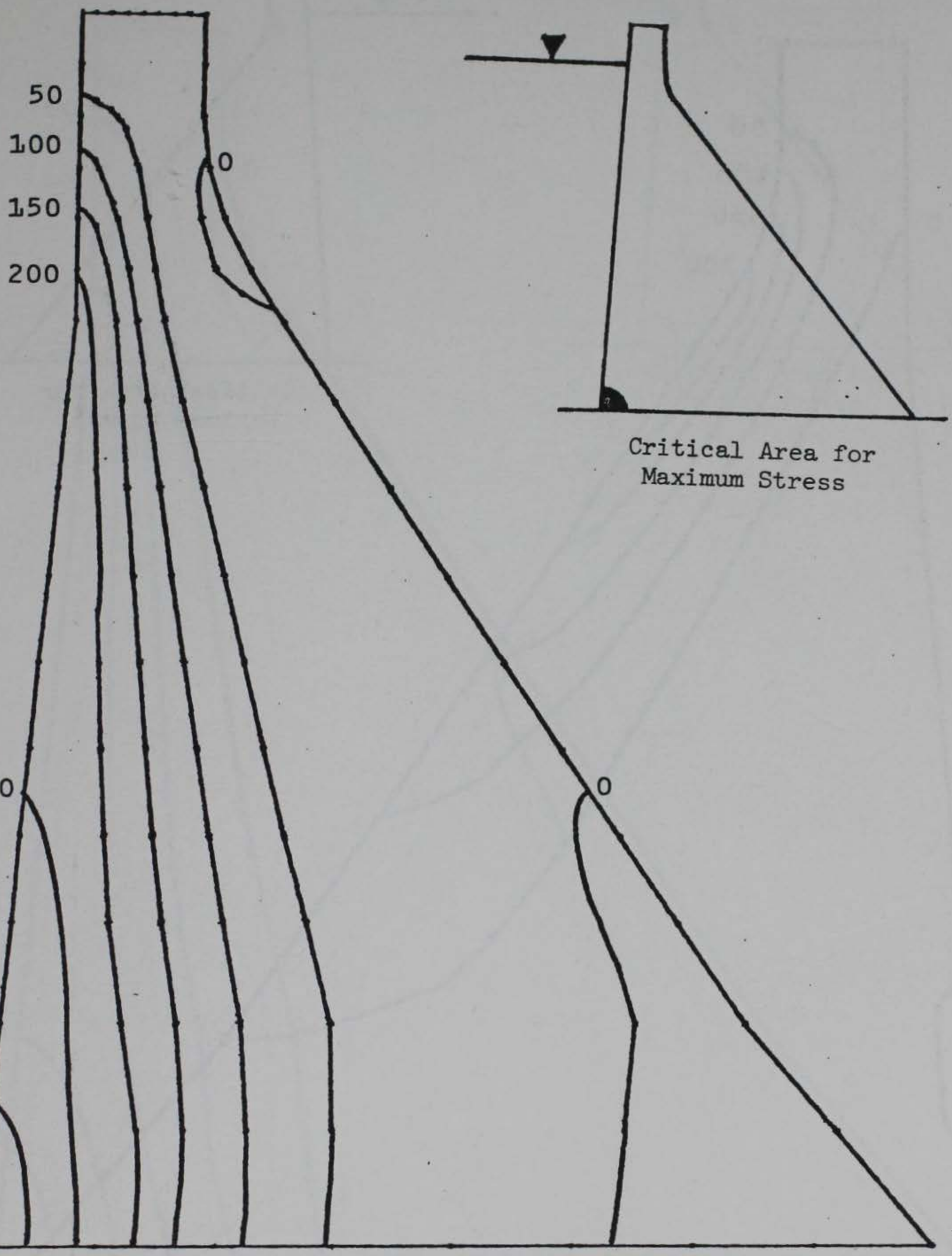

Critical Area for
Maximum Stress

d. Maximum principal stresses
in psi at 2.875 seconds.

Figure 18 (sheet 4 of 4).

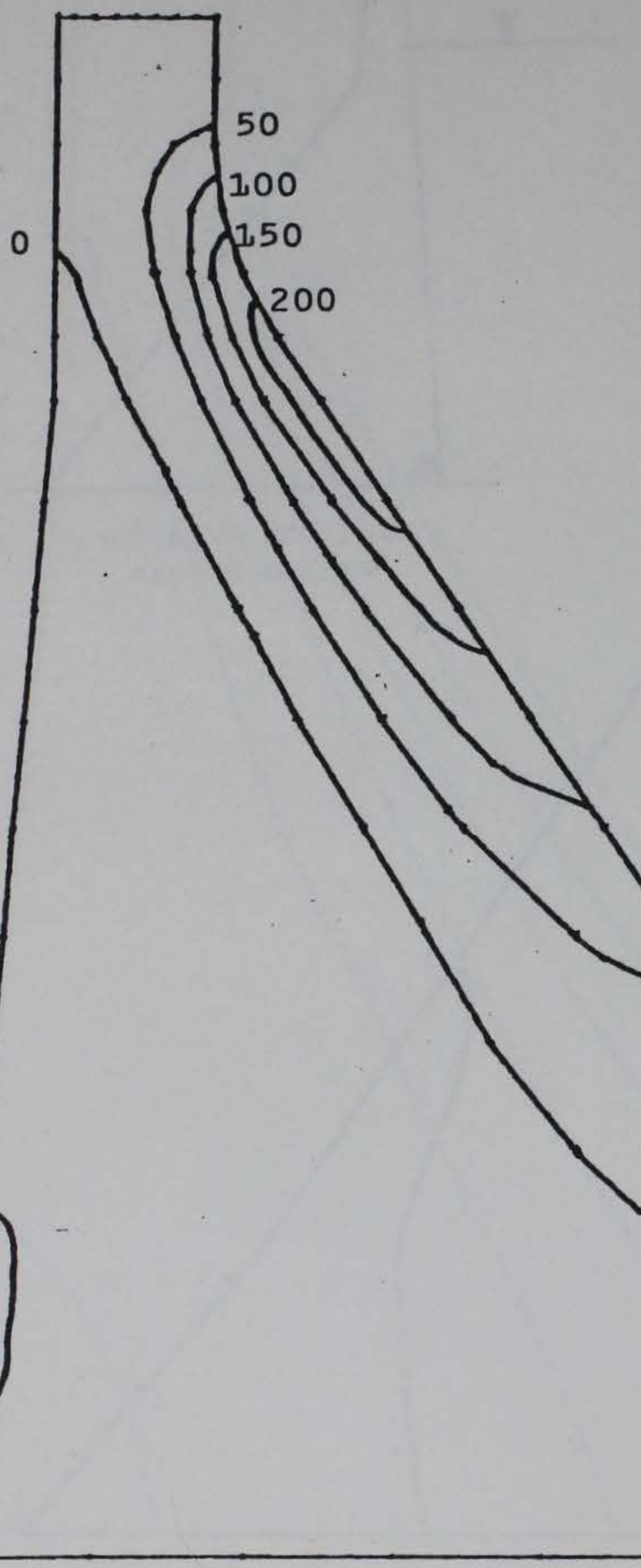

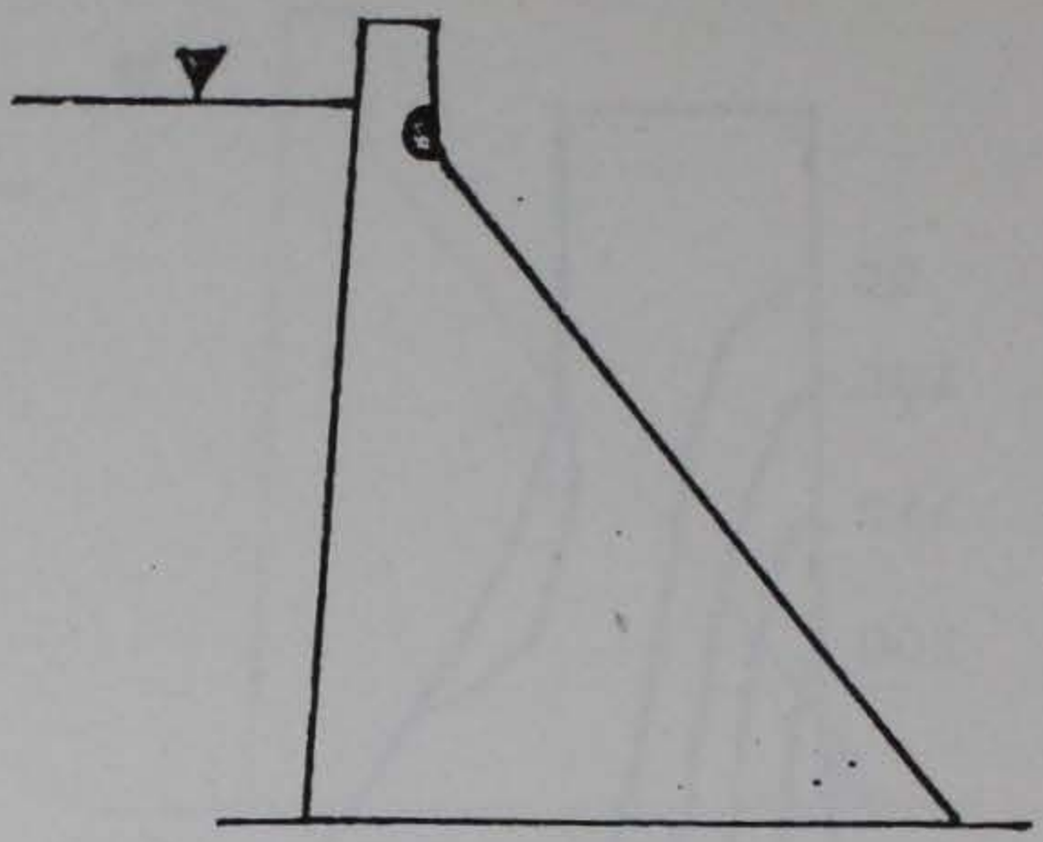

Critical Area for
Maximum Stress

a. Maximum principal stresses
in psi at 2.645 seconds.

Figure 19 Maximum principal stresses in Richard B. Russell Dam due to SOOW and vertical components of Helena Earthquake, 10 percent damping (sheet 1 of 4).

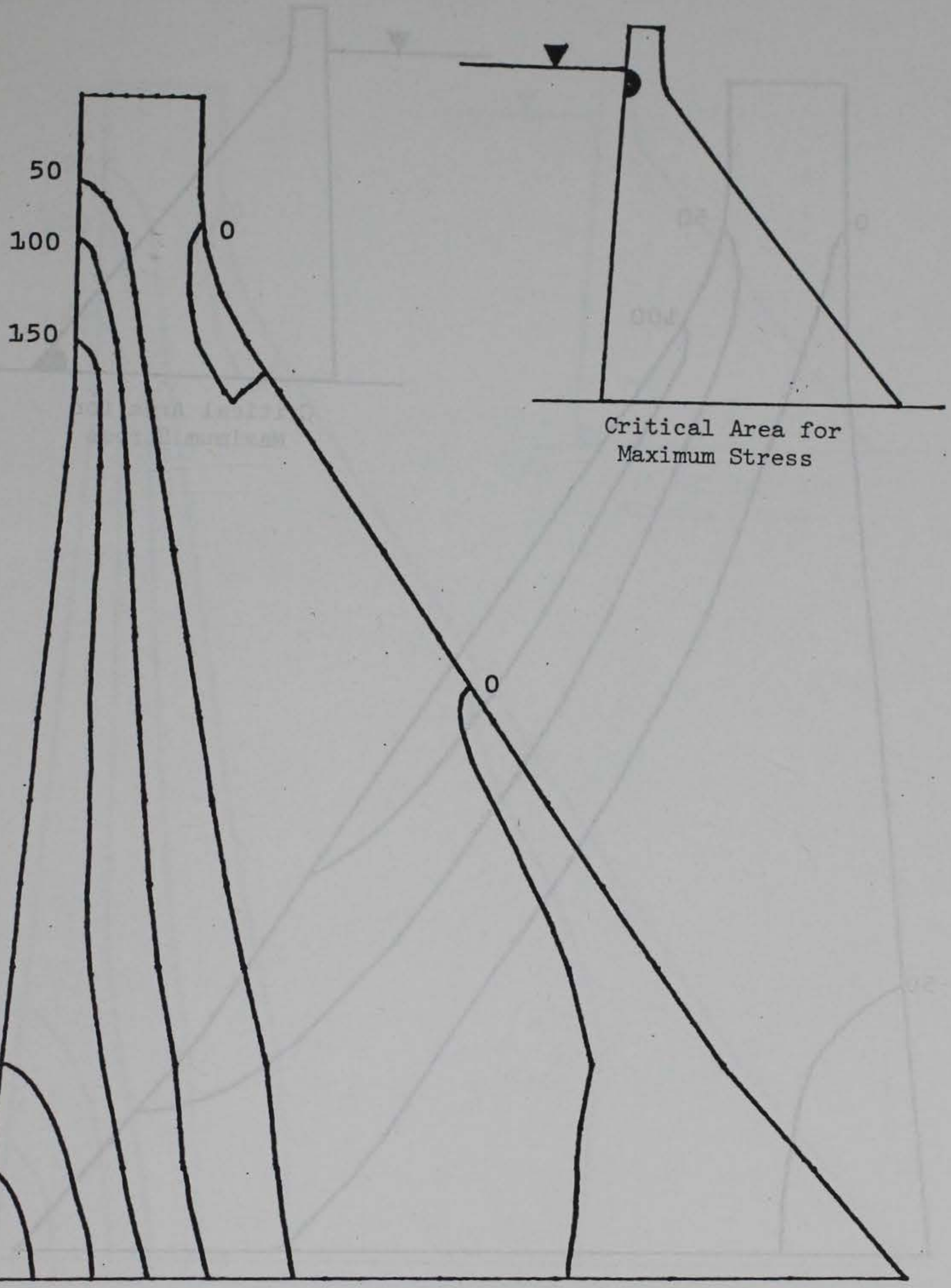

b. Maximum principal stresses
in psi at 2.87 seconds.

Figure 19 (sheet 2 of 4).

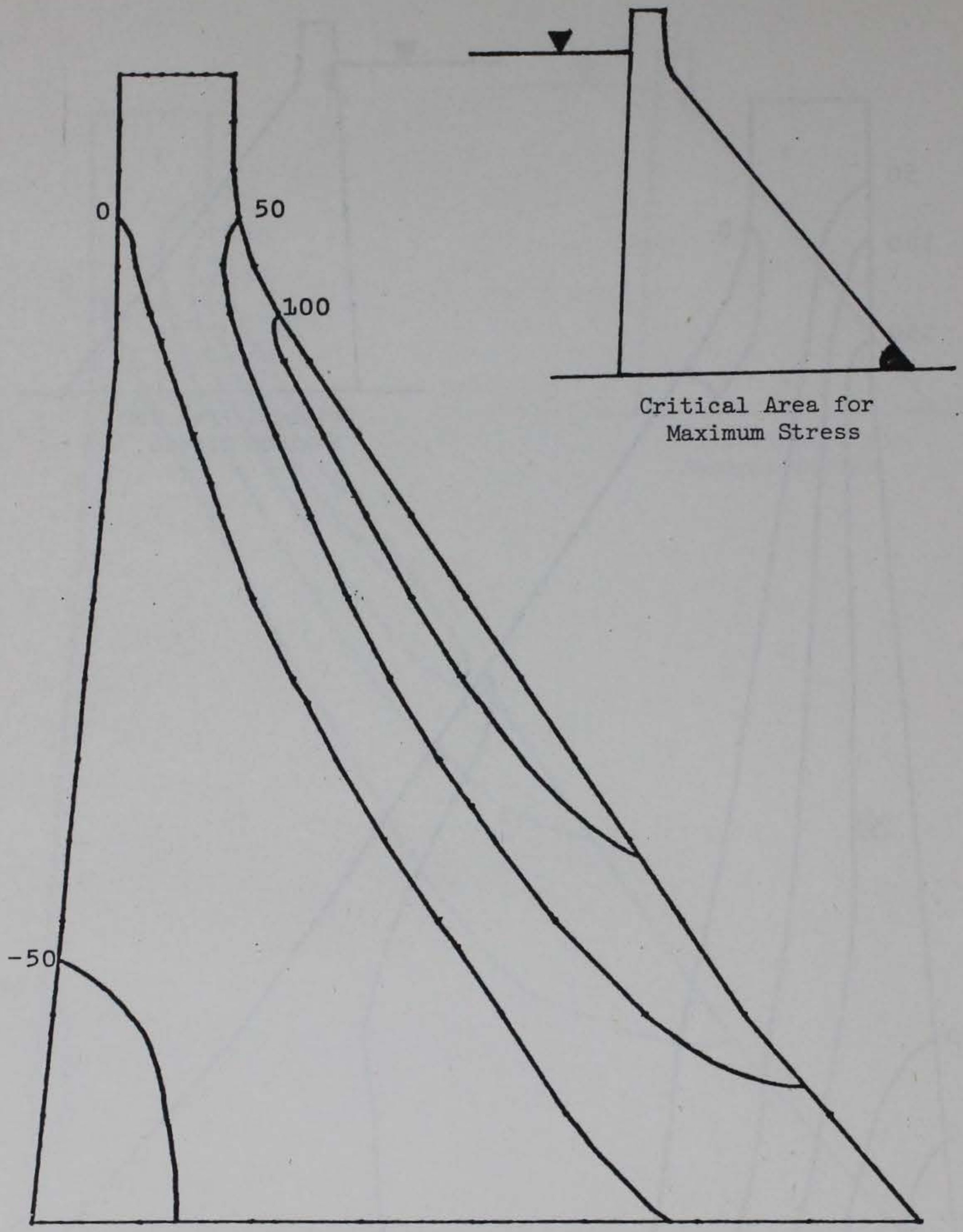

Critical Area for
Maximum Stress

c. Maximum principal stresses
in psi at 2.62 seconds.

Figure 19 (sheet 3 of 4).

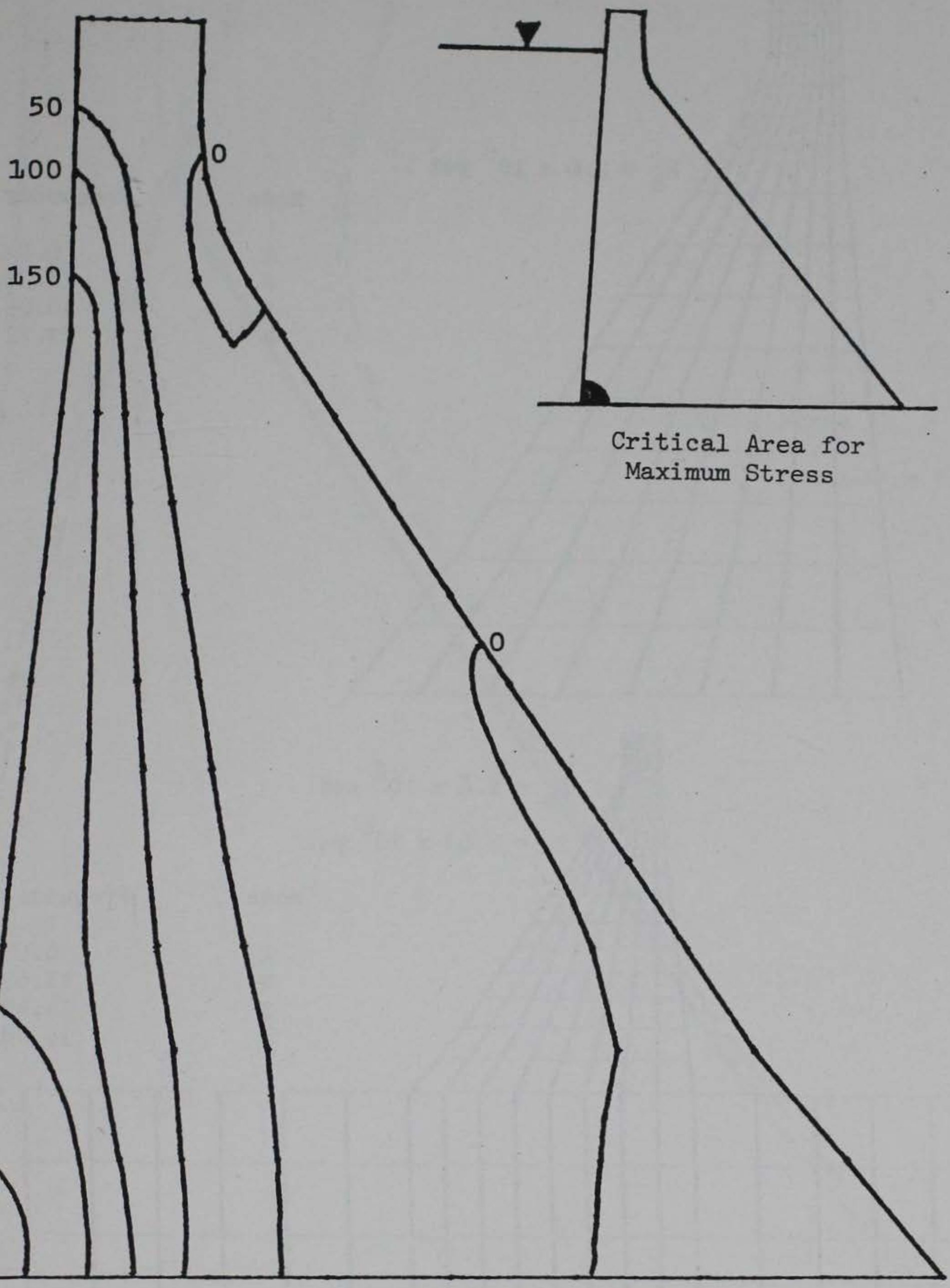

Critical Area for
Maximum Stress

d. Maximum principal stresses
in psi at 2.87 seconds.

Figure 19 (sheet 4 of 4).

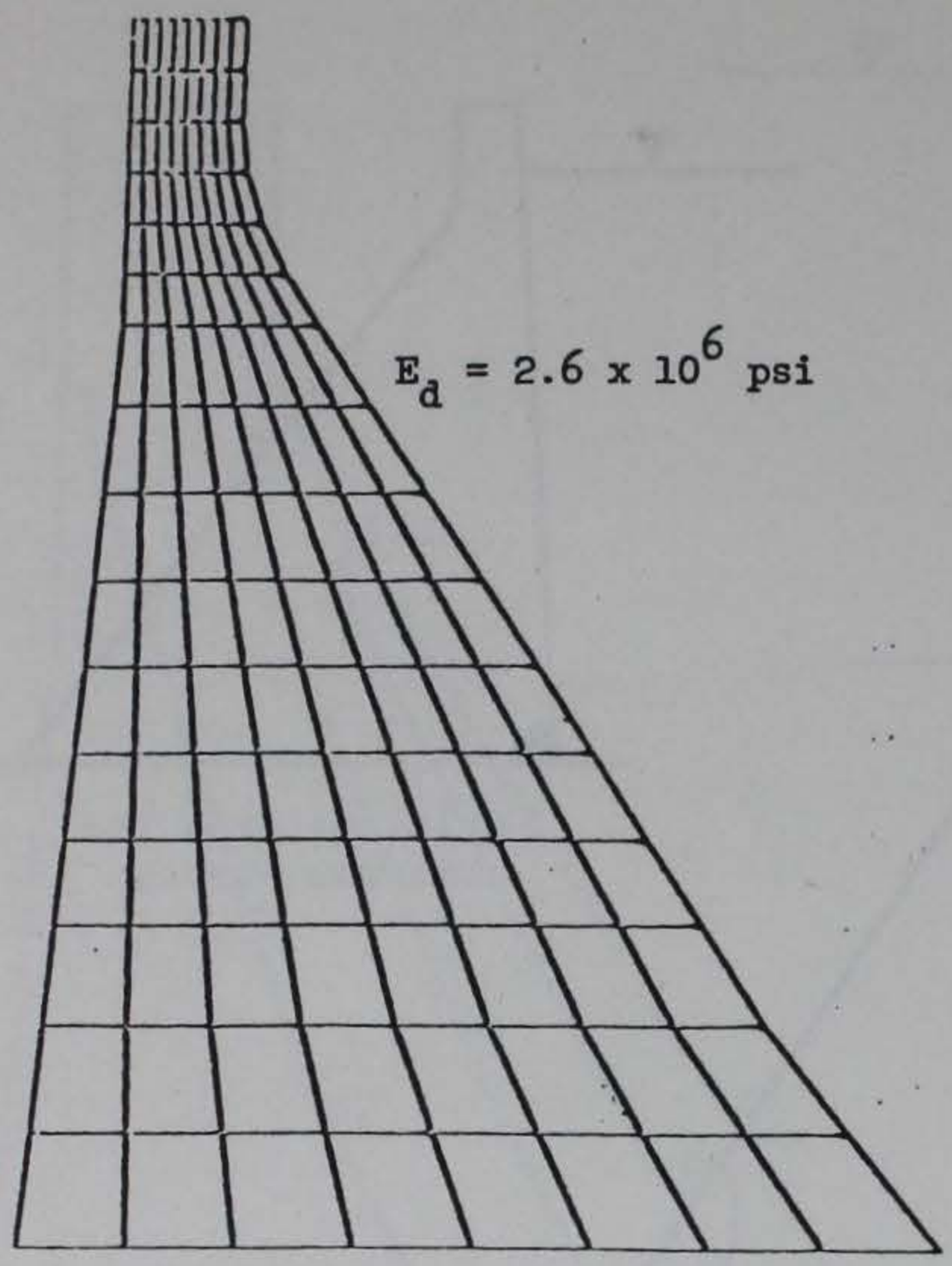

$E_d = 2.6 \times 10^6$ psi

Mode	Frequency (Hz)
1	6.541
2	14.30
3	19.05
4	25.22

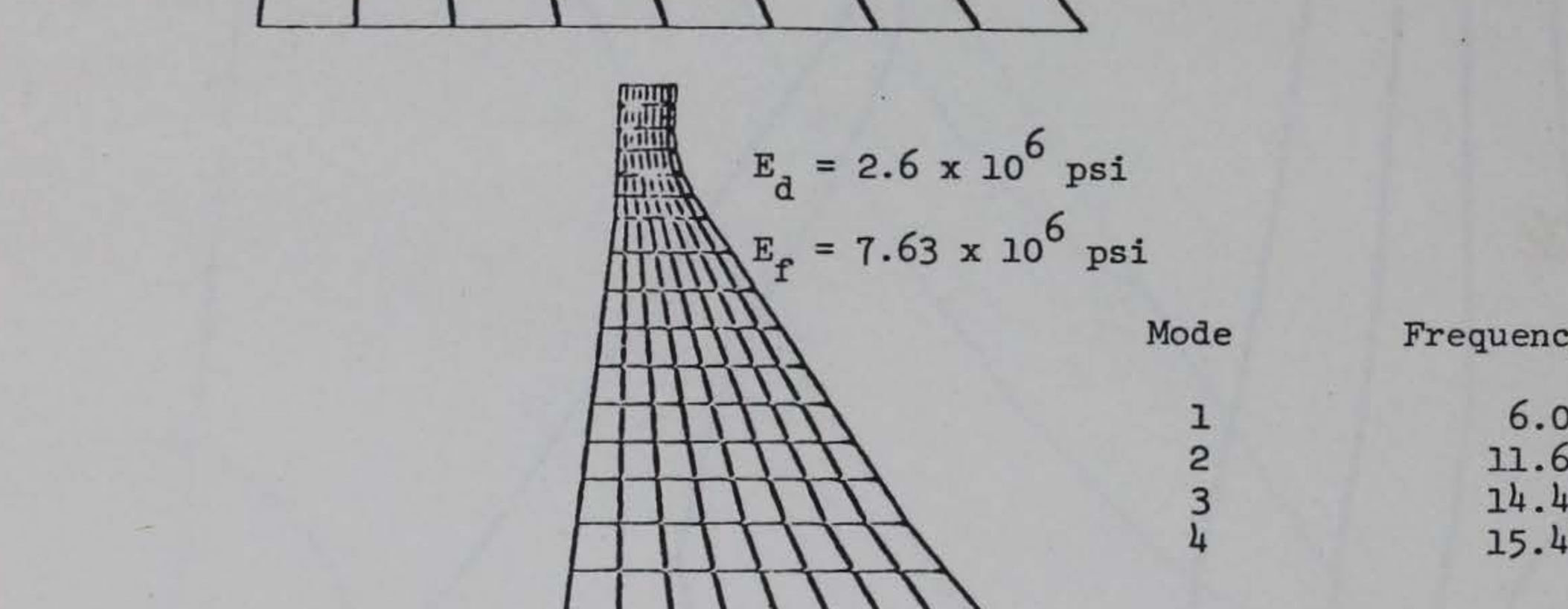

$E_d = 2.6 \times 10^6$ psi

$E_f = 7.63 \times 10^6$ psi

Mode	Frequency (Hz)
1	6.034
2	11.63
3	14.49
4	15.48

Figure 20. Elastic moduli and natural frequencies for the Richard B. Russell Dam, for the case of a fixed base and that with foundation included.

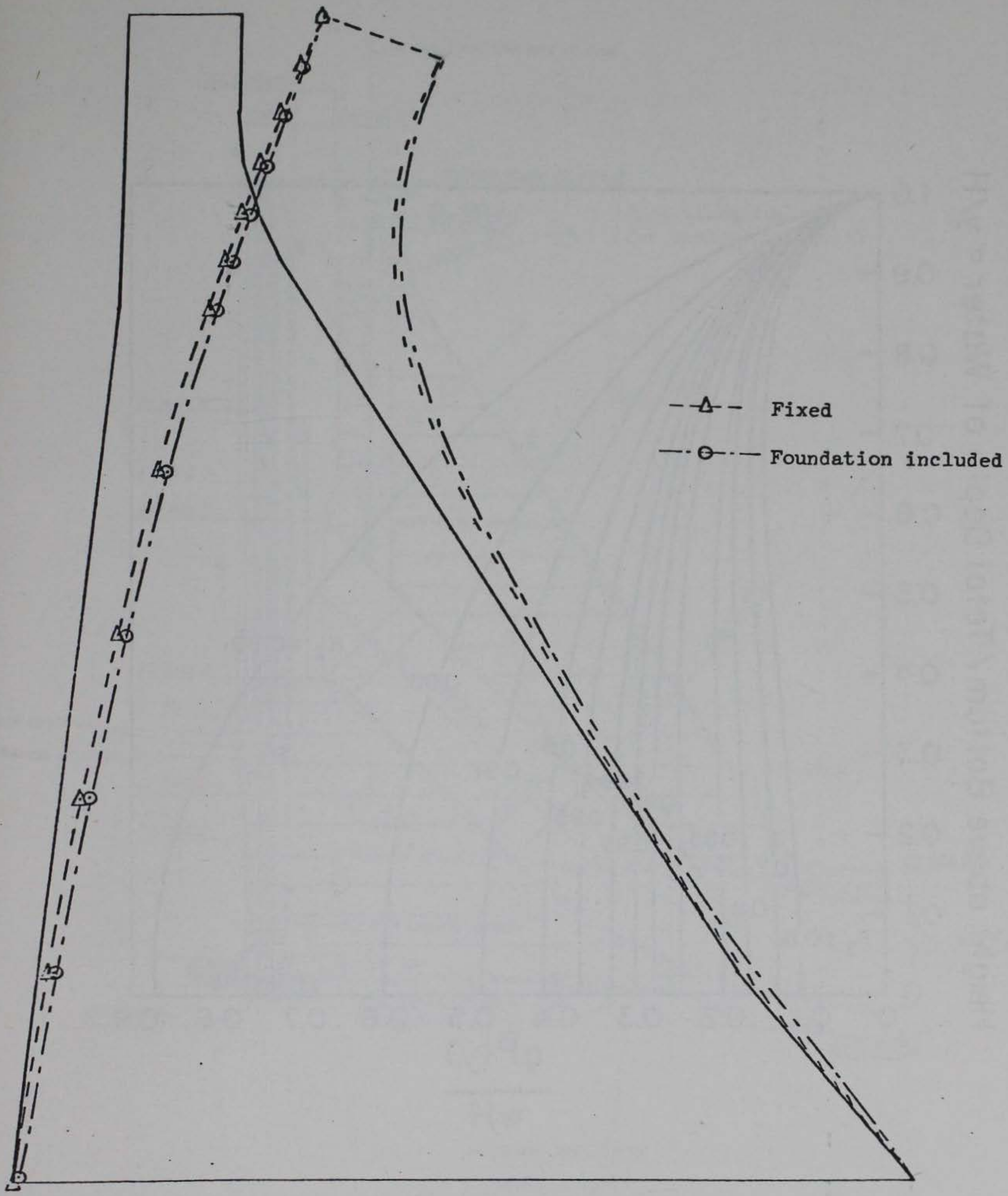

Figure 21. Normalized fundamental mode shapes for Richard B. Russell nonoverflow monolith. Foundation conditions are those illustrated in Figure 20.

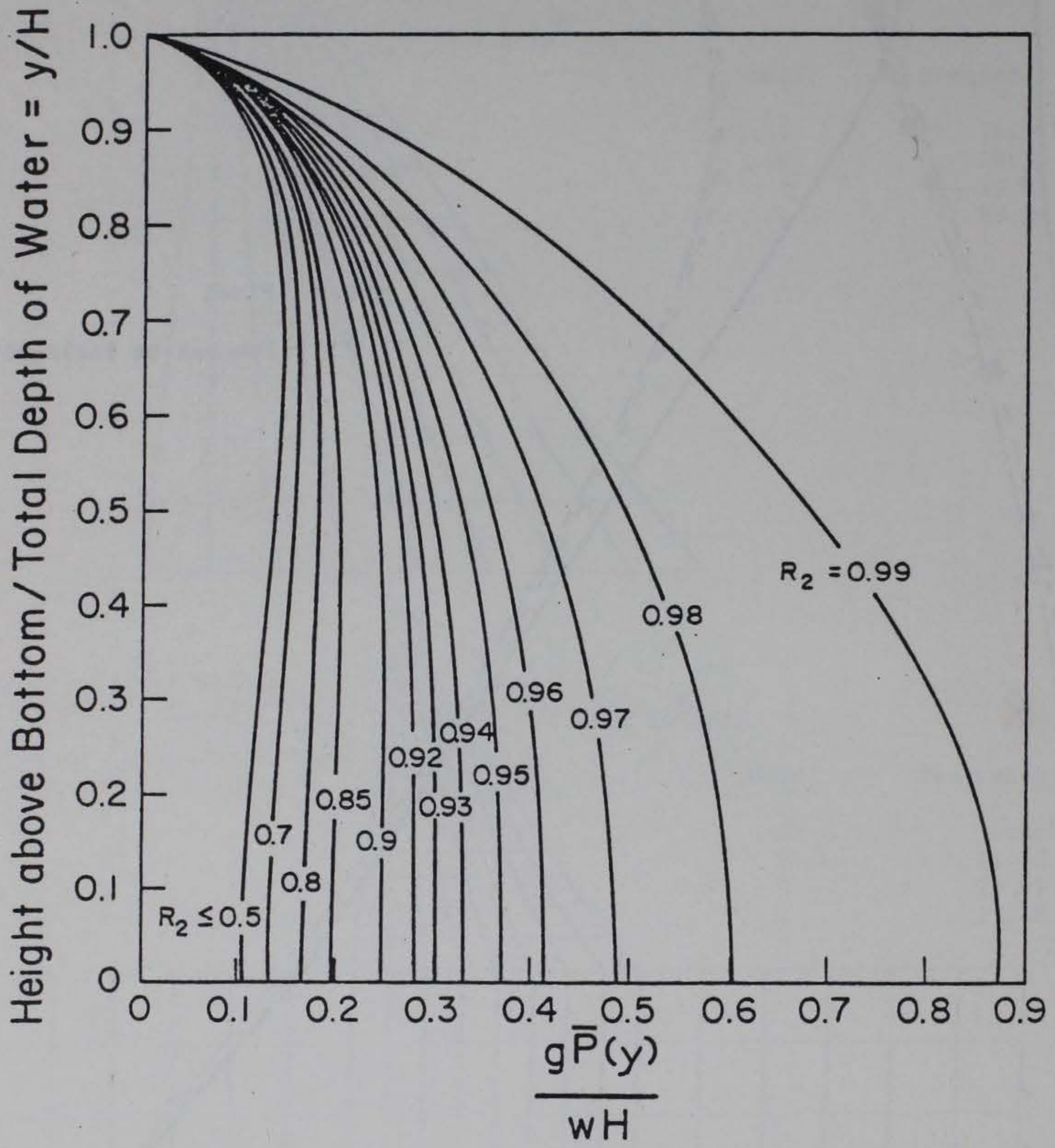

Figure 22 Standard plots for variation of $\bar{P}(y)$ over the depth of water for $H/H_s = 1$ and various values of R_2.

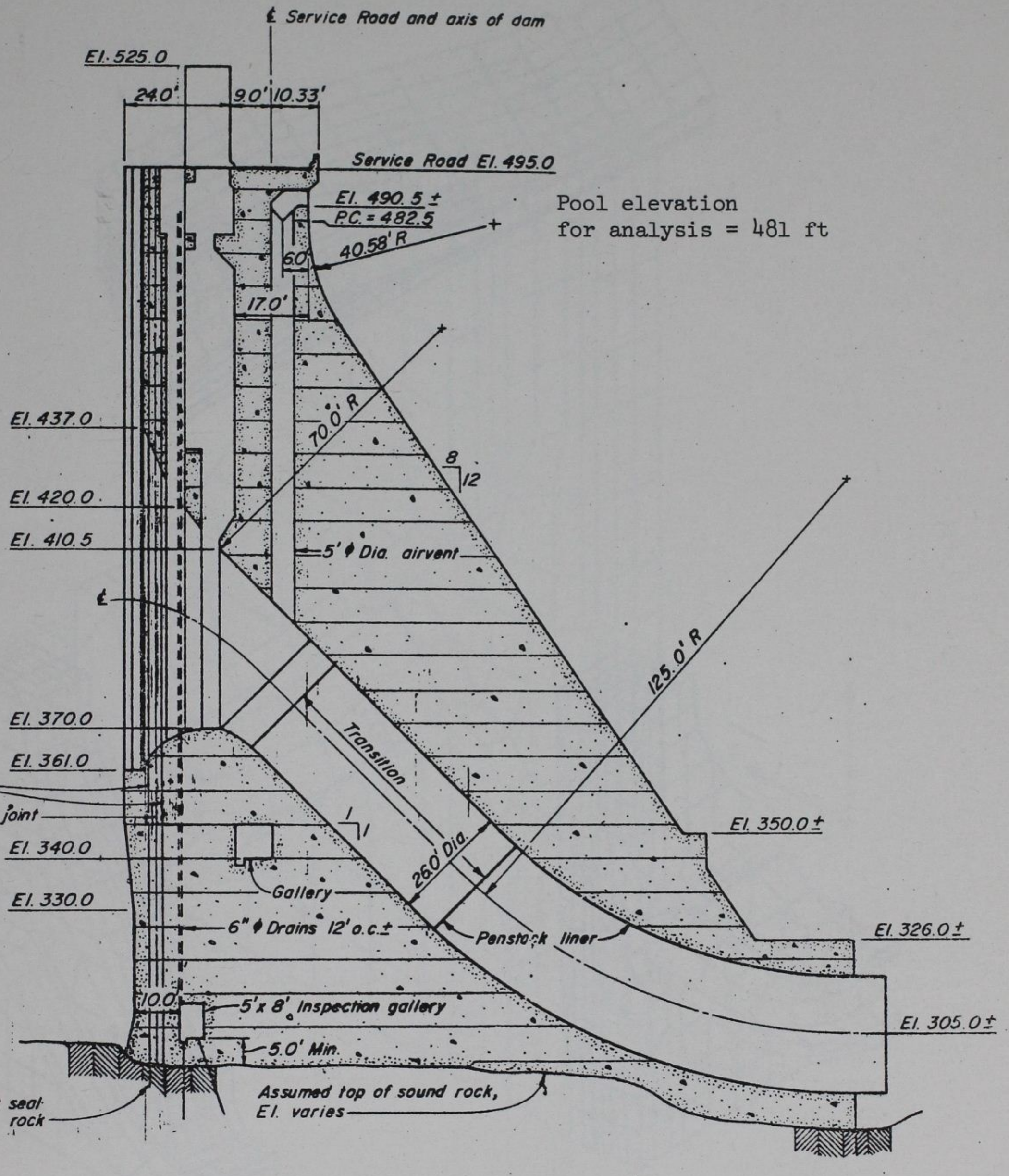

INTAKE SECTION

SCALE: 1" = 20'

Figure 23 Intake section, Richard B. Russell Dam.

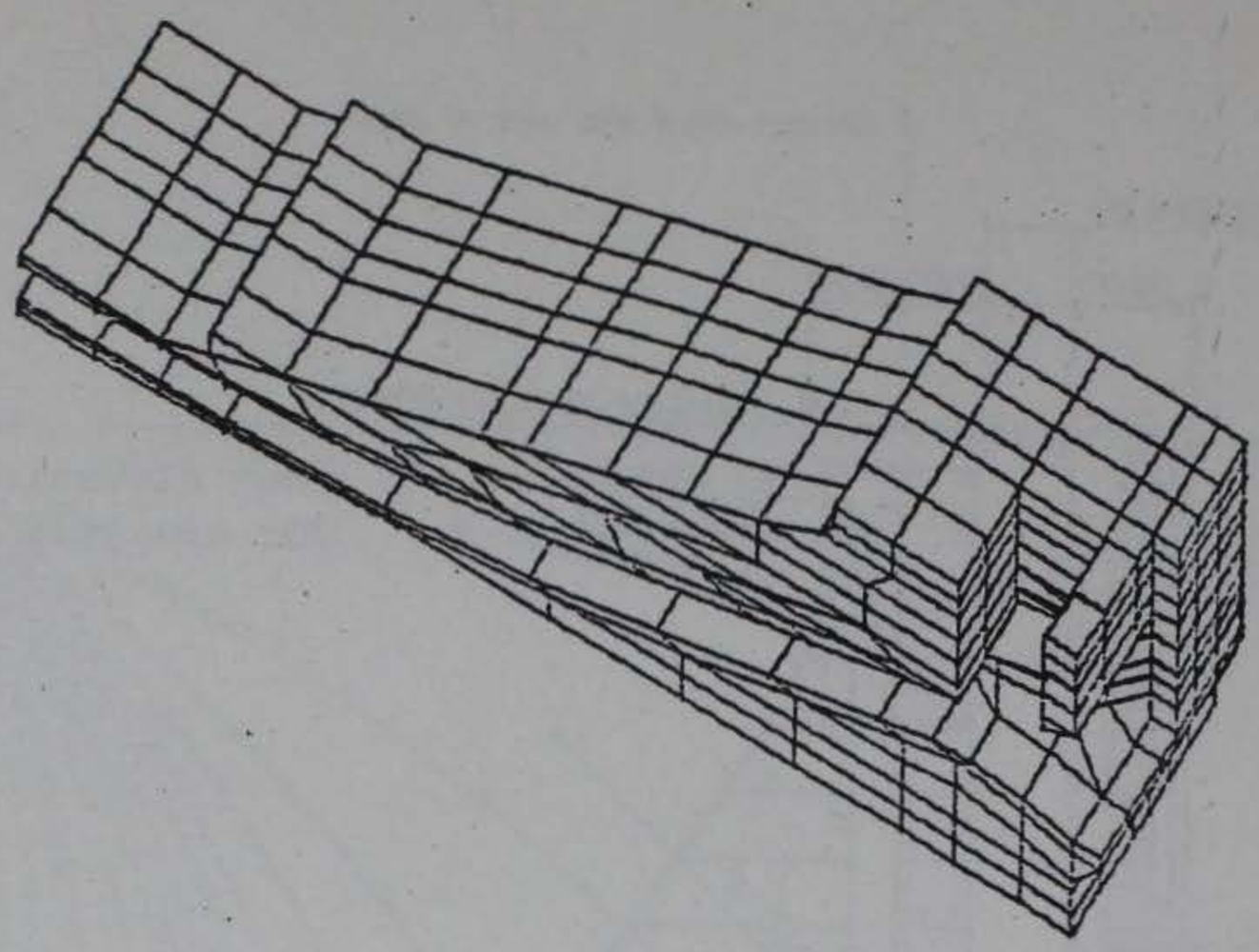

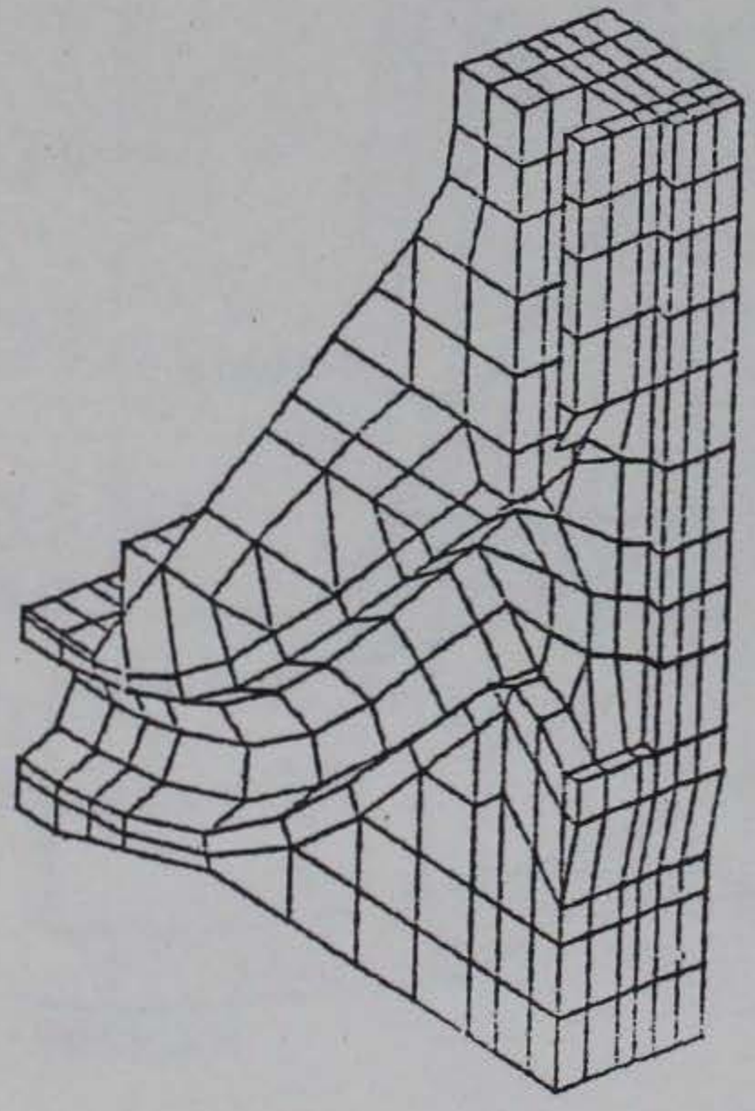

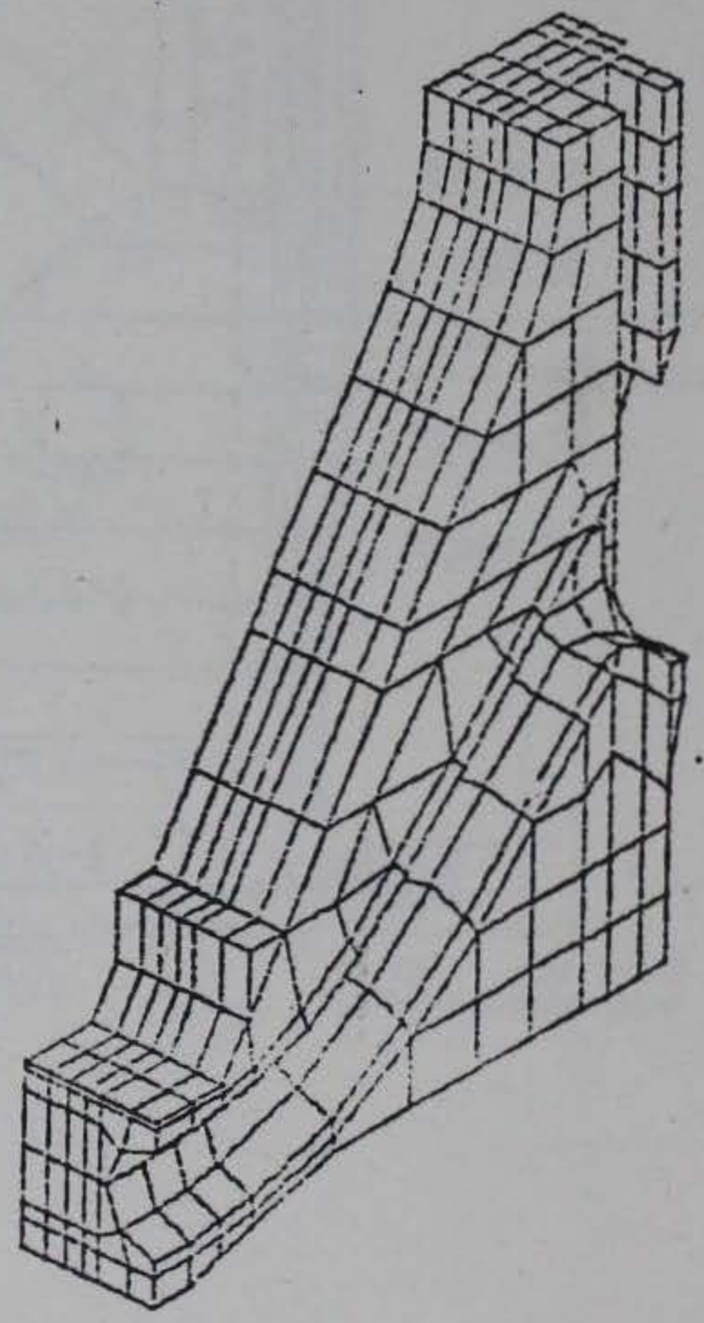

Figure 24 Finite element grid, intake section, Richard B. Russell Dam.

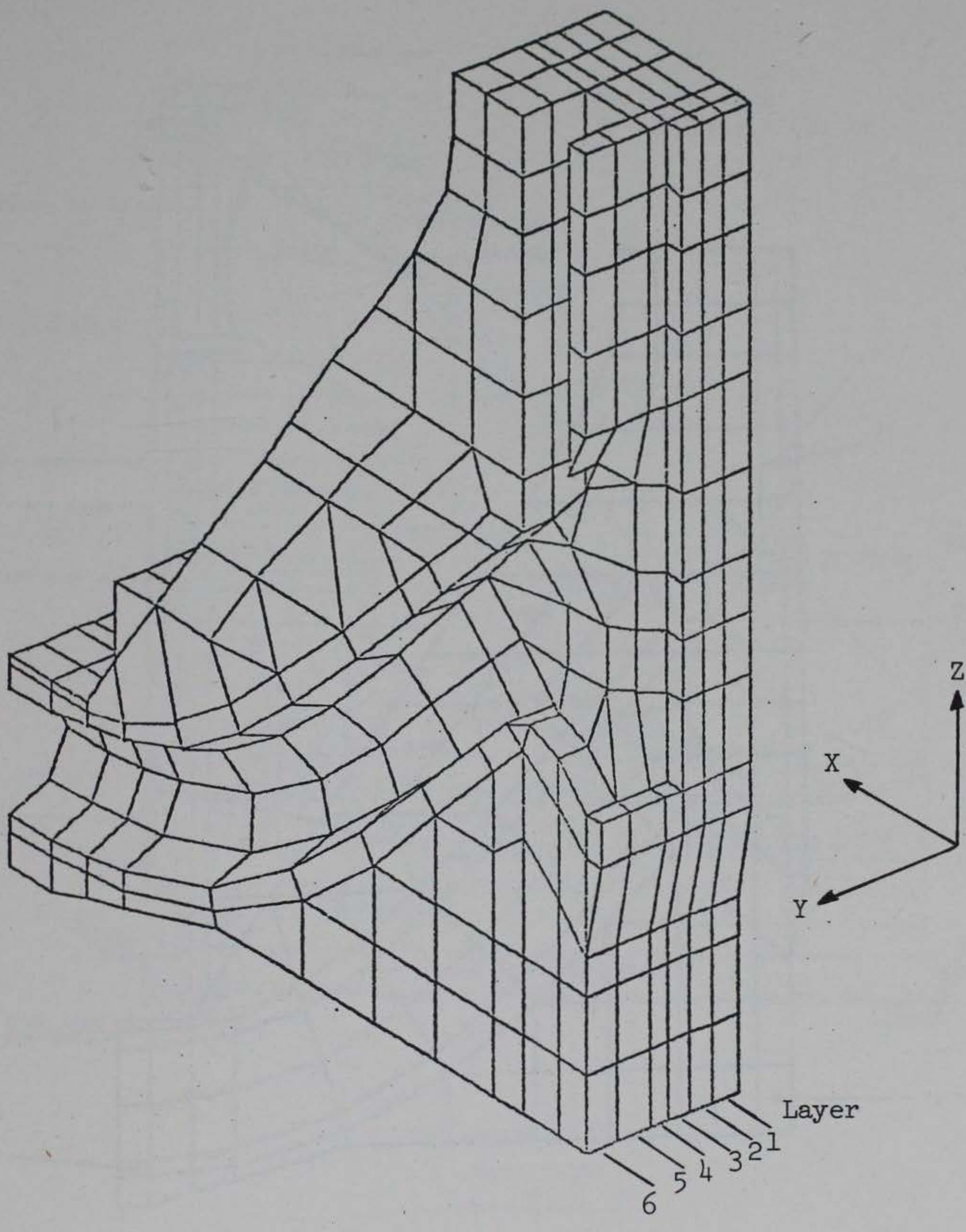

Figure 25 Layering of intake section finite element grid.

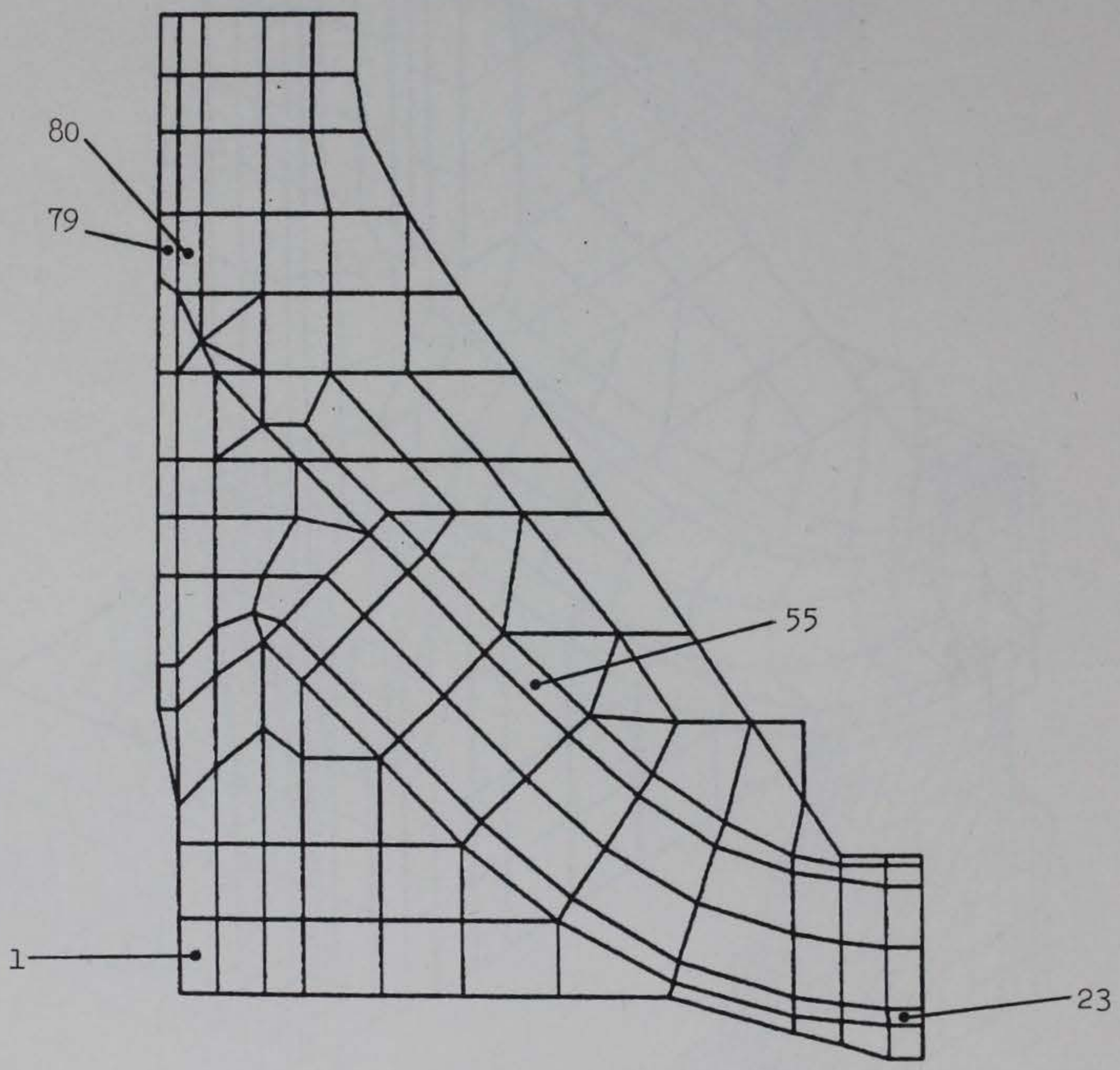

Figure 26 Finite element grid, intake section
(critical elements identified)

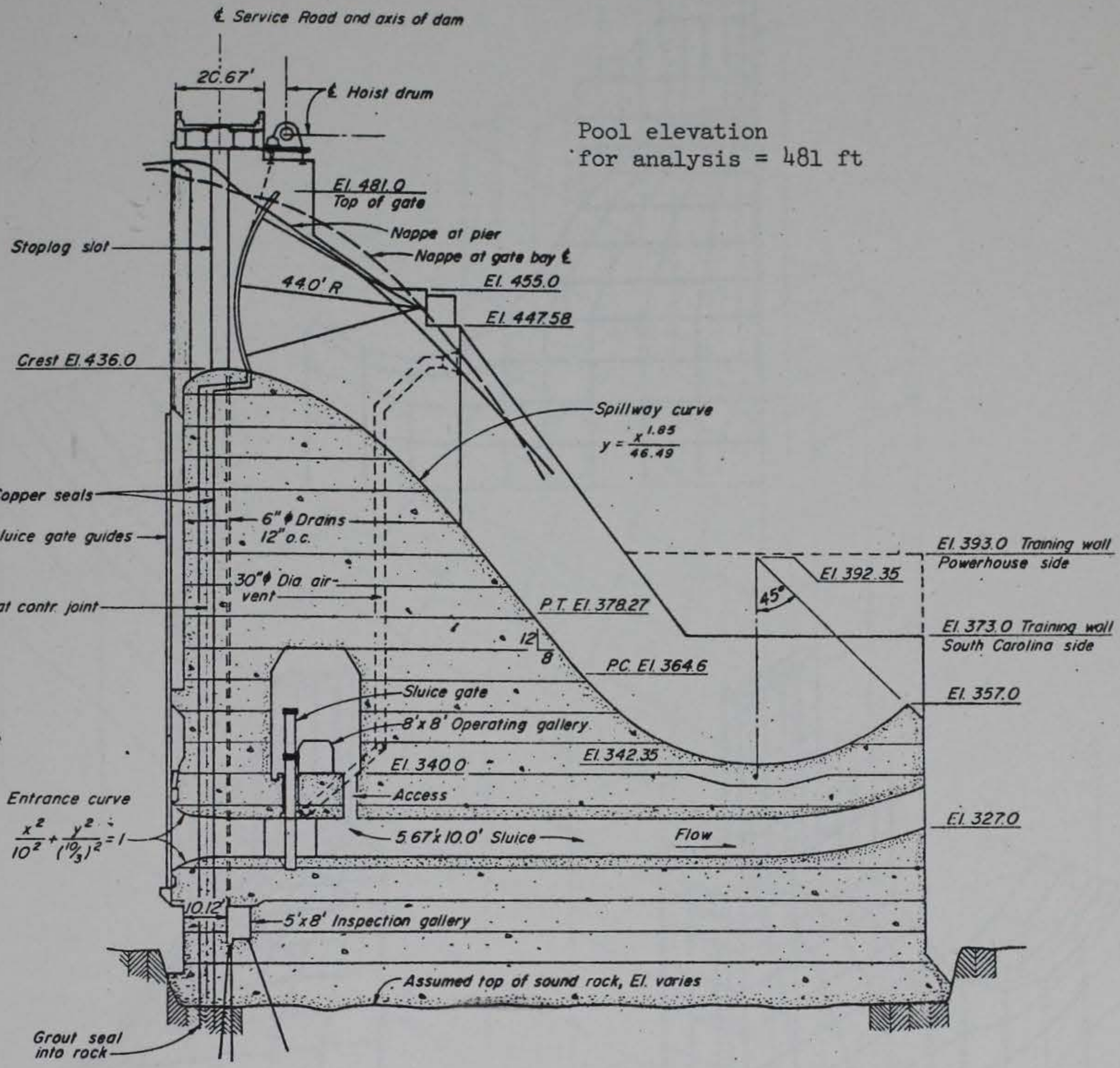

Pool elevation
for analysis = 481 ft

SPILLWAY SECTION

SCALE 1" = 20'

20' 0 20'

Figure 27 Overflow section, Richard B. Russell Dam.

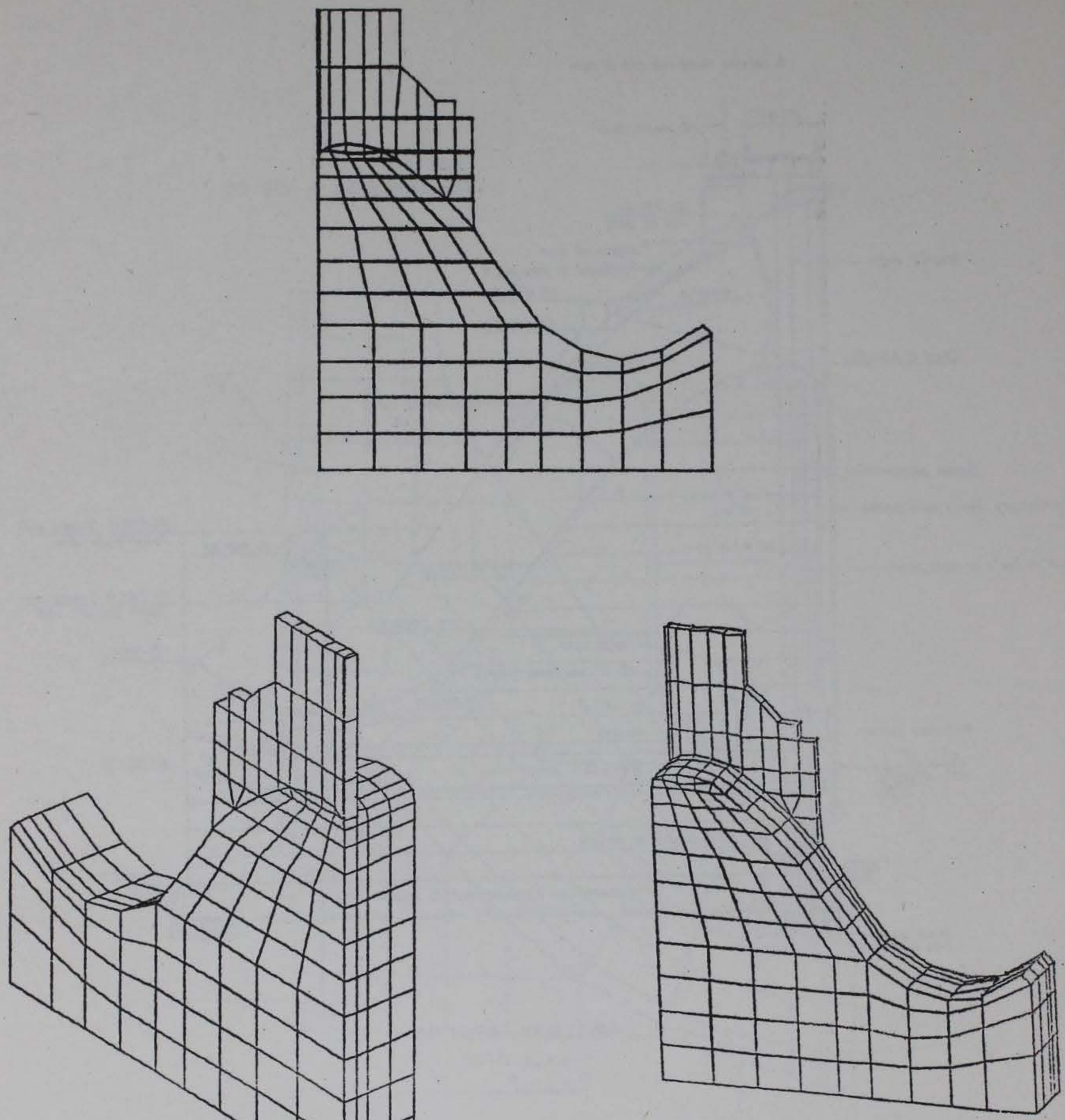

Figure 28 Finite element grid, overflow section,
Richard B. Russell Dam.

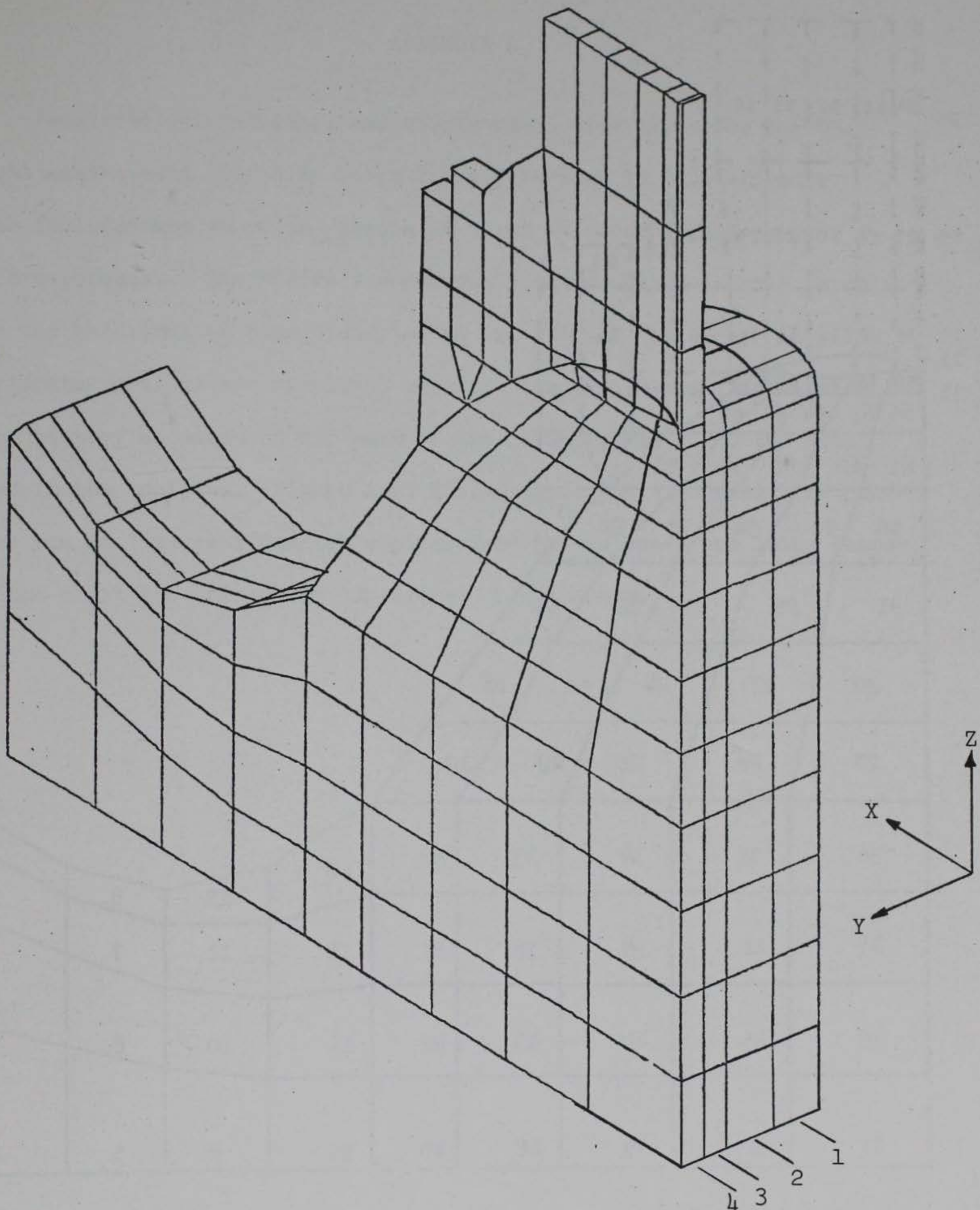

Figure 29 Layering of overflow section finite element grid.

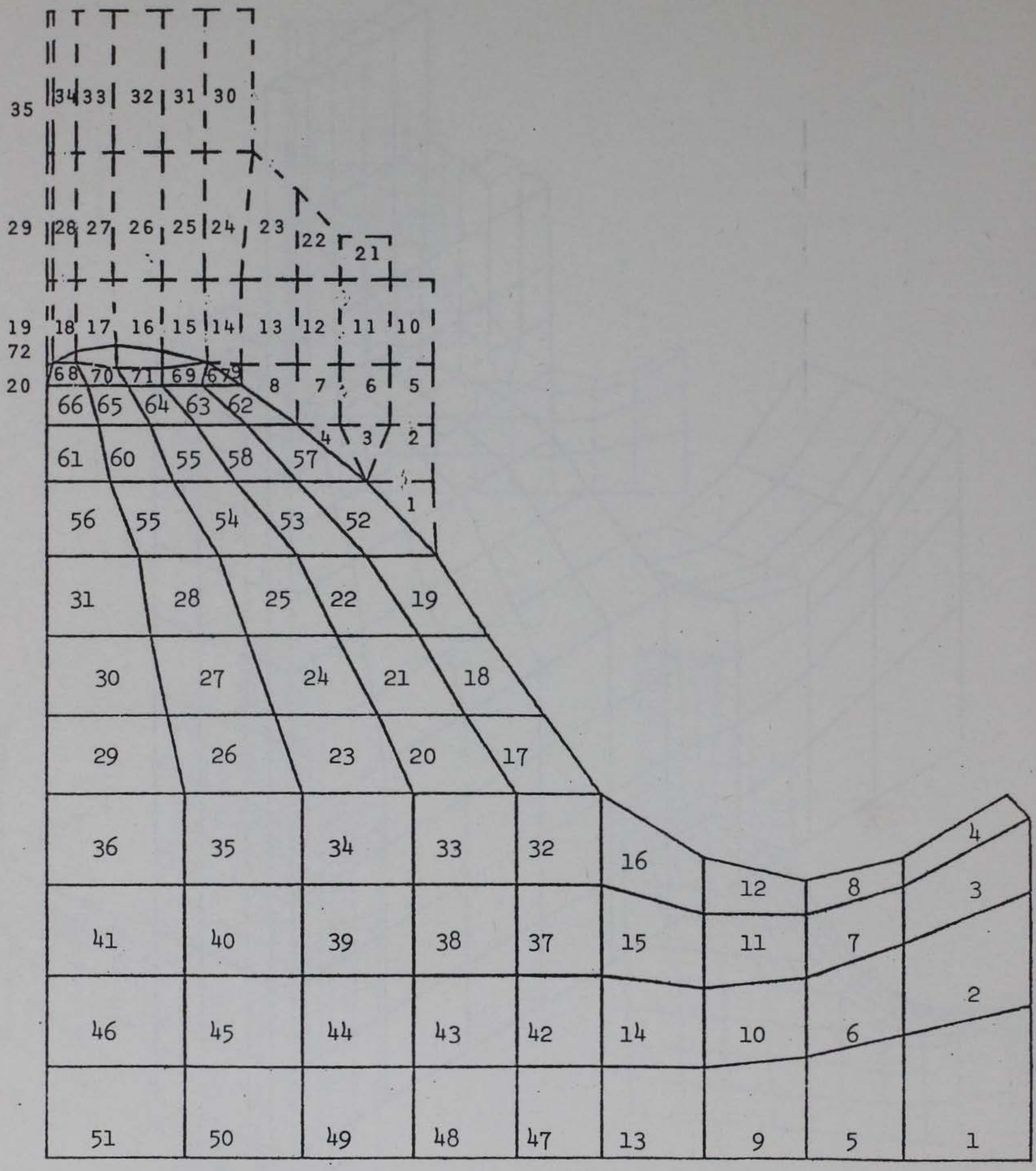

Figure 30 Element identification, overflow section finite element grid.

APPENDIX A

Acceleration, velocity, and displacement time histories for the eight earthquakes listed in Table 2 are presented in this appendix. Also included are response spectra at 5 and 10 percent damping for each earthquake. The finite element analyses discussed in this report use the acceleration time histories as the driving function. Only the horizontal motions are displayed herein. However, the actual vertical time history as measured for each of the listed earthquakes was also used in the analyses. Figure A.25 displays the NRC 1.60 design response spectrum at 5 percent damping superimposed on the upper and lower bounds of the eight time histories considered in this study.

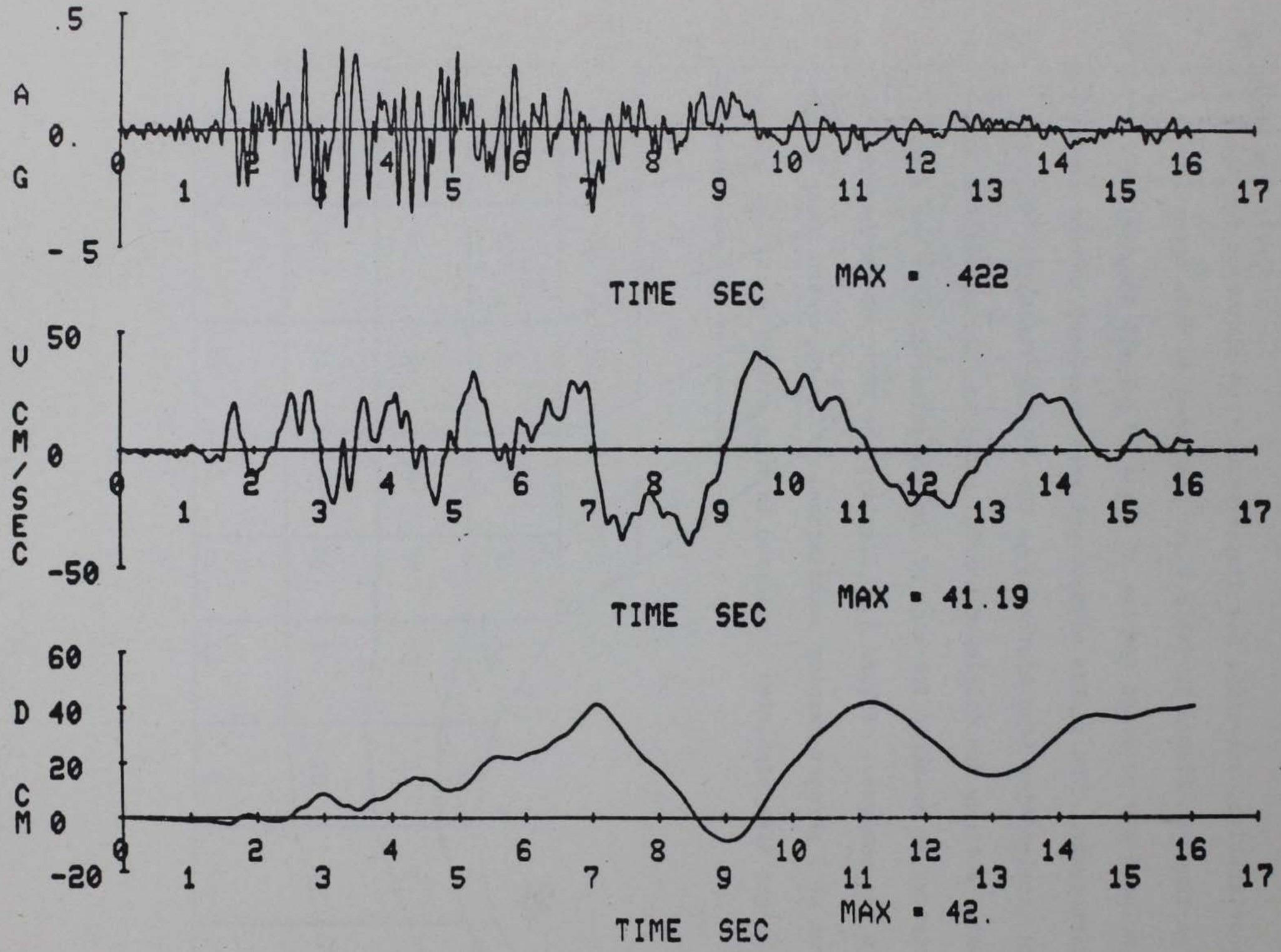

Figure A.1 San Fernando Earthquake, Hollywood Storage P.E. Lot, CIT D058, N90E component.

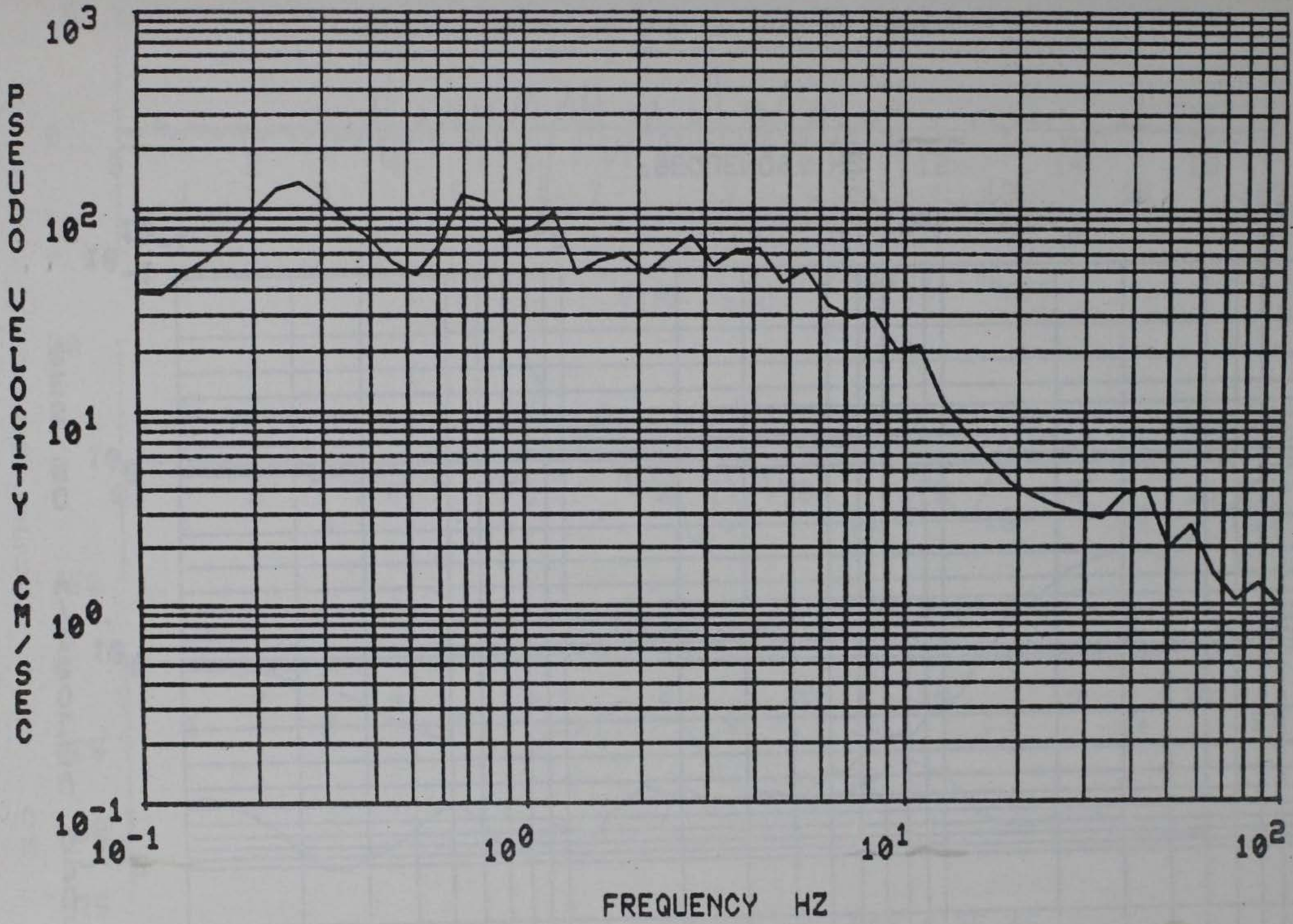

Figure A.2 Response spectrum, 5 percent damping, San Fernando Earthquake, Hollywood Storage P.E. Lot, CIT D058, N90E component.

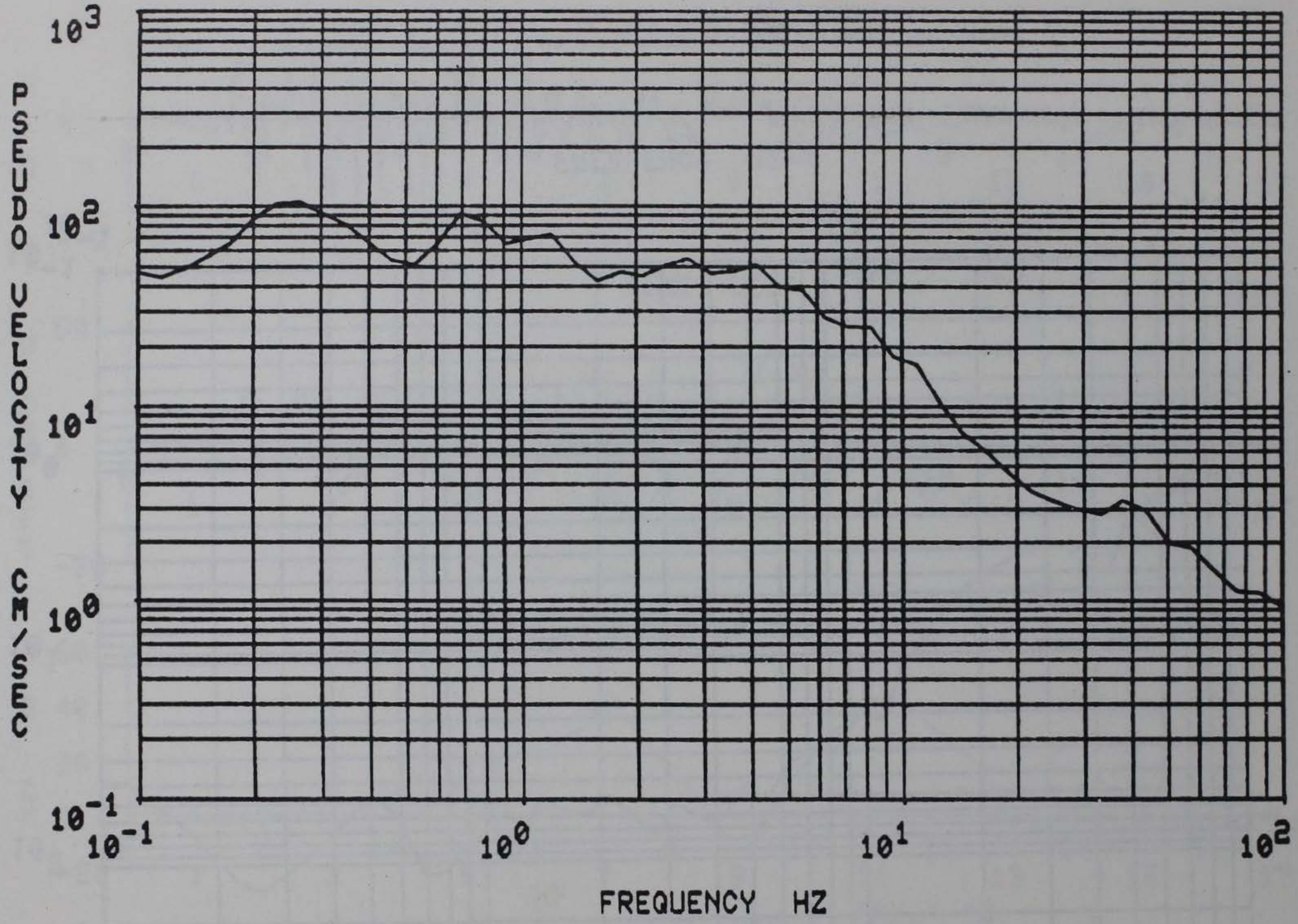

Figure A.3 Response spectrum, 10 percent damping, San Fernando Earthquake, Hollywood Storage P.E. Lot, CIT D058, N90E component.

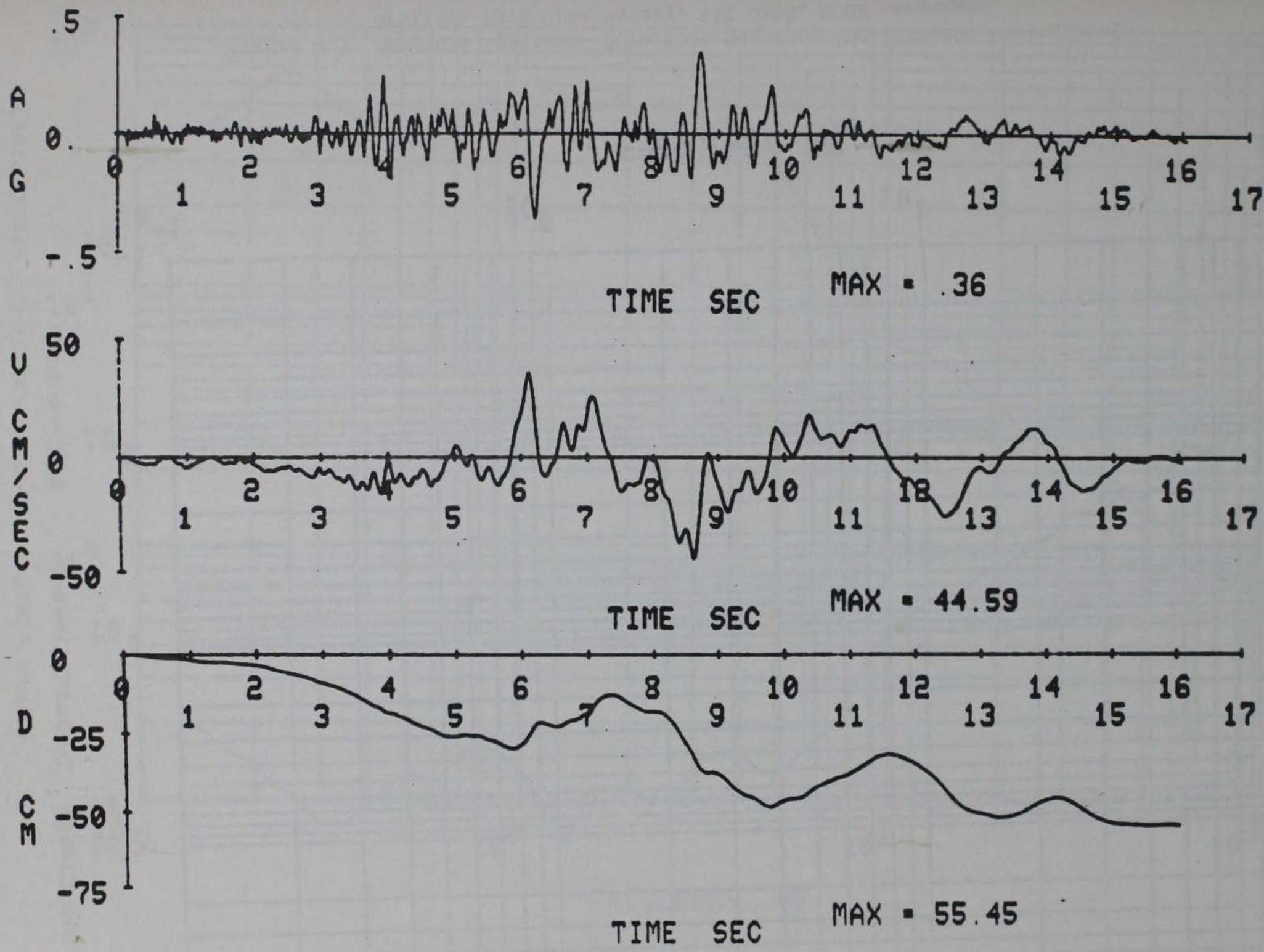

Figure A.4 San Fernando Earthquake, Griffith Park Observatory, CIT 0198, S00W component.

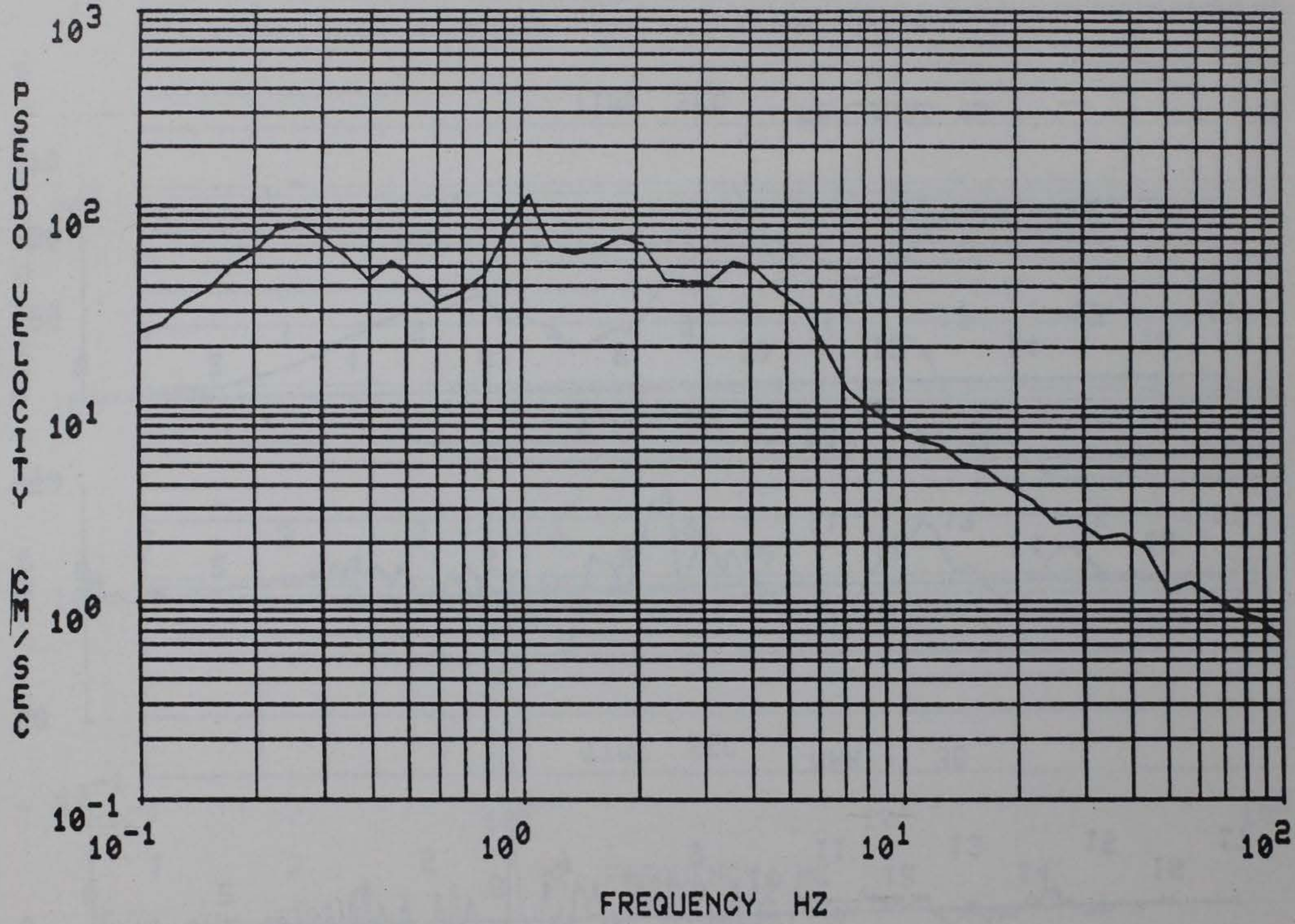

Figure A.5 Response spectrum, 5 percent damping, San Fernando Earthquake, Griffith Park Observatory, CIT 0198, S00W component.

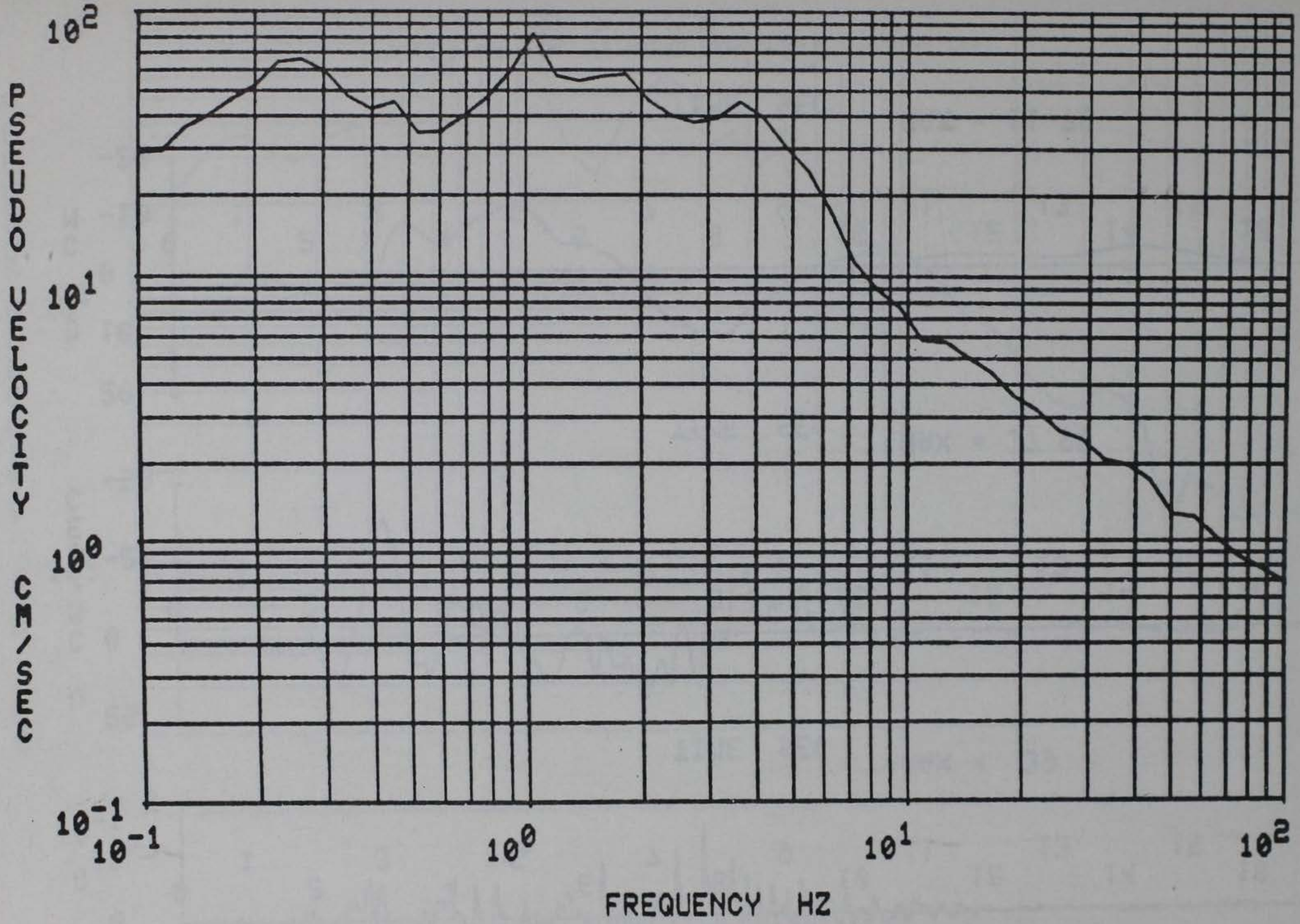

Figure A.6 Response spectrum, 10 percent damping, San Fernando Earthquake, Griffith Park Observatory, CIT 0198, S00W component.

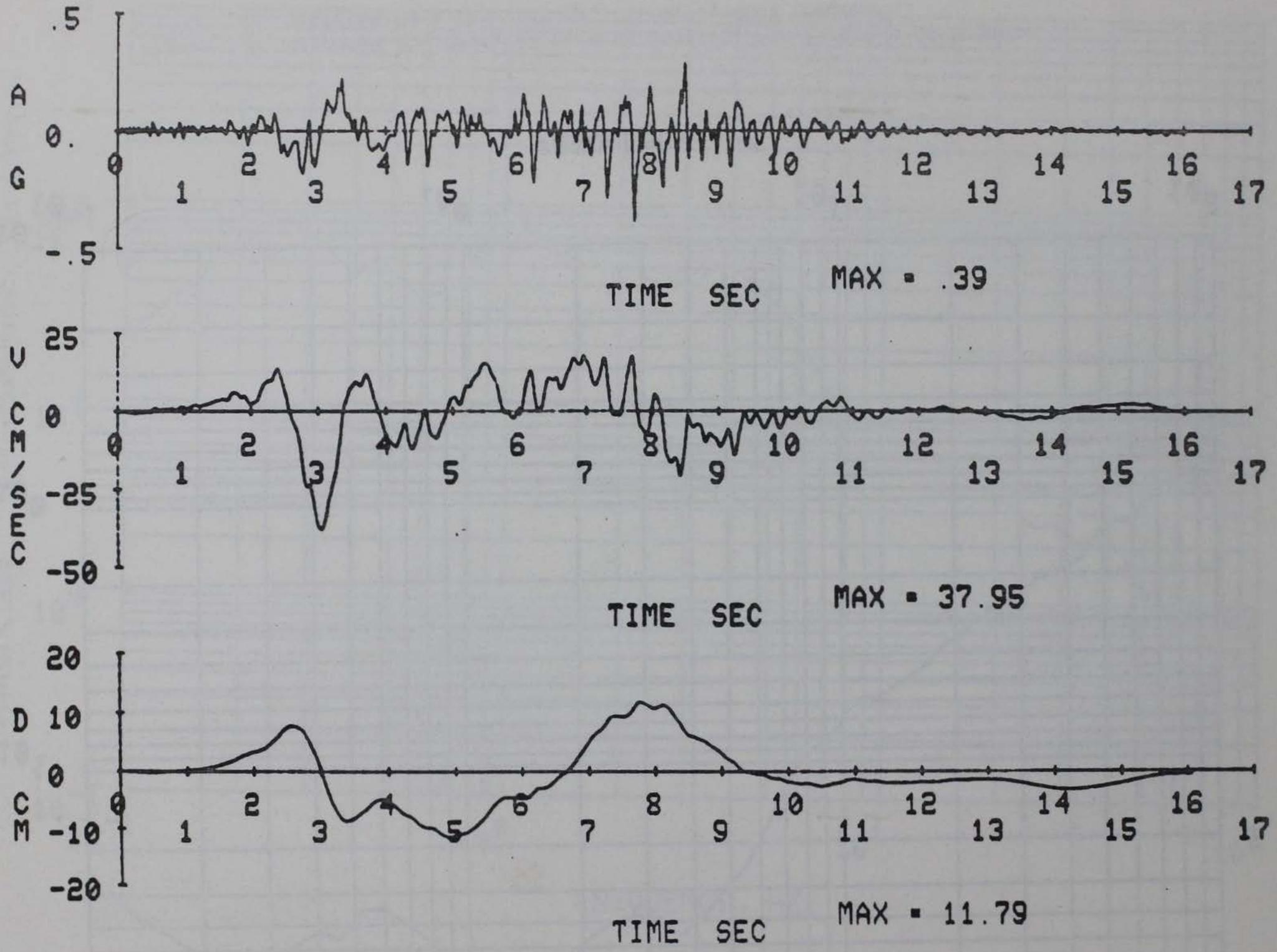

Figure A.7 San Fernando Earthquake, Pacoima Dam, CIT C041, S16E component.

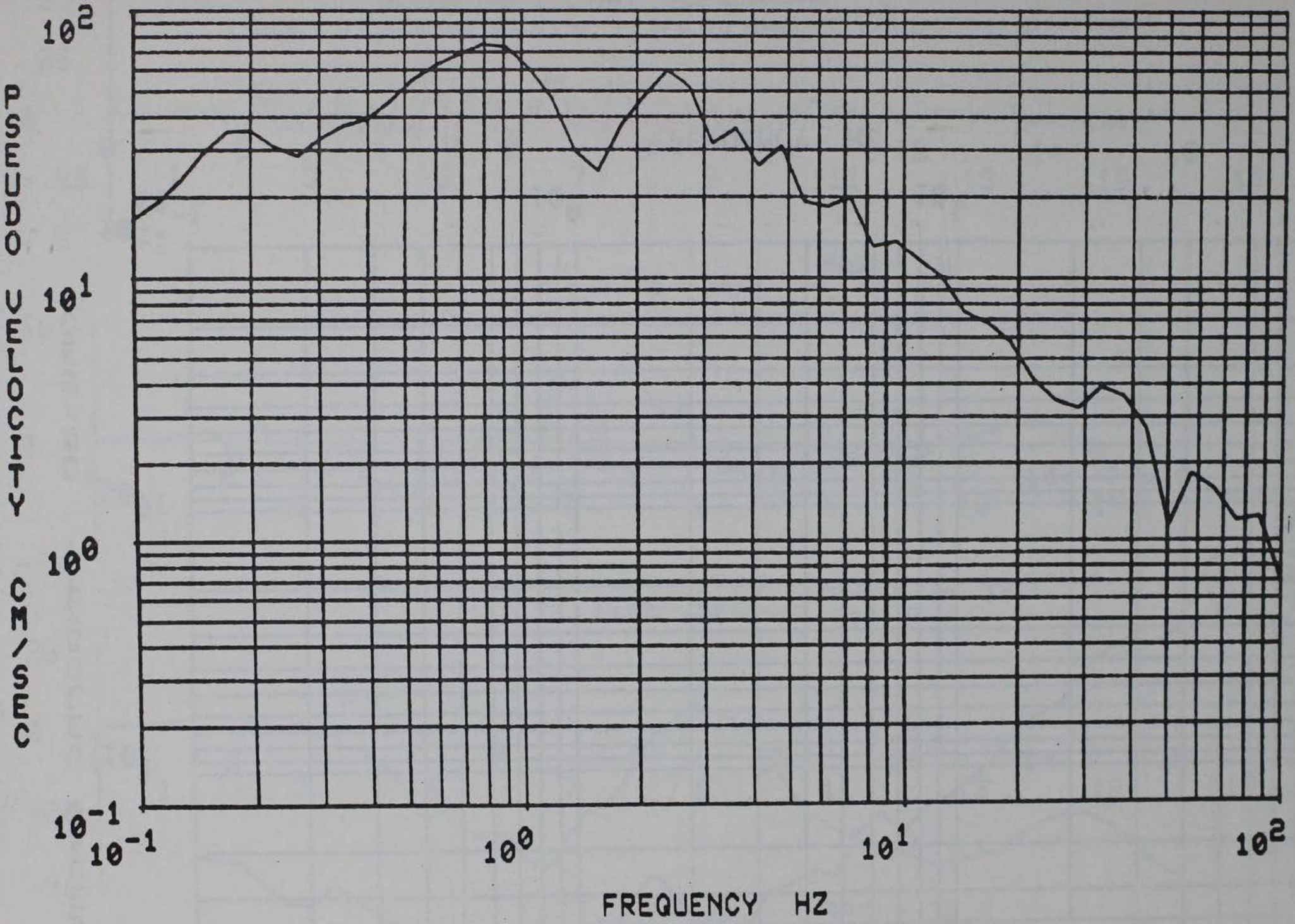

Figure A.8 Response spectrum, 5 percent damping, San Fernando Earthquake, Pacoima Dam, CIT C041, S16E component.

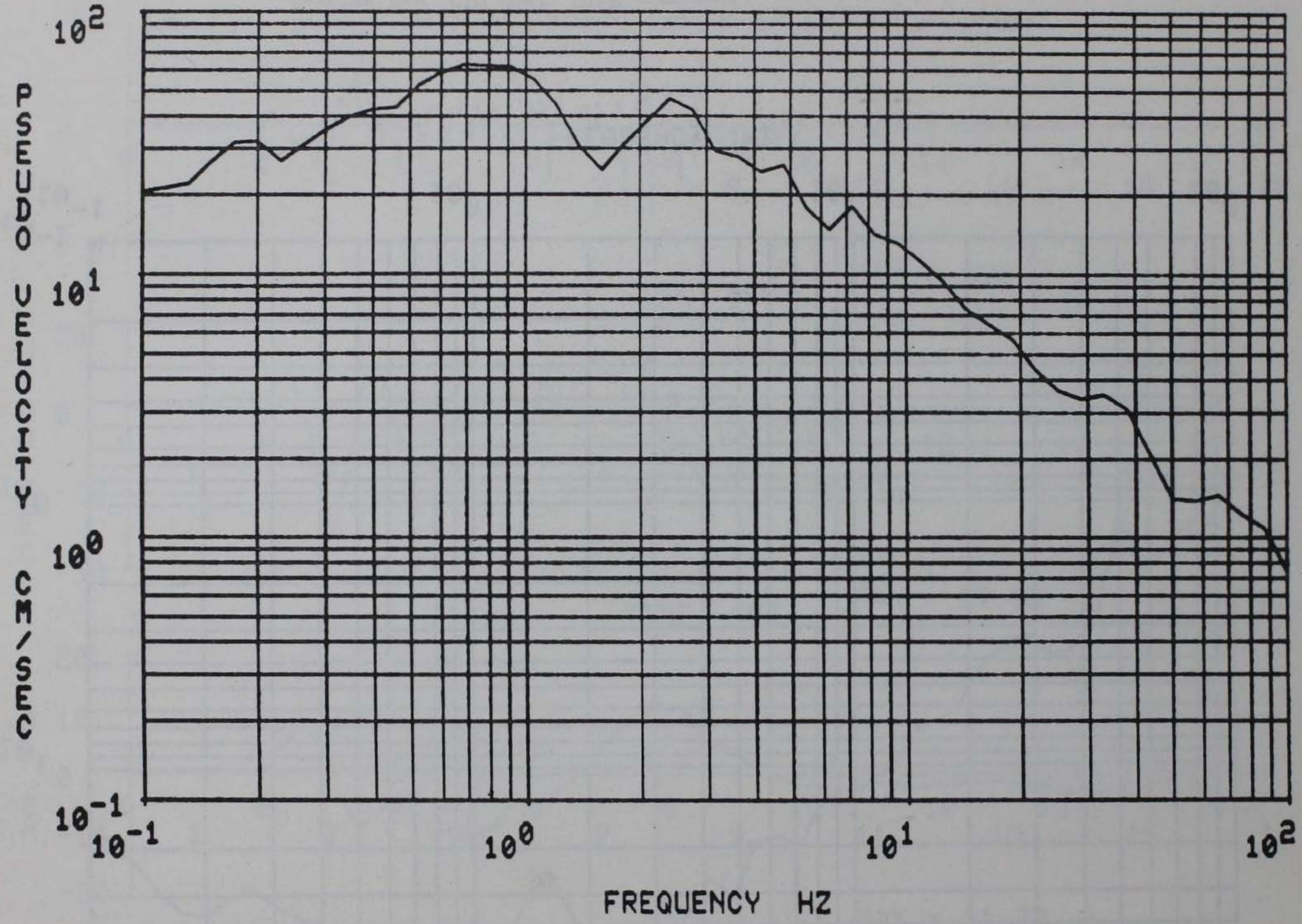

Figure A.9 Response spectrum, 10 percent damping, San Fernando Earthquake, Pacoima Dam, CIT C041, S16E component.

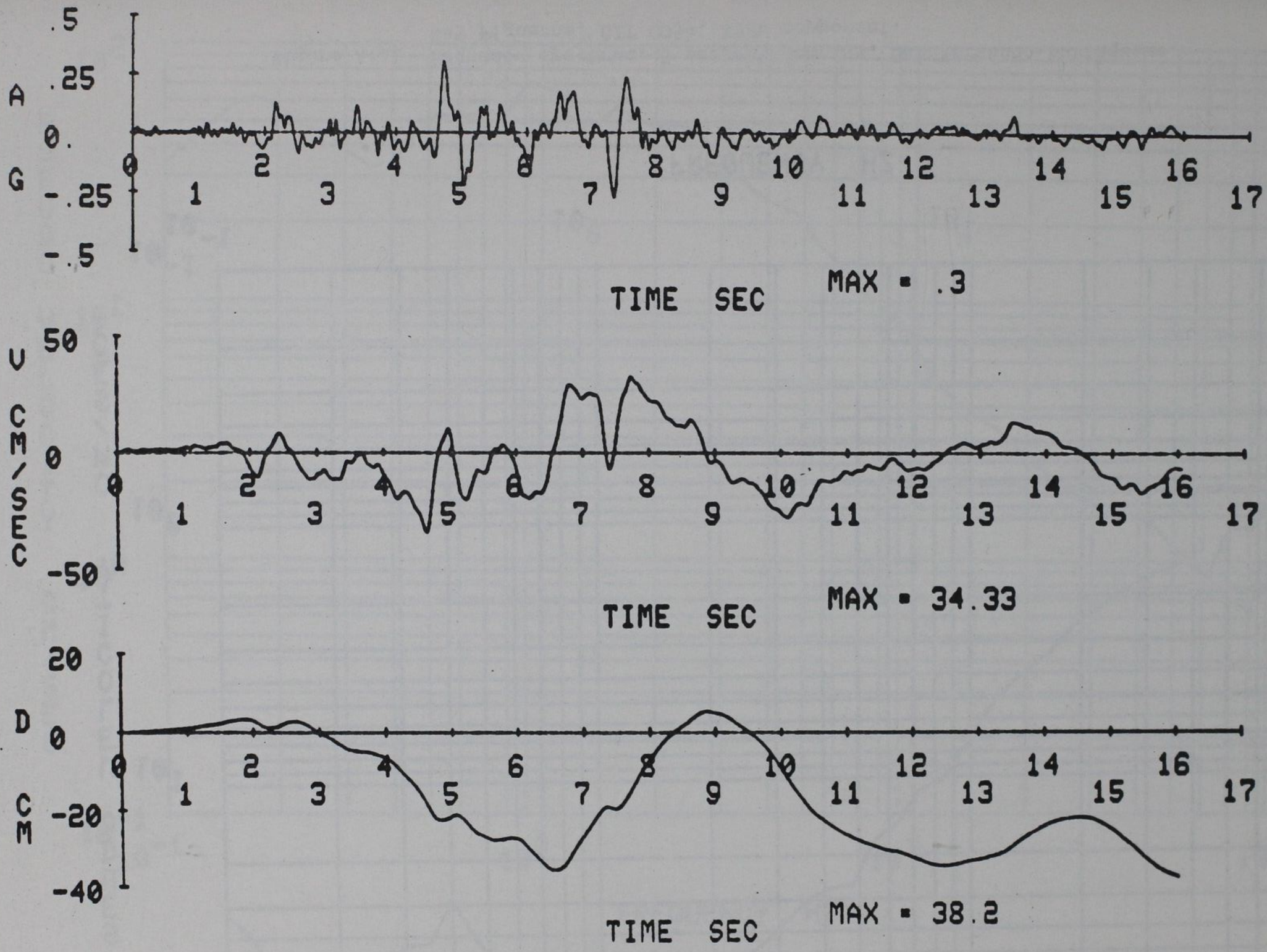

Figure A.10 San Fernando Earthquake, 445 Figueroa, CIT C054, N52W component.

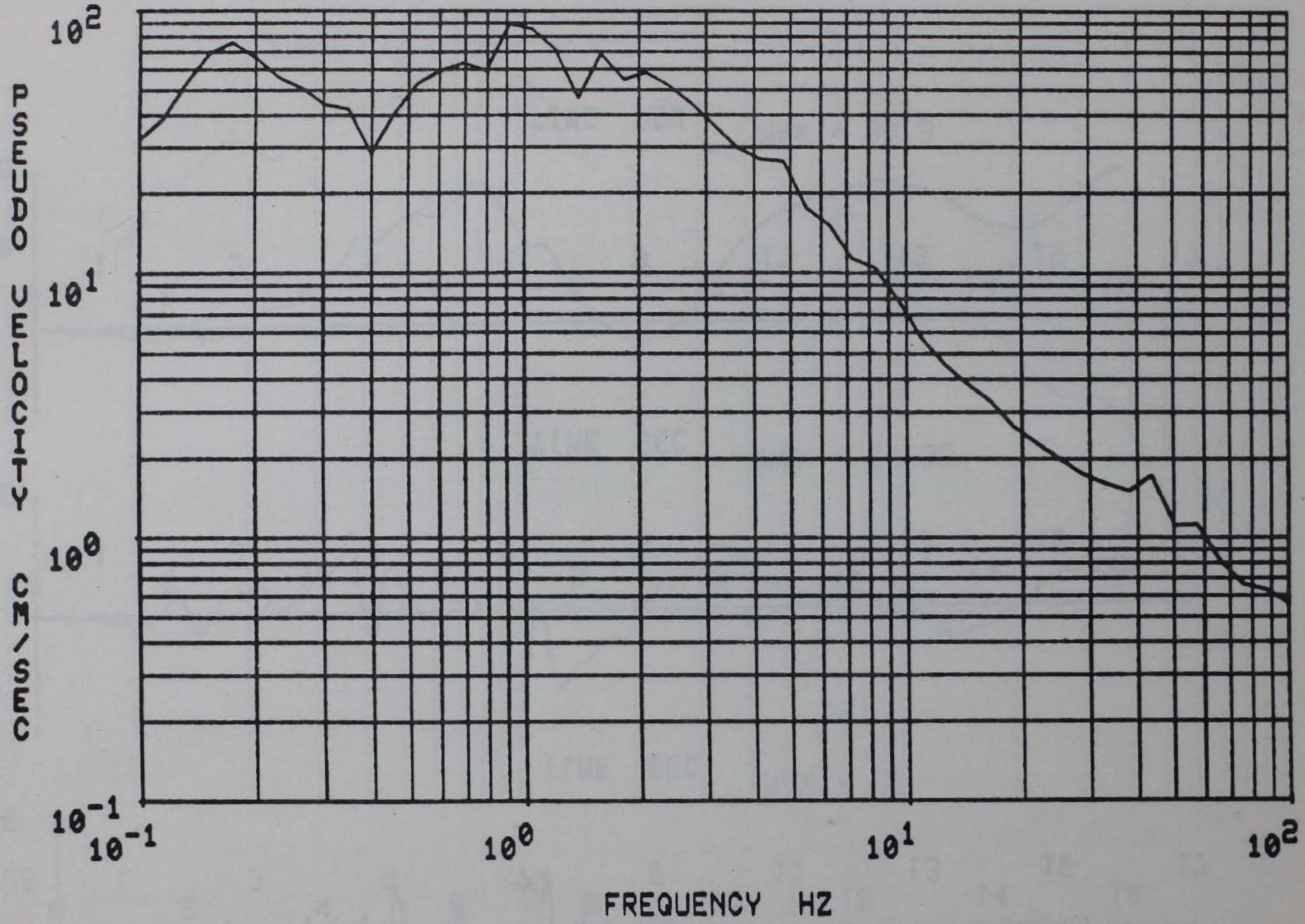

Figure A.11 Response spectrum, 5 percent damping, San Fernando Earthquake, 445 Figueroa, CIT C054, N52W component.

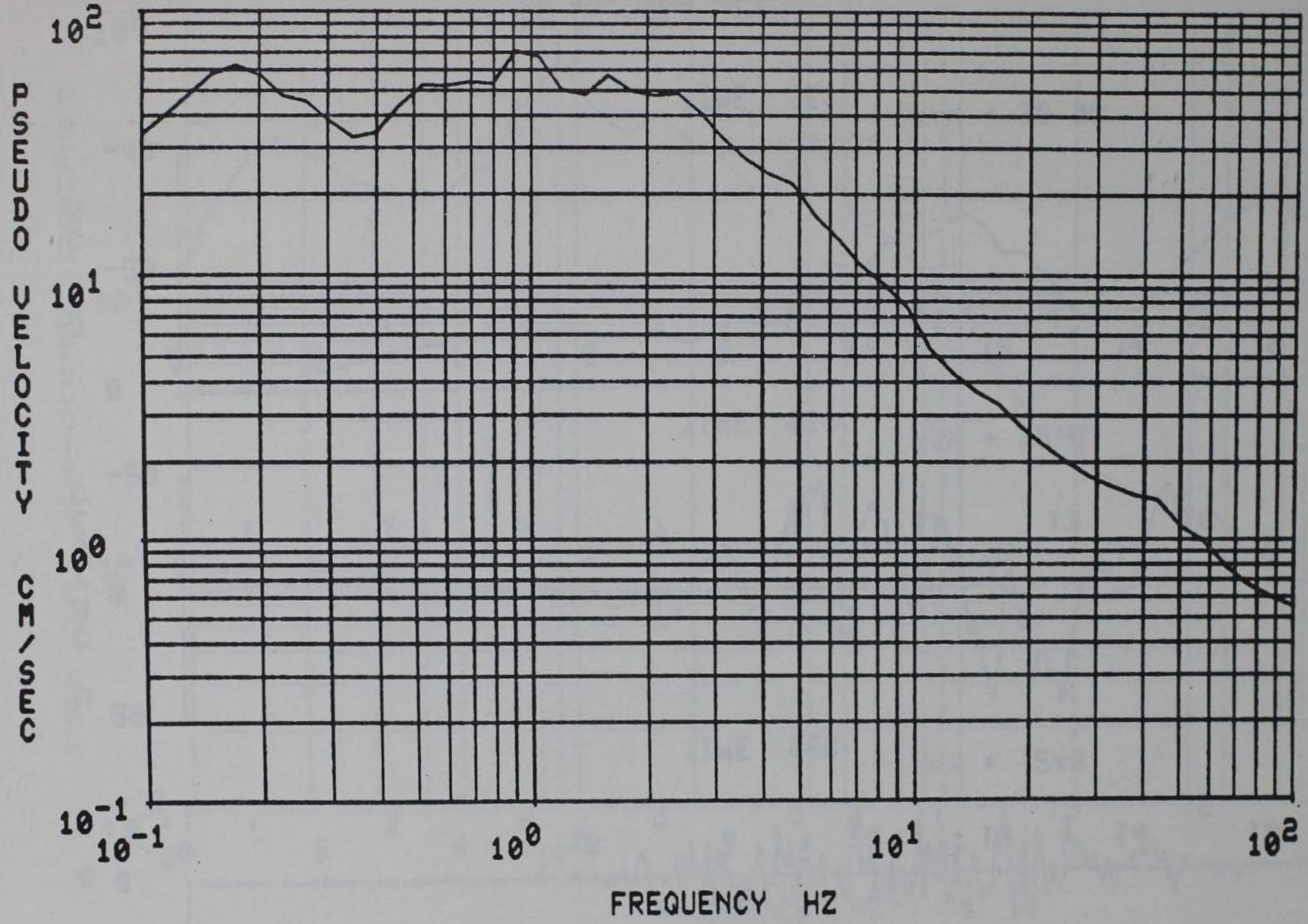

Figure A.12 Response spectrum, 10 percent damping, San Fernando Earthquake, 445 Figueroa, CIT C054, N52W component.

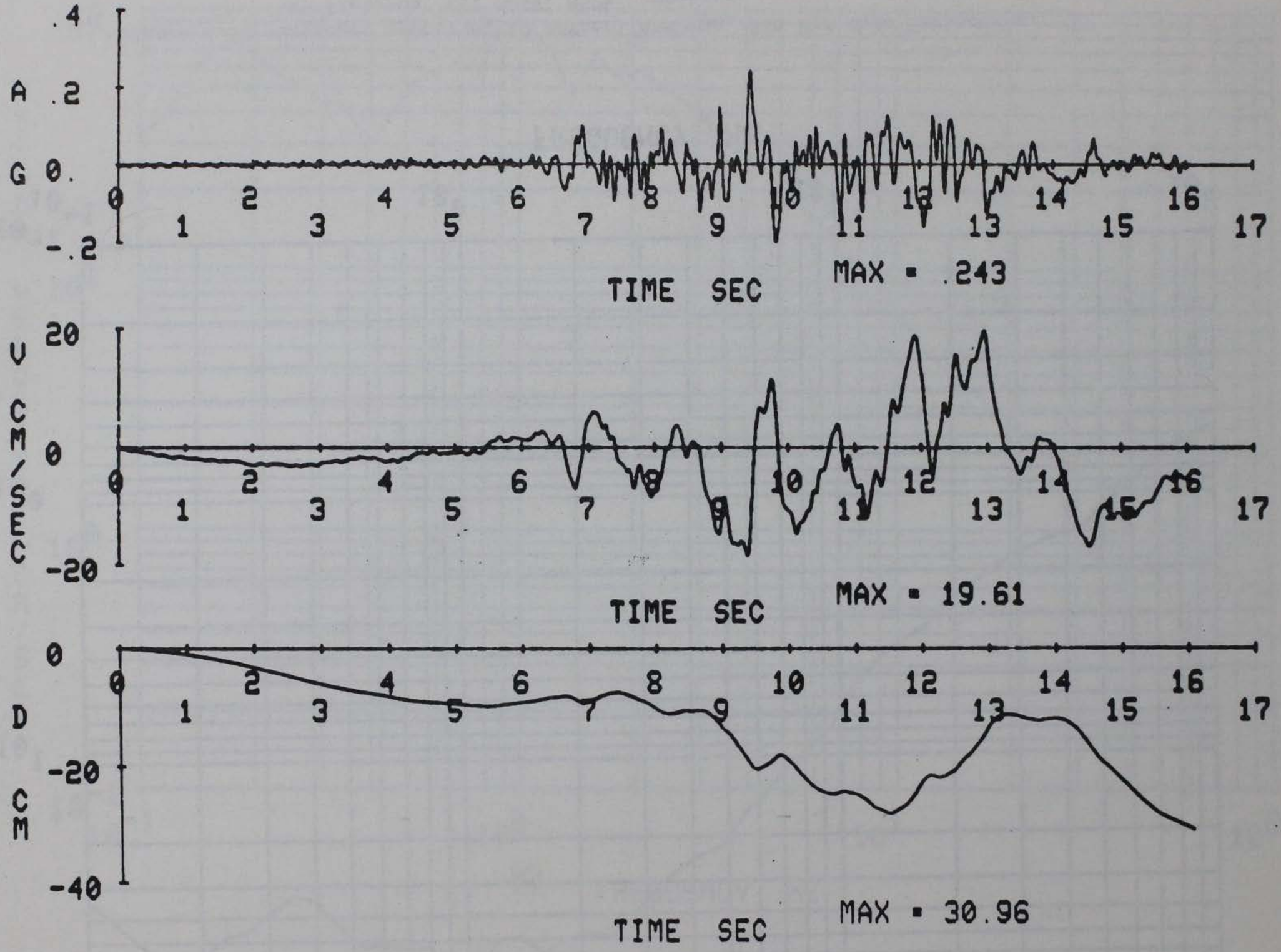

Figure A.13 San Fernando Earthquake, 1625 Olympic Blvd, CIT 0199, N62W component.

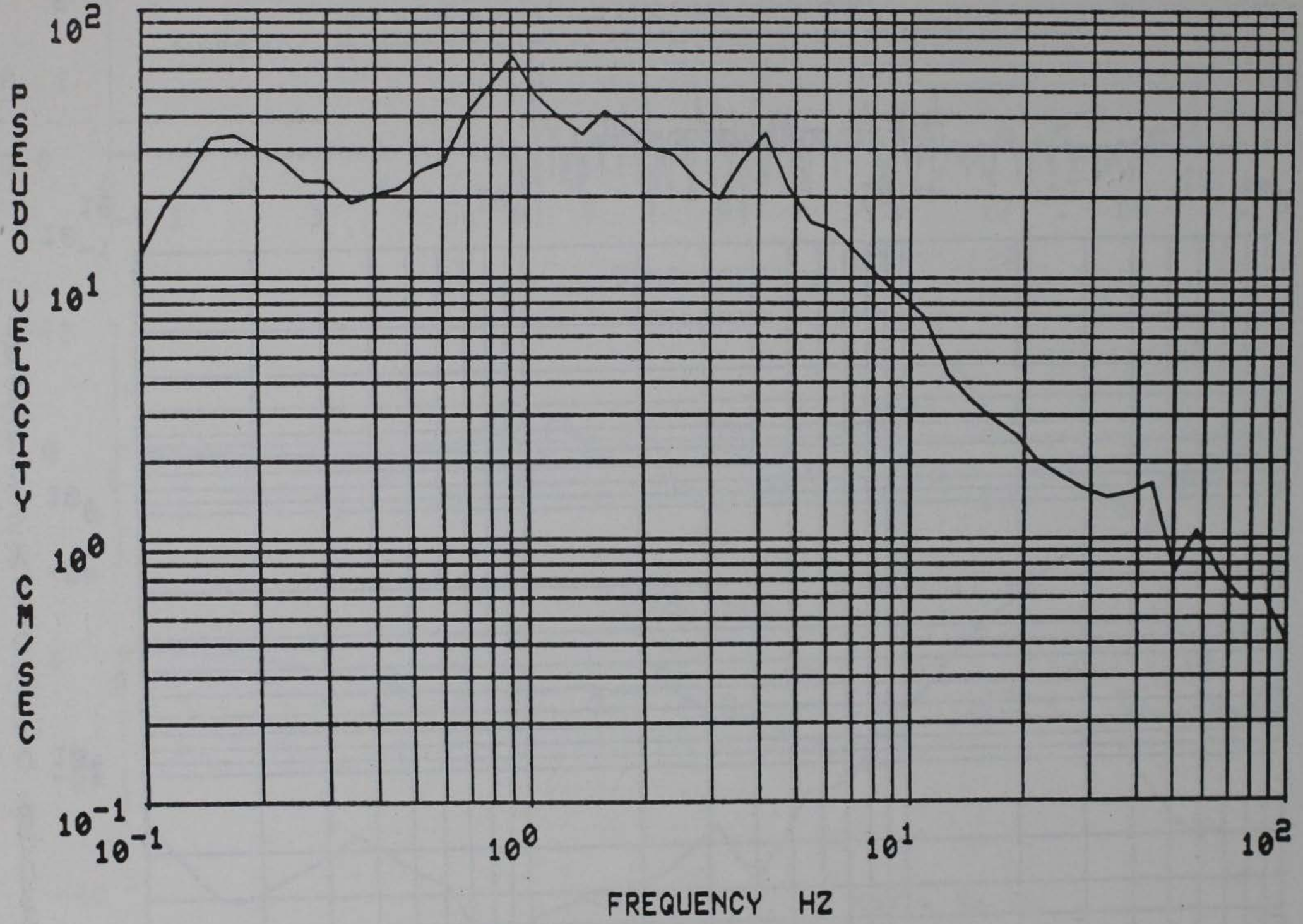

Figure A.14 Response spectrum, 5 percent damping, San Fernando Earthquake, 1625 Olympic Blvd, CIT 0199, N62W component.

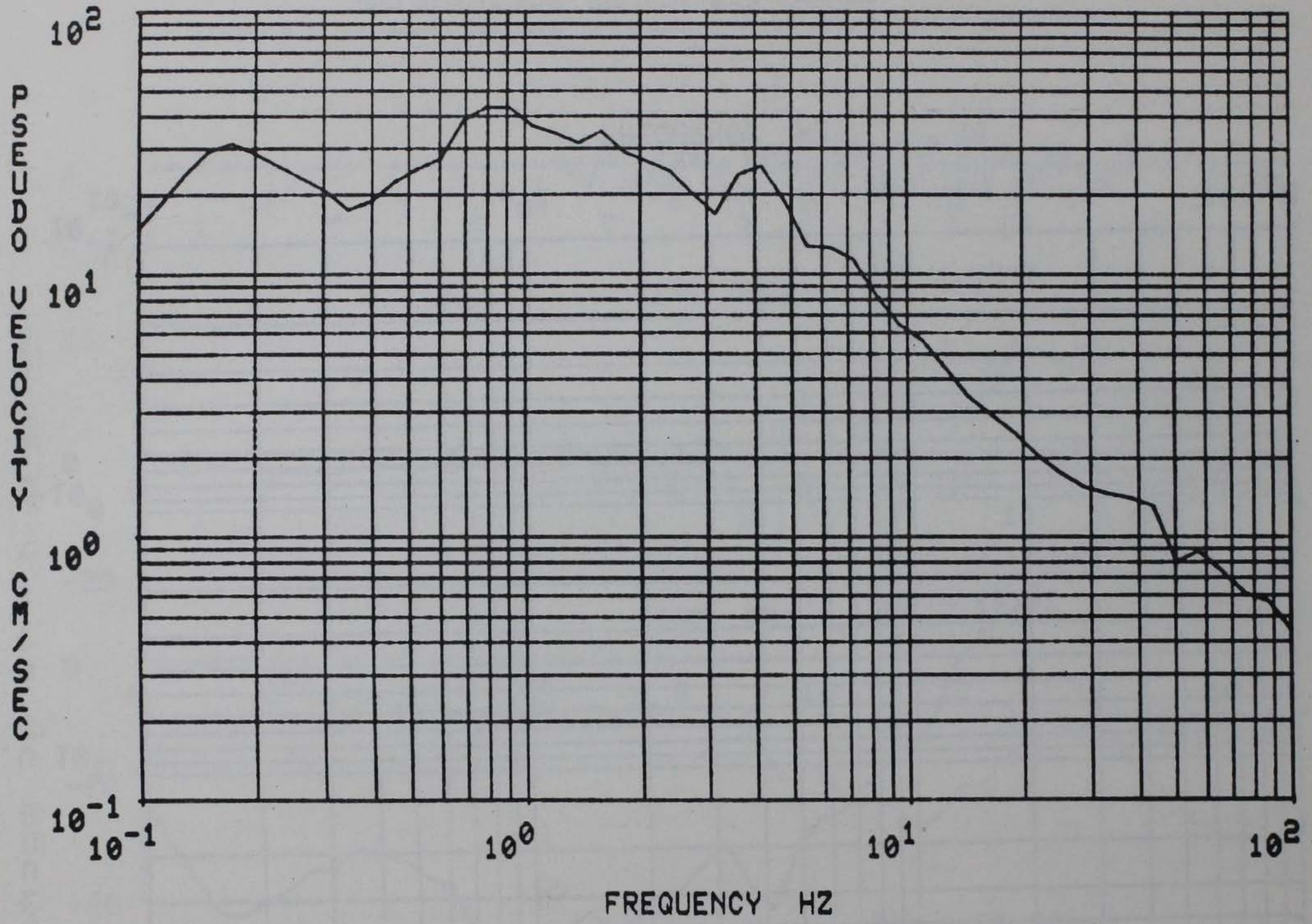

Figure A.15 Response spectrum, 10 percent damping, San Fernando Earthquake, 1625 Olympic Blvd, CIT 0199, N62W component.

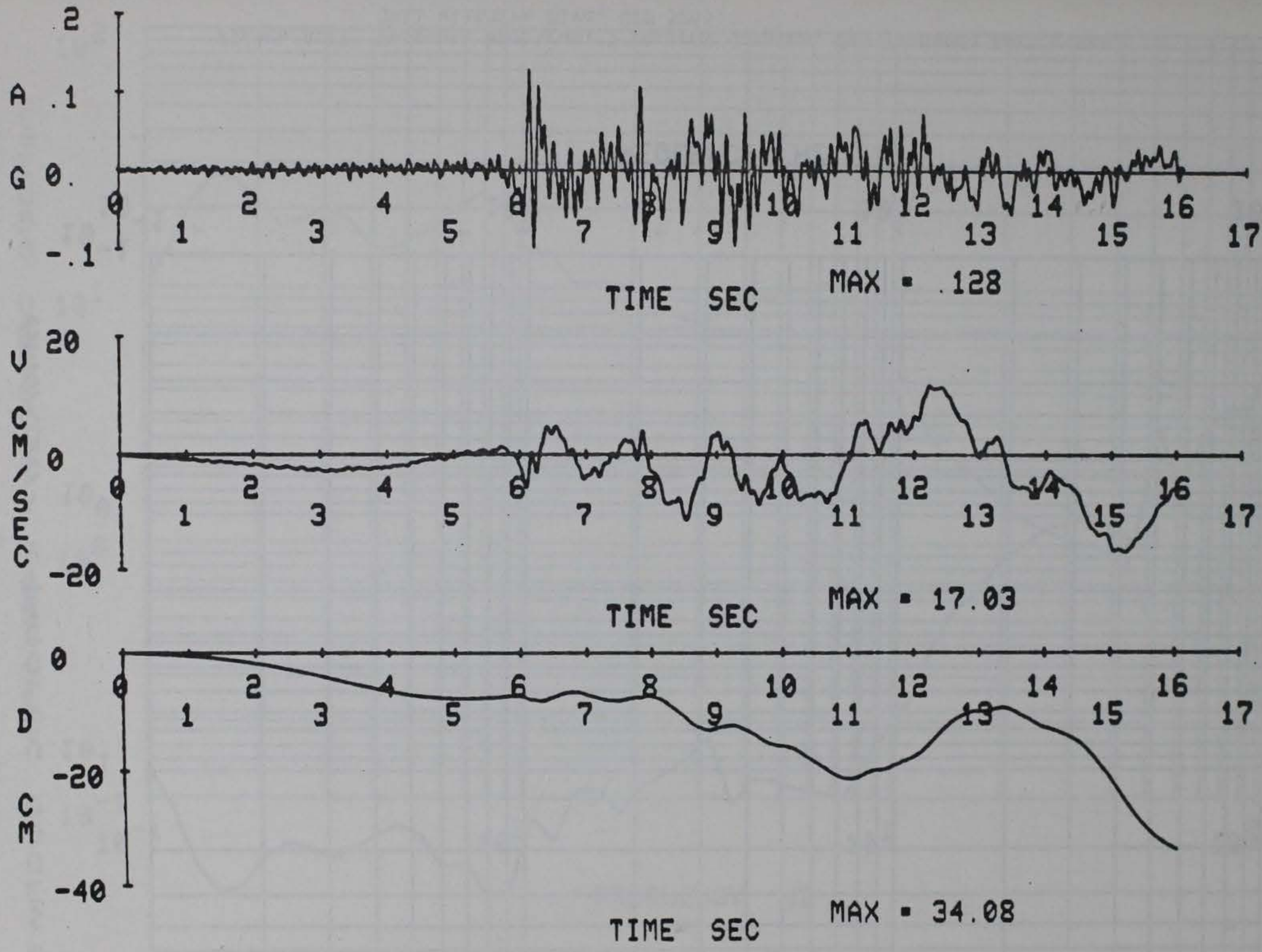

Figure A.16 San Fernando Earthquake, 3411 Wilshire Blvd, CIT 5265.

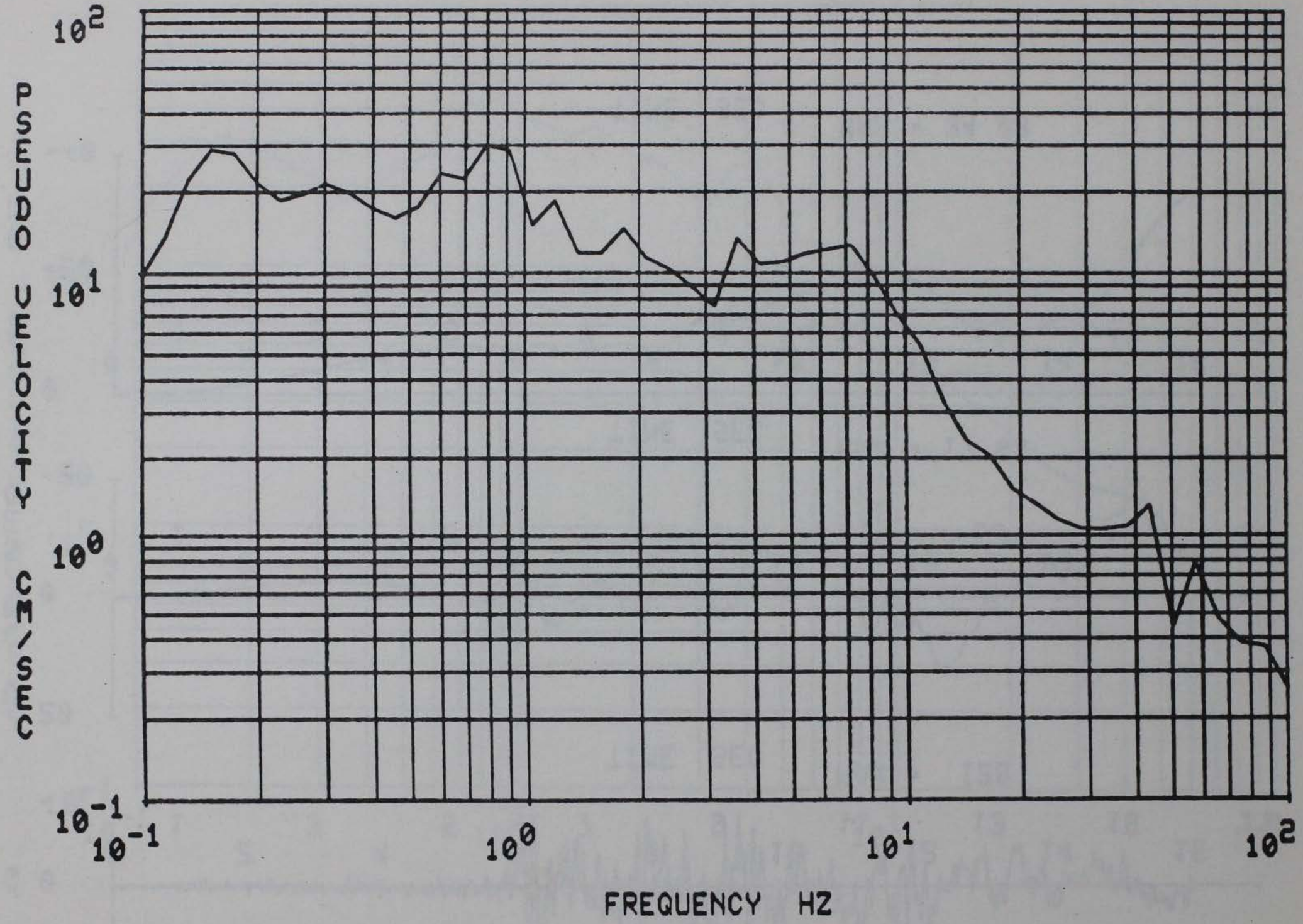

Figure A.17 Response spectrum, 5 percent damping, San Fernando Earthquake, 3411 Wilshire Blvd, CIT 5265.

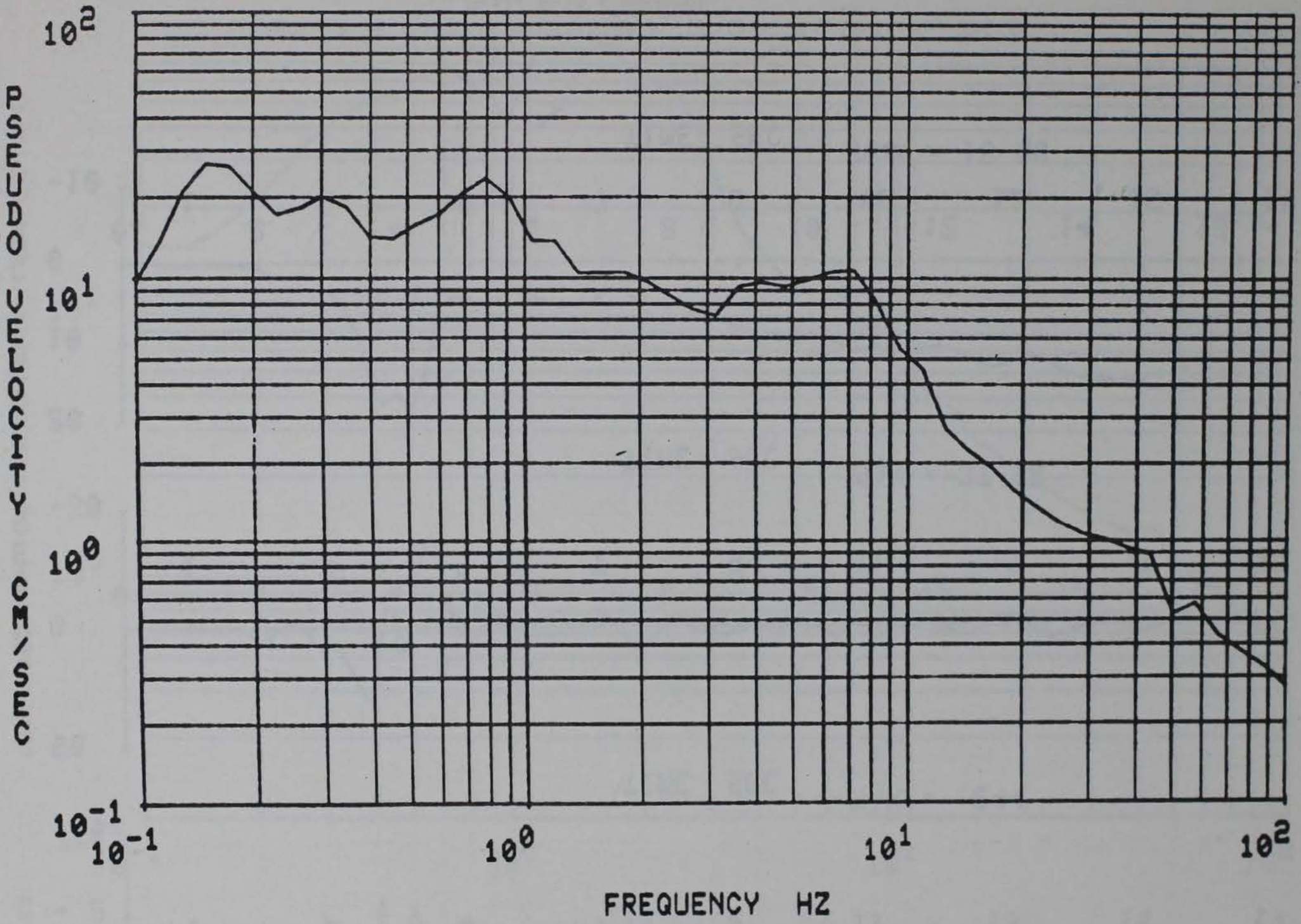

Figure A.18 Response spectrum, 10 percent damping, San Fernando Earthquake, 3411 Wilshire Blvd, CIT 5265.

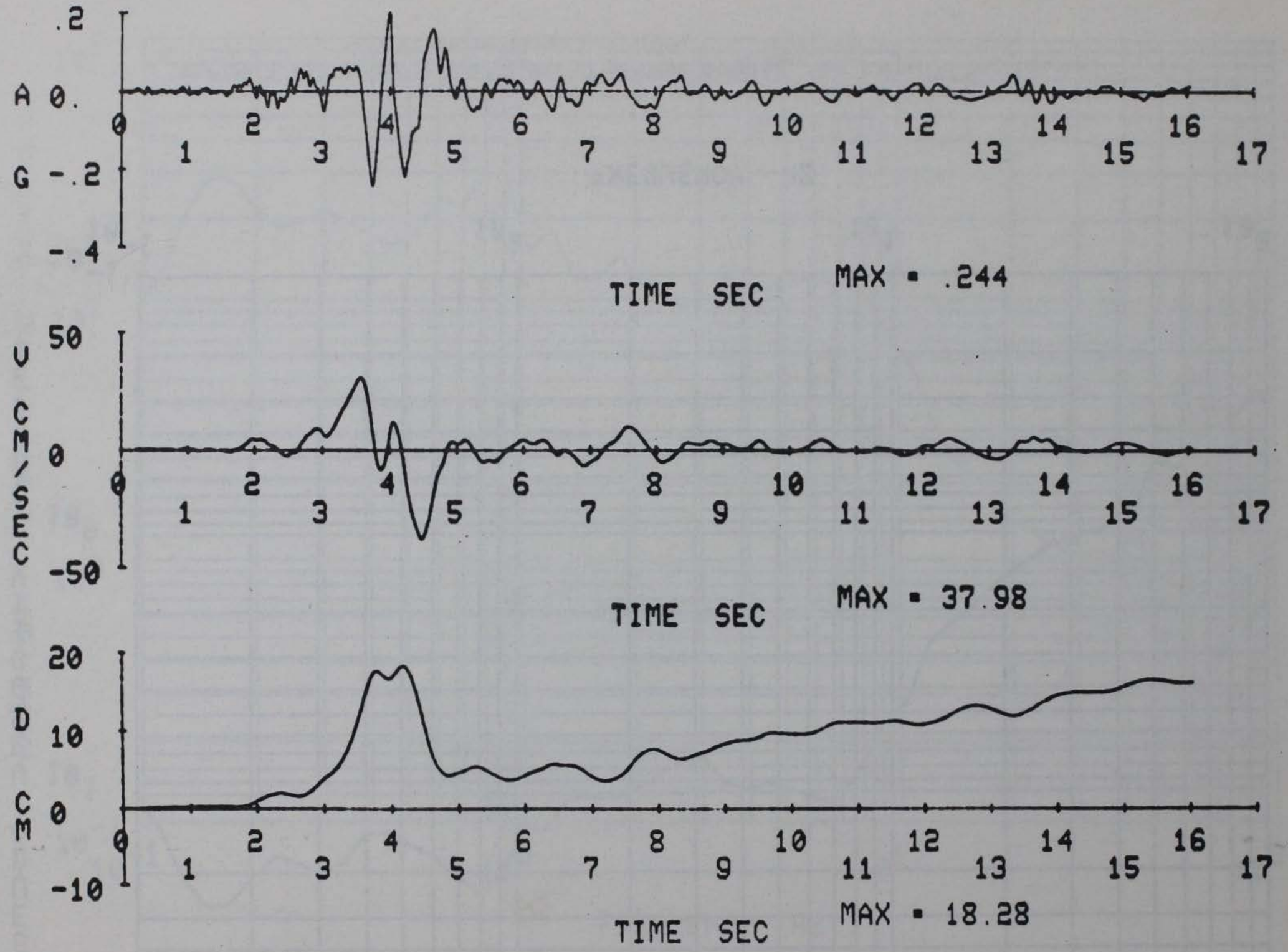

Figure A.19 Parkfield Earthquake, Cholame Shandon Array No. 2, CIT B033, N65E component.

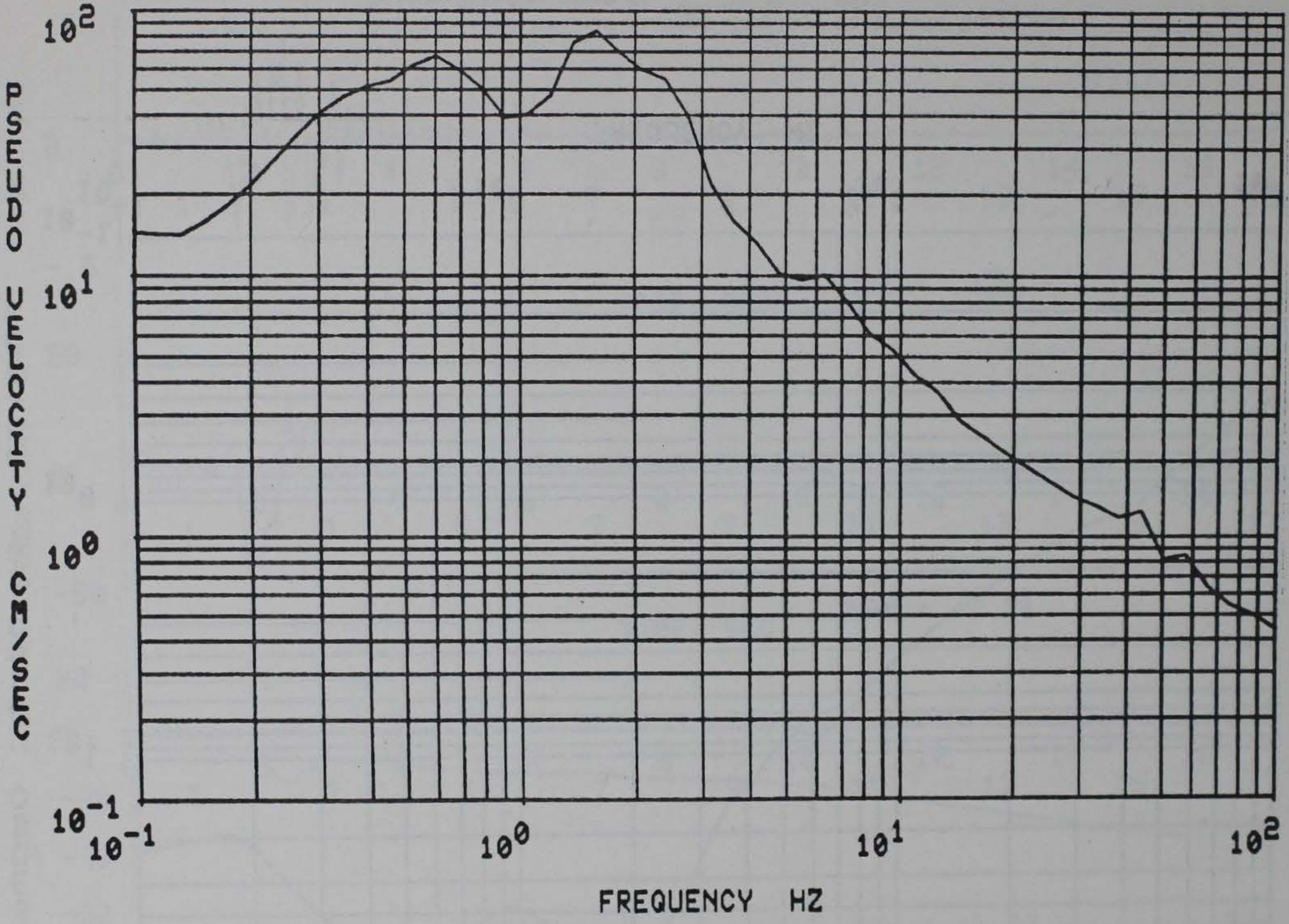

Figure A.20 Response spectrum, 5 percent damping, Parkfield Earthquake, Cholame Shandon Array No. 2, CIT B033, N65E component.

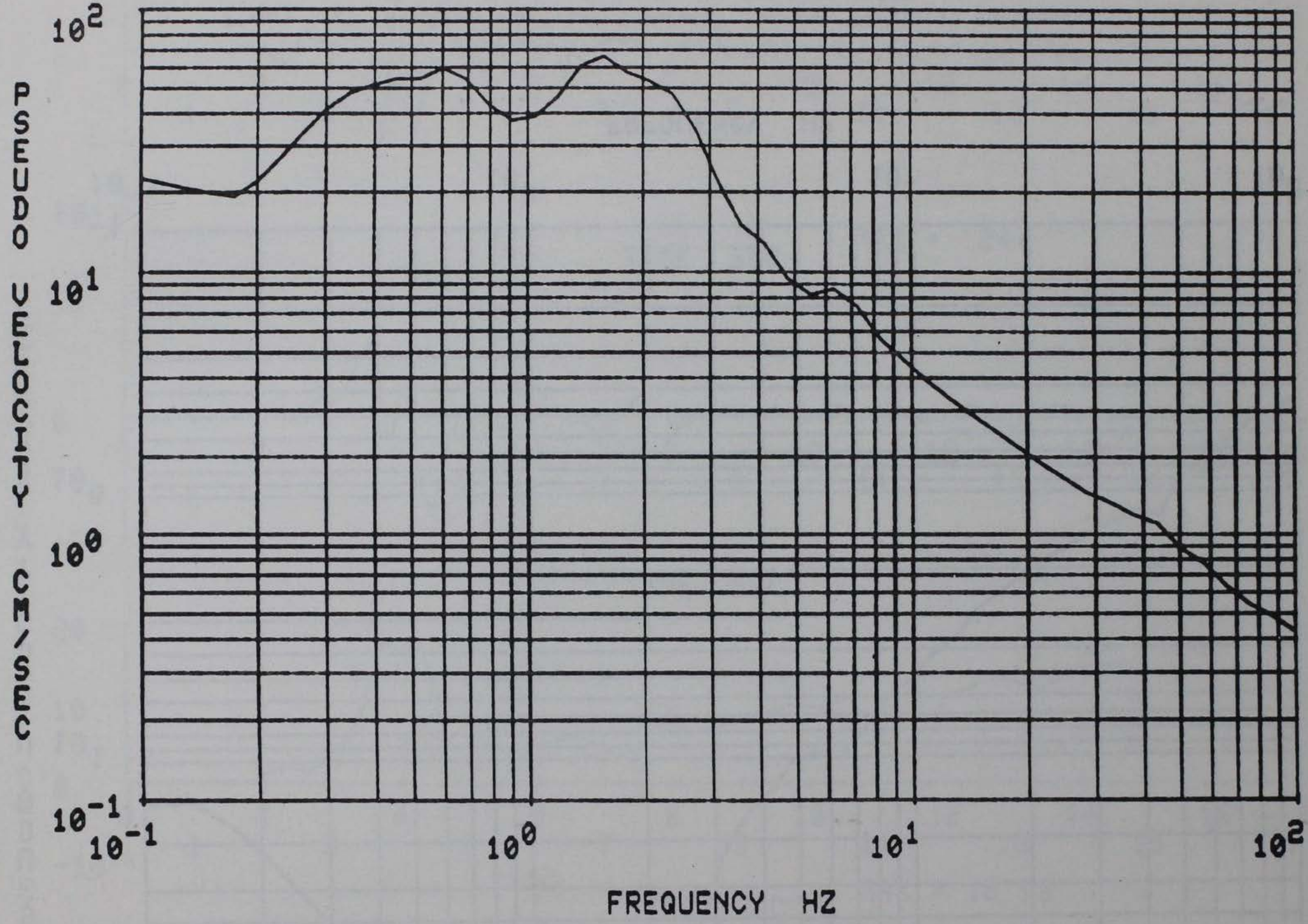

Figure A.21 Response spectrum, 10 percent damping, Parkfield Earthquake, Cholame Shandon Array No. 2, CIT B033, N65E component.

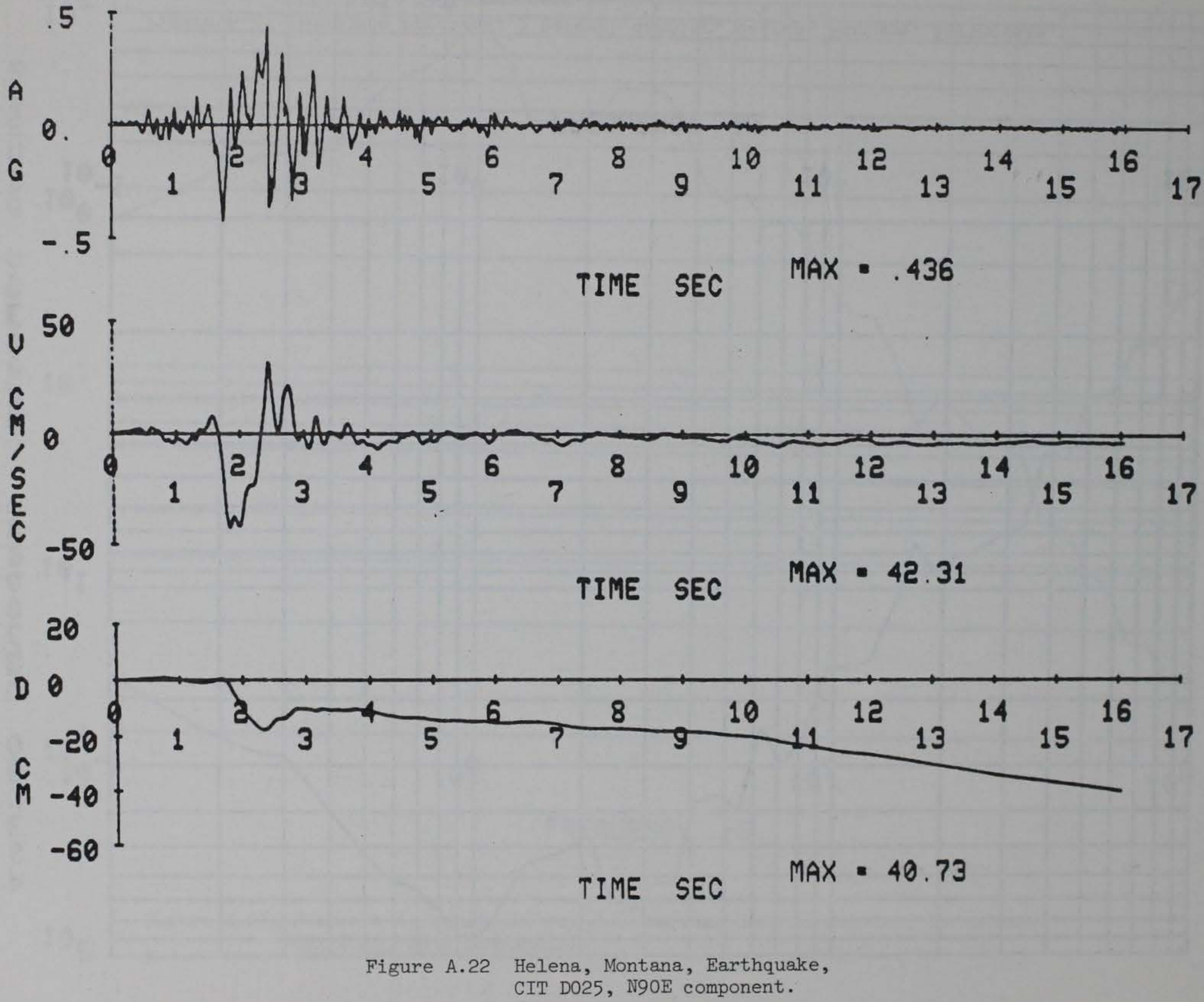

Figure A.22 Helena, Montana, Earthquake,
CIT D025, N90E component.

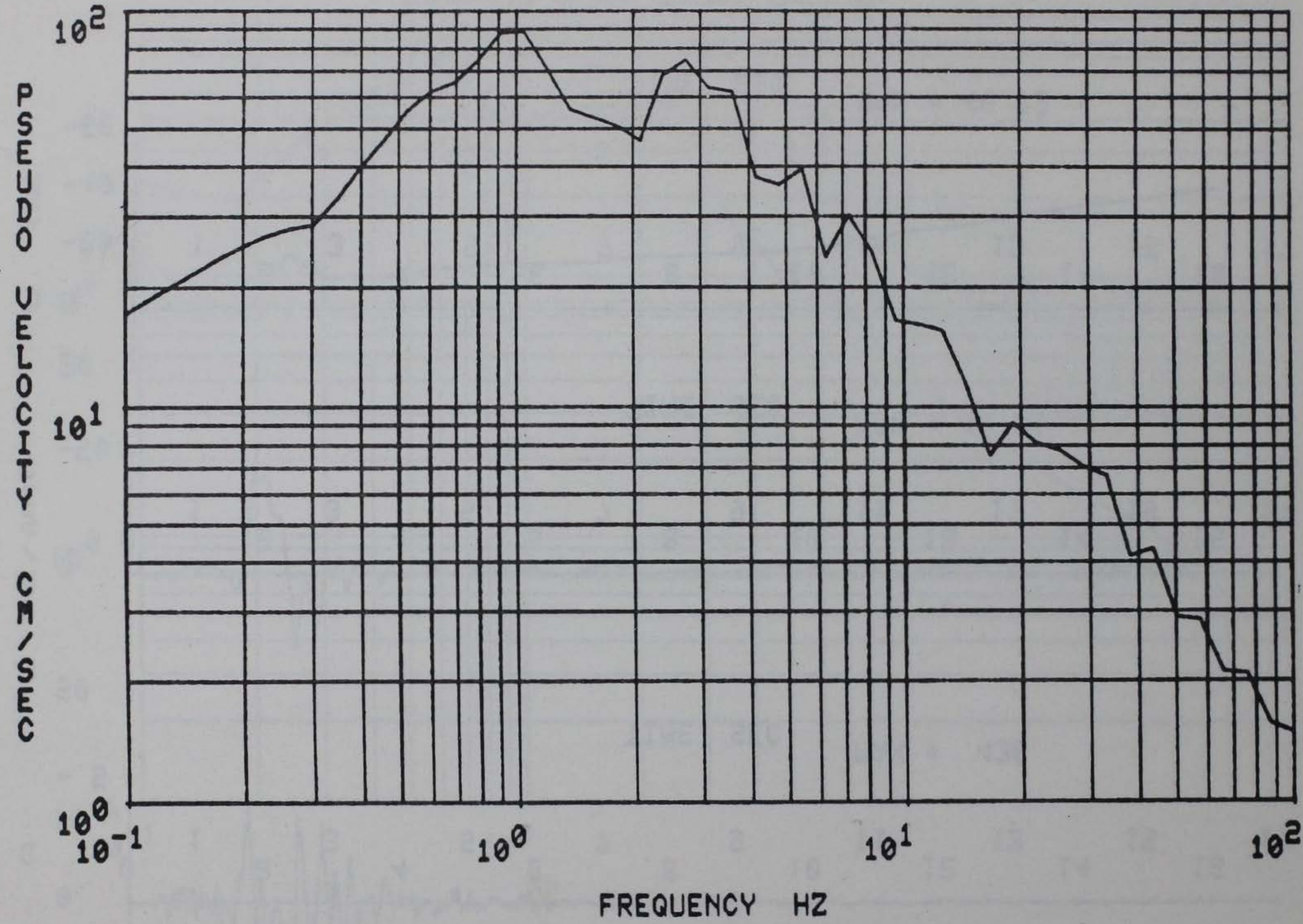

Figure A.23 Response spectrum, 5 percent damping, Helena, Montana, Earthquake, CIT D025, N90E component.

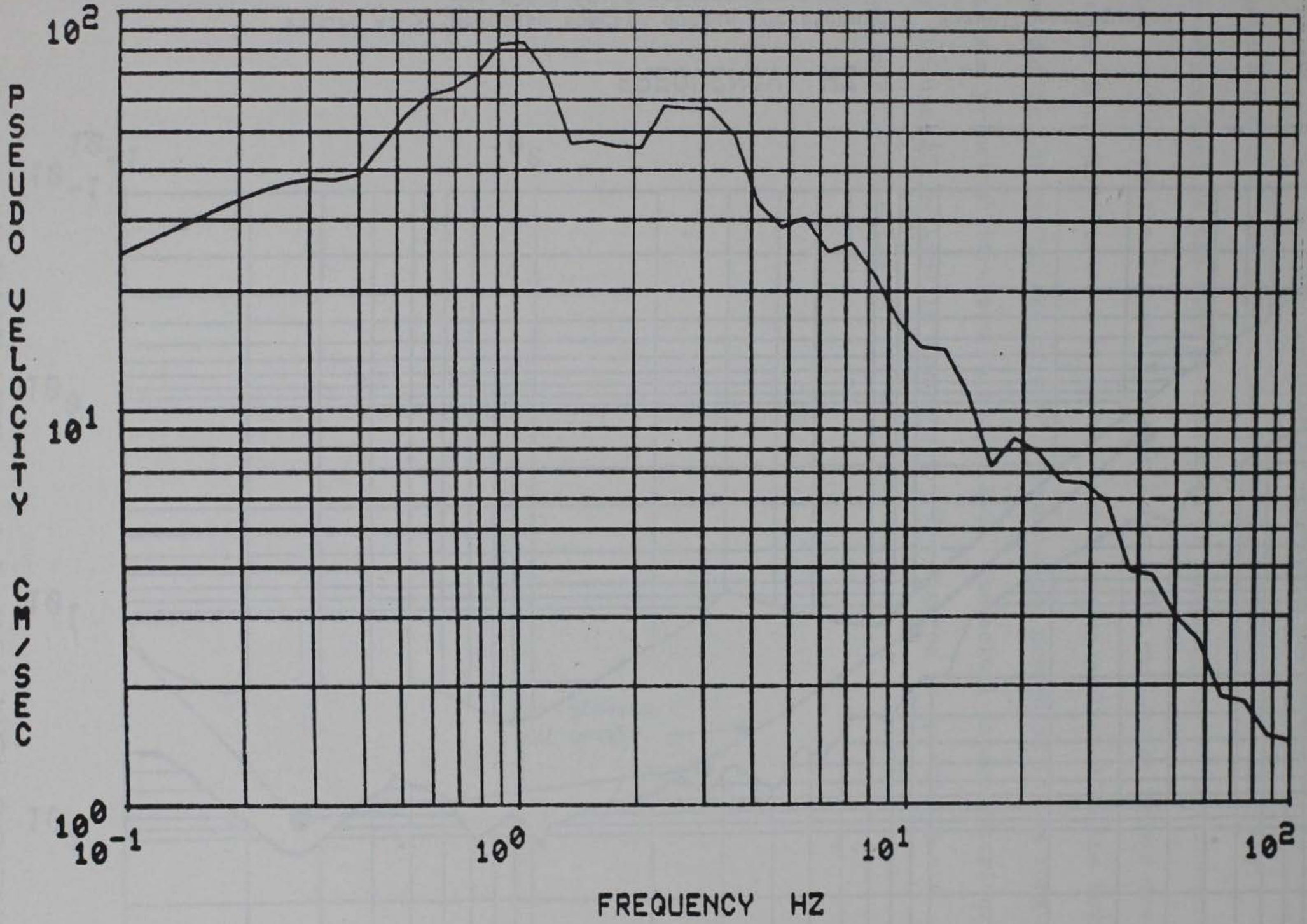

Figure A.24 Response spectrum, 10 percent damping, Helena, Montana, Earthquake, CIT D025, N90E component.

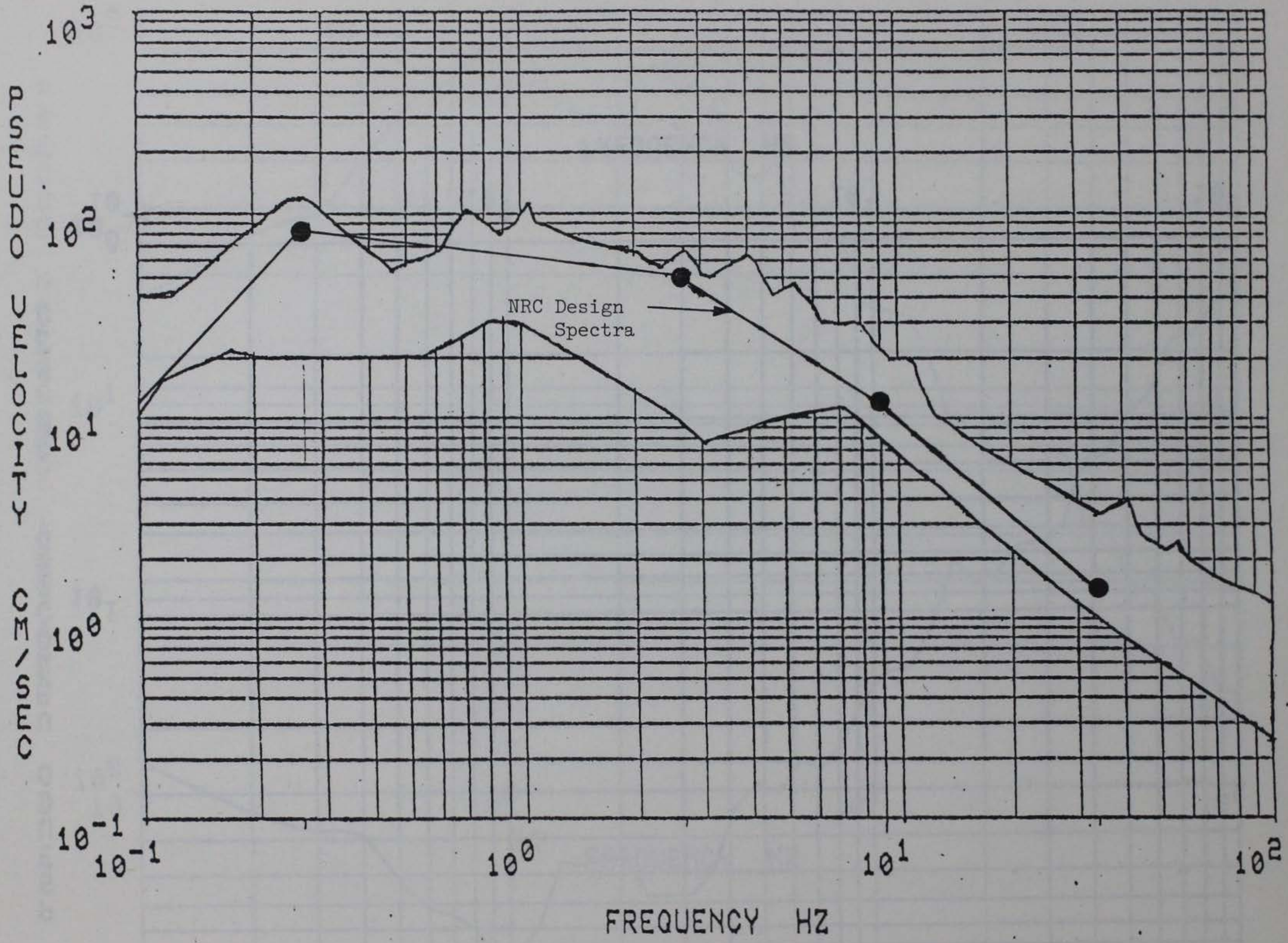

Figure A.25 Response spectra bounds for Richard B. Russell earthquakes and NRC 1.60, 5 percent damping.

APPENDIX B

The purpose of this appendix is to present the results of an earthquake structural analysis of the Koyna Dam of India. The analysis procedure used is the same as that used in the analysis of the nonoverflow section of the Richard B. Russell Dam. The earthquake record used in the analysis (Figure B.1) is the actual record monitored on the Koyna Dam during the earthquake of 1963. Results are presented in the form of maximum principal stresses in Figure B.2. The actual damage experienced by the dam can be seen in Figure B.3. The figures in Appendix B are from References 9 and 10.

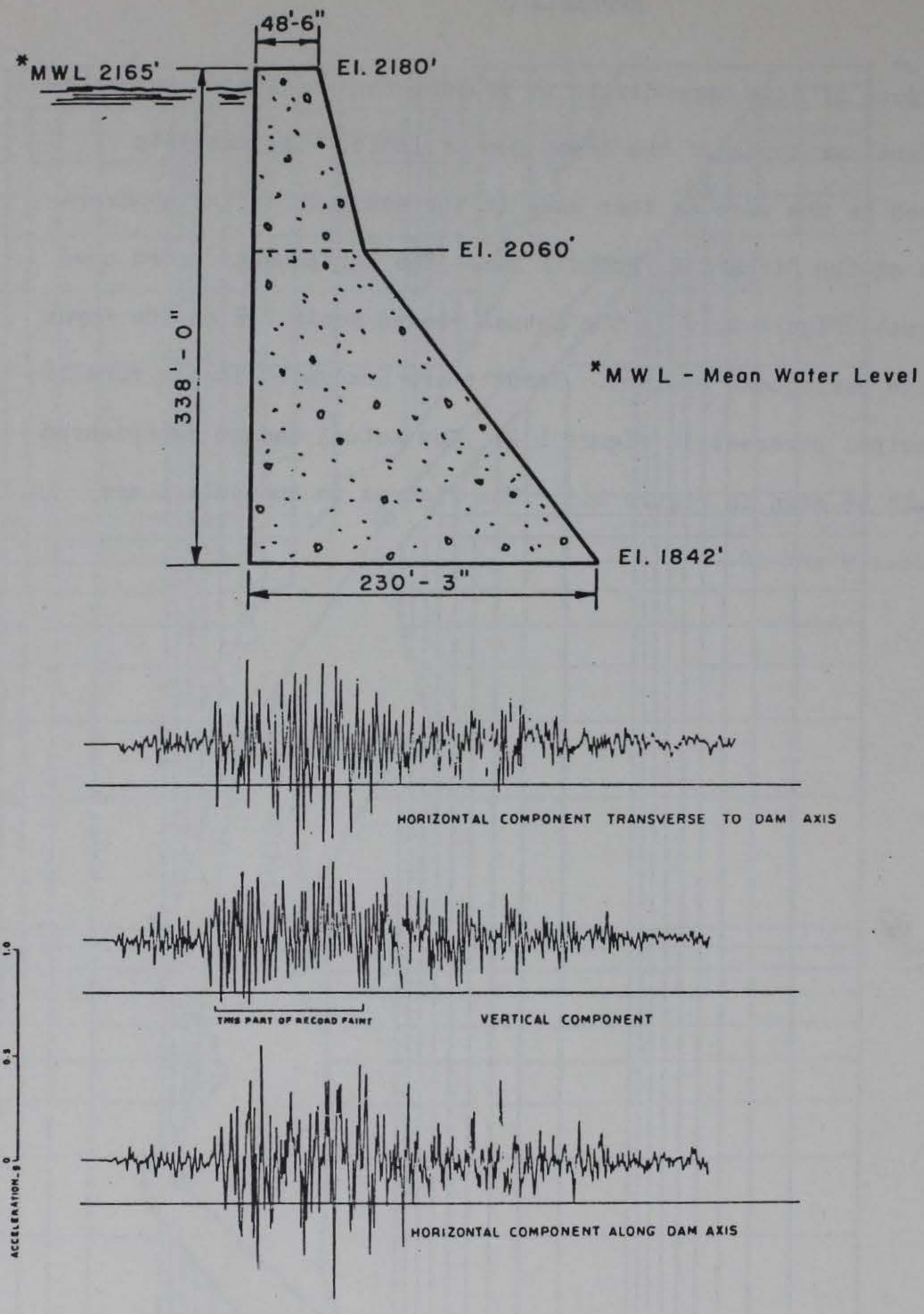

Figure B.1 Cross section geometry of Koyna Dam, accelerogram recorded in block 1-A during the December 11, 1967 earthquake.

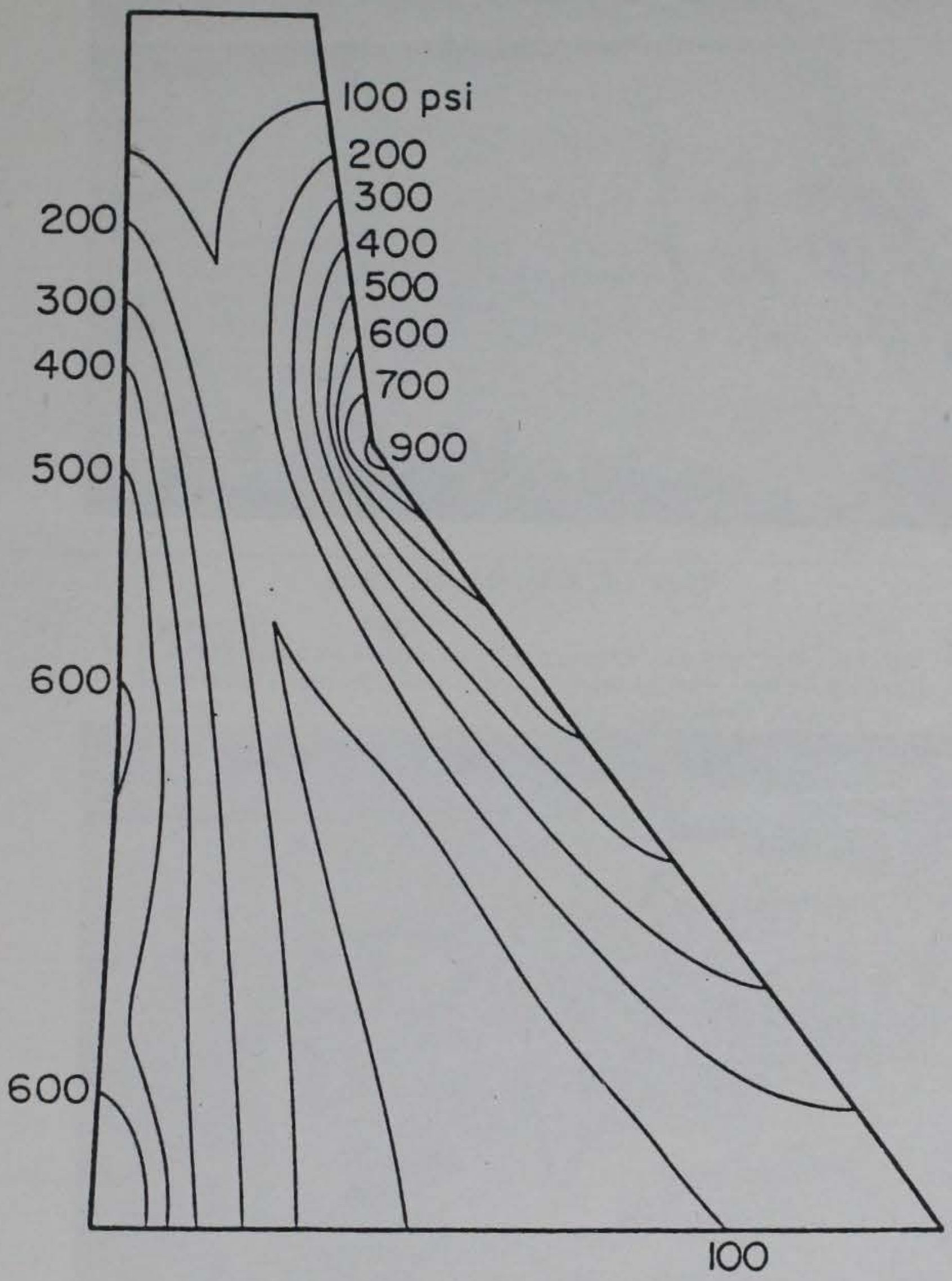

Figure B.2 Envelope values of maximum principal stresses (maximum tension or minimum compression) for a nonoverflow monolith of Koyna Dam due to Koyna Earthquake. Static and dynamic stresses are combined.

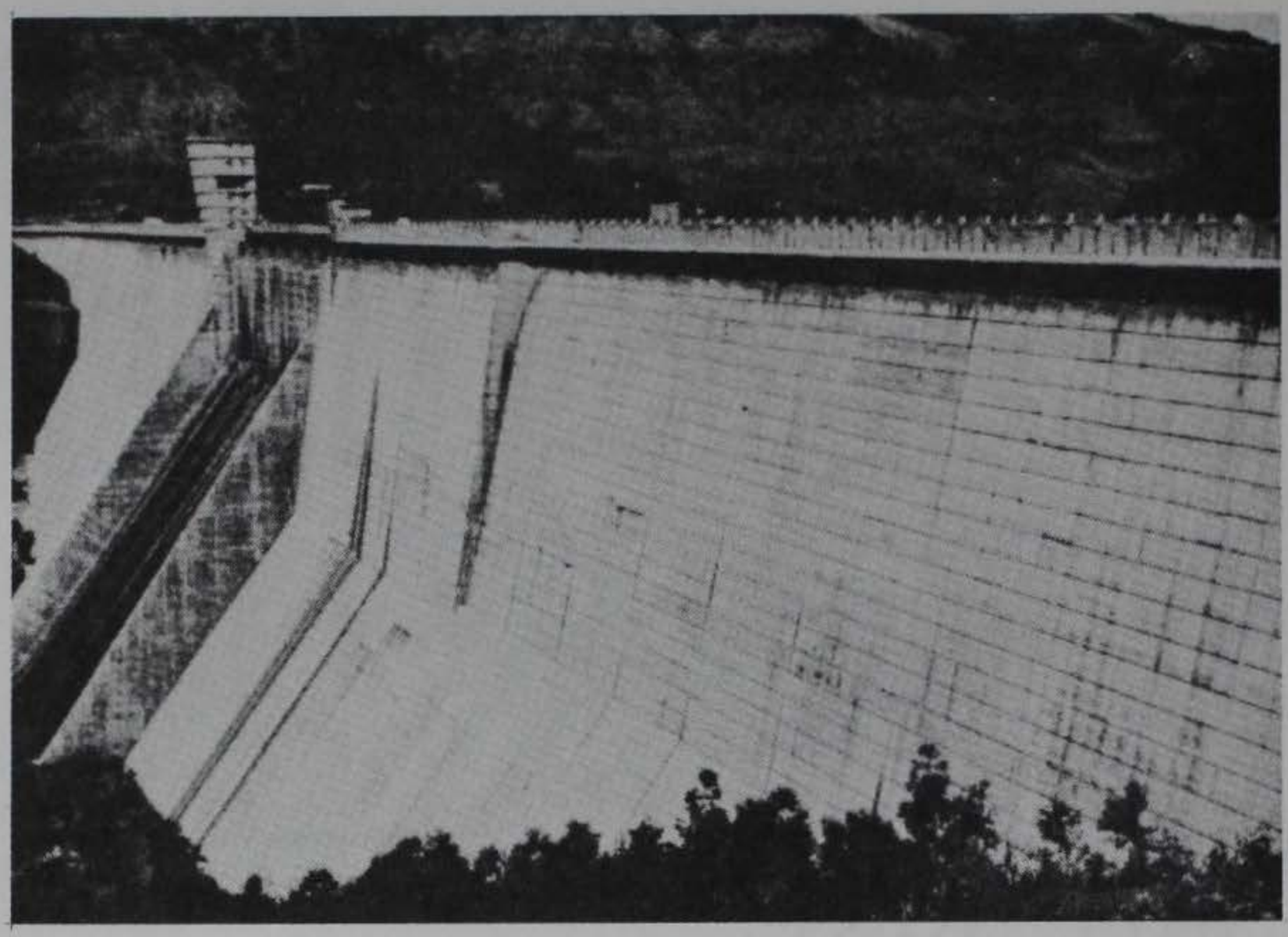

a. View of downstream face.

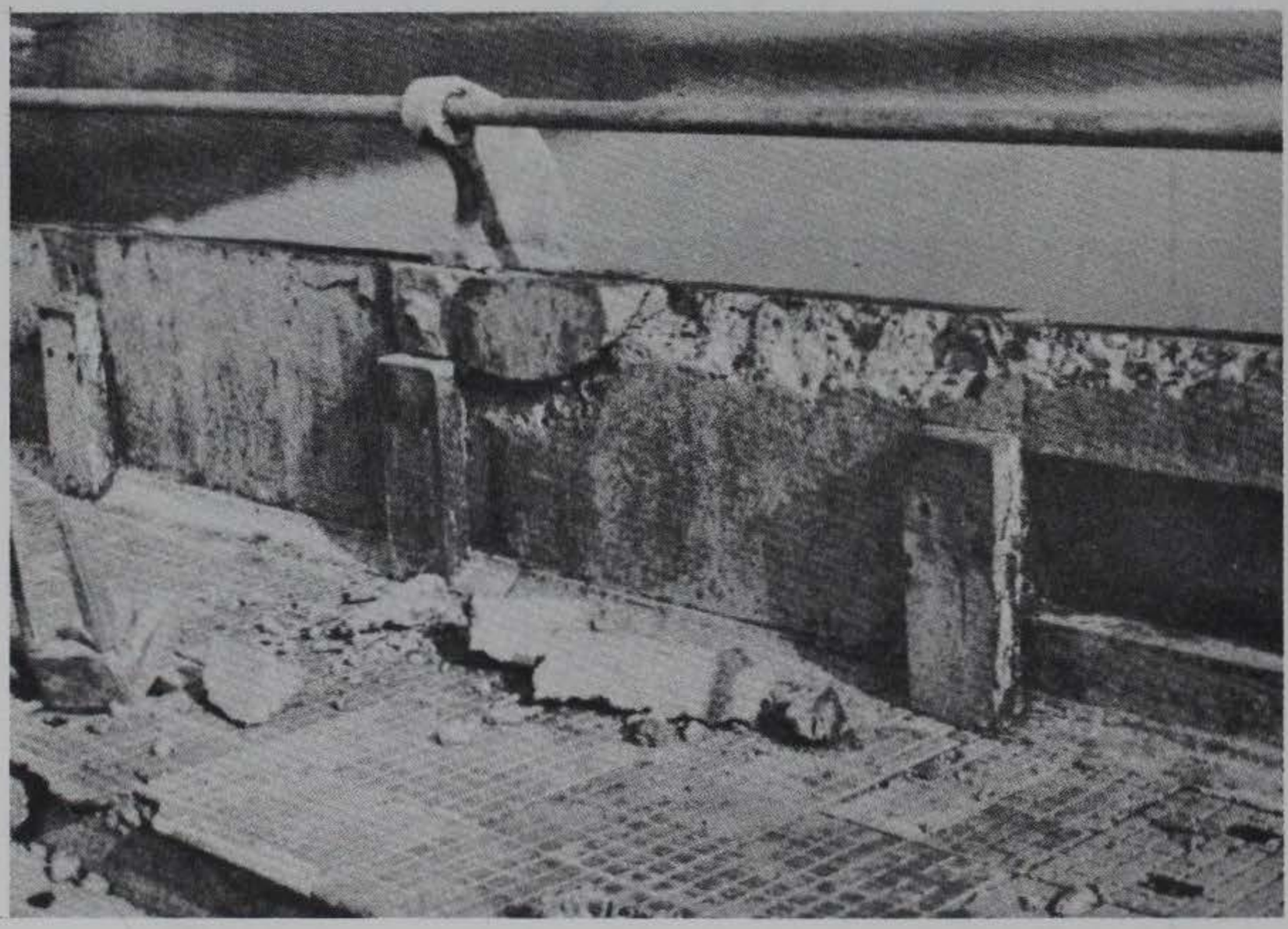

b. Damage sustained by guardrail on crest of dam.

Figure B.3 Damage to Koyna Dam during earthquake of December 11, 1967. (Photographs by G. V. Berg.)